

Fiscal Year 2017: First Quarter

Progress Report  
**Advanced Battery Materials  
Research (BMR) Program**

Released March 2017  
for the period of October – December 2016

*Approved by*

Tien Q. Duong, Advanced Battery Materials Research Program Manager  
Vehicle Technologies Office, Energy Efficiency and Renewable Energy

---

## TABLE OF CONTENTS

<b>A Message from the Advanced Battery Materials Research Program Manager</b> .....	<b>xv</b>
<b>Task 1 – Advanced Electrode Architectures</b> .....	<b>1</b>
Task 1.1 – Higher Energy Density via Inactive Components and Processing Conditions (Vincent Battaglia, Lawrence Berkeley National Laboratory) .....	2
Task 1.2 – Prelithiation of Silicon Anode for High-Energy Lithium-Ion Batteries (Yi Cui, Stanford University).....	4
Task 1.3 – Electrode Architecture-Assembly of Battery Materials and Electrodes (Karim Zaghib, HydroQuebec) .....	7
Task 1.4 – Design and Scalable Assembly of High-Density, Low-Tortuosity Electrodes (Yet-Ming Chiang, Massachusetts Institute of Technology) .....	9
<b>Task 2 – Silicon Anode Research</b> .....	<b>11</b>
Task 2.1 – High-Capacity and Long Cycle Life Silicon-Carbon Composite Materials and Electrodes (Gao Liu, Lawrence Berkeley National Laboratory) .....	12
Task 2.2 – Development of Silicon-Based High-Capacity Anodes (Ji-Guang Zhang and Jun Liu, Pacific Northwest National Laboratory; Prashant Kumta, University of Pittsburgh) .....	14
<b>Task 3 – High-Energy-Density Cathodes for Advanced Lithium-Ion Batteries</b> .....	<b>17</b>
Task 3.1 – Studies on High-Capacity Cathodes for Advanced Lithium-Ion Systems (Jagjit Nanda, Oak Ridge National Laboratory).....	18
Task 3.2 – High-Energy-Density Lithium Battery (Stanley Whittingham, SUNY Binghamton) .....	21
Task 3.3 – Development of High-Energy Cathode Materials (Ji-Guang Zhang and Jianming Zheng, Pacific Northwest National Laboratory) .....	24
Task 3.4 – <i>In Situ</i> Solvothermal Synthesis of Novel High-Capacity Cathodes (Feng Wang and Jianming Bai, Brookhaven National Laboratory) .....	28
Task 3.5 – Novel Cathode Materials and Processing Methods (Michael M. Thackeray and Jason R. Croy, Argonne National Laboratory) .....	30
Task 3.6 – Advanced Cathode Materials for High-Energy Lithium-Ion Batteries (Marca Doeff, Lawrence Berkeley National Laboratory) .....	33
Task 3.7 – Exploiting Cobalt and Nickel Spinels in Structurally Integrated Composite Electrodes (Michael M. Thackeray and Jason R. Croy, Argonne National Laboratory) .....	36
Task 3.8 – Discovery of High-Energy Lithium-Ion Battery Materials (Wei Tong, Lawrence Berkeley National Laboratory) .....	38

<b>Task 4 – Electrolytes</b> .....	<b>41</b>
Task 4.1 – Understanding and Mitigating Interfacial Reactivity Between Electrode and Electrolyte (Khalil Amine, Larry A. Curtiss, and Nenad Markovic, Argonne National Laboratory) .....	42
Task 4.2 – Advanced Lithium-Ion Battery Technology: High-Voltage Electrolyte (Joe Sunstrom, Daikin) .....	45
Task 4.3 – Multi-Functional, Self-Healing Polyelectrolyte Gels for Long-Cycle-Life, High-Capacity Sulfur Cathodes in Lithium-Sulfur Batteries (Alex Jen and Jihui Yang, University of Washington).....	47
Task 4.4 – Development of Ion-Conducting Inorganic Nanofibers and Polymers (Nianqiang (Nick) Wu, West Virginia University; Xiangwu Zhang, North Carolina State University).....	50
Task 4.5 – High Conductivity and Flexible Hybrid Solid-State Electrolyte (Eric Wachsman, Liangbing Hu, and Yifei Mo, University of Maryland) .....	54
Task 4.6 – Self-Forming Thin Interphases and Electrodes Enabling 3D Structured High-Energy-Density Batteries (Glenn Amatucci, Rutgers University).....	57
Task 4.7 – Dual Function Solid-State Battery with Self-Forming, Self-Healing Electrolyte and Separator (Esther Takeuchi, Stony Brook University).....	58
<b>Task 5 – Diagnostics</b> .....	<b>61</b>
Task 5.1 – Model System Diagnosis for High-Energy Cathode Development (Guoying Chen, Lawrence Berkeley National Laboratory).....	62
Task 5.2 – Interfacial Processes – Diagnostics (Robert Kostecki, Lawrence Berkeley National Laboratory) .....	65
Task 5.3 – Advanced <i>In Situ</i> Diagnostic Techniques for Battery Materials (Xiao-Qing Yang and Seongmin Bak, Brookhaven National Laboratory) .....	68
Task 5.4 – Nuclear Magnetic Resonance and Magnetic Resonance Imaging Studies of Solid Electrolyte Interphase, Dendrites, and Electrode Structures (Clare Grey, Cambridge University) .....	71
Task 5.5 – Optimization of Ion Transport in High-Energy Composite Cathodes (Shirley Meng, University of California – San Diego) .....	74
Task 5.6 – <i>In Situ</i> Diagnostics of Coupled Electrochemical-Mechanical Properties of Solid Electrolyte Interphases on Lithium-Metal Rechargeable Batteries (Xingcheng Xiao, GM) .....	77
Task 5.7 – Microscopy Investigation on the Fading Mechanism of Electrode Materials (Chongmin Wang, Pacific Northwest National Laboratory).....	80
Task 5.8 – Characterization and Computational Modeling of Structurally Integrated Electrodes (Michael M. Thackeray and Jason R. Croy, Argonne National Laboratory) .....	83

---

<b>Task 6 – Modeling Advanced Electrode Materials .....</b>	<b>85</b>
Task 6.1 – Predicting and Understanding Novel Electrode Materials from First Principles (Kristin Persson, Lawrence Berkeley National Laboratory).....	86
Task 6.2 – Addressing Heterogeneity in Electrode Fabrication Process (Dean Wheeler and Brian Mazzeo, Brigham Young University) .....	88
Task 6.3 – Understanding and Strategies for Controlled Interfacial Phenomena in Lithium-Ion Batteries and Beyond (Perla Balbuena, Texas A&M University).....	91
Task 6.4 – First Principles Modeling of SEI Formation on Bare and Surface/Additive Modified Silicon Anode (Perla Balbuena, Texas A&M University) .....	93
Task 6.5 – A Combined Experimental and Modeling Approach for the Design of High Current Efficiency Silicon Electrodes (Xingcheng Xiao, General Motors, and Yue Qi, Michigan State University) .....	96
Task 6.6 – Electrode Materials Design and Failure Prediction (Venkat Srinivasan, Lawrence Berkeley National Laboratory).....	99
Task 6.7 – First Principles Calculations of Existing and Novel Electrode Materials (Gerbrand Ceder, Lawrence Berkeley National Laboratory).....	102
<b>Task 7 – Metallic Lithium and Solid Electrolytes .....</b>	<b>104</b>
Task 7.1 – Mechanical Properties at the Protected Lithium Interface (Nancy Dudney, Oak Ridge National Lab; Erik Herbert, Michigan Technological University; Jeff Sakamoto, University of Michigan).....	106
Task 7.2 – Solid Electrolytes for Solid-State and Lithium-Sulfur Batteries (Jeff Sakamoto, University of Michigan).....	108
Task 7.3 – Composite Electrolytes to Stabilize Metallic Lithium Anodes (Nancy Dudney and Frank Delnick, Oak Ridge National Laboratory).....	110
Task 7.4 – Overcoming Interfacial Impedance in Solid-State Batteries (Eric Wachsman, Liangbing Hu, and Yifei Mo, University of Maryland, College Park).....	113
Task 7.5 – Nanoscale Interfacial Engineering for Stable Lithium-Metal Anodes (Yi Cui, Stanford University).....	116
Task 7.6 – Lithium Dendrite Suppression for Lithium-Ion Batteries (Wu Xu and Ji-Guang Zhang, Pacific Northwest National Laboratory).....	119
Task 7.7 – Lithium Batteries with Higher Capacity and Voltage (John B. Goodenough, University of Texas – Austin) .....	122
Task 7.8 – Advancing Solid State Interfaces in Lithium-Ion Batteries (Nenad Markovic and Larry A. Curtiss, Argonne National Laboratory) .....	124
Task 7.9 – Engineering Approaches to Dendrite-Free Lithium Anodes (Prashant Kumta, University of Pittsburgh).....	126

<b>Task 8 – Lithium–Sulfur Batteries .....</b>	<b>128</b>
Task 8.1 – New Lamination and Doping Concepts for Enhanced Lithium–Sulfur Battery Performance (Prashant N. Kumta, University of Pittsburgh) .....	130
Task 8.2 – Simulations and X-Ray Spectroscopy of Lithium–Sulfur Chemistry (Nitash Balsara, Lawrence Berkeley National Laboratory) .....	133
Task 8.3 – Novel Chemistry: Lithium Selenium and Selenium Sulfur Couple (Khalil Amine, Argonne National Laboratory) .....	136
Task 8.4 – Multi-Functional Cathode Additives for Lithium-Sulfur Battery Technology (Hong Gan, Brookhaven National Laboratory, and Co-PI Esther Takeuchi, Brookhaven National Laboratory and Stony Brook University) .....	139
Task 8.5 – Development of High-Energy Lithium–Sulfur Batteries (Jun Liu and Dongping Lu, Pacific Northwest National Laboratory) .....	142
Task 8.6 – Nanostructured Design of Sulfur Cathodes for High-Energy Lithium-Sulfur Batteries (Yi Cui, Stanford University) .....	145
Task 8.7 – Addressing Internal “Shuttle” Effect: Electrolyte Design and Cathode Morphology Evolution in Lithium-Sulfur Batteries (Perla Balbuena, Texas A&M University) .....	148
Task 8.8 – Investigation of Sulfur Reaction Mechanisms (Deyang Qu, University of Wisconsin - Milwaukee; Xiao-Qing Yang, Brookhaven National Laboratory) .....	151
Task 8.9 – Statically and Dynamically Stable Lithium–Sulfur Batteries (Arumugam Manthiram, U Texas Austin) .....	153
Task 8.10 – Electrochemically Responsive, Self-Formed Lithium-Ion Conductors for High-Performance Lithium-Metal Anodes (Donghai Wang, Pennsylvania State University) .....	156
<b>Task 9 – Lithium-Air Batteries .....</b>	<b>159</b>
Task 9.1 – Rechargeable Lithium–Air Batteries (Ji-Guang Zhang and Wu Xu, Pacific Northwest National Laboratory) .....	160
Task 9.2 – Efficient Rechargeable Li/O <sub>2</sub> Batteries Utilizing Stable Inorganic Molten Salt Electrolytes (Vincent Giordani, Liox) .....	163
Task 9.3 – Lithium–Air Batteries (Khalil Amine and Larry A. Curtiss, Argonne National Laboratory) .....	166
<b>Task 10 – Sodium-Ion Batteries .....</b>	<b>169</b>
Task 10.1 – Exploratory Studies of Novel Sodium-Ion Battery Systems (Xiao-Qing Yang and Xiqian Yu, Brookhaven National Laboratory) .....	170

## TABLE OF FIGURES

Figure 1. Laminate calendered at 100°C to 30% porosity. Notice flattened and cracked particles. ....	3
Figure 2. Rate performance of a laminate calendered at different temperatures.....	3
Figure 3. Cycling performance. ....	3
Figure 4. (a, b) Scanning electron microscopy (SEM) images of Ge nanoparticles (NPs) before (a) and after (b) thermal lithiation. (c) X-ray diffraction patterns of Ge NPs before (upper) and after (bottom) thermal lithiation. (d, e) SEM images of GeO <sub>2</sub> NPs before (d) and after (e) thermal lithiation. (f) First-cycle delithiation capacities of lithiated Ge NPs (blue) and lithiated GeO <sub>2</sub> NPs (red). The capacity is based on the mass of Ge or GeO <sub>2</sub> in the anode. (g) First-cycle delithiation capacities of lithiated Ge NPs (blue) and lithiated GeO <sub>2</sub> NPs (red) before (solid) and after (dash) exposure to ambient-air condition (30%~40% RH) for 6 h. ....	5
Figure 5. Full cell performance of 1.5 Ah pouch-type cell: (a) assembled cell; (b) voltage profile during charge-discharge between 2.75 V and 4.4 V at 0.2C rate; (c) rate capability with different current; and (d) cycle life at room temperature. ....	8
Figure 6. Electrochemical test results of half-cells and full cells that contain electrodes prepared by non-sintering magnetic alignment process. (a) Voltage versus areal capacity plot of a LCO cathode. (b) Voltage versus areal capacity plot of a MCMB graphite anode. (c) Charge-discharge voltage profile of a LCO-MCMB full cell.....	10
Figure 7. Sample silicon materials library. ....	13
Figure 8. Silicon particles of different average diameter sizes: (a) 30-50 nm, (b) 50-70 nm, (c) 70-130 nm, and (d) 1µm. ....	13
Figure 9. Thermogravimetric analysis of a few carbon precursor candidates, at a heating rate of 5°C/min from room temperature to 800°C, under nitrogen atmosphere. ....	13
Figure 10. <i>In situ</i> measurement of the electrode swelling upon discharge-discharge process. ....	15
Figure 11. Cycling performance of porous silicon obtained by the low-temperature thermite reaction.....	15
Figure 12. Specific discharge capacity versus cycle numbers for the low-temperature, solid-state reduction (LTSR) approach derived silicon/carbon-nanfiber nanocomposite. The current rate for first three cycles is 300 mA/g and for the remaining cycles is 1 A/g.....	15
Figure 13. Cyclic voltammetry during first and second charge-discharge cycle for Li <sub>2</sub> Cu <sub>0.4</sub> Ni <sub>0.6</sub> O <sub>2</sub> synthesized using sol-gel method using a chelating agent adipic acid.....	19
Figure 14. Scanning electron microscopy micrograph of Li <sub>2</sub> Cu <sub>0.4</sub> Ni <sub>0.6</sub> O <sub>2</sub> cathode particles without (left) adipic acid (AA) and with (right) 0.75 M AA). ....	19
Figure 15. X-ray diffraction patterns of the prelithiated Sn-Fe in comparison to the pristine and standard diffraction patterns of the corresponding phases by contacting the electrode with lithium metal (left) and the corresponding charge/discharge curve of the prelithiated Sn <sub>y</sub> Fe (right). ....	22

Figure 16. (a) Scanning electron microscopy image of $\text{Ni}_{0.68}\text{Mn}_{0.22}\text{Co}_{0.10}(\text{OH})_2$ precursor. (b) Initial discharge profiles at C/10, (c) cycling performance and (d) capacity retention of $\text{Li}(\text{Ni}_{0.68}\text{Mn}_{0.22}\text{Co}_{0.10})_{0.99}\text{M}_{0.01}\text{O}_2$ (M = Mg, Al, V, and Y) during cycling at C/3 after 3 formation cycles at C/10 (1C = 200 mA g <sup>-1</sup> ). Cathode electrode loading is ~4 mg cm <sup>-2</sup> . .....	25
Figure 17. (a) Initial discharge profiles at C/10. (b) Cycling performance and retention of $\text{Li}(\text{Ni}_{0.76}\text{Mn}_{0.14}\text{Co}_{0.10})_{1-x}\text{Al}_x\text{O}_2$ during cycling at C/3 after 3 formation cycles at C/10. ....	25
Figure 18. <i>In situ</i> , temperature-resolved X-ray diffraction for tracking structural evolution of intermediates in preparing (a) $\text{LiNiO}_2$ and (b) $\text{LiNi}_{0.7}\text{Co}_{0.15}\text{Mn}_{0.15}\text{O}_2$ from hydroxides (via solid-state reaction in O <sub>2</sub> with a heating rate of 5°C/min). ....	28
Figure 19. Depiction of the crystal structure of $\text{Sn}_3(\text{PO}_4)_2$ with space group P 21/c showing large channels that may prove beneficial lithium diffusion. O (red), P (purple), Sn (gray). ....	31
Figure 20. (a) Capacity versus cycling of the baseline $\text{Li}_{1.18}\text{Mn}_{0.54}\text{Co}_{0.18}\text{Ni}_{0.28}\text{O}_2$ (~6% spinel) with and without treatments of $\text{Li}_3\text{PO}_4$ , $\text{Li}_{2.8}\text{Ni}_{0.1}\square_{0.1}\text{PO}_4$ , and $\text{Sn}_3(\text{PO}_4)_2$ . (b) Corresponding rate performance of the samples in (a) at a constant charge rate of 15 mA/g, and various discharge rates as labeled (mA/g); first-cycle activation between 4.6-2.0 V; thereafter, 4.45 V-2.5 V. (c) Scanning electron microscopy images of the as-prepared, baseline powder. ....	31
Figure 21. 2D state-of-charge mapping for: (a) pristine $\text{Li}_1\text{Ni}_{0.6}\text{Mn}_{0.2}\text{Co}_{0.2}\text{O}_2$ particles and (b) chemically delithiated $\text{Li}_{0.5}\text{Ni}_{0.6}\text{Mn}_{0.2}\text{Co}_{0.2}\text{O}_2$ imaged at the Ni K-edge. Five different views were investigated to get better statistics. ....	34
Figure 22. Figure 22. (a) Voltage profile of Li/LT-LiCo <sub>0.9</sub> Ni <sub>0.1</sub> O <sub>2</sub> cell showing points where ex situ X-ray diffraction (XRD) data were collected. (b) Corresponding ex situ XRD patterns. (c) Magnified region for (311) and (400) peaks. (d) Simulated XRD patterns of {Li}{tet}[Co <sub>2</sub> O <sub>4</sub> ] spinel and {Li <sub>2</sub> }{oct}[Co <sub>2</sub> O <sub>4</sub> ] lithiated spinel. ....	37
Figure 23. Li (de)intercalation mechanism predicted by density functional theory. ....	37
Figure 24. X-ray diffraction patterns of $\text{Li}_{1.2}\text{Mn}_{0.6}\text{Ni}_{0.2}\text{O}_2$ samples prepared by a solid-state method. Samples are denoted by milling energy followed by milling time, and annealing time. ....	39
Figure 25. The first-cycle voltage profiles of $\text{Li}_{1.2}\text{Mn}_{0.6}\text{Ni}_{0.2}\text{O}_2$ samples prepared by a solid-state method. Cells were cycled between 4.8 and 2 V at a current of 25 mA/g. ....	39
Figure 26. (a) Picture of a 16-channel high precision leakage current measuring system. (b) Schematics showing the connection between the leakage current and the rate of parasitic reactions. (c) A typical current relaxation curve collected to extract the static leakage current. ....	43
Figure 27. Evolution of the static parasitic current as a function of the holding potential for (a) carbon black cast on aluminum foil, and (b) the bare aluminum foil. The electrolyte used was 1.2 M LiPF <sub>6</sub> in EC/EMC (3:7 by mass). ....	43
Figure 28. The initial inductively coupled plasma with mass spectrometry (ICP-MS) results of Co dissolution upon electrochemical polarization using a stationary probe rotating disk electrode system. Working electrode: $\text{LiCoO}_2/\text{C}/\text{PVDF}$ . Electrolyte: 1M LiPF <sub>6</sub> in EC:EMC (3:7 by mass). ....	44

Figure 29. Volume change as function of voltage at 4.2, 4.5 and 4.6 V for both cathode and anode exposed to hydrocarbon and fluorocarbon electrolyte. ....	46
Figure 30. Baseline gas chromatography – mass spectrometry data for baseline fluorinated electrolyte.....	46
Figure 31. First-generation organic starting materials for novel polyelectrolyte gels, all of which have now been synthesized or acquired commercially. ....	48
Figure 32. Mixing solutions containing model pyrene and NDI species results in a new absorption peak at 500 nm (visible as a deep red color).....	48
Figure 33. (a) Symmetric cell with TFSI-only room-temperature ionic liquid (RTIL) electrolyte displays high overpotential that quickly grows out of control. (b) FSI-only RTIL electrolyte, with the same pyrrolidinium cation and Li <sup>+</sup> molar concentration, displays low and continuously decreasing overpotential (note the change in scale), even at increasing current rates. ....	49
Figure 34. Elimination of overcharge (polysulfide redox shuttle) in Li-S cells with room-temperature ionic liquid electrolyte, as opposed to additive-free organic electrolytes, which cause severe overcharge issues. ....	49
Figure 35. Photographs of (a) as-spun precursor nanofibers, and (b) calcinated Al-doped inorganic nanofibers.....	51
Figure 36. (a) Infrared spectrum. (b) Photograph (pale yellow liquid) of 4-vinylbenzenesulfonyl chloride.....	52
Figure 37. (a) Infrared spectrum. (b) Photograph of 4-vinylbenzenesulfonyl amine. ....	52
Figure 38. Infrared spectra of N-Sulfinyltrifluoromethanesulfonamide (CF <sub>3</sub> SO <sub>2</sub> N=S=O): (a) without catalyst and (b) with catalyst.....	53
Figure 39. Scanning electron microscopy images of garnet nanofibers before (top) and after (bottom) calcination. ....	55
Figure 40. (a) Electrochemical impedance spectroscopy profiles of the flexible electrolyte membrane at different temperatures (25°C, 40°C, and 90°C). (b) Arrhenius plot of the flexible electrolyte membrane at elevated temperatures.....	55
Figure 41. Digital photo (left) and X-ray diffraction pattern (right) of 4cm by 4cm conductive garnet textile. ....	55
Figure 42. Structures of AgI β-phase (left), AgI γ-phase (center), and LiI (right).....	59
Figure 43. Electrochemical impedance spectroscopy for silver iodide as a function of temperature. ....	59
Figure 44. Equivalent circuit used for data analysis. ....	59
Figure 45. Resistance as a function of temperature.....	59
Figure 46. (a) Scanning electron microscopy image. (b-c) Rietveld refinements of synchrotron X-ray diffraction and neutron patterns of Li <sub>1.3</sub> Nb <sub>0.3</sub> Mn <sub>0.4</sub> O <sub>2</sub> crystal sample.....	63
Figure 47. Synchrotron X-ray diffraction patterns of chemically delithiated Li <sub>x</sub> Nb <sub>0.3</sub> Mn <sub>0.4</sub> O <sub>2</sub> (0 < x ≤ 1.3) crystal samples.....	63



Figure 48. (a) NMC and NMC/R electrodes capacity retention. (b-d) Charge discharge voltage profiles.....	66
Figure 49. Nyquist plots of coin cells with NMC (a) and NMC/R (b) cathodes. $R_s$ and $R_{ct}$ extracted from the impedance data for NMC (c) and NMC/R (d) electrodes. ....	66
Figure 50. (a) Illustration of pair distribution function (PDF) showing that peaks correspond to characteristic bond lengths. (b) <i>Ex situ</i> PDF data of pristine sample and “OCV—1V—3V” sample. (c) Zoomed in data on the short-range region of <i>ex situ</i> PDF data. (d) Zoomed in data on the long-range region of <i>ex situ</i> PDF data. ....	69
Figure 51. Differential capacity versus voltage plots of the $\text{Na}_{2/3}\text{Mn}_{1-\gamma}\text{Mg}_\gamma\text{O}_2$ ( $\gamma = 0.0, 0.05, 0.1$ ) compositions.....	72
Figure 52. <i>Ex situ</i> $^{23}\text{Na}$ magic angle spinning solid-state nuclear magnetic resonance (NMR) spectra collected on cells stopped at different points along the first electrochemical charge/discharge cycle of $\text{Na}_{2/3}\text{Mn}_{1-\gamma}\text{Mg}_\gamma\text{O}_2$ , where $\gamma = 0.0, 0.05, 0.1$ for (a), (b), and (c), respectively. Spectra are scaled according to number of scans collected during the experiment, amount of sample in the rotor, and NMR signal decay obtained from $T_2$ relaxation time measurements. Hashes indicate samples for which a lack of experimental data prevents proper scaling of the spectrum. Asterisks indicate spinning sidebands. ....	72
Figure 53. (a) Aberration corrected high-angle annular dark field (HAADF) scanning transmission electron microscopy image. (b) Spatially resolved O K-edge and Mn L-edge electron energy loss spectroscopy (EELS) spectra. (c) Mn $L_3/L_2$ ratio fit results from the EELS spectra. ....	75
Figure 54. First charge and discharge profiles of silicon with CMC and PAA binders. ....	75
Figure 55. PVD system integrated with glovebox for making lithium thin-film electrode and protective coatings. ....	78
Figure 56. (a) Typical L-D curves with different indentation strain rates (F/F). (b) Typical L-D curves with different loading rates (F). ....	78
Figure 57. The effect of elastic modulus on the L-D curves. The L-D curves with $E \geq 3.5$ GPa nearly overlap with each other.....	78
Figure 58. Scanning transmission electron microscopy – electron energy loss spectroscopy (STEM–EELS) analysis valence mapping of the 40 cycles and its correlation with the $\text{Al}_2\text{O}_3$ coating layer. (a-c) Uncoated samples. (d-f) Coated samples. (a) Annular dark field (ADF) image. (b) Estimated Mn valence state map based on EELS chemical shift. (c) Mn EELS spectra from surface and inner region in (a). (d) ADF image. (e) Estimated Mn valence state map from EELS chemical shift. (f) Mn EELS spectra from surface and inner region in (d). ....	81
Figure 59. The compositional phase space of a layered (L)-layered (L)-spinel (S) system. $\text{Li}_2\text{MnO}_3 \bullet \text{LiNi}_{0.5}\text{Mn}_{0.5}\text{O}_2 \bullet \text{LiNi}_{0.5}\text{Mn}_{1.5}\text{O}_4$ . ....	84
Figure 60. Rietveld refinement results of (a) synchrotron X-ray and (b) neutron diffraction of the $x = 0.75$ sample. (c) Synchrotron X-ray diffraction of the $x = 1.0$ sample.....	84

Figure 61. Spontaneous oxygen evolution and its impact on the nearest cation. For instance, surface $Mn^{4+}$ (purple octahedral site) to $Mn^{3+}$ (yellow site) by first oxygen evolution (yellow site in c/d). .....	87
Figure 62. The d-orbital density of state (DOS) of the defect site in the surface (top) and at the bulk (bottom). Cr defect prefers the surface as reflected by the bulk versus surface DOS behavior (a). Ni shows the opposite behavior (b). .....	87
Figure 63. Side-by-side comparison of the rigid micro-N-line probe consisting of metal deposited on a glass substrate (left), and the flexible micro-flex-line probe consisting of metal deposited on a polyimide substrate (right). .....	89
Figure 64. Effect of electrolyte composition on lithiation and SEI formation in a silicon cluster. (a) EC/LiPF <sub>6</sub> . (b) EC only. (c) Same as (b) with enlarged silicon atoms. Si (yellow), Li (purple), O (red), C (grey), H (white), F (light blue). .....	92
Figure 65. Snapshot of a classical molecular dynamics simulation of a model silicon anode after a constant electric field of 1 V/Å is applied. The model anode is in a larger cell containing also the electrolyte phase and the cathode. The charge is simulated by applying a constant potential to the cell. Si (blue), Li (yellow), Li (electrolyte, pink), C (green), H (white), O (red), P (orange), F (light blue). .....	92
Figure 66. (left) Nucleation of Li <sub>2</sub> CO <sub>3</sub> over graphite electrode. Lithium ions interact with adsorbed oxygen atoms at the graphite edge. (right) Electrostatic potential (eV) of the nucleating phase on the solid electrode. Note the discontinuity at the interface (highlighted).....	94
Figure 67. Gaussian fit to the “self” part of van Hove function suggests Li <sub>2</sub> EDC (left) is crystalline compared to pure EC (right). Correlations are calculated for ps compared to ns in the Li <sub>2</sub> EDC case. ....	94
Figure 68. Schematic showing deformation of patterned silicon island during cycling, and the resulting impact of volume changes on SEI formation and failure. ....	97
Figure 69. (a) Finite element model of a sliding silicon island electrode on a current collector; (b) Length change of the silicon island versus cycle number. ....	97
Figure 70. (a) The number of lithium atoms reached silicon thin film after 150ps molecular dynamic simulations, and the corresponding structure of silicon initially coated with (b) SiO <sub>2</sub> , (c) SiO <sub>2</sub> -LiF, and (d) LiF. ....	97
Figure 71. (a-c) According to the pre-stressed lithium scenario, tensile stresses act within lithium metal, and compressive stresses act inside electrolyte. (d-f) Relaxed lithium assumes stress-free condition for lithium metal and electrolyte. During operation, when fresh lithium gets deposited, bulk lithium metal, electrolyte, and the newly deposited lithium experience compression. ....	100
Figure 72. (a-b) Variation in effective exchange current density around the dendritic protrusion. If the current at the peak is greater than that at the valley, dendrites grow. (a) For pre-stressed lithium. (b) For initially relaxed lithium. (c) Ratio of the effective exchange current density at the protrusion peak over that at the valley. For initially relaxed lithium, dendrite growth never occurs at low current operation. ....	100

Figure 73. Maximal transition metal site distortion relative to the original bond lengths in ordered LiTMO <sub>2</sub> ground state structures and in cation-disordered LiTMO <sub>2</sub> structures. Contribution of the four symmetry-breaking normal modes, $v_2$ through $v_5$ , to the site distortions are shown. ....	103
Figure 74. Energy and relative transition metal (TM) site distortion in LiNi <sub>0.5</sub> Ti <sub>0.5</sub> O <sub>2</sub> and LiMn <sub>0.5</sub> Ni <sub>0.5</sub> O <sub>2</sub> . Each data point corresponds to a single atomic structure. The error bars indicate the range of distortions for all sites of one TM species within that structure. ....	103
Figure 75. Performed first attempts at characterizing mechanical properties of lithium films post electro-chemical cycling. ....	107
Figure 76. (a) 20- $\mu$ m thick lithium film. (b) 5- $\mu$ m thick lithium film. The residual hardness impressions are approximately 11 $\mu$ m along each face. ....	107
Figure 77. First-generation Li-LLZO-Sulfur+carbon cells. By wt.; 46% S, 37% KJB, 8.5% PVDF, and 8.5% Super P. Cycled at 0.06 mA/cm <sup>2</sup> in 1M LiTFSI, DOL:DME. Electrodes were ~30- to 35- $\mu$ m thick; 0.8 mg <sub>(S)</sub> /cm <sup>2</sup> loading. (a) Schematic diagram of test cell. LLZO membrane physically isolated lithium from the liquid electrolyte. (b) First two cycles comparing a typical all-liquid cell (red) and hybrid cell (blue data). Specific capacities normalized by grams S. (c) Sulfur specific capacity versus cycle number, and Coulombic efficiency versus cycle number. All-liquid cell (red), hybrid cell (blue) data.....	109
Figure 78. (left) Room-temperature conductivity comparing the composites with (red) and without (orange) plasticizers. TEGDME is added to the spray coat and DMC to the melt samples. (right) Arrhenius results for the spray-coated electrolytes are shown along with those for the single-phase Ohara (blue) and polymer (black) electrolytes. ....	111
Figure 79. (left) Room temperature conductivity of the spray-coated composite with different amounts of the Ohara ceramic. The conductivity was recorded after heating the composite to 80°C and cooling. (right) Similar results for composites formed with different concentrations of dissolved lithium triflate salt. ....	111
Figure 80. Characterization of bi-layer garnet and performance of NMC battery. (a) Cross sectional scanning electron microscopy (SEM) image of bi-layer garnet. (b) SEM of garnet grains coated with carbon nanotube (CNT). (c) Cyclic voltammetry of the NMC battery with CNT anode. (d). Electrochemical impedance spectroscopy of the NMC battery with CNT anode after lithiation. (e) Cycling performance of the NMC battery at 0.1 C rate. (f) Rate test of the NMC battery at 0.1C and 0.05 C rates. ....	114
Figure 81. CE of artificial SEI protected Cu foil and bare Cu foil at a current density of (a) 1 mA cm <sup>-2</sup> (cycling capacity 1 mAh cm <sup>-2</sup> ; Inset: the corresponding voltage profiles at the 20 <sup>th</sup> cycle) and (b) 0.25 mA cm <sup>-2</sup> (cycling capacity 0.5 mAh cm <sup>-2</sup> ). ....	117
Figure 82. Top-view scanning electron microscopy images and corresponding digital photographs of lithium deposition after five cycles on (a/c) artificial SEI protected Cu and (b/d) bare Cu foil. (e) Configuration of nano-indentation measurements. (f) Elastic modulus versus depth for indentation test. ....	117

Figure 83. (a) Highest occupied molecular orbital (HOMO) and lowest unoccupied molecular orbital (LUMO) energies of lithium salts (LiPF <sub>6</sub> , LiTFSI, LiBOB) and solvents (EC, EMC). The vertical lines indicate the electrochemical stability window of related lithium salts and solvents. (b) Schematic illustration demonstrating that LiPF <sub>6</sub> additive in LiTFSI-LiBOB dual-salt electrolyte improves the stability of the Al current collector and the Li-metal anode.....	120
Figure 84. (a) The impedance plots of a Li-S battery. (b) Charge and discharge voltage profiles of a Li-S battery with LLZT and LLZT–2LiF as a separator. (c) Charge and discharge voltage profiles of a Li-S battery with LLZT–2LiF at different current densities. (d) Capacity retention and cycling efficiency of the Li-S battery. ....	123
Figure 85. Cycling stability and CE of the Li-S cell without solid electrolyte nor LiNO <sub>3</sub> additive. ....	123
Figure 86. X-ray photoelectron spectroscopy results for 1s lithium peak to establish Li-O interaction. ....	125
Figure 87. X-ray photoelectron spectroscopy results for titanium 2p peaks to track valence state of titanium. ....	125
Figure 88. (a) Density functional theory calculated reaction path for lithium migration from Li <sub>2</sub> CO <sub>3</sub> to the Li(100) surface. (b) Illustration showing migration of one lithium (blue) across the interface. ....	125
Figure 89. Significant improvement in Coulombic efficiency of lithium afforded by use of multilayer porous foams.....	127
Figure 90. Voltage hysteresis plot of composite polymer electrolytes (black) showing superior Coulombic efficiency and stability as compared to commercial separators with liquid electrolyte (red). ....	127
Figure 91. Scanning electron microscopy images of the morphology of (a) lithium electrode and (b) lithium structurally isomorphous alloy (Li-SIA) electrode cycled at high current density ~ 1 A/g (30 cycles). A clear absence of dendritic structures observed in the Li-SIA electrode. ....	127
Figure 92: Mechanical behavior of composite polymer electrolyte showing superior strength of engineered synthesis method. ....	131
Figure 93. (a) Fourier transform infrared spectra of composite polymer electrolyte (CPE) after cycling. (b) Flammability test result of the CPE. ....	131
Figure 94. Structure of C-S nanospheres. (a) Schematic of the 60 wt% (left) and 30 wt% (right) carbon nanosphere morphology. (b) Associated high-angle annular dark-field images. (c) Simulated (bottom) and measured X-ray absorption spectra of 30 wt% (green) and 60 wt% (brown) loaded carbon nanoshells. Dashed vertical lines indicate the positions of peak maximum. Bottom insets: Models used when calculating the X-ray absorption spectroscopy of the 30-wt% and 60-wt% nanoshells, respectively. (d) Energy dispersive X-ray spectra of nanoshells at the carbon and sulfur edges.....	134
Figure 95. Schematic for the voltage profile and polysulfides solubility test of Li/Se-S cell in two different electrolytes. ....	137

Figure 96. (a) Estimated maximum sulfur and selenium loading versus pore volume of carbon materials. (b) Pore size distribution of a newly developed carbon material for high-loading Se-S system. (c) X-ray diffraction pattern showing crystalline selenium formation in the composite. ....	137
Figure 97. TiS <sub>2</sub> effect on sulfur utilization. ....	140
Figure 98. Energy density at electrode level. ....	140
Figure 99. Slurry mixing process methods versus TiS <sub>2</sub> distribution (energy dispersive spectroscopy) within coated cathode. ....	141
Figure 100. (a) Dependence of electrode porosity on thickness. (b) Calculated electrolyte amount for electrodes with different porosities. (c) Dependence of volumetric energy density on electrode thickness. (d) Cycling stability of electrodes at different thicknesses. ....	143
Figure 101. Crystal structures and calculated band structures for bulk phases of (a) Ni <sub>3</sub> S <sub>2</sub> , (b) SnS <sub>2</sub> , (c) FeS, (d) CoS <sub>2</sub> , (e) VS <sub>2</sub> , and (f) TiS <sub>2</sub> . The red dashed lines mark the Fermi energy level. ....	146
Figure 102. (a) First-cycle charge voltage profiles of Ni <sub>3</sub> S <sub>2</sub> -Li <sub>2</sub> S, SnS <sub>2</sub> -Li <sub>2</sub> S, FeS-Li <sub>2</sub> S, CoS <sub>2</sub> -Li <sub>2</sub> S, VS <sub>2</sub> -Li <sub>2</sub> S, TiS <sub>2</sub> -Li <sub>2</sub> S, and G/CNT-Li <sub>2</sub> S electrodes. (b) Energy profiles for the decomposition of Li <sub>2</sub> S cluster on Ni <sub>3</sub> S <sub>2</sub> , SnS <sub>2</sub> , FeS, CoS <sub>2</sub> , VS <sub>2</sub> , TiS <sub>2</sub> , and graphene. Top view schematic representations of the corresponding decomposition pathways for (c) Ni <sub>3</sub> S <sub>2</sub> , (d) SnS <sub>2</sub> , (e) FeS, (f) CoS <sub>2</sub> , (g) VS <sub>2</sub> , (h) TiS <sub>2</sub> and (i) graphene. Here, green, yellow, grey, purple, brown, blue, red, cyan, and beige balls symbolize lithium, sulfur, nickel, tin, iron, cobalt, vanadium, titanium, and carbon atoms, respectively. S <sub>m</sub> represents the sulfur atom in the Li <sub>2</sub> S cluster. ....	146
Figure 103. First coordination shell of a lithium ion (purple) surrounded by DME molecules (left) at 1M LiFSI concentration, and solvated by salt anions and DME molecules at 4M LiFSI concentration (right). Camacho Forero, Smith, Balbuena, JPCC, 2017. O (red), C (grey), S (yellow), N (blue). ....	149
Figure 104. Cell performance is affected by chemical reactions in the anode side: (a) effect of chemical reaction kinetics; and (b) effect of discharge rate. ....	149
Figure 105. DME-based electrolytes with elemental sulfur contacted with lithium metal at different times. From top to bottom: electrolytes with sulfur and without Li metal, electrolytes with sulfur and Li metal for 1 day, electrolytes with sulfur with Li metal for 2 days, electrolytes with sulfur with Li metal for 4 days, and electrolytes with sulfur with Li metal for 8 days. From left to right: LiTFS/DME electrolyte, LiTFSi/DME electrolyte, LiDFOB/DME electrolyte, LiBOB/DME electrolyte, LiBF <sub>4</sub> /DME electrolyte, LiPF <sub>6</sub> /DME electrolyte, LiClO <sub>4</sub> /DME electrolyte, LiTFSi/DME/DOL electrolyte. ....	152
Figure 106. <i>In situ</i> electrochemical optical cell (left bottom). Full set up (left top). Example photos at various stages of galvanostatic charge (a-f). ....	152
Figure 107. Dynamic cycling performance of the cells fabricated with (a) spherical carbon – single-walled carbon nanotube (SWCNT)-coated separators, (b) layer-by-layer (LBL) carbon nanofiber (CNF)-coated separators, and (c) LBL CNT-coated separators. ....	154

Figure 108. Initial discharge-charge profiles of KB-S70 cathodes in (a) conventional, (b) 0.25 M polysulfide-containing, and (c) 50 vol% dimethyl disulfide (DMDS)-containing electrolytes with electrolyte/ sulfur ratios of 5 and 10 mL g <sup>-1</sup> at a current density of 0.2 mA cm <sup>-2</sup> , with (d) their corresponding cycling performance. ....	157
Figure 109. Cycling performance of 2 wt% sulfur-containing polymers with different sulfur contents as additives. (a) PSD containing different sulfur contents. (b) PST containing different sulfur contents.....	157
Figure 110. Morphologies of lithium metal deposited onto stainless steel substrate. Scanning electron microscopy images of lithium metal deposited onto bare stainless steel substrate in the electrolyte with the addition of 8 wt% the sulfur composite product (SCP)-90. ....	157
Figure 111. Discharge curves of Li-O <sub>2</sub> cells using carbon nanotube air electrodes and 1 M LiClO <sub>4</sub> -DME electrolyte cycled at various temperatures (from 40°C to -20°C) and at a discharge current density of 0.1 mA cm <sup>-2</sup> .....	161
Figure 112. Morphological images of the discharged products on the carbon nanotube (CNT)-based air electrodes after discharge at various temperatures (a-g) and the pristine CNTs air electrode (h). ....	161
Figure 113. (a) Galvanostatic discharge curves for Li/O <sub>2</sub> cell containing a LiNO <sub>3</sub> -KNO <sub>3</sub> electrolyte and a carbon-based air electrode (T= 150°C, PO <sub>2</sub> = 1.4 atm, j= 0.32 mA/cm <sup>2</sup> ). (b) Cycling profile of a molten nitrate Li/O <sub>2</sub> cell containing a carbon-free air electrode (T= 150°C, j= 0.13 mA/cm <sup>2</sup> , boron carbide loading: 5-7 mg/cm <sup>2</sup> ). (c) Corresponding <i>in situ</i> pressure analysis for cell depicted in (b).....	164
Figure 114. (a) Lithium plating/stripping onto Cu (A <sub>Li</sub> =A <sub>Cu</sub> =0.502 cm <sup>2</sup> ) at j= 0.5 mA/cm <sup>2</sup> , at 150°C, under Ar, in LiNO <sub>3</sub> -KNO <sub>3</sub> melt (Inset: Q vs cycle number and lithium plating/stripping load curve). (b) Cycling curve comparison between Li-Li symmetric cell and Li-Cu cell employing LiNO <sub>3</sub> -KNO <sub>3</sub> melt, at 0.5 mA/cm <sup>2</sup> , at 150°C. (c) Electrochemical impedance spectroscopy data derived from cycled Li-Li symmetric cell (estimated electrolyte thickness: 0.5 mm, A <sub>Li</sub> = 0.502 cm <sup>2</sup> ). ....	164
Figure 115. (a) Transmission electron microscopy (TEM) image of Platinum-hollow graphene nanocages (Pt-HGNs). (b,c) High-magnification TEM images of Pt-HGNs. (d) Dark-field scanning transmission electron microscopy (DF-STEM) image of Pt-HGNs. ....	167
Figure 116. Galvanostatic discharge/charge profiles of Li-O <sub>2</sub> batteries with (a) hollow graphene nanocages (HGNs) and (b) Pt-HGNs as+ cathode catalysts at 100 mA/g in the voltage range of 2.2 – 4.5 V vs. Li+/Li with the fixed capacity of 1000 mAh/g. Discharge/charge profiles of Li–O <sub>2</sub> batteries with (c) Pristine HGNs and (d) Pt-HGNs cathode catalysts at different current densities.....	167
Figure 117. (a) <i>Ex situ</i> X-ray diffraction patterns (left) for V <sub>2</sub> CT <sub>x</sub> upon electrochemical sodiation/desodiation cycling (right). (b) Schematic illustration of the expansion/contraction behavior of V <sub>2</sub> CT <sub>x</sub> during sodiation/desodiation process: the interlayer distance of V <sub>2</sub> CT <sub>x</sub> is increased upon Na <sup>+</sup> intercalation during sodiation process, then partially reduced upon Na <sup>+</sup> deintercalation due to the trapped Na <sup>+</sup> between V <sub>2</sub> CT <sub>x</sub> layers that behaves as a pillar during desodiation process. ....	171

## TABLE OF TABLES

Table 1. Experimental conductivity results (with 95% confidence intervals) from using $\mu$ NLP and $\mu$ FLP on the same electrode sample.....	89
Table 2. Formulation design. ....	140

## A MESSAGE FROM THE ADVANCED BATTERY MATERIALS RESEARCH PROGRAM MANAGER

The Advanced Battery Materials Research (BMR) Program continues to expand its portfolio to include new materials and processes that have the potential to reduce the cost and improve the performance of batteries. With this comes the addition of several world renowned investigators to our already diverse Team. A list of the new efforts is provided below:

- *In situ* Diagnostics of Coupled Electrochemical-Mechanical Properties of Solid Electrolyte Interphases on Lithium Metal for Rechargeable Batteries; Xingcheng Xiao, General Motors
- Advanced Microscopy and Spectroscopy for Probing and Optimizing Electrode-Electrolyte Interphases in High-Energy Lithium Batteries; Shirley Meng, University of California – San Diego
- Advanced Li-Ion Battery Technology: High-Voltage Electrolyte; Joe Sunstrom, Daikin America
- Multi-Functional, Self-Healing Polyelectrolyte Gels for Long-Cycle-Life, High-Capacity Sulfur Cathodes in Li-S Batteries; Jihui Yang, University of Washington
- Solid-State Inorganic Nanofiber Network-Polymer Composite Electrolytes for Lithium Batteries; Nianqiang Wu, West Virginia University
- High Conductivity and Flexible Hybrid Solid-State Electrolyte; Eric Wachsman, University of Maryland
- Self-Forming Thin Interphases and Electrodes Enabling 3D Structured High-Energy-Density Batteries; Glenn Amatucci, Rutgers University
- Dual Function Solid-State Battery with Self-Forming, Self-Healing Electrolyte and Separator; Esther Takeuchi, Stony Brook University
- Self-Assembling Rechargeable Lithium Batteries from Alkali and Alkaline-Earth Halides; Yet-Ming Chiang, Massachusetts Institute of Technology
- Engineering Approaches to Dendrite-Free Lithium Anodes; Prashant Kumta, University of Pittsburgh
- Dendrite Growth Morphology Modeling in Liquid and Solid Electrolytes; Yue Qi, Michigan State University
- Understanding and Strategies for Controlled Interfacial Phenomena in Li-Ion Batteries and Beyond; Perla Balbuena, Texas A&M University
- First Principles Modeling and Design of Solid-State Interfaces for the Protection and Use of Li-Metal Anodes; Gerbrand Ceder, University of California – Berkeley
- Electrochemically Responsive Self-Formed Li-ion Conductors for High-Performance Li-Metal Anodes; Donghai Wang, Pennsylvania State University (Penn State)

A few notable achievements for this quarter include:

- LiF was used to stabilize the LLZO solid electrolyte against moisture and CO<sub>2</sub> in air. In a Li-S battery, this solid electrolyte blocked the shuttle reaction, reduced the interface resistance, and improved the Coulombic efficiency. (Task 7.7, John B. Goodenough)
- A method was demonstrated for surface lattice doping to enhance the cycling stability of Ni-rich NMC cathode materials at a high charge cut-off voltage of 4.5 V. (Task 3.3, Ji-Guang Zhang and Jianming Zheng)



- The existence of the reconstruction rock-salt layer on NMC-532 surface was found to improve cell performance by inhibiting impedance growth during cycling. (Task 5.2, Robert Kostecki)
- It was demonstrated that prelithiated Ge and GeO nanoparticles can be incorporated into a silicon electrode and used as a prelithiation agent. (Task 2.2, Yi Cui)

Sincerely,

*Tien Q. Duong*

Tien Q. Duong  
Manager, Advanced Battery Materials Research (BMR) Program  
Energy Storage R&D  
Vehicle Technologies Office  
Energy Efficiency and Renewable Energy  
U.S. Department of Energy

## TASK 1 – ADVANCED ELECTRODE ARCHITECTURES

### Summary and Highlights

Energy density is a critical characterization parameter for batteries for electric vehicles (EVs) as there is only so much room for the battery and the vehicle needs to travel over 200 miles. The U.S. Department of Energy (DOE) targets are 500 Wh/L on a system basis and 750 Wh/L on a cell basis. Not only do the batteries have to have high energy density, they need to do so and still deliver 1000 Wh/L for 30 seconds on the system level. To meet these requirements not only entails finding new, high-energy-density electrochemical couples, but also highly efficient electrode structures that minimize inactive material content, allow for expansion and contraction for several thousand cycles, and allow full access to the active materials by the electrolyte during pulse discharges. In that vein, the DOE Vehicle Technologies Office (VTO) supports two projects in the Advanced Battery Materials Research (BMR) Program under Task 1 – Advanced Electrode Architectures: Task 1.1 – Higher Energy Density via Inactive Components and Processing Conditions, Lawrence Berkeley National Laboratory (LBNL); and Task 1.2 – Pre-Lithiation of Silicon Anode for High-Energy Li-Ion Batteries, Stanford University (Stanford).

The two tasks take different general engineering approaches to improving the energy density. Task 1.1 attempts to increase energy density by making thicker electrodes and reducing the overall amount of inactive components per cell. Task 1.2 attempts to increase the energy density of Li-ion cells by replacing graphitic anodes with high-capacity Si-based active materials and a process for prelithiating the anode to make up for the poor first-cycle irreversible capacity loss. Both attempts insist on establishing an appropriate methodology for introducing the changes.

The problem being addressed with the first approach is that as electrode thickness increases, the drying time can decrease, which allows additional time for segregation of the electrode components. Another problem being addressed is that thick electrodes may still have to be wound around a mandrel in a cylindrical cell configuration. For a thicker electrode, winding leads to more hoop stress on the outer portion of the laminate. Both problems can result in delamination of the laminate from the current collector. Another problem with thicker electrodes is that they tend to not cycle as well as thinner electrodes and thus reach the end-of-life condition sooner, delivering fewer cycles. The source of the cycling problem is still not clear.

The problem being addressed by the second approach is that although silicon offers higher specific capacity for lithium, it experiences a 300% increase in volume during the lithiation process. The change in volume results in freshly exposed surface area to electrolyte during the charging process and in a large amount of lithium ions to be consumed in forming the solid electrolyte interphase (SEI) on the anode. Thus, the full advantage of silicon cannot be realized because excess cathode material is needed to supply the lithium for SEI formation on the anode.

**Highlight.** This quarter, Task 1.2 (Cui's Group) has demonstrated the ability to prelithiate germanium and germanium oxide nanoparticles that can then be incorporated into a silicon electrode as a prelithiation agent.

## Task 1.1 – Higher Energy Density via Inactive Components and Processing Conditions (Vincent Battaglia, Lawrence Berkeley National Laboratory)

**Project Objective.** Thicker electrodes with small levels of inactive components that can still deliver most of their energy at C-rates of C/3 should result in batteries of higher energy density. Higher energy density should translate to more miles per charge or smaller, less expensive batteries. Unfortunately, the limit to making thicker electrodes is not based on power capability but on mechanical capability, that is, the thicker electrodes delaminate from the current collector during calendaring or slicing. The objective of this research is to produce a high-energy-density electrode with typical Li-ion components that does not easily delaminate and still meets the EV power requirements through changes to the components and concomitant changes to the processing conditions.

**Project Impact.** Today's batteries cost too much on a per kWh basis and have too low of an energy density to allow cars to be driven over 300 miles on a single charge. The project's research addresses both problems simultaneously. By developing thicker, higher energy-density electrodes, the fraction of cost relegated to inactive components is reduced and the amount of energy that can be introduced to a small volume can be increased. Macroscopic modeling suggests that this could have as much as a 20% impact on both numbers.

**Out-Year Goals.** In the outgoing years, the project will make changes to the binder molecular weight, conductive additive, and size distribution of the active material and whatever changes are necessitated by electrode processing conditions to increase the energy density while maintaining power capability. Changes in the processing conditions can include the time of mixing, the rate of casting, the temperature of the slurry during casting, drying conditions, and hot calendaring. Chemical modifications may include multiple binder molecular weights and changes in the conductive additive size and shape.

**Collaborations.** This project collaborates with Zaghbi's group (HydroQuebec, HQ) for materials and cell testing; Wheeler's group (Brigham Young University, BYU) for modeling analysis; Liu's group (LBNL) on polymer properties; Arkema for binders; and a commercial cathode material supplier.

### Milestones

1. Fabricate "thick" laminates of NCM and establish the effect of calendaring at different temperatures. (Q1 – Complete)
2. Determine to what extent electrode performance can be improved through the use of an active material of two particle size distributions. (Q2)
3. Determine the degree to which several updates in materials and processing are affecting cyclability. (Q3)
4. *Go/No-Go.* Determine if a binder of a mixture of molecular weights is worth pursuing to achieve thicker electrodes based on ease of processing and level of performance. If no, pursue a path of a single molecular weight binder. (Q4)

## Progress Report

**Milestone 1 (Complete) – Fabricate “thick” laminates of NCM and establish the effect of calendaring at different temperatures.** Electrodes were calendared between 25 and 125°C. The electrode at 100°C showed slightly lower rate performance, but significantly better cycling performance.

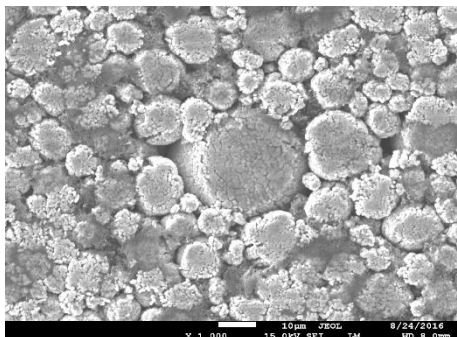


**Figure 1. Laminate calendared at 100°C to 30% porosity. Notice flattened and cracked particles.**

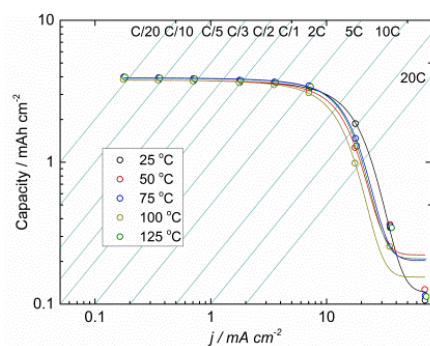


**Figure 2. Rate performance of a laminate calendared at different temperatures.**

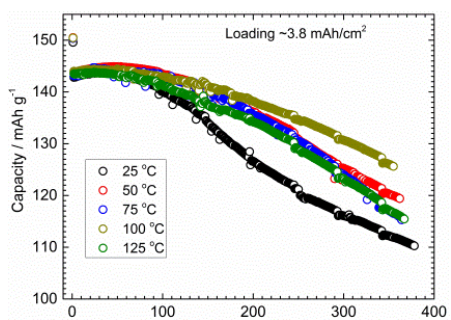


**Figure 3. Cycling performance.**

A single laminate of NCM of approximately 4 mAh/cm<sup>2</sup> was fabricated and allowed to dry by natural convection in the glovebox. Once dry, the calendaring machine was turned on, and the temperature of the rollers was adjusted and allowed to come to equilibrium at several different temperatures (27, 50, 75, 100, and 125 °C). A section of the laminate was calendared to the 30% porosity at each of the different temperatures. A scanning electron microscopy (SEM) image was taken of the compressed electrode. The SEM revealed that for all of the electrodes, the secondary particles of NCM were flattened and, for some particles, cracked. An example is provided in Figure 1, which shows the laminate calendared at 100°C.

Once the electrodes were calendared, they were assembled in coin cells for electrochemical testing. The electrodes were put through a rate performance test and long-term cycling. The rate tests revealed that the laminate calendared at 100°C showed the poorest rate capability at approximately 5 C (Figure 2). The cell calendared at 100°C and a 5 C discharge rate was completely discharged in 3 minutes, instead of 12 minutes like the others.

Once the rate performance test was completed, the cells were put on full charge and discharge cycling tests at C/3. The electrodes calendared at 100°C cycled the best. At 350 cycles, these electrodes only displayed a 12.5% capacity fade. The others were very near to or greater than 20% capacity fade, which is considered end-of-life.

The project continues to gather information regarding processing conditions. Many findings, such as this one, require additional investigation. It is not understood why the rate performance and the cycling performance would be counter to each other. It could be speculated that the particles calendared at 100°C remain fully encapsulated by binder, which promotes cohesion among the particles but also limits the transport of salt to the active material surface. Further investigation is needed.

## Task 1.2 – Prelithiation of Silicon Anode for High-Energy Lithium-Ion Batteries (Yi Cui, Stanford University)

**Project Objective.** Prelithiation of high-capacity electrode materials such as silicon is an important means to enable those materials in high-energy batteries. This study pursues two main directions: (1) developing facile and practical methods to increase first-cycle Coulombic efficiency (CE) of Li-ion batteries, and (2) synthesizing fully lithiated silicon and other lithium compounds for pre-storing lithium.

**Project Impact.** The first-cycle CE of lithium-ion batteries will be increased dramatically via prelithiation. Prelithiation of high-capacity electrode materials will enable those materials in next-generation, high-energy-density batteries. This project's success will make high-energy-density Li-ion batteries for EVs.

**Out-Year Goals.** Compounds containing a large quantity of lithium will be synthesized for pre-storing lithium ions inside batteries. First-cycle CE (1<sup>st</sup> CE) will be improved and optimized (over 95%) by prelithiation with the synthesized Li-rich compounds. The stability of prelithiation reagents in the air conditions and solvents will be improved.

**Collaborations.** The project works with the following collaborators: (1) BMR principal investigators (PIs), (2) Stanford Linear Accelerator Center (SLAC): *in situ* X-ray, Dr. Michael Toney, and (3) Stanford: mechanics, Professor Nix.

### Milestones

1. Synthesize LiF/metal nanocomposite for cathode prelithiation with high capacity and good air stability (> 500 mAh/g). (March 2016 – Complete)
2. Synthesize  $\text{Li}_x\text{Si-Li}_2\text{O}$  composites for anode prelithiation with improved stability in ambient air with 40% relative humidity. (June 2016 – Complete)
3. Synthesize stabilized  $\text{Li}_3\text{N}$  for cathode prelithiation with high capacity of > 1700 mAh/g. (September 2016 – Complete)
4. Synthesize  $\text{Li}_x\text{Ge}$  nanoparticles and  $\text{Li}_x\text{Ge-Li}_2\text{O}$  composites for anode prelithiation with improved air-stability. (January 2017 – In progress)

## Progress Report

Previously, the project demonstrated that metallurgically synthesized  $\text{Li}_x\text{Si}$  nanoparticles (NPs) can serve as a high-capacity prelithiation reagent to effectively increase the 1<sup>st</sup> CE of anode materials. Group IV elements such as germanium have relatively high specific capacities (1640 mAh/g for Ge) and similar volumetric capacities to silicon (2574 mAh/cm<sup>3</sup> for Si; 2275 mAh/cm<sup>3</sup> for Ge), making them also suitable for pre-storing lithium. Ball-milled Ge NPs and  $\text{GeO}_2$  NPs were used as the starting materials to form  $\text{Li}_x\text{Ge}$  alloy and  $\text{Li}_x\text{Ge-Li}_2\text{O}$  composite materials, respectively. SEM was utilized to characterize the morphology of the Ge and  $\text{GeO}_2$  NPs before and after lithiation. After ball milling, the size of Ge NPs is in the range of 100 to 300 nm, while that of  $\text{GeO}_2$  NPs is in the range of 150 to 350 nm, as shown in Figure 4a/d. The sizes of the derived  $\text{Li}_x\text{Ge}$  alloy and  $\text{Li}_x\text{Ge-Li}_2\text{O}$  composite were larger than those of the starting materials because of the volume expansion (Figure 4b/e).

X-ray diffraction (XRD) confirms the crystal-line nature of ball-milled Ge powder (PDF no. 00-004-0545) and a small portion of  $\text{GeO}_2$  (PDF no. 00-036-1463) resulting from the high-energy ball-milling process in air (Figure 4c, upper). XRD confirms the complete transformation of Ge in both Ge powder and the intrinsic oxide  $\text{GeO}_2$  to crystalline  $\text{Li}_{22}\text{Ge}_5$  (PDF no. 01-081-6059) during the thermal alloying process (Figure 4c, lower). The small peaks of  $\text{Li}_2\text{O}$  (PDF no. 00-012-0254) come from the conversion of the small amount of intrinsic oxide  $\text{GeO}_2$ . XRD analysis also shows the complete formation of crystalline  $\text{Li}_{22}\text{Ge}_5$  and  $\text{Li}_2\text{O}$  during the thermal alloying process of  $\text{GeO}_2$  powder and molten lithium. To measure the prelithiation capacities of the  $\text{Li}_x\text{Ge}$  alloy and  $\text{Li}_x\text{Ge-Li}_2\text{O}$  composite, the electrodes were charged to 1.5 V directly at a slow rate of C/20 (1C = 1640 mA/g for Ge and 1126 mA/g for  $\text{GeO}_2$ ). The prelithiation capacities were 1335 mAh/g and 892 mAh/g based on the masses of Ge and  $\text{GeO}_2$  in the anode, respectively (Figure 4f). To test the air stability of  $\text{Li}_x\text{Ge}$ ,  $\text{Li}_x\text{Ge}$  NPs were exposed to ambient air (30% to 40% relative humidity) for 6 h, exhibiting a high extraction capacity of 947 mAh/g (30% capacity loss, Figure 4g). Although the specific capacity is relatively lower,  $\text{Li}_x\text{Ge-Li}_2\text{O}$  NPs exhibit superior ambient-air stability with a higher capacity retention of 85% (15% capacity loss) compared to bare  $\text{Li}_x\text{Ge}$  NPs.

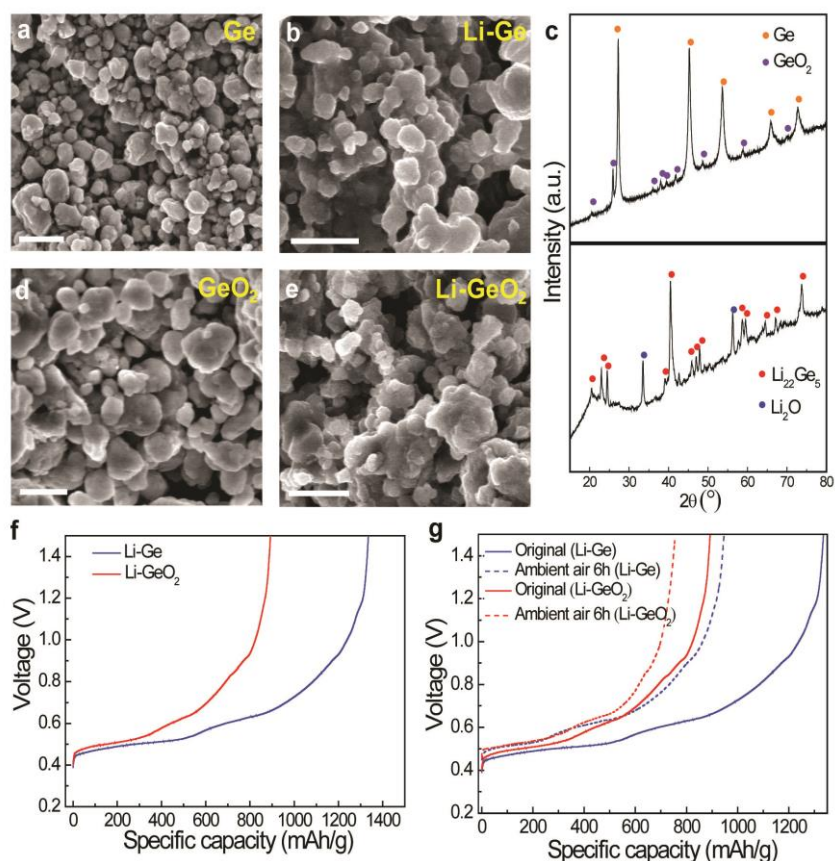


**Figure 4.** (a, b) Scanning electron microscopy (SEM) images of Ge nanoparticles (NPs) before (a) and after (b) thermal lithiation. (c) X-ray diffraction patterns of Ge NPs before (upper) and after (bottom) thermal lithiation. (d, e) SEM images of  $\text{GeO}_2$  NPs before (d) and after (e) thermal lithiation. (f) First-cycle delithiation capacities of lithiated Ge NPs (blue) and lithiated  $\text{GeO}_2$  NPs (red). The capacity is based on the mass of Ge or  $\text{GeO}_2$  in the anode. (g) First-cycle delithiation capacities of lithiated Ge NPs (blue) and lithiated  $\text{GeO}_2$  NPs (red) before (solid) and after (dash) exposure to ambient-air condition (30%~40% RH) for 6 h.

## Patents/Publications/Presentations

### Publication

- Zhao, J. Sun, and A. Pei, K. Yan, G. Zhou, Y. Liu, D. Lin, and Y. Cui.\* “A General Prelithiation Approach for Group IV Elements and Corresponding Oxides.” *JACS*, under review.

## Task 1.3 – Electrode Architecture-Assembly of Battery Materials and Electrodes (Karim Zaghib, HydroQuebec)

**Project Objective.** The project goal is to develop an electrode architecture based on nano-Si materials and design a full cell having high energy density and long cycle life. To achieve the objective, this project investigates the structure of nano-Si materials that provide acceptable volume change to achieve long cycle life, while still maintaining the high-capacity performance of silicon. The project scope includes control of the particle size distribution of nano-Si materials, crystallinity, silicon composition, and surface chemistry of the nano-Si materials. The focus is to develop electrode formulations and electrode architectures based on nano-Si materials, which require optimized nano-Si/C composites and functional binders, as well as a controlled pore distribution in the electrode and the related process conditions to fabricate the electrode.

**Project Impact.** Silicon is a promising alternative anode material with a capacity of ~4200 mAh/g, which is more than a magnitude higher than that of graphite. However, many challenges remain unresolved, inhibiting commercialization of silicon; this is mainly due to the large volume variations of silicon during charge/discharge cycles that result in pulverization of the particle and poor cycling stability. Successful development of highly reversible silicon electrodes with acceptable cost will lead to higher-energy-density and lower-cost batteries that are in high demand, especially for expanding the market penetration for EVs.

**Approach.** The project approach will encompass the following:

- Explore various synthesis methods to produce low-cost, nano-Si materials with controlled purity and particle morphology.
- Develop an appropriate silicon anode architecture that can tolerate volumetric expansion and provide an acceptable cycle life with low capacity fade.
- Identify a binder and electrode composition by investigating parameters that define the electrode structure, such as porosity, loading, and electrode density. The optimized Si-anode will be matched with a high-voltage NMC cathode to fabricate large format Li-ion cells.
- Use *in situ* techniques such as SEM and impedance spectroscopy to monitor the particle and electrode environment changes during cycling.
- Achieve cost reduction by moving from more costly silicon (> \$50/kg) to metallurgical silicon, which is projected to be \$3~\$5/kg.

**Out-Year Goals.** At this stage of the project, a major effort will be allocated to failure mode analysis of nano-Si anodes before and after cycling. Dual-beam (electron + ion) microscopy and TOF-SIM (Time-of-Flight Secondary Ion Mass Spectrometry) techniques will be used to analyze the residual lithium contents in the structure of delithiated nano-Si anodes. This analysis will help to understand the failure mode of the anode and help guide the effort to improve the particle morphology and the electrode architecture.

**Collaborations.** This project collaborates with several BMR PIs: V. Battaglia and G. Liu (LBNL), C. Wong and Jason Zhang (Pacific Northwest National Laboratory, PNNL), and J. Goodenough (University of Texas, UT).

### Milestones

1. Failure mode analysis of the nano-Si/C composite electrode before and after cycling. Improve the structure of the nano-Si/C composite based on the results of failure mode analysis. (March 2017 – In progress)



## Progress Report

Li-ion pouch laminated cells based on NMC//nano-Si/C composite with a capacity of 1.5 Ah were assembled (Figure 5a). The loadings are 2.2 and 10.3 mg/cm<sup>2</sup> for the anode and cathode, respectively. The anode/cathode ratio was 1.15 based on the capacities obtained with the half cells of the cathode and anode materials. The electrochemical performance (formation capacity, rate capability and cycle stability) was evaluated. The capacity of the cell at 0.2C rate revealed a discharge capacity around 1400 mAh between 2.75 V and 4.4 V, which is 95% of the designed cell capacity (Figure 5b).

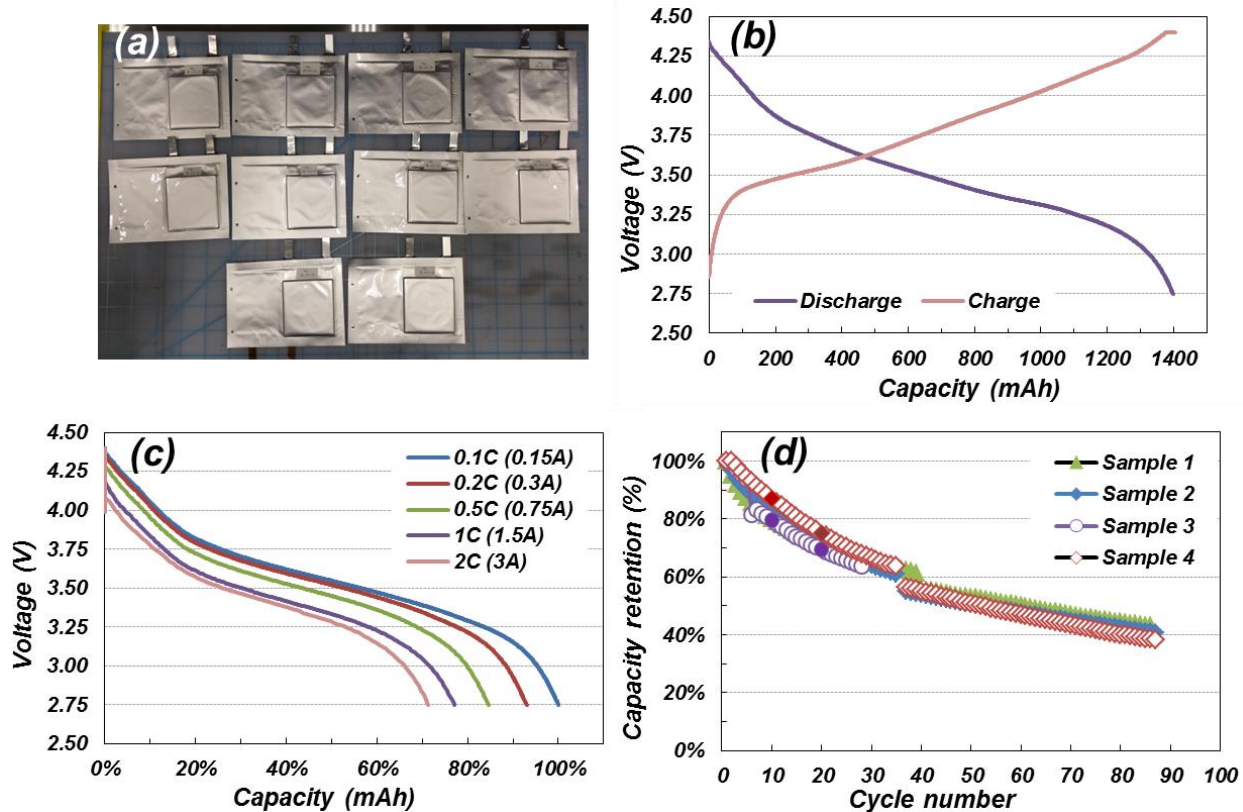


Figure 5. Full cell performance of 1.5 Ah pouch-type cell: (a) assembled cell; (b) voltage profile during charge-discharge between 2.75 V and 4.4 V at 0.2C rate; (c) rate capability with different current; and (d) cycle life at room temperature.

The rate capability of the cells was evaluated with different currents (0.1 to 2C). At 2C, the cell delivered 70% of the capacity obtained at 0.1C (Figure 5c). The voltage profiles showed similar behavior at the different rates, and the cells have low IR drop. However, the cycling stability of these cells shows high capacity fade (Figure 5d). During the 90 cycles, the capacity decreases continuously with cycle number, with a retention of just 40%. This capacity fade is attributed to the instability of the anode material. The loss of contact between silicon anode particles and the mechanical disintegration of the anode film are the main causes of this capacity fade. Post-mortem analysis is planned to improve understanding of the low cycling performance of this Li-ion cell chemistry.

## Task 1.4 – Design and Scalable Assembly of High-Density, Low-Tortuosity Electrodes (Yet-Ming Chiang, Massachusetts Institute of Technology)

**Project Objective.** The project objective is to develop scalable, high-density, low-tortuosity electrode designs and fabrication processes enabling increased cell-level energy density compared to conventional Li-ion technology. It will also characterize and optimize the electronic and ionic transport properties of controlled porosity and tortuosity cathodes as well as densely-sintered reference samples. Success is measured by the area capacity (mAh/cm<sup>2</sup>) that is realized at defined C-rates or current densities.

**Project Impact.** The high cost (\$/kWh) and low energy density of current automotive Li-ion technology is in part due to the need for thin electrodes and associated high inactive materials content. If successful, this project will enable use of electrodes based on known families of cathode and anode actives, but with at least three times the areal capacity (mAh/cm<sup>2</sup>) of current technology while satisfying the duty cycles of vehicle applications. This will be accomplished via new electrode architectures fabricated by scalable methods with higher active materials density and reduced inactive content, and will in turn enable higher-energy-density and lower-cost EV cells and packs.

**Approach.** Two techniques are used to fabricate thick, high-density electrodes with low tortuosity porosity oriented normal to the electrode plane: (1) directional freezing of aqueous suspensions; and (2) magnetic alignment. Characterization includes measurement of single-phase material electronic and ionic transport using blocking and non-blocking electrodes with ac and dc techniques, electrokinetic measurements, and drive-cycle tests of electrodes using appropriate battery scaling factors for EVs.

**Out-Year Goals.** Identify anodes and fabrication approaches that enable full cells in which both electrodes have high area capacity under EV operating conditions. Anode approach will include identifying compounds amenable to same fabrication approach as cathode, or use of very high capacity anodes such as stabilized lithium or Si-alloys that in conventional form can capacity-match the cathodes. Use data from best-performing electrochemical couple in techno-economic modeling of EV cell and pack performance parameters.

**Collaborations.** Within BMR, this project collaborates with Antoni P. Tomsia (LBNL) in fabrication of low-tortuosity, high-density electrodes by directional freeze-casting, and with Gao Liu (LBNL) in evaluating silicon anodes. Externally, the project collaborates with Randall Erb (Northeastern University) on magnetic alignment fabrication methods for low-tortuosity electrodes.

### Milestones

1. *Go/No-Go:* Fabricate and test half-cells and full Li-ion cell in which both cathode and anode are prepared by magnetic alignment, and in which at least one electrode is prepared by non-sintering process. Criteria: Measured area capacity of a half-cell is at least 10 mAh/cm<sup>2</sup> and of a full cell is at least 8 mAh/cm<sup>2</sup>. (December 2016 – Complete)

## Progress Report

**Go/No-Go Milestone.** Fabricate and test half-cells and full Li-ion cell in which both cathode and anode are prepared by magnetic alignment, and in which at least one electrode is prepared by non-sintering process. Measured area capacity of a half-cell is at least 10 mAh/cm<sup>2</sup> and of a full cell is at least 8 mAh/cm<sup>2</sup>.

This quarter, results are reported for half-cells containing LiCoO<sub>2</sub> (Umicore) cathodes and MCMB 6-28 (Osaka Gas) anodes, respectively, that are prepared by non-sintering magnetic alignment process. Results of full Li-ion cells consisting of LiCoO<sub>2</sub> cathode and MCMB anode are also reported.

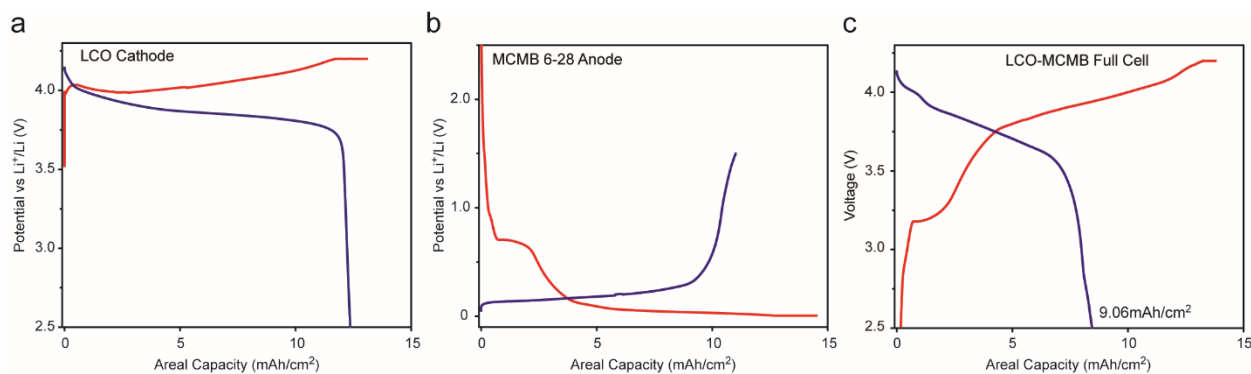


**Figure 6. Electrochemical test results of half-cells and full cells that contain electrodes prepared by non-sintering magnetic alignment process. (a) Voltage versus areal capacity plot of a LCO cathode. (b) Voltage versus areal capacity plot of a MCMB graphite anode. (c) Charge-discharge voltage profile of a LCO-MCMB full cell.**

Figure 6a shows the first-cycle charge-discharge voltage versus areal capacity profile of a low-tortuosity LiCoO<sub>2</sub> cathode (430 μm in thickness, LCO:carbon black:binder = 95:2.5:2.5). This electrode was first charged at 1/15 C to 4.2 V and then held at 4.2 V until the current dropped to 1/40 C. Then the LCO electrode was discharged at 1/15 C to a low cut-off voltage of 2.5 V, which delivered 12.58 mAh/cm<sup>2</sup> areal capacity, 96.4% of its theoretical areal capacity. Figure 6b shows the first-cycle lithiation-delithiation voltage versus capacity profile of the low-tortuosity MCMB anode (MCMB:carbon black:binder = 96:2:2). This electrode was lithiated at C/20 to 10 mV and then delithiated to 1.5 V, which delivered 11.01 mAh/cm<sup>2</sup> areal capacity.

Figure 6c shows the first charge-discharge voltage profile of a LCO-MCMB full cell tested at C/20. Both electrodes were prepared by the emulsion-based magnetic alignment approach. The LCO cathode is 429 μm in thickness and has a theoretical areal capacity of 13.3 mAh/cm<sup>2</sup>. The MCMB anode is 419 μm in thickness and has a slightly higher theoretical areal capacity of 16.4 mAh/cm<sup>2</sup>, so that the AC ratio is ~1.23:1. Upon charge to 4.2 V (CC-CV charge), the LCO-MCMB full cell reaches a capacity of 145 mAh/g (calculated based on the weight of the LCO cathode). However, during discharge the full cell only delivers a capacity of 95.1 mAh/g, ~66% of the charge capacity. Based on the result from the MCMB-Li half-cell test (Figure 6b), the first-cycle capacity loss of the full cell should mostly be attributed to the loss at the MCMB anode, which clearly requires further improvement. Nevertheless, the LCO-MCMB full cell delivers an areal capacity of **9.06 mAh/cm<sup>2</sup>**. The results above meet this quarter's *Go/No Go* milestone.

## Task 2 – Silicon Anode Research

### Summary and Highlights

Most Li-ion batteries used in state-of-the-art EVs contain graphite as their anode material. Limited capacity of graphite ( $\text{LiC}_6$ , 372 mAh/g) is one barrier that prevents the long-range operation of EVs required by the EV Everywhere Grand Challenge proposed by the DOE Office of Energy Efficiency & Renewable Energy (EERE). In this regard, silicon is one of the most promising candidates as an alternative anode for Li-ion battery applications. Silicon is environmentally benign and ubiquitous. The theoretical specific capacity of silicon is 4212 mAh/g ( $\text{Li}_{21}\text{Si}_5$ ), which is 10 times greater than the specific capacity of graphite. However, the high specific capacity of silicon is associated with large volume changes (more than 300 percent) when alloyed with lithium. These extreme volume changes can cause severe cracking and disintegration of the electrode and can lead to significant capacity loss.

Significant scientific research has been conducted to circumvent the deterioration of Si-based anode materials during cycling. Various strategies, such as reduction of particle size, generation of active/inactive composites, fabrication of Si-based thin films, use of alternative binders, and the synthesis of one-dimensional silicon nanostructures have been implemented by several research groups. Fundamental mechanistic research also has been performed to better understand the electrochemical lithiation and delithiation processes during cycling in terms of crystal structure, phase transitions, morphological changes, and reaction kinetics. Although significant progress has been made on developing Si-based anodes, many obstacles still prevent their practical application. Long-term cycling stability remains the foremost challenge for Si-based anode, especially for the high loading electrode ( $> 3\text{mAh/cm}^2$ ) required for many practical applications. The cyclability of full cells using Si-based anodes is also complicated by multiple factors, such as diffusion-induced stress and fracture, loss of electrical contact among silicon particles and between silicon and current collector, and the breakdown of SEI layers during volume expansion/contraction processes. The design and engineering of a full cell with a Si-based anode still needs to be optimized. Critical research remaining in this area includes, but is not limited to, the following:

- Low-cost manufacturing processes must be found to produce nano-structured silicon with the desired properties.
- The effects of SEI formation and stability on the cyclability of Si-based anodes need to be further investigated. Electrolytes and additives that can produce a stable SEI layer need to be developed.
- A better binder and a conductive matrix need to be developed. They should provide flexible but stable electrical contacts among silicon particles and between particles and the current collector under repeated volume changes during charge/discharge processes.
- The performances of full cells using silicon-based anode need to be investigated and optimized.

The main goal of this project is to have a fundamental understanding on the failure mechanism on Si-based anode and improve its long-term stability, especially for thick electrode operated at full-cell conditions. Success of this project will enable Li-ion batteries with a specific energy of  $>350\text{ Wh/kg}$  (in cell level), 1000 deep-discharge cycles, 15-year calendar life, and less than 20% capacity fade over a 10-year period to meet the goal of the EV Everywhere Grand Challenge.

**Highlight.** The PNNL group developed a low-temperature thermite reaction ( $\sim 300^\circ\text{C}$ ) method to synthesis porous silicon anode with stable cyclability.

## Task 2.1 –High-Capacity and Long Cycle Life Silicon Carbon Composite Materials and Electrodes (Gao Liu, Lawrence Berkeley National Laboratory)

**Project Objective.** This project will synthesize Si/C anode composite materials at 1,000 mAh/g capacity at a cost less than \$10/kg and fabricate a long-cycle-life electrode similar to a graphite electrode for high-energy-density Li-ion batteries.

**Project Impact.** Low energy density and limited lifetime are two major drawbacks of the automobile Li-ion batteries for EV and plug-in hybrid electric vehicle (PHEV) applications. The project will develop high-capacity and long-life Si/C composite anodes to prolong battery cycling and storage lifetime, and to provide an in-depth understanding of silicon electrode design strategies to stabilize silicon material volume change and to prevent surface side reactions. This research effort will generate new intellectual properties based on the fundamental discovery of novel materials and new synthesis processes, and will bridge the R&D gaps between the fundamental research and the applied materials discovery, to pave the way for the successful commercialization of silicon materials.

**Approach.** This work combines novel materials design and innovative synthesis process to synthesize mechanically robust and dimensionally stable Si/C composite materials. In addition, it will use low-cost Si/C precursor materials and a scalable process to generate low-cost Si/C product.

**Out-Year Goals.** The work progresses toward study of the physical and chemical properties and of electrochemical properties of the low-cost precursor materials. Novel synthesis strategy will be developed and used to fabricate materials to tailor the morphology, structure, composite component, and electrochemical properties of the Si/C composite materials. The morphologic and structural features and electrochemical properties will be characterized for the as-prepared Si/C composited with functional binder during electrochemical testing. The goal is to achieve a high-capacity, long-life Li-ion battery using this Si/C composite anode.

**Collaborations.** This project is a single investigator project. However, the proposed work requires extensive collaboration with DOE user facilities at national laboratories and industries. These include the National Center for Electron Microscopy (NCEM) and the Advance Light Sources (ALS) program at LBNL, *in situ* electrochemical transmission electron microscopy (TEM) facilities at the Environmental Molecular Sciences Laboratory (EMSL), the national user facility at PNNL, IREQ General Motors (GM) R&D Center, and LBNL BMR laboratories. The project will also involve collaboration with BMR participants at LBNL, including Dr. Marca Doeff's group and Dr. Vince Battaglia's group.

### Milestones

1. Set up the silicon materials and carbon precursors library, and finish characterizing the starting materials. (December 2016 – Complete)
2. Conduct preliminary tests to generate Si/C composite particles with the spray methods. (March 2017 – In progress)
3. Electron microscopy image analyses of the Si/C samples and development of functional binders based on Si/C composite structures. (June 2017)
4. Electrochemical analysis to demonstrate  $> 1000$  mAh/g and  $> 3$  mAh/cm<sup>2</sup> of the Si/C composite electrodes. (September 2017)

## Progress Report

The Si/C materials library has been established, including a wide size-range of silicon particles and various types of organics as carbon precursors. Figure 7 is an example of the silicon materials library. The initial materials library will be enriched during this project as new silicon materials and organic precursors become available on the market and in the literature. Nano- to micro-scale silicon powders of diameters from 20 nm to 10  $\mu\text{m}$  have been acquired for this project. The silicon materials also have different levels of purity, ranging from metallurgic grade to high pure samples. The silicon samples come with different morphologies, as shown in Figure 8 (increasing particle size, 8a-d). However, samples a/b are fused nano-particles, while samples c/d are separated micron-size particles. The electrochemical properties of these silicon materials are being evaluated. The binders being considered for this work include LBNL's functional conductive polymer binders, industrial binders such as CMC, PVDF, and another commonly used binder, PAA. Various organics and polymers were selected as the carbon precursors. Figure 9 shows high-temperature decomposition of selected organics under thermogravimetric analysis (TGA) evaluation.

Chemical Name	type	Particle size	Purity	Vendor
Silicon Nanopowder	Nano Powder	30-50 nm	98%	Nanostructured & Amorphous Materials Inc.
Silicon Nanopowder	Nano Powder	50-70 nm	98%	Nanostructured & Amorphous Materials Inc.
Silicon Nanopowder	Nano-Micro Powder	70-130 nm	99%	Nanostructured & Amorphous Materials Inc.
Silicon (Si) Powder	Micro Powder	1 $\mu\text{m}$	99%	US Research Materials Inc.
Silicon (Si) Powder	Micro Powder	1 $\mu\text{m}$	99.99%	US Research Materials Inc.

Figure 7. Sample silicon materials library.

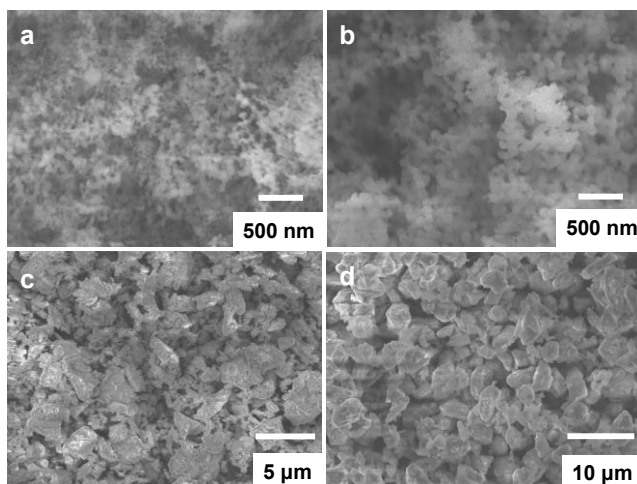


Figure 8. Silicon particles of different average diameter sizes: (a) 30-50 nm, (b) 50-70 nm, (c) 70-130 nm, and (d) 1 $\mu\text{m}$ .

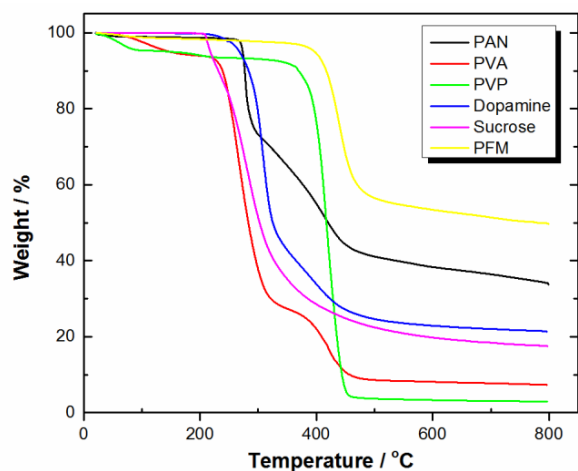


Figure 9. Thermogravimetric analysis of a few carbon precursor candidates, at a heating rate of 5 $^{\circ}\text{C}/\text{min}$  from room temperature to 800 $^{\circ}\text{C}$ , under nitrogen atmosphere.

## Task 2.2 – Development of Silicon-Based High-Capacity Anodes (Ji-Guang Zhang and Jun Liu, Pacific Northwest National Laboratory; Prashant Kumta, University of Pittsburgh)

**Project Objective.** The project objective is to develop high-capacity and low-cost Si-based anodes with good cycle stability and rate capability to replace graphite in Li-ion batteries. In one approach, the low-cost Si-graphite-carbon (SGC) composite will be developed to improve long-term cycling performance while maintaining a reasonably high capacity. Si-based secondary particles with a nano-Si content of ~10 to 15 wt% will be embedded in the matrix of active graphite and inactive conductive carbon materials. Controlled void space will be pre-created to accommodate the volume change of silicon. A layer of highly graphitized carbon coating at the outside will be developed to minimize the contact between silicon and electrolyte, and hence minimize the electrolyte decomposition. New electrolyte additives will be investigated to improve the stability of the SEI layer. In another approach, nanoscale silicon and Li-ion conducting lithium oxide composites will be prepared by *in situ* chemical reduction methods. The stability of Si-based anode will be improved by generating the desired nanocomposites containing nanostructured amorphous or nanocrystalline silicon as well as amorphous or crystalline lithium oxide (Si+Li<sub>2</sub>O) by the direct chemical reduction of a mixture and variety of silicon sub oxides (SiO and SiO<sub>x</sub>) and/or dioxides. Different synthesis approaches comprising direct chemical reduction using solution, solid-state, and liquid-vapor phase methods will be utilized to generate the Si+Li<sub>2</sub>O nanocomposites. The electrode structures will be modified to enable high utilization of thick electrode.

**Project Impact.** Si-based anodes have much larger specific capacities compared with conventional graphite anodes. However, the cyclability of Si-based anodes is limited because of the large volume expansion characteristic of these anodes. This work will develop a low-cost approach to extend the cycle life of high-capacity, Si-based anodes. The success of this work will further increase the energy density of Li-ion batteries and accelerate market acceptance of EVs, especially for the PHEVs required by the EV Everywhere Grand Challenge.

**Out-Year Goals.** The main goal of the proposed work is to enable Li-ion batteries with a specific energy of > 200 Wh/kg (in cell level for PHEVs), 5000 deep-discharge cycles, 15-year calendar life, improved abuse tolerance, and less than 20% capacity fade over a 10-year period.

**Collaborations.** This project collaborates with Xingcheng Xiao (GM): *In situ* measurement of thickness swelling silicon anode.

### Milestones

1. Synthesize micron-sized silicon with the desired porosity and *in situ* grown graphene coating. (Q1 – In progress)
2. Synthesize low-cost Si-based nanocomposite anode materials using high-energy mechanical milling (HEMM) and other economical template derived methods. (Q2 – In progress)
3. Identify new electrolyte additive to improve the stable operation of Si-based anode. (Q3)
4. Fabricate and characterize Si-based anode with desired electrode capacity (~3 mAh/cm<sup>2</sup>). (Q4)

## Progress Report

This quarter, the swelling of the porous-Si-graphite composite electrode was investigated. First, through collaboration with the GM team, electrode swelling was measured by *in situ* electrochemical dilatometer. The electrode loading is  $\sim 3 \text{ mAh cm}^{-2}$  with porous Si/C and graphite in 1:2 ratio. Figure 10 shows the charge-discharge profiles (black curves) and the electrode thickness change (red curves). Initial electrode swelling is  $\sim 20\%$  after full lithiation and  $\sim 7\%$  after delithiation. The *ex situ* SEM study further corroborates that the composite electrodes have limited swelling upon cycling. The pristine electrode before cycling has a thickness of  $\sim 72 \mu\text{m}$ . The cycled electrode at lithiated state is  $\sim 90 \mu\text{m}$  thickness, while  $\sim 80 \mu\text{m}$  at delithiated state. The electrode swelling at delithiated and lithiated state is  $\sim 11\%$  and  $25\%$ , respectively. Calendering effect to the electrode performance was also investigated. The electrode can be calendered to a density of  $\sim 1.5 \text{ g/cc}$ . The porous silicon structure can be maintained after calendering. Hence, electrochemical performance was not affected significantly by calendering. The electrode after calendering still shows good cycling stability, with capacity retention of  $\sim 90\%$  after 200 cycles. In another effect, a low-temperature thermite reaction was developed. The reaction initiating temperature can be as low as  $300^\circ\text{C}$  by adding selected salt into the reaction system. Preliminary results (Figure 11) show that the porous silicon obtained can deliver a high specific capacity of  $\sim 2100 \text{ mAh/g}$  and good cycling stability of  $\sim 85\%$  retention over 100 cycles.

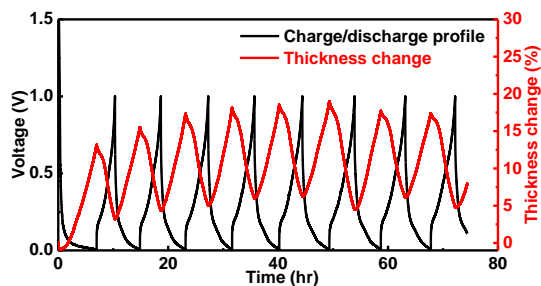


Figure 10. *In situ* measurement of the electrode swelling upon discharge-discharge process.

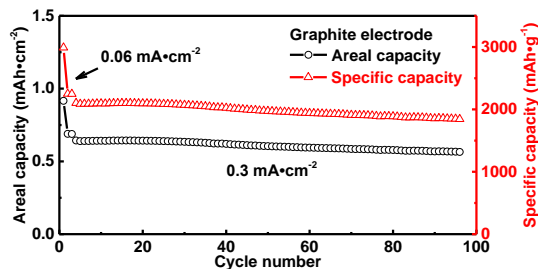


Figure 11. Cycling performance of porous silicon obtained by the low-temperature thermite reaction.

Electrochemically active silicon was obtained by the reduction of silicon precursor ( $\text{SiX}$ ) utilizing inorganic reductants (IR) by a low-temperature, solid-state reduction (LTSR) approach. Commercially obtained ( $\sim 40 \mu\text{m}$ ) IR was ball milled for 2 h in argon atmosphere to reduce particle size to below  $2 \mu\text{m}$ . A homogenous mixture of HEMM derived IR ( $\sim 2 \mu\text{m}$ ) and supporting precursor serving as a flux along with stoichiometric amount of  $\text{SiX}$  was sealed in stainless steel autoclave in argon atmosphere. The sealed mixture was heated and maintained at  $200^\circ\text{C}$  for 6 h to complete the reaction. The XRD pattern of the heat-treated mixture indicates formation of silicon, but no peaks corresponding to IR after reduction of  $\text{SiX}$  at  $200^\circ\text{C}$  for 6 h. The undesired intermediate phases were dissolved in  $1\text{M HCl}$  to obtain silicon. The high reaction conversion efficiency ( $\sim 90 - 95\%$ ) of this approach shows its potential commercial viability.

The LTSR-derived silicon was then embedded in carbon nanofibers (CNF) using a solution coating technique followed by thermally induced carbonization at  $700^\circ\text{C}$  for 1 h and then followed by testing as an active anode material for Li-ion application. At a current rate of  $\sim 50 \text{ mA/g}$ , the Si/CNF material showed a first-cycle discharge and charge capacity of  $\sim 2870 \text{ mAh/g}$  and  $\sim 2067 \text{ mAh/g}$ , respectively, with first-cycle irreversible loss of  $\sim 25 - 30\%$ . During initial cycles of the long-term cycle test (Figure 12), Si/CNF show a capacity of  $\sim 2161 \text{ mAh/g}$  and  $\sim 1210 \text{ mAh/g}$  at current rates of  $0.3 \text{ A/g}$  and  $1 \text{ A/g}$ , respectively. More efforts are in progress to further improve stability of this promising Si-based anode material.

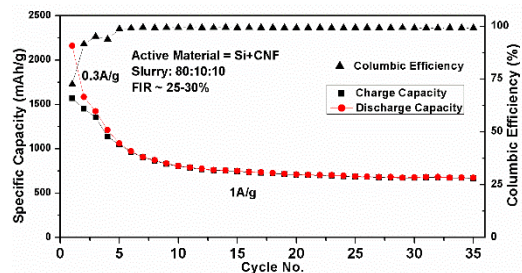


Figure 12. Specific discharge capacity versus cycle numbers for the low-temperature, solid-state reduction (LTSR) approach derived silicon/carbon-nanofiber nanocomposite. The current rate for first three cycles is  $300 \text{ mA/g}$  and for the remaining cycles is  $1 \text{ A/g}$ .



## Patents/Publications/Presentations

### Publications

- Gattu, Bharat, and Rigved Epur, Prashanth H. Jampani, Ramalinga Kuruba, Moni K. Datta, and Prashant N. Kumta. “Silicon-Carbon Core-Shell (C@Si@C) Hollow Nanotubular Configuration – High Performance Lithium-Ion Anodes.” *Journal of Physical Chemistry - C*, 2017, under review.
- Gattu, Bharat, and Prashanth H. Jampani, Moni K. Datta, and Prashant N. Kumta. “Water-Soluble Template Derived Nanoscale Silicon Nano-Flakes and Nano-Rods Morphologies: Stable Architectures for Lithium Ion Anodes.” *Nanoresearch*, 2017, under review.

## TASK 3 – HIGH-ENERGY-DENSITY CATHODES FOR ADVANCED LITHIUM-ION BATTERIES

### Summary and Highlights

Development of high-energy-density, low-cost, thermally stable, and environmentally safe electrode materials is a key enabler for advanced batteries for transportation. High energy density is synonymous with reducing cost per unit weight or volume. One major technical barrier toward developing high-energy-density Li-ion batteries is the lack of robust, high-capacity cathodes. As an example, the most commonly used anode material for Li-ion batteries is graphitic carbon, which has a specific capacity of 372 mAh/g, while even the most advanced cathodes such as NMC or NCA have a maximum capacity of ~180 mAh/g. Thus, there is an immediate need to develop high-capacity (and high-voltage) cathodes that have stable reversible capacities of > 250 mAh/g. High volumetric energy density is also critical for transportation application. Alternative high-capacity cathode chemistries such as those based on conversion compounds, lithium-sulfur, and metal-air chemistries still have fundamental issues that need to be addressed. Successful demonstration of practical high-energy cathodes will enable high-energy cells that meet or exceed the DOE cell level targets of 400 Wh/kg and 600 Wh/L with a system level cost target of \$125/kWh.

During the last decade, many high-voltage cathode chemistries were developed under the BMR (previously BATT) program including Li-rich NMC and Ni-Mn spinels. Current efforts are directed toward new synthesis methods and modifications for high capacity Ni-rich NMC to improve their structural and oxidative stability at higher voltage (Zhang, PNNL; Doeff, LBNL; Wang, Brookhaven National Laboratory, BNL). Thackeray and Croy's effort at Argonne National Laboratory (ANL) is focused on synthesis of composite layered-layered spinel (LLS) and layered spinel (LS) high-voltage cathodes including Co- and Ni-based spinel phases. Nanda's effort at Oak Ridge National Laboratory (ORNL) is targeted toward synthesis and stabilization of multi-lithium cathode oxides based on Ni-Cu and other high-voltage compositions to address the issue of oxygen evolution. Whittingham's effort at State University of New York (SUNY) – Binghamton is directed at high volumetric energy density Sn/Li<sub>x</sub>VOPO<sub>4</sub> full cells and performance optimization.

**Highlights.** The highlights for this quarter are as follows:

- **Task 3.1.** Developed a sol-gel synthesis method for carbon-coated, Ni-rich Li<sub>2</sub>Ni<sub>x</sub>Cu<sub>1-x</sub>O<sub>2</sub> cathodes.
- **Task 3.2.** Developed methods to prelithiate SnyFe anodes and chemically lithiate LiVOPO<sub>4</sub>.
- **Task 3.3.** Demonstrated a method for surface lattice doping to enhance the cycling stability of Ni-rich NMC cathode materials at a high charge cut-off voltage of 4.5 V.
- **Task 3.4.** Studied *in situ* phase changes using synchrotron XRD for Ni- and Co-based TM oxide cathodes prepared with hydroxide precursors under varied reaction conditions.
- **Task 3.5.** Surface treatment of Li<sub>3</sub>PO<sub>4</sub>, Li<sub>2.8</sub>Ni<sub>0.1□</sub><sub>0.1</sub>PO<sub>4</sub>, and Sn<sub>3</sub>(PO<sub>4</sub>)<sub>2</sub> on LLS cathode, Li<sub>1.18-δ</sub>Mn<sub>0.54</sub>Co<sub>0.18</sub>Ni<sub>0.28</sub>O<sub>2</sub> improved capacity retention and rate performance compared to the untreated cathode.
- **Task 3.6.** Studied the chemical heterogeneity and state of charge (SOC) variation of pristine and chemically delithiated Li<sub>1</sub>Ni<sub>0.6</sub>Mn<sub>0.2</sub>Co<sub>0.2</sub>O<sub>2</sub> particles.
- **Task 3.7.** Developed a new sol-gel synthesis method for Al-substitution in LiCoO<sub>3</sub> at low temperature.
- **Task 3.8.** Optimized synthesis and processing conditions for Li<sub>1.2</sub>Mn<sub>0.6</sub>Ni<sub>0.2</sub>O<sub>2</sub> cathodes and used this as guide for other Ni-rich systems.

## Task 3.1 – Studies on High-Capacity Cathodes for Advanced Lithium-Ion Systems (Jagjit Nanda, Oak Ridge National Laboratory)

**Project Objective.** The project goal is to develop high-energy-density Li-ion battery electrodes for EV and PHEV applications that meet and/or exceed the DOE energy-density and life-cycle targets based on the USDRIVE/USABC roadmap. Specifically, this project aims to mitigate technical barriers associated with high-voltage (and high-capacity) cathode compositions. These include Li-rich, transition metal (TM) based oxides and multi-lithium compositions such as  $\text{Li}_2\text{M}_x^{\text{I}}\text{M}_{1-x}^{\text{II}}\text{O}_2$  and  $\text{Li}_2\text{M}_x^{\text{I}}\text{M}_{1-x}^{\text{II}}\text{O}_3$  and where  $\text{M}^{\text{I}}$  and  $\text{M}^{\text{II}}$  are TMs that may or may not include manganese or cobalt. Major emphasis is placed on developing new material modifications and synthetic approaches for stabilizing high-voltage cathodes to enable reversible capacities in the range of 250 mAh/g at an average nominal voltage  $> 3.7$  V versus Li/Li<sup>+</sup>. Major technical barriers to be addressed include the following: (1) preventing structural transitions during repeated electrochemical cycling, (2) improving oxidative stability at higher redox potential by addressing interfacial stability, and (3) reducing voltage hysteresis by improving kinetics and transport at the materials level. The cathode synthesis and optimization will utilize various advanced characterization and diagnostic methods at the electrode and/or cell level for studying cell and/or electrode degradation under abuse conditions. The techniques include electrochemical impedance spectroscopy (EIS), micro-Raman spectroscopy, aberration corrected electron microscopy combined with electron energy loss spectroscopy (EELS), X-ray photoelectron spectroscopy (XPS), inductively coupled plasma – atomic emissions spectroscopy (ICP-AES), X-ray absorption near edge spectroscopy (XANES), and X-ray and neutron diffraction.

**Project Impact.** The project has both short-term and long-term deliverables directed towards VTO Energy Storage 2015 and 2022 goals. Specifically, it involves work on advanced electrode couples that have cell-level energy density targets exceeding 400 Wh/kg and 700 Wh/l for 5000 cycles. Increasing the energy density per unit mass or volume ultimately reduces the cost of battery packs consistent with the DOE 2022 EV Everywhere Grand Challenge goal of \$125/kWh.

**Out-Year Goals.** The goal is to develop new cathode materials that have high capacity, use low-cost materials, and meet the DOE road map in terms of safety and cycle life. Over the last few years, the PI has worked on improving the cycle life and performance of high-capacity, high-voltage cathodes by utilizing new synthesis and interfacial approaches such as surface modification. The cathode chemistries include lithium-manganese-rich NMC and multi-lithium TM oxides such as nickel-copper and manganese. In coming years, the PI plans to improve the anionic (oxidative) stability of cathode compositions and develop new synthesis approaches to create disorder cathodes that would avoid structural transformation and improve electrochemical stability.

**Collaborations.** This project collaborates with Johanna Weker, Stanford Synchrotron Radiation Lightsource (SSRL), SLAC: X-ray imaging and XANES; Pengfei and Chongmin Wang, PNNL: Electron Microscopy; Feng Wang, BNL: X-ray synchrotron spectroscopy and microscopy; and Jason Croy, ANL.

### Milestones

1. Synthesize Ni-rich  $\text{Li}_2\text{Cu}_x\text{Ni}_{1-x}\text{O}_2$  cathodes with  $x = 0.25$  and  $0.4$ , and evaluate their high-voltage capacity and oxidative stability [ $> 225$  mAh/g, 25 cycles]. (December 2016 – In progress, 50%)
2. Complete *in situ* and *ex situ* X-ray, neutron, and spectroscopic studies of Ni-rich  $\text{Li}_2\text{Cu}_x\text{Ni}_{1-x}\text{O}_2$  and related high-voltage cathode compositions. (March 2017 – In progress)
3. Synthesize one particular class and composition of disordered cathodes- $\text{Li}_2\text{MoO}_3$  and Cr-substituted  $\text{Li}_2\text{MoO}_3$ . (June 2017)
4. Complete structural and electrochemical performance analysis of disordered cathodes- $\text{Li}_2\text{MoO}_3$  and Cr-substituted  $\text{Li}_2\text{MoO}_3$ . (September 2017)

## Progress Report

Last year the project successfully synthesized  $\text{Li}_2\text{CuO}_2$  and  $\text{Li}_2\text{Cu}_{0.5}\text{Ni}_{0.5}\text{O}_2$  compositions and studied their capacity retention, oxidative stability, and structural transformation. Substituting 50% nickel at Cu sites improved the redox voltage and stability. This quarter, the project focused on stabilizing Ni-rich  $\text{Li}_2\text{Cu}_x\text{Ni}_{1-x}\text{O}_2$  with a Ni content of around 60%. This was necessary before trying to achieve a higher Ni content of around 75%. Additionally, the project aimed to improve the electrochemical kinetics by using adipic acid (AA) as a chelating agent that leads to an amorphous carbon coating and reduces the primary particle size.

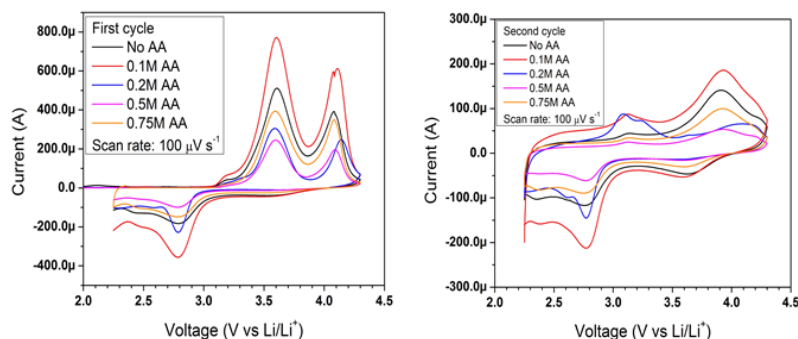


**Figure 13. Cyclic voltammetry during first and second charge-discharge cycle for  $\text{Li}_2\text{Cu}_{0.4}\text{Ni}_{0.6}\text{O}_2$  synthesized using sol-gel method using a chelating agent adipic acid.**

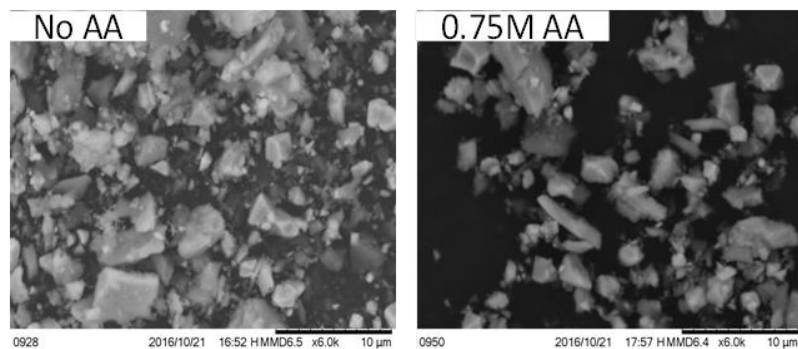


**Figure 14. Scanning electron microscopy micrograph of  $\text{Li}_2\text{Cu}_{0.4}\text{Ni}_{0.6}\text{O}_2$  cathode particles without (left) adipic acid (AA) and with (right) 0.75 M AA.**

Energy dispersive spectroscopy (EDS) analysis (not shown here) confirms the presence of carbon, which results due to thermal decomposition of AA. Figure 14 shows typical SEM micrographs of  $\text{Li}_2\text{Cu}_{0.4}\text{Ni}_{0.6}\text{O}_2$  powders synthesized with no AA and with 0.75 M AA. The 0.75 M AA samples have a smaller average particle size compared to those prepared without chelating agent.

Preliminary electrochemical test data so far show lower capacity for  $\text{Li}_2\text{Cu}_{0.4}\text{Ni}_{0.6}\text{O}_2$  powders compared to  $\text{Li}_2\text{Cu}_{0.5}\text{Ni}_{0.5}\text{O}_2$ , but the capacity increased with increasing AA molar ratio to about  $\sim 150$  mAh/g for the 0.75 M AA composition. The project is optimizing the synthesis conditions with higher AA content that would further improve electrochemical performance.

The  $\text{Li}_2\text{Cu}_{0.4}\text{Ni}_{0.6}\text{O}_2$  powders were synthesized through a sol-gel route using acetate precursors of nickel and copper and using AA as a chelating agent. The powders were reacted initially at  $400^\circ\text{C}$  for 6 h and then at  $800^\circ\text{C}$  for 24 h to obtain the final phase. Initial XRD results showed  $\text{Li}_2\text{CO}_3$  as an impurity phase.

Figure 13 shows cyclic voltammograms (CV) of  $\text{Li}_2\text{Cu}_{0.4}\text{Ni}_{0.6}\text{O}_2$  synthesized with molar ratios of AA ranging from 0 to 0.75 M relative to the overall metal-ion content. During the first charge cycle, as reported earlier, the material undergoes an irreversible structural transition from orthorhombic to trigonal phase accompanied by oxygen activity or loss. The second-cycle CV represents the signature of  $\text{Li}_2\text{Cu-NiO}_2$  redox activity with primarily two broad oxidation peaks at 3.9 and 3 V. The corresponding reduction peaks are shifted by 300 mV toward lower voltage, implying significant kinetic

## Patents/Publications/Presentations

### Publications

- Zhou, H., and K. Ann, S. Allu, S. Pannala, J. Li, H. Z. Bilheux, S. K. Martha, and J. Nanda. “Probing Multiscale Transport and Inhomogeneity in a Lithium-Ion Pouch Cell Using *In Situ* Neutron Methods.” *ACS Energy Letters* 1 (2016): 981-86.
- Nanda, J., and Rose Ruther. “High Capacity Multi-Lithium Cathodes for Advance Lithium-Ion.” U.S. Drive Highlights – Energy Storage, DOE (2016).

### Presentation

- Eleventh International Symposium on Advances in Electrochemical Science and Technology (ISAEST-11), Chennai, India (December 8-10, 2016): “Electrochemical Energy Storage Materials: From Transportation to Grid Storage”; Jagjit Nanda.

## Task 3.2 – High-Energy-Density Lithium Battery (Stanley Whittingham, SUNY Binghamton)

**Project Objective.** The project objective is to develop the anode and cathode materials for high-energy-density cells for use in PHEVs and EVs that offer substantially enhanced performance over current batteries used in PHEVs and with reduced cost. Specifically, the primary objectives are to:

- Increase the volumetric capacity of the anode by a factor of 1.5 over today’s carbons
  - Using a SnFeC composite conversion reaction anode.
- Increase the capacity of the cathode
  - Using a high-capacity conversion reaction cathode, CuF<sub>2</sub>, and/or
  - Using a high-capacity 2 lithium intercalation reaction cathode, VOPO<sub>4</sub>.
- Enable cells with an energy density exceeding 1 kWh/liter.

**Project Impact.** The volumetric energy density of today’s Li-ion batteries is limited primarily by the low volumetric capacity of the carbon anode. If the volume of the anode could be cut in half, and the capacity of the cathode to over 200 Ah/kg, then the cell energy density can be increased by over 50% to approach 1 kWh/liter (actual cell). This will increase the driving range of vehicles.

Moreover, smaller cells using lower cost manufacturing will lower the cost of tomorrow’s batteries.

**Out-Year Goals.** The long-term goal is to enable cells with an energy density of 1 kWh/liter. This will be accomplished by replacing both the present carbon used in Li-ion batteries with anodes that approach double the volumetric capacity of carbon, and the present intercalation cathodes with materials that significantly exceed 200 Ah/kg. By the end of this project, it is anticipated that cells will be available that can exceed the volumetric energy density of today’s Li-ion batteries by 50%.

**Collaborations.** The Advanced Photon Source (APS) at ANL and, when available, the National Synchrotron Light Source II at BNL will be used to determine the phases formed in both *ex situ* and *operando* electrochemical cells. University of Colorado – Boulder, and University of Michigan will provide some of the electrolytes to be used.

### Milestones

1. Determine cyclability of Sn/Li<sub>x</sub>VOPO<sub>4</sub>. (12/31/16 – Completed).
2. Demonstrate cyclability of Sn/CuF<sub>2</sub>. (March 2017).
3. Choose optimum couple. (June 2017).
4. Supply cells to the DOE. (September 2017).

## Progress Report

The goal of this project is to synthesize tin-based anodes that have 1.5 times the volumetric capacity of the present carbons, and conversion and intercalation cathodes with capacities over 200 Ah/kg.

The major efforts in this first quarter of year three were to continue the efforts to demonstrate a lithiation method for a full cell containing the Sn/Fe/C conversion anode and either a  $\text{Li}_x\text{VOPO}_4$  or a  $\text{CuF}_2$  cathode. As noted last quarter, the effort is now focused on the cathode  $\text{Li}_x\text{VOPO}_4$ .

**Milestone 1: “Demonstrate cyclability of the Sn/Li<sub>x</sub>VOPO<sub>4</sub> couple. The cells will be cycled until failure. The results of this cell will be reported.”** Last quarter, the project demonstrated and reported the cyclability of electrochemically  $\text{Sn}_y\text{Fe}$  in a  $\text{Sn}_y\text{Fe}/\text{VOPO}_4$  full cell. This quarter, it reports several practical approaches of incorporating lithium into either the anode or cathode; the optimum approach will be determined in the future. The approaches studied this quarter include:

- **Prelithiation of  $\text{Sn}_y\text{Fe}$ .** This was achieved by using either stabilized lithium metal powder (SLMP) or lithium metal. The fabricated electrode was shorted by bringing it into direct contact with lithium metal/SLMP or by mixing it with SLMP. Either process led to formation of the lithiated product,  $\text{Li}_{22}\text{Sn}_5$ , as confirmed by the XRD patterns in Figure 15 (left). The impact of the  $\text{Sn}_y\text{Fe}$  prelithiation was further confirmed by half-cell electrochemical testing of the prelithiated electrode. The results showed that such a process can greatly reduce the initial irreversible excess capacity, as shown in Figure 15 (right).
- To obtain the discharge products of  $\text{CuF}_2$ , the project used a direct synthesis method by ball-milling LiH and  $\text{CuF}_2$  to form nano composite of Cu/LiF, as confirmed by SEM and XRD. The composite is the conversion discharge products of the  $\text{CuF}_2$ .
- $\text{LiVOPO}_4$  was chemically reacted with butyllithium to form  $\text{Li}_2\text{VOPO}_4$ , as confirmed by ICP and XRD results. The lattice parameters of the pristine  $\text{LiVOPO}_4$  are  $a = 6.742 \text{ \AA}$ ,  $b = 7.202 \text{ \AA}$ ,  $c = 7.919 \text{ \AA}$ , and  $V = 342.69 \text{ \AA}^3$ ; those of the lithiated phase are  $a = 7.202 \text{ \AA}$ ,  $b = 7.104 \text{ \AA}$ ,  $c = 7.780 \text{ \AA}$ , and  $V = 356.78 \text{ \AA}^3$ . These results confirm successful lithiation.

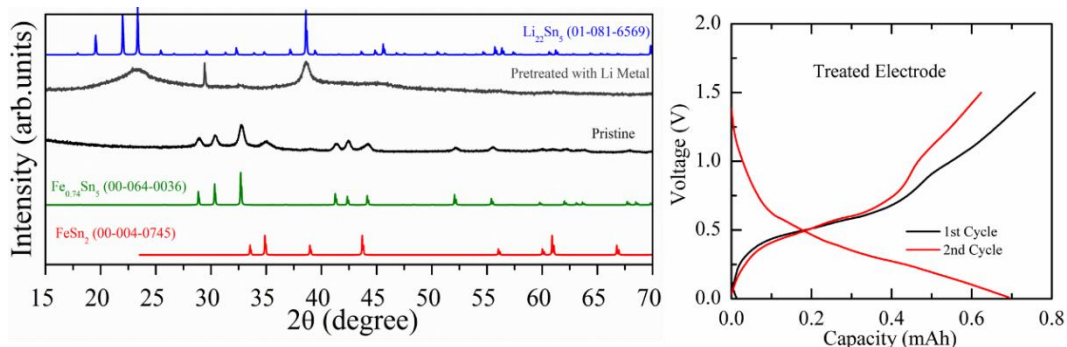


**Figure 15.** X-ray diffraction patterns of the prelithiated Sn-Fe in comparison to the pristine and standard diffraction patterns of the corresponding phases by contacting the electrode with lithium metal (left) and the corresponding charge/discharge curve of the prelithiated  $\text{Sn}_y\text{Fe}$  (right).

## Patents/Publications/Presentations

### Presentations

- National Renewable Energy Laboratory (NREL), Golden, Colorado (September 22, 2016): “What are the Ultimate Limits of Intercalation Reactions for Li-Batteries, and Some Approaches to Get There?”; M. S. Whittingham.
- American Chemical Society (ACS) Northeast Regional Meeting (NERM), Binghamton, New York (October 7, 2016): “FeSn<sub>2</sub> and FeSn<sub>5</sub> Alloy with High and Stable Capacity as Anodes in Lithium-Ion Batteries”; Fengxia Xin.
- ACS Northeast Regional Meeting (NERM), Binghamton, New York (October 6, 2016): “Intrinsic Challenges in Creating a Reversible Copper(II) Fluoride Cathode for Lithium-Ion Batteries”; Nik Zagarella.
- ACS NERM, Binghamton, New York (October 6, 2016): “Synthesis, Characterization and Optimization of Vanadium Phosphates as Cathode Material for Lithium-Ion Batteries”; Yong Shi.
- 2016 Materials Research Society (MRS) Fall Meeting, Boston (November 30, 2016): Enhanced Performance of LiVOPO<sub>4</sub> Cathodes with Sol-Gel Synthesis”; Hui Zhou.



## Task 3.3 – Development of High-Energy Cathode Materials (Ji-Guang Zhang and Jianming Zheng, Pacific Northwest National Laboratory)

**Project Objective.** The project objective is to develop high-energy-density, low-cost, cathode materials with long cycle life. The previous investigation demonstrates that synthesis condition, synthesis approach, and surface modification have significant effects on the performances of high-voltage spinel and LMR-NCM cathodes. These valuable understandings will be used to guide development of high-energy-density, enhanced long-term cycling stability of Ni-rich  $\text{LiNi}_x\text{Mn}_y\text{Co}_z\text{O}_2$  (NMC) cathode materials that can deliver a high discharge capacity with long-term cycling stability.

**Project Impact.** Although state-of-the-art layered structure cathode materials such as  $\text{LiNi}_{1/3}\text{Mn}_{1/3}\text{Co}_{1/3}\text{O}_2$  and  $\text{LiNi}_{0.4}\text{Mn}_{0.4}\text{Co}_{0.2}\text{O}_2$ , have relatively good cycling stability at charge to 4.3 V, their energy densities need to be further improved to meet the requirements of EVs. This work focuses on the two closely integrated parts: (1) Develop the high-energy-density NMC layered cathode materials for Li-ion batteries; and (2) characterize the structural properties of the NMC materials by various diagnostic techniques including scanning transmission electron microscopy (STEM)/EELS, energy dispersive X-ray (EDX) mapping and SIMS, and correlate with the first part. The success of this work will increase energy density of Li-ion batteries and accelerate market acceptance of EVs, especially for PHEVs required by the EV Everywhere Grand Challenge.

**Approach.** In FY 2016, the compositions of NMC cathode materials and the charge cutoff voltage were optimized. Ni-rich NMC cathode materials with initial discharge capacity higher than  $200 \text{ mAh g}^{-1}$  and capacity retention of 90% after 100 cycles were successfully achieved. However, the long-term cycling stability is still unsatisfactory and requires further improvement. In FY 2017, several strategies will be carried out to further enhance the long-term cycling stability as well as the thermal stability of NMC cathode materials, including (1) cationic/anionic lattice doping; (2) surface modification; and/or (3) introduction of effective electrolyte formulas/additives.

**Out-Year Goals.** The long-term goal of the proposed work is to enable Li-ion batteries with a specific energy of  $> 96 \text{ Wh kg}^{-1}$  (for PHEVs), 5000 deep-discharge cycles, 15-year calendar life, improved abuse tolerance, and less than 20% capacity fade over a 10-year period.

**Collaborations.** This project engages with the following collaborators:

- Dr. Bryant Polzin (ANL) – NMC electrode supply
- Dr. X. Q. Yang (BNL) – *In situ* XRD characterization during cycling
- Dr. Kang Xu (U.S. Army Research Laboratory, ARL) – New electrolyte

### Milestones

1. Complete lattice doping to enhance cycling stability of NMC at high charge cutoff voltages, and identify the effect of dopants in NMC during cycling using quantitative atomic level mapping. (December 2016 – Complete)
2. Identify appropriate solvents for surface modification of NMC, and reveal the structural changes of different NMC materials after wash with water. (March 2017 – In progress)
3. Complete surface modification to enhance the cycling stability of NMC at high charge cutoff voltages. (June 2017)
4. Achieve NMC performance improvement of  $200 \text{ mAh g}^{-1}$  and 80% capacity retention after 200 cycles. (September 2017)

## Progress Report

This quarter's milestone is complete. Surface lattice doping has been adopted to enhance the cycling stability of Ni-rich NMC cathode materials at a high charge cutoff voltage of 4.5 V.

Using the spherical  $\text{Ni}_{0.68}\text{Mn}_{0.22}\text{Co}_{0.10}(\text{OH})_2$  precursor, the effects of dopants on the electrochemical performance of  $\text{Li}(\text{Ni}_{0.68}\text{Mn}_{0.22}\text{Co}_{0.10})_{0.99}\text{M}_{0.01}\text{O}_2$  ( $M = \text{Mg}, \text{Al}, \text{V}, \text{and Y}$ ) were firstly investigated. The lattice doped materials were prepared by mixing the  $\text{Ni}_{0.68}\text{Mn}_{0.22}\text{Co}_{0.10}(\text{OH})_2$  precursor of  $\sim 10 \mu\text{m}$  secondary particle size (Figure 16a) and the dopant precursors, which was further blended with lithium hydroxides and then annealed at the optimum calcination temperature of  $775^\circ\text{C}$  for 24 h. The cycling performance of the 1% metal doped cathode materials was then evaluated in coin-type cells with similar electrode loading ( $\sim 4 \text{ mg cm}^{-2}$ ). Electrochemical performance results showed that the additional lattice doping slightly reduced discharge capacity due to the electrochemical inactivity of the dopants (Figure 16b). During long-term cycling, only the aluminum doping showed positive effect in improving the capacity retention, while the other dopants (magnesium, vanadium, and yttrium) deteriorated the cyclability of the Ni-rich NMC cathodes (Figure 16c,d).

The effect of aluminum doping content on the electrochemical performance of another Ni-rich NMC  $\text{Li}(\text{Ni}_{0.76}\text{Mn}_{0.14}\text{Co}_{0.10})_{1-x}\text{Al}_x\text{O}_2$  of higher capacity was systematically investigated. It is found that discharge capacity decreases with the increase of doping amount, owing to the electrochemical inactivity of aluminum and the lowered lithium-ion diffusion kinetics (Figure 17a). It was also noticed that the doping amount had significant effect on the long-term cycling performance on Ni-rich NMC  $\text{Li}(\text{Ni}_{0.76}\text{Mn}_{0.14}\text{Co}_{0.10})_{1-x}\text{Al}_x\text{O}_2$  (Figure 17b). With 1 mol% aluminum doping, the capacity retention in 200 cycles of Ni-rich NMC cathode was improved from 88.5% to 89.0%. Further increasing the aluminum doping amount to be higher than 1 mol% resulted in the faster capacity degradation. This may be because only a small amount of Al precursor could be successfully doped into the layered structure lattice; further increase of aluminum doping can only form a thick coating layer on the surface of particles, which dramatically increased the kinetic barrier for Li-ion transportation and the reversible Li-ion de/intercalation processes. The results suggest that the surface lattice doping has very limited improvement in the cycling stability of Ni-rich NMCs at high charge cutoff voltages, as the particle cracking is considered the primary reason for the capacity degradation (see FY 2016 Q2 report). Further efforts will focus on the synthesis of NMC hydroxide precursor with homogeneous aluminum elemental distribution, to enhance the structural integrity of secondary particles and thus improve the long-term cycle life of Ni-rich NMC cathodes.

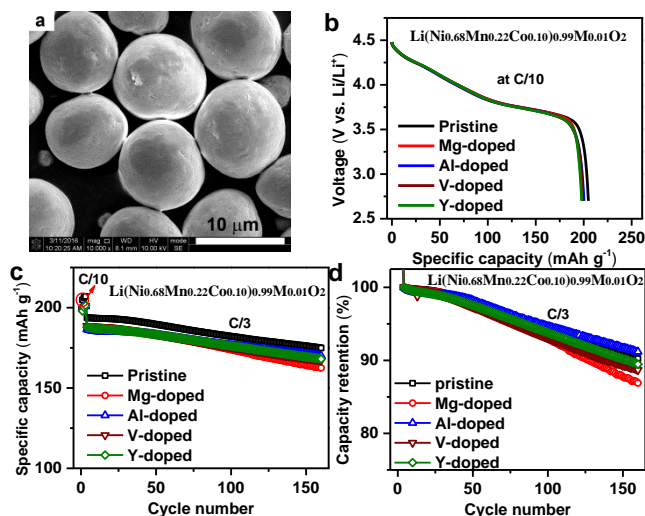


**Figure 16.** (a) Scanning electron microscopy image of  $\text{Ni}_{0.68}\text{Mn}_{0.22}\text{Co}_{0.10}(\text{OH})_2$  precursor. (b) Initial discharge profiles at C/10, (c) cycling performance and (d) capacity retention of  $\text{Li}(\text{Ni}_{0.68}\text{Mn}_{0.22}\text{Co}_{0.10})_{0.99}\text{M}_{0.01}\text{O}_2$  ( $M = \text{Mg}, \text{Al}, \text{V}, \text{and Y}$ ) during cycling at C/3 after 3 formation cycles at C/10 ( $1\text{C} = 200 \text{ mA g}^{-1}$ ). Cathode electrode loading is  $\sim 4 \text{ mg cm}^{-2}$ .

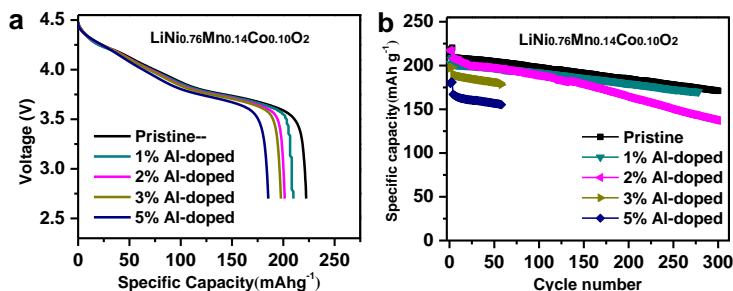


**Figure 17.** (a) Initial discharge profiles at C/10. (b) Cycling performance and capacity retention of  $\text{Li}(\text{Ni}_{0.76}\text{Mn}_{0.14}\text{Co}_{0.10})_{1-x}\text{Al}_x\text{O}_2$  during cycling at C/3 after 3 formation cycles at C/10.

## Patents/Publications/Presentations

### Publication

- Zheng, Jianming, and Seung Myeong, Woongrae Cho, Pengfei Yan, Jie Xiao, Chongmin Wang, Jaephil Cho, and Ji-Guang Zhang. “Li- and Mn-Rich Cathode Materials: Challenges to Commercialization.” *Advanced Energy Materials* (2016). doi: 10.1002/aenm.201601284.

### Presentation

- 2016 MRS Fall Meeting, Boston (November 28, 2016): “An Artificial Solid Electrolyte Interface Layer for Stable Nickel-Rich Cathode Materials”; Jianming Zheng, Pengfei Yan, Jian Liu, Xueliang Sun, Chongmin Wang, and Ji-Guang Zhang.

## Task 3.4 – *In Situ* Solvothermal Synthesis of Novel High-Capacity Cathodes (Feng Wang and Jianming Bai, Brookhaven National Laboratory)

**Project Objective.** The goal is to develop novel high-capacity cathodes with precise control of the phase, stoichiometry, and morphology. Despite considerable interest in developing low-cost, high-energy cathodes for Li-ion batteries, designing and synthesizing new cathode materials with the desired phases and properties have proven difficult, due to complexity of the reactions involved in chemical synthesis. Building on established *in situ* capabilities/techniques for synthesizing and characterizing electrode materials, this project will undertake *in situ* studies of synthesis reactions under real conditions to identify the intermediates and to quantify the thermodynamic and kinetic parameters governing the reaction pathways. The results of such studies will enable strategies to “dial in” desired phases and properties, opening a new avenue for synthetic control of the phase, stoichiometry, and morphology during preparation of novel high-capacity cathodes.

**Project Impact.** Present-day Li-ion batteries are incapable of meeting the targeted miles of all-electric-range within the weight and volume constraints, as defined by the DOE in the EV Everywhere Grand Challenge. New cathodes with higher energy density are needed for Li-ion batteries so that they can be widely commercialized for plug-in electric vehicle (PEV) applications. The effort will focus on increasing energy density (while maintaining the other performance characteristics of current cathodes) using synthesis methods that have the potential to lower cost.

**Out-Year Goals.** This project is directed toward developing novel high-capacity cathodes, with a focus on Ni-rich layered oxides. Specifically, synthesis procedures will be developed for making  $\text{LiNiO}_2$  and a series of Co/Mn substituted solid solutions,  $\text{LiNi}_{1-x}\text{M}_x\text{O}_2$  (M=Co, Mn); through *in situ* studies, this project undertakes systematic investigations of the impact of synthesis conditions on the reaction pathways and cationic ordering processes toward the final layered phases. The structural and electrochemical properties of the synthesized materials will be characterized using scanning XRD, neutron scattering, TEM, EELS, and various electrochemical techniques. The primary goal is to develop a reversible cathode with an energy density of 660 Wh/kg or higher.

**Collaborations.** This project engages with the following collaborators: Lijun Wu and Yimei Zhu at BNL; Khalil Amine, Zonghai Chen, and Yang Ren at ANL; Jagjit Nanda and Ashfia Huq at ORNL; Nitash Balsara, Wei Tong, and Gerbrand Ceder at LBNL; Arumugam Manthiram at UT Austin; Scott Misture at Alfred University; Peter Khalifha at SUNY; Kirsuk Kang at Seoul National University; Brett Lucht at University of Rhode Island; and Jason Graetz at HRL Laboratories.

### Milestones

1. Identify the synthesis reactions and involved structural ordering in both Ni-based and Co-based layered oxides through *in situ* synchrotron X-ray studies. (December 2016 – Complete)
2. Develop neutron scattering based techniques for *in situ* probing the dynamics of cation ordering in NMC layered oxides under real synthesis conditions. (March 2017 – On schedule)
3. Identify synthesis procedures for kinetic control of structural ordering in NMC layered oxides through combined *in situ/ex situ* synchrotron X-ray and neutron studies. (June 2017)
4. Complete the evaluation of synthesis conditions, specifically identifying the effect of temperature and time on the structural ordering and electrode performance of Ni-rich NMC layered cathodes. (September 2017)

## Progress Report

Previously, *in situ* XRD techniques were developed for real-time probing of synthesis reactions in preparing  $\text{LiNiO}_2$  and the Co-substituted variant,  $\text{LiNi}_{0.8}\text{Co}_{0.2}\text{O}_2$ , thereby gaining insights into synthetic control of structural/electrochemical properties of the materials. This quarter, the developed approaches were applied broadly to studies of synthesis reactions in preparing Co-based and Ni-based TM layered oxides, ranging from  $\text{LiCoO}_2$ , to  $\text{LiNiO}_2$ , and solid solution  $\text{LiNi}_{1-x}(\text{CoMn})_x\text{O}_2$  (of varying stoichiometry), wherein lithium and TM hydroxides were used as precursors. Synchrotron X-ray was employed for acquisition of high-quality diffraction data with wide collection angle and high angular resolution within short time (seconds), allowing access to intermediates and short-lived phases. The *in situ* studies revealed a strong dependence of reaction pathway on constituent TM elements in the precursors, indicating that presence of Co and Mn in Ni-based hydroxides is favorable for phase transformation to layered oxides at low temperatures.

Precursors were made from mixtures of  $\text{LiOH}$  with  $\text{TM}(\text{OH})_2$  (TM = Ni, Co, Mn of varying molar ratios) that were synthesized using co-precipitation method. Time-resolved synchrotron XRD patterns were recorded from the hydroxide mixtures upon heating from low to high temperatures. Figure 18 shows representative contour plots of the XRD patterns recorded from intermediates at low temperatures ( $\leq 500^\circ\text{C}$ ) in preparing  $\text{LiNiO}_2$  and  $\text{LiNi}_{0.7}\text{Co}_{0.15}\text{Mn}_{0.15}\text{O}_2$ . In these two cases, the phase transformation process is overall similar, both from initial hydroxides (space group:  $p\text{-}3m1$ ) to the eventual layered oxides ( $R\text{-}3m$ ). But due to the different chemical reactivity between Ni, Co, and Mn, complex reaction occurred in  $\text{Ni}_{0.7}\text{Co}_{0.15}\text{Mn}_{0.15}(\text{OH})_2$ , along a much different pathway than that in those precursors containing only nickel or cobalt. For example, heat treatment led to decomposition of  $\text{Ni}(\text{OH})_2$  at  $\sim 230^\circ\text{C}$ , giving rise to rock-salt ( $\text{NiO}$ ), and no layered phase was observed at temperatures up to  $500^\circ\text{C}$  (Figure 18a). In contrast,  $\text{Ni}_{0.7}\text{Co}_{0.15}\text{Mn}_{0.15}(\text{OH})_2$  transformed into structurally similar intermediates at temperatures between  $218\text{--}313^\circ\text{C}$ , and layered phase thereafter, through local anionic exchange and cationic migration/re-ordering (Figure 18b). Results from *ex situ* XRD measurements showed that, with elongated sintering time, the transformation from  $\text{Ni}_{0.7}\text{Co}_{0.15}\text{Mn}_{0.15}(\text{OH})_2$  to intermediates occurred at  $120^\circ\text{C}$ , and then to the layered at temperature as low as  $200^\circ\text{C}$ . Quantitative structure analysis is under way, for better understanding of the synthesis process in preparing Ni-rich layered oxides and their dependence on precursors.

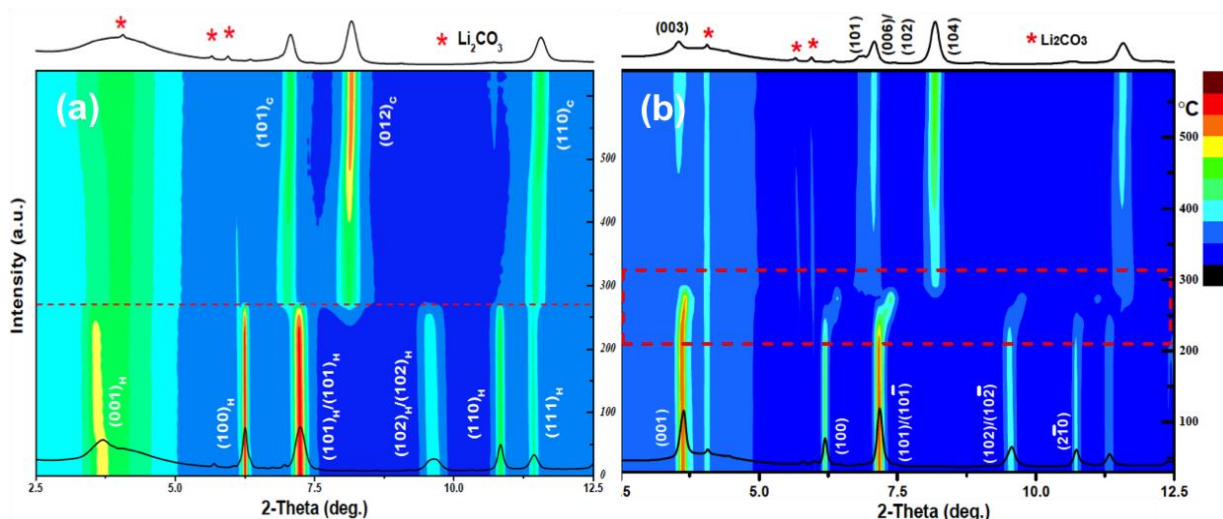


Figure 18. *In situ*, temperature-resolved X-ray diffraction for tracking structural evolution of intermediates in preparing (a)  $\text{LiNiO}_2$  and (b)  $\text{LiNi}_{0.7}\text{Co}_{0.15}\text{Mn}_{0.15}\text{O}_2$  from hydroxides (*via* solid-state reaction in  $\text{O}_2$  with a heating rate of  $5^\circ\text{C}/\text{min}$ ).

## Patents/Publications/Presentations

### Patent

- Wang, F., and X. Wang, J. Graetz, and P. Khalifah. Nanostructured Copper Vanadium Oxides as High-Capacity Cathodes for Lithium-ion Batteries, U.S. patent (filed).

### Publication

- Zhao, J., and W. Zhang, A. Huq, S. T. Misture, B. Zhang, S. Guo, L. Wu, Y. Zhu, Z. Chen, K. Amine, F. Pan, J. Bai, and F. Wang. “*In Situ* Probing and Synthetic Control of Cationic Ordering in Ni-Rich Layered Oxide Cathodes.” *Adv. Energy Mater.* 1601266 (2016): in press.

### Presentation

- 2016 MRS Fall Meeting, Boston (November 27 – December 2, 2016): “Developing High-Capacity Ni-rich Layered Oxide Cathodes for Li-ion Batteries via *In Situ* Synthetic Control of the Structure and Material Properties”; D. Wang, J. Bai, J. Zhao, W. Zhang, and Feng Wang.

## Task 3.5 – Novel Cathode Materials and Processing Methods (Michael M. Thackeray and Jason R. Croy, Argonne National Laboratory)

**Project Objective.** The project goal is to develop low-cost, high-energy, and high-power Mn-oxide-based cathodes for Li-ion batteries that will meet the performance requirements of PHEVs and EVs. Improving the design, composition, and performance of advanced electrodes with stable architectures and surfaces, facilitated by an atomic-scale understanding of electrochemical and degradation processes, is a key objective.

**Project Impact.** Standard Li-ion battery technologies are unable to meet the demands of the next-generation EVs and PHEVs. Battery developers and scientists will take advantage of both the applied and fundamental knowledge generated from this project to advance the field. This knowledge should enable progress toward meeting DOE goals for 40-mile, all-electric range PHEVs.

**Approach.** This project will exploit the concept and optimize the electrochemical properties of structurally integrated “composite” electrode structures with a prime focus on LLS materials. Alternative processing routes will be investigated. The comprehensive characterization facilities at ANL will be used to explore novel surface and bulk structures by both *in situ* and *ex situ* techniques in pursuit of advancing the electrochemical performance of state-of-the-art cathode materials. A theoretical component will complement the experimental work of this project.

**Out-Year Goals.** The out-year goals are as follows:

- Identify high-capacity (LL and LS) composite electrode structures and compositions that are stable to electrochemical cycling at high potentials (~ 4.5 V).
- Identify and characterize surface chemistries and architectures that allow fast Li-ion transport and mitigate or eliminate TM dissolution.
- Use complementary theoretical approaches to further understanding of electrode structures and electrochemical processes to accelerate progress of materials development.
- Scale-up, evaluate, and verify promising cathode materials in conjunction with scale-up and cell fabrication facilities at ANL.

**Collaborators.** This project engages with the following collaborators: Arturo Gutierrez, Eungje Lee, and Roy Benedek in Chemical Sciences and Engineering (CSE) at ANL.

### Milestones

1. Explore the energy content, and stabilization thereof, of moderate  $\text{Li}_2\text{MnO}_3$ -content ( $25\% < x < 50\%$ )  $y[\text{xLi}_2\text{MnO}_3 \cdot (1-x)\text{LiMO}_2] \cdot (1-y)\text{LiM}_2\text{O}_4$  (M=Mn, Ni, Co), LL and LLS electrodes; target capacity  $\geq 220$  mAh/g. (December 2016 – In progress)
2. Identify surface-treatment strategies that enable LLS electrodes to maintain high capacities ( $\geq 220$  mAh/g) and high rate performance (~200 mAh/g at 1C). (March 2017 – In progress)
3. Demonstrate oxide energy densities  $\geq 750$  Wh/kg<sub>oxide</sub> in full-cell testing of surface-modified, LLS electrodes. (September 2017)

## Progress Report

As part of the project's objective to design unique surface structures that can enable high capacities ( $\sim 200$  mAh/g) at 1C, several surface treatments of the phosphate materials  $\text{Li}_3\text{PO}_4$ ,  $\text{Li}_{2.8}\text{Ni}_{0.1}\square_{0.1}\text{PO}_4$ , and  $\text{Sn}_3(\text{PO}_4)_2$  ( $\square$  = lithium vacancy) have been investigated. The  $\text{PO}_4$  polyanions in these compounds possess strong covalent bonding; a property that might protect cathode surfaces under high voltage cycling. In addition, the inherent structures of some phosphates may lend themselves to fast Li-ion diffusion. For instance, the structure of  $\text{Sn}_3(\text{PO}_4)_2$  consists of large, open channels ( $\sim 4.44$  Å) as illustrated in Figure 19. The above-mentioned materials were evaluated for their efficacy as effective surface treatments for the project's baseline, LLS cathode  $\text{Li}_{1.18}\text{Mn}_{0.54}\text{Co}_{0.18}\text{Ni}_{0.28}\text{O}_2$  with a targeted  $\sim 6\%$  spinel content.

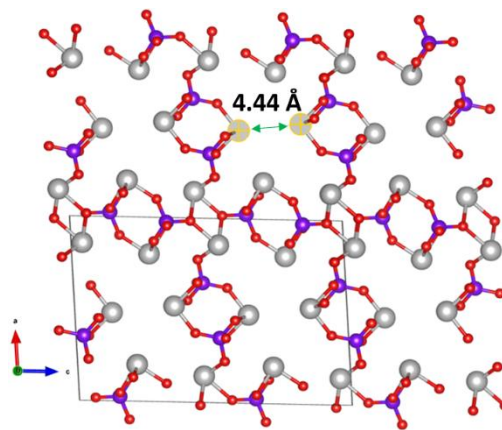


Figure 19. Depiction of the crystal structure of  $\text{Sn}_3(\text{PO}_4)_2$  with space group P 21/c showing large channels that may prove beneficial lithium diffusion. O (red), P (purple), SN (gray).

Surface treatments were conducted via wet-chemical methods and included preliminary optimization of phosphate concentration (wt%) and post-synthesis annealing. It was found, in general, that the capacity of treated samples increased as the concentration of surface phosphate dropped. Figure 20a shows the capacity versus cycle performance of Li-half cells containing a baseline, LLS cathode, and cathodes fabricated from the baseline material treated nominally with 1 wt%  $\text{Li}_3\text{PO}_4$ ,  $\text{Li}_{2.8}\text{Ni}_{0.1}\square_{0.1}\text{PO}_4$ , or  $\text{Sn}_3(\text{PO}_4)_2$ . The cycling protocol (at room temperature) was: first cycle: 4.6 - 2.0 V, and thereafter, 4.45 - 2.5 V, 15 mA/g. Figure 20b shows the corresponding rate performance of the cells after the first-cycle activation when cells were discharged to 2.5 V at various rates. Each of the treated cathodes delivered an initial capacity roughly equivalent to that of the baseline, but provided improved capacity and cycling stability relative to the baseline electrode after  $\sim 10$  cycles. In addition, Figure 20b shows that both  $\text{Li}_3\text{PO}_4$ - and  $\text{Li}_{2.8}\text{Ni}_{0.1}\square_{0.1}\text{PO}_4$  treated samples delivered a higher capacity than the baseline electrode for most rates. These results align with the initial reasoning cited with respect to phosphate materials. The baseline material, as-prepared in a continuously stirred tank reactor is shown in Figure 20c and remains representative of the morphology of the samples after surface treatments (not shown). Further spectroscopic, structural, and electrochemical analyses are under way to understand the reasons behind the improved performance.

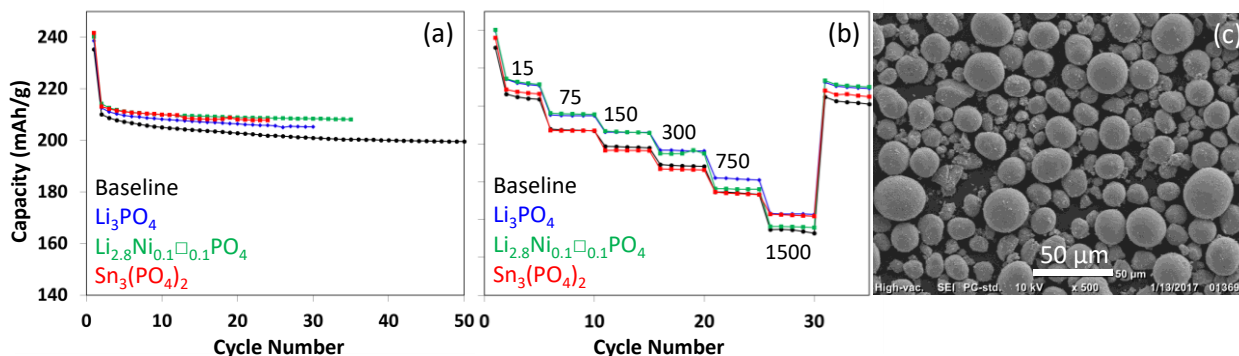


Figure 20. (a) Capacity versus cycling of the baseline  $\text{Li}_{1.18}\text{Mn}_{0.54}\text{Co}_{0.18}\text{Ni}_{0.28}\text{O}_2$  ( $\sim 6\%$  spinel) with and without treatments of  $\text{Li}_3\text{PO}_4$ ,  $\text{Li}_{2.8}\text{Ni}_{0.1}\square_{0.1}\text{PO}_4$ , and  $\text{Sn}_3(\text{PO}_4)_2$ . (b) Corresponding rate performance of the samples in (a) at a constant charge rate of 15 mA/g, and various discharge rates as labeled (mA/g); first-cycle activation between 4.6-2.0 V; thereafter, 4.45 V-2.5 V. (c) Scanning electron microscopy images of the as-prepared, baseline powder.



## Patents/Publications/Presentations

### Publication

- University of Illinois – Chicago (November 8, 2016): “The Next Generation of Li-ion Batteries for Transportation Applications: Perception, Promises and Problems”; Arturo Gutierrez. Invited.

## Task 3.6 – Advanced Cathode Materials for High-Energy Lithium-Ion Batteries (Marca Doeff, Lawrence Berkeley National Laboratory)

**Project Objective.** Microscopy and synchrotron X-ray absorption and photoemission techniques will be used to study the phenomenon of surface reconstruction to rock salt on NMC particle surfaces as a function of composition, synthesis method, surface chemistry, and electrochemical history. Because the surface reconstruction is implicated in capacity fading and impedance rise during high-voltage cycling, a thorough understanding of this phenomenon is expected to lead to principles that can be used to design robust, high-capacity NMC materials for Li-ion cells. The emphasis will be on stoichiometric NMCs with high Ni contents such as 622 and 523 compositions.

**Project Impact.** To increase the energy density of Li-ion batteries, cathode materials with higher voltages and/or higher capacities are required, but safety and cycle life cannot be compromised. Ni-rich NMCs can provide higher capacities and lower cost in comparison with low Ni content NMCs, but surface reactivity is an issue. A systematic evaluation of the effects of synthesis method, composition, and cell history on the surface reconstruction phenomenon will lead to higher capacity, robust, and structurally stable positive electrode materials that result in higher energy density Li-ion cells than are currently available.

**Out-Year Goals.** The information generated by the in-depth characterization will be used to design robust NMC materials that can withstand cycling to high potentials and deliver > 200 mAh/g.

**Collaborations.** Transmission X-ray microscopy (TXM) has been used this quarter to characterize NMC materials, with work done in collaboration with Yijin Liu (SSRL). Synchrotron and computational efforts continued in collaboration with Professor M. Asta (University of California – Berkeley, UCB); and Dr. Dennis Nordlund, Dr. Yijin Liu, and Dr. Dimosthenis Sokaras (SSRL). The TEM effort is in collaboration with Dr. Huolin Xin (BNL).

### Milestones

1. Complete thermal characterization of Ni-rich NMC materials by TXM and X-ray Raman. (December 2016 – Complete)
2. Synthesize Ti-substituted Ni-rich NMCs by conventional and spray pyrolysis methods. (March 2017 – On schedule)
3. Complete electrochemical characterization of Ti-substituted Ni-rich NMCs (June 2017)
4. *Go/No Go*: Core-shell composites made by infiltration and re-firing of spray-pyrolyzed hollow spherical particles. (September 2016 – No-go decision made)

## Progress Report

This quarter, the thermal stability of Ni-rich NMCs was investigated at different states of charge. Highly delithiated  $\text{Li}_{1-x}\text{Ni}_{0.6}\text{Mn}_{0.2}\text{Co}_{0.2}\text{O}_2$  was prepared by a chemical delithiation method. In comparison with electrochemical delithiation, chemical delithiation can prepare a large quantity of samples for different characterizations. However, it is possible that chemical delithiation could lead to some discrepancies due to the uncontrolled delithiation rate.

To answer the question, pristine samples and chemically delithiated samples were investigated using a transmission X-ray microscope that is sensitive to the TM oxidation states. It is challenging to directly monitor the lithium distribution within the sample. However, the valence state of nickel is a good indicator to track the SOC distribution because nickel is the main redox active element in this material. To get better statistics, more than five views were studied; five representative views are presented in Figure 21. As shown in Figure 21a, the pristine material shows some degree of SOC heterogeneity. After chemical delithiation (Figure 21b), the K-edge energy increased, which indicates the oxidation of nickel as expected. Moreover, the oxidation state distribution (that is, SOC distribution) becomes more homogeneous. Considering the chemical delithiation process is carried out in solution, the homogeneity could be related to uniform removal and redistribution of lithium within the particles.

A no-go decision was made for Milestone 4 because of the general observation of a graded composition for particles made by spray pyrolysis; a core-shell composite is not necessary to make materials with Ni-poor surfaces.

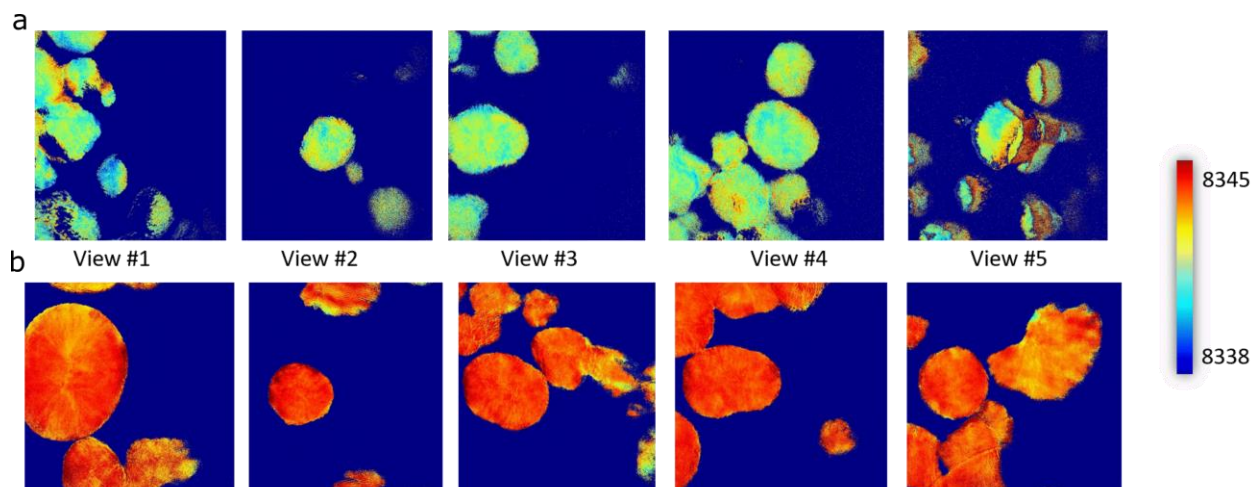


Figure 21. 2D state-of-charge mapping for: (a) pristine  $\text{Li}_{1-x}\text{Ni}_{0.6}\text{Mn}_{0.2}\text{Co}_{0.2}\text{O}_2$  particles and (b) chemically delithiated  $\text{Li}_{0.5}\text{Ni}_{0.6}\text{Mn}_{0.2}\text{Co}_{0.2}\text{O}_2$  imaged at the Ni K-edge. Five different views were investigated to get better statistics.

## Patents/Publications/Presentations

### Publications

- Ludwig, Jennifer, and Dennis Nordlund, Marca M. Doeff, and Thomas Nilges. “Synthesis and Characterization of Metastable, 20-nm-sized  $\text{Pn}_{a_2}1\text{-LiCoPO}_4$  Nanospheres.” *J. Solid State Chem.* (2017). doi:10.1016/j.jssc.2017.01.015.
- Xu, J., and F. Lin, M. Doeff, and W. Tong. “A Review of Ni-based Layered Oxides for Rechargeable Li-ion Batteries.” *J. Mater. Chem. A* (2016). doi: 10.1039/C6TA07991A
- Evans, Tyler, and Daniela Molina Piper, Huaxing Sun, Timothy Porcelli, Seul Cham Kim, Sang Sub Han, Yong Seok Choi, Chixia Tian, Dennis Nordlund, Marca M. Doeff, Chunmei Ban, Sung-Jin Cho, Kyu Hwan Oh, and Se-Hee Lee. “*In Situ* Engineering of the Electrode-Electrolyte Interface for Stabilized Over-lithiated Cathodes.” *Adv. Mater.* (2017). doi: 10.1002/adma.201604549.

### Presentations

- 2016 Pacific Rim Meeting on Electrochemical and Solid-State Science (PRIME), Honolulu (October 2-7, 2016): “Structural Stability of Nickel-Rich Layered Cathode Materials”; Chixia Tian, Yahong Xu, Dennis Nordlund, Huolin Xin, Yijin Liu, and Marca Doeff.
- 2016 SSRL User Meeting (October 6, 2016): “Cycling Failure Mechanism of Nickel-Rich Layered Cathode Materials”; Chixia Tian, Yahong Xu, Dennis Nordlund, Dimosthenis Sokaras, Huolin Xin, Yijin Liu, and Marca Doeff.
- Second International Symposium on Renewable Energy Technologies, Sydney, Australia (November 30 – December 4, 2016): “Recent Progress on Battery Materials”; Marca M. Doeff. Invited.
- Energy Harvesting USA, Santa Clara, California (November 16-17, 2016): “Illuminating Performance Characteristics of Battery Materials Using Synchrotron Techniques: Advanced NMCs, Sodium-Ion Batteries, and Solid Garnet-Type Electrolytes”; Marca M. Doeff. Invited.
- The Northern California Chapter of The American Vacuum Society, San Jose, California (November 16, 2016): “The Future of Solid State Batteries for Electric Vehicles”; Marca M. Doeff. Invited.
- 2016 SSRL / Linac Coherent Light Source (LCLS) User Meeting, Menlo Park, California (October 5-7, 2016): “Synchrotron Studies of Battery Materials”; Marca M. Doeff.

## Task 3.7 – Exploiting Cobalt and Nickel Spinel in Structurally Integrated Composite Electrodes (Michael M. Thackeray and Jason R. Croy, Argonne National Laboratory)

**Project Objective.** The goal of this project is to stabilize high capacity, composite ‘layered-layered’ electrode structures with lithium-cobalt-oxide and lithium-nickel-oxide spinel components (referred to as LCO-S and LNO-S, respectively), or solid solutions thereof (LCNO-S), which can accommodate lithium at approximately 3.5 V vs. metallic lithium. This approach and the motivation to exploit the electrochemical and structural LCO-S and LNO-S spinel structures, about which relatively little is known, is unique.

**Project Impact.** State-of-the art lithium-ion batteries are currently unable to satisfy the performance goals for plug-in hybrid- (PHEV) and all-electric (EV) vehicles. If successful, this project will impact the advance of energy storage for electrified transportation as well as other applications, such as portable electronic devices and the electrical grid.

**Approach.** This work will focus on the design and synthesis of new spinel compositions and structures that operate above 3 V and below 4 V and to determine their structural and electrochemical properties through advanced characterization. This information will be used subsequently to select the most promising spinel materials as stabilizers in high capacity composite electrode structures.

**Out-Year Goals.** The electrochemical capacity of most high potential lithium-metal oxide insertion electrodes is generally severely compromised by their structural instability and surface reactivity with the electrolyte at low lithium loadings (i.e., at highly charged states). Although some progress has been made by cation substitution and structural modification, the practical capacity of these electrodes is still restricted to approximately 160-170 mAh/g. This project proposes a new structural and compositional approach with the goal of producing electrode materials that can provide 200-220 mAh/g without significant structural or voltage decay for 500 cycles. If successful, the materials processing technology will be transferred to Argonne’s Materials Engineering and Research Facility (MERF) for scale up and further evaluation.

**Collaborations.** This project collaborates with Eungje Lee, Arturo Gutierrez, and Roy Benedek (CSE, ANL); and Vinayak Dravid, Soo Kim, and Chris Wolverton (Northwestern University).

### Milestones

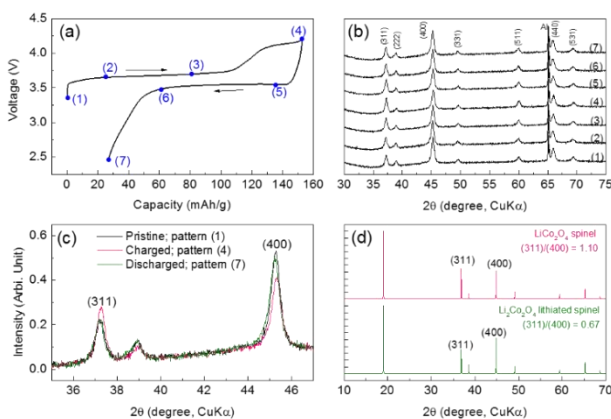
1. Explore solution-based synthesis routes to optimize the structure and performance of Co-based spinel and structurally-integrated LS electrodes. (Q4 – In progress)
2. Determine structure/electrochemical property relationships of Co-based spinel materials and when structurally-integrated in composite LS electrodes. (Q4 – In progress; see text)
3. Investigate bulk and surface modifications of Co-based spinel and LS electrodes. (Q4 – In progress)

## Progress Report

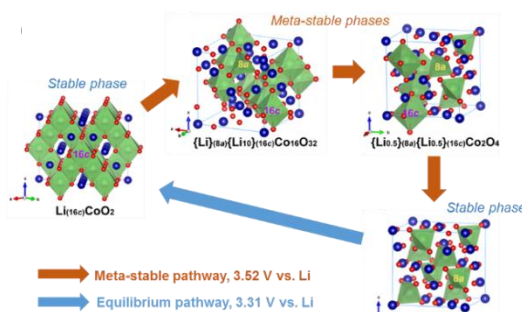
This project aims to stabilize high capacity, composite ‘layered-layered’ electrode structures with lithiated lithium-cobalt-oxide (LCO) and lithium-nickel-oxide (LNO) spinel components, or solid solutions thereof, which can release and accommodate lithium at approximately 3.5 V versus metallic lithium. The synthesis, structure, and electrochemistry of these lithiated spinel materials, prepared at moderately low temperature (LT), has been reported previously<sup>1</sup>. The reversible lithium extraction and reinsertion reactions that occur at approximately 3.7 V and 3.5 V during charge and discharge, respectively, exhibit a distinct hysteresis, which is more pronounced than it is for layered  $\text{Li}_{1-x}\text{CoO}_2$  and spinel  $\text{Li}_{1-x}\text{Mn}_2\text{O}_4$  electrode systems. Refinement of experimental XRD data coupled to structural calculations using density functional theory (DFT) were performed this quarter to gather insight into the reasons for this hysteresis.

Figure 22a shows the initial charge/discharge profile of a typical Li/LT- $\text{LiCo}_{0.9}\text{Ni}_{0.1}\text{O}_2$  cell. *Ex situ* XRD patterns of the LT- $\text{LiCo}_{0.9}\text{Ni}_{0.1}\text{O}_2$  electrodes were collected during charge and discharge at points (1) to (7) on this profile; these data remain essentially unchanged during charge and discharge, consistent with the stability of a  $[\text{Co}_{0.9}\text{Ni}_{0.1}\text{O}_2]$  (or  $[\text{Co}_{1.8}\text{Ni}_{0.2}\text{O}_4]$ ) spinel framework during lithium insertion/extraction reactions. However, a careful examination of the XRD data reveals that there is a reversible change in the relative intensities of the (311) and (400) peaks (that is, the  $I_{(311)}/I_{(400)}$  ratio) during the charge-discharge cycle and, more specifically, that the  $I_{(311)}/I_{(400)}$  ratio increases during charge and decreases during discharge (Figure 22c). For example,  $I_{(311)}/I_{(400)} = 0.44, 0.64,$  and  $0.45$  for patterns (1), (4), and (7), respectively. The  $I_{(311)}/I_{(400)}$  ratio is dependent on the relative  $\text{Li}^+$  occupancies of tetrahedral ( $T_d$ ) vs. octahedral ( $O_h$ ) sites in the spinel structure, as shown in Figure 22d, in which it can be clearly seen that  $I_{(311)}/I_{(400)}$  ratio is greater in the simulated XRD pattern of the  $\{\text{Li}\}_{[\text{tet}]}\text{Co}_2\text{O}_4$  spinel structure than it is in the pattern of the  $\{\text{Li}_2\}_{[\text{oct}]}\text{Co}_2\text{O}_4$  lithiated spinel structure, consistent with the reversible  $\text{Li}^+$  migration from  $O_h$  to  $T_d$  sites during charge and from  $T_d$  to  $O_h$  sites during discharge.

DFT calculations on a model  $\text{Li}_{16-x}\text{Co}_{16}\text{O}_{32}$  super structure were performed to validate the XRD analysis of the  $\text{Li}_{2-x}[\text{Co}_{1.8}\text{Ni}_{0.2}\text{O}_4]$  system above. It was found that: (1)  $\text{Li}^+$  migration from  $O_h$  to  $T_d$  sites is favorable during charge, as expected; (2) meta-stable lithium-deficient structures such as  $\{\text{Li}\}_{[\text{tet}]\{\text{Li}_{10}\}_{[\text{oct}]}\text{Co}_{16}\text{O}_{32}$  (or  $\text{Li}_{1.375}[\text{Co}_2]\text{O}_4$ ) in which lithium occupies both tetrahedral and octahedral sites form during charge until the  $\{\text{Li}_{0.5}\}_{[\text{tet}]\text{Co}_2\text{O}_4$  spinel composition is reached; (3) the discharge process follows equilibrium reaction pathway between  $\{\text{Li}_{0.5}\}_{[\text{tet}]\text{Co}_2\text{O}_4$  and  $\{\text{Li}\}_{[\text{oct}]\text{Co}_2\text{O}_4$ ; and (4) the voltage for the meta-stable reaction pathway is  $\sim 0.2$  V higher than the equilibrium path, which is consistent with the experimentally-observed hysteresis.



**Figure 22. (a) Voltage profile of Li/LT- $\text{LiCo}_{0.9}\text{Ni}_{0.1}\text{O}_2$  cell showing points where *ex situ* X-ray diffraction (XRD) data were collected. (b) Corresponding *ex situ* XRD patterns. (c) Magnified region for (311) and (400) peaks. (d) Simulated XRD patterns of  $\{\text{Li}\}_{[\text{tet}]\text{Co}_2\text{O}_4$  spinel and  $\{\text{Li}_2\}_{[\text{oct}]\text{Co}_2\text{O}_4$  lithiated spinel.**



**Figure 23. Li (de)intercalation mechanism predicted by density functional theory.**

[1] E. Lee, J. R. Croy, M. M. Thackeray et al., ACS Appl. Mater. & Interfaces 8, 27720 (2016).

## Task 3.8 – Discovery of High-Energy Lithium-Ion Battery Materials (Wei Tong, Lawrence Berkeley National Laboratory)

**Project Objective.** This project aims to develop a cathode that can cycle  $> 200$  mAh/g while exhibiting minimal capacity and voltage fade. The emphasis will be on oxides with high nickel contents. This task focuses on the compositions in the Li-Ni-O phase space, which will be explored using a combinatorial materials approach to search for new high-capacity cathodes. The specific objectives of this project are to: (1) investigate and understand the correlation between the synthesis and electrochemical performance of Ni-based compounds, and (2) design, synthesize, and evaluate the potential new high-capacity cathodes within Li-Ni-O composition space using the percolation theory as a guideline.

**Project Impact.** In commercial Li-ion batteries, the well-ordered, close-packed oxides, particularly, layered lithium TM oxides ( $\text{LiTmO}_2$ , Tm is transition metal) are widely used. However, the energy density needs to be at least doubled to meet the performance requirements of EVs (300 to 400 miles). Although capacities approaching 300 mAh/g have been reported in Li-, Mn-rich layered oxide compounds, capacity decay and voltage fading in the long-term cycling are always observed. Therefore, new materials are urgently needed to make the breakthrough in Li-ion battery technology.

**Approach.** The recent discovery of high-capacity materials with lithium excess provides new insights into design principles for potential high-capacity cathode materials. According to the percolation theory, lithium excess is required to access 1 lithium exchange capacity in  $\text{LiTmO}_2$  compounds. This seems to be independent of TM species; therefore, it could open a composition space for the search of new materials with high capacity. The interesting  $\text{Ni}^{2+}/\text{Ni}^{4+}$  redox is selected as the electrochemically active component, and combinatorial materials design concept will be used to discover the potential cathode material candidates in the Li-Ni-O phase space.

**Out-Year Goals.** The long-term goal is to search new high-energy cathodes that can potentially meet the performance requirements of EVs with a 300- to 400-mile range in terms of cost, energy density, and performance. Work will progress from the understanding of the known compounds,  $\text{LiNiO}_2$  and  $\text{Li}_2\text{NiO}_2$ , toward the development of new Ni-based high-energy cathode oxides.

**Collaborations.** The project closely collaborates with M. Doeff (LBNL) on soft X-ray absorption spectroscopy (XAS), C. Ban (NREL) on ALD coating, B. McCloskey (LBNL) for differential electrochemical mass spectrometry (DEMS), and R. Kostecki (LBNL) for Raman spectroscopy. Collaboration is also in progress with other BMR PIs (X.-Q. Yang and F. Wang, BNL; and K. Persson, LBNL) for crystal structure evolution on cycling and material computation.

### Milestones

1. Use Li-, Mn-rich oxide as the baseline material; develop synthesis that can be used to screen the second TMs for Li-rich Ni-based oxides. (December 2016 – Complete)
2. Design the Li-rich Ni-based oxide compositions, and perform the synthesis of the designed compositions. (March 2017 – In progress)
3. Complete the electrochemical tests on the synthesized Li-rich Ni-based oxides. Down select one composition that shows promising electrochemical performance with an initial capacity  $> 200$  mAh/g. (June 2017)
4. Complete the structural characterization of the selected composition, and compare the performance with Li-, Mn-rich oxide baseline. (September 2017)

## Progress Report

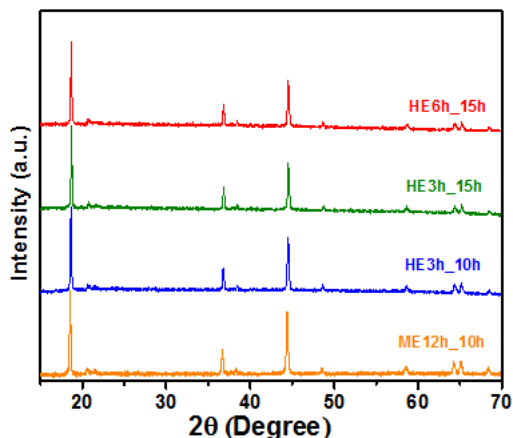


Figure 24. X-ray diffraction patterns of  $\text{Li}_{1.2}\text{Mn}_{0.6}\text{Ni}_{0.2}\text{O}_2$  samples prepared by a solid-state method. Samples are denoted by milling energy followed by milling time, and annealing time.

After the  $\text{Li}_{1.2}\text{Mn}_{0.6}\text{Ni}_{0.2}\text{O}_2$  samples were prepared, they were formulated into electrodes and subjected to an electrochemical test to investigate the effect of synthetic conditions on the electrochemical performance. The first-cycle voltage profiles of these four samples are shown in Figure 25. The cells were cycled between 2 and 4.8 V at a current density of 25 mA/g (C/10, capacity at 1C was defined as 250 mAh/g). Overall, all samples demonstrated similar voltage profiles, consisting of a plateau region at a voltage around 4.5 V during the first charge that is often referred to as electrochemical activation process, as well as a sloping region during the discharge. Despite invisible difference in XRD patterns, a difference was evidenced by a prolonged profile toward the end of charging and discharging. It can be clearly seen that the  $\text{Li}_{1.2}\text{Mn}_{0.6}\text{Ni}_{0.2}\text{O}_2$  sample prepared at a high energy for 3 h and annealing for 15 h delivered the highest discharge capacity (259 mAh/g) that is associated with 0.82 lithium per formula. In comparison, the discharge capacity of the sample prepared at a medium energy was only 215 mAh/g. This capacity was about 17% lower compared to the best sample (HE3h\_15h), although the XRD patterns of these two samples were similar. This clearly translates into the difference in  $\text{Li}_{1.2}\text{Mn}_{0.6}\text{Ni}_{0.2}\text{O}_2$  active material rather than process variables (that is, slurry formulation, electrode fabrication, and cell assembly). Simply comparing these two samples led to a combined effect of milling method and annealing time. In contrast to the crystallographic information extracted from XRD, the project clearly observed the effect of synthetic conditions on the electrochemical performance. It would be interesting to elucidate the correlation between the synthesis and performance and identify the key variables that govern the electrochemical properties. Additionally, the optimal synthetic condition for  $\text{Li}_{1.2}\text{Mn}_{0.6}\text{Ni}_{0.2}\text{O}_2$  will be used to prepare other Li-rich oxide cathodes.

The  $\text{Li}_{1.2}\text{Mn}_{0.6}\text{Ni}_{0.2}\text{O}_2$  samples were synthesized via a solid-state method using  $\text{Li}_2\text{CO}_3$ ,  $\text{Ni}(\text{OH})_2$ , and  $\text{MnCO}_3$  precursors. Raw materials were mixed by a mechanical milling process, and then annealed at 950°C. The synthetic variables include milling energy, milling time, and annealing time. This information is used to denote the samples prepared under varied conditions. For example,  $\text{Li}_{1.2}\text{Mn}_{0.6}\text{Ni}_{0.2}\text{O}_2$  sample that was prepared at a medium energy (ME) for 12 h, and annealing for 10 h, is denoted as ME12h\_10h. HE3h\_15h represents the precursors that were mixed at a high energy (HE) for 3 h, then annealed for 15 h. Figure 24 shows the XRD patterns of all four  $\text{Li}_{1.2}\text{Mn}_{0.6}\text{Ni}_{0.2}\text{O}_2$  samples. Generally, all samples demonstrated similar XRD patterns consistent with those reported in the literature. Based on the results, no significant effect of the synthetic condition on the crystal structure of  $\text{Li}_{1.2}\text{Mn}_{0.6}\text{Ni}_{0.2}\text{O}_2$  was detected by XRD.

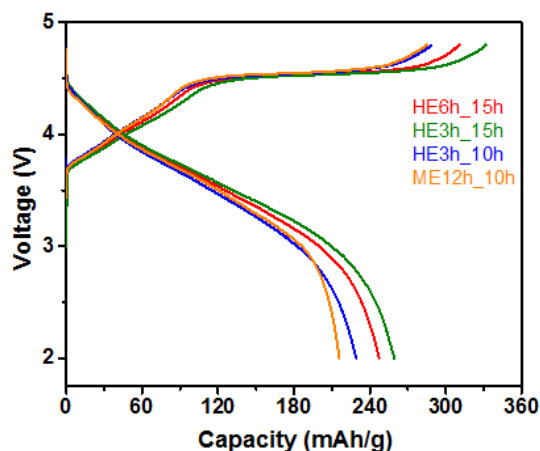


Figure 25. The first-cycle voltage profiles of  $\text{Li}_{1.2}\text{Mn}_{0.6}\text{Ni}_{0.2}\text{O}_2$  samples prepared by a solid-state method. Cells were cycled between 4.8 and 2 V at a current of 25 mA/g.



## Patents/Publications/Presentations

### Publication

- Xu, Jing, and En-Yuan Hu, Dennis Nordlund, Apurva Mehta, Steven N. Ehrlich, Xiao-Qing Yang, and Wei Tong. “Understanding the Degradation Mechanism of Lithium Nickel Oxide Cathode for Li-ion Batteries.” *ACS Applied Materials & Interfaces* 8 (2016): 31677–31683.
- Xu, Jing, and Feng Lin, Marca M. Doeff, and Wei Tong. “A Review of Ni-based Layered Oxides for Rechargeable Li-ion Batteries.” *Journal of Materials Chemistry A* 5 (2017): 874–901.

### Presentations

- 12<sup>th</sup> Annual Lithium Battery Power, Bethesda, Maryland (November 2016): “High-Capacity Ni-Based Layered Oxide Cathode for Li-Ion Batteries”; Wei Tong and Jing Xu. Invited.
- Electrochemical Society (ECS), 230<sup>th</sup> Meeting, Honolulu (October 2016): “Understanding the Degradation Mechanism of Lithium Nickel Oxide Cathode for Li-Ion Batteries”; Wei Tong and Jing Xu.

## TASK 4 – ELECTROLYTES

### Summary and Highlights

The goal of the BMR Program is to develop long-life batteries superior to commercial Li-ion systems in terms of cost, vehicle range, and safety. The BMR Program addresses the fundamental problems of electrode chemical and mechanical instabilities that have slowed development of affordable, high performance, automotive batteries. The aim is to identify electrode/electrolyte materials that yield enhanced battery performance and lead to greater acceptance of EVs.

Currently, the VTO supports seven projects in the BMR Program under the Electrolytes area. These projects can be categorized into three general topics:

- **Liquid.** The projects for liquid electrolyte aim to develop an atomic/molecular level understanding of the stability of electrochemical interfaces during charge-discharge cycling to stabilize solid /liquid interfaces in Li-ion batteries. In addition, electrolyte formulations, based on fluoro-chemistries, will be developed to achieve significantly improved operating voltage, increased durability, and increased energy density of Li-ion batteries at a reasonable cost.
- **Polymer.** The target of polymer electrolyte projects is mainly for use in Li-S batteries. Inorganic/polymer and polymer/gel hybrid electrolytes that have flexibility, mechanical strength, thermal stability, high ionic conductivity, stable interfaces against lithium metal, and polysulfide-trapping capability will be developed to enable energy densities twice that of the start-of-the-art Li-ion batteries, with comparable cycle life.
- **Self-Forming & Self-Healing.** The self-forming and self-healing electrolyte projects focus on developing and implementing Li-metal-based metal fluorite and metal iodide batteries, capable of energy densities > 400-500 Wh/kg and 1000 Wh/L.

**Highlights.** This quarter, the ANL group demonstrated the first-of-its-kind experiment of *in situ* dissolution of cobalt monitored by using a SPRDE-ICP-MS (stationary probe rotating disk electrode, and inductively coupled plasma with mass spectrometry) setup. The work is to underpin the instabilities of  $\text{LiCoO}_2$  at higher potentials.

## Task 4.1 – Understanding and Mitigating Interfacial Reactivity between Electrode and Electrolyte (Khalil Amine, Larry A. Curtiss, and Nenad Markovic, Argonne National Laboratory)

**Project Objective.** This project aims to develop an understanding, at atomic/molecular levels, of the stability of electrochemical interfaces during charge-discharge cycling and use the knowledge for stabilizing solid/liquid interfaces in Li-ion batteries. The goal is to improve the stability of solid/liquid interfaces using insights into the atomic/molecular processes that limit stability during cycling. The core of this proposal is to identify, rationalize, and understand the dynamics of the dissolution processes of 3D-TM cations in the cathode materials, the stability of various commercial and highly purified electrolytes comprised of organic solvents, salts, and additives, and the evolution of O<sub>2</sub> and other gaseous products formed from the electrode material or the electrolyte during the charging-discharging of the Li-ion battery.

**Project Impact.** The instability of the solid-liquid interfaces during cycling limits use of novel cathodes such as 6:2:2 and 8:1:1 NMC cathodes with higher voltage and higher power densities. Stabilization of solid/liquid interfaces in Li-ion batteries can lead to enhanced performance and increased safety.

**Approach.** This project follows an integrated program focused on solid-liquid interfaces in Li-ion batteries using state-of-the-art *in situ* characterization tools and computational modeling to understand and design interfaces with enhanced stability. The range of high-end analytical tools includes: (1) a three-electrode RDE setup; (2) ICP-MS; (3) Gas Chromatography with Triple Quadrupole MS (GC-QqQ) in Headspace sampling (HS) mode; and (4) DEMS. High precision electrochemical measurements in combination with *in situ* measurements and characterization are highly suitable to investigate correlation of stability with a number of electrochemical, structural, and compositional properties of the interfaces. Computational methods that provide reaction energies and barriers as well as structural information at the atomic level will be used to predict and test possible reactions that affect the stability of solid-liquid interfaces.

**Out-Year Goals.** Work will progress toward more comprehensive *in situ* characterization and integrated modeling capabilities with applications to solid liquid interfaces of electrolytes and 6:2:2 NMC cathodes. If the project can harness the complexity that governs instability of the interface, it should be possible to move far beyond the current state-of-the-art Li-ion systems as well as create new avenues for the design and deployment of cathode materials and electrolytes.

**Collaborations.** This project funds work at ANL and PNNL. Zonghai Chen, Sanja Tepavcevic, Pietro Papa Lopes, and Peter Zapol, all of ANL, contribute to the project.

### Milestones

1. Perform first *ex situ* measurements of electrode/electrolyte decomposition products using ICP-MS and GC-MS. (Q1)
2. Develop protocol for calculating electrochemical reactions at electrolyte-electrode interfaces. (Q1)
3. Build a new 16-channel high-precision electrochemical measurement system dedicated to this project. (Q2)
4. Benchmark the kinetics of direct electrochemical oxidation of baseline electrolyte at different potentials. (Q3)
5. Coupling of ICP-MS with electrochemical cell for the direct *in situ* investigation of the metal dissolution from the cathode. (Q4)

## Progress Report

Figure 26 shows the home-built high precision electrochemical measurement system, as well as a schematic of its use to characterize the kinetics of parasitic reactions occurring at the surface of working electrodes. In principle, the half-cells are constant-voltage charged/discharged to a desired potential, and the potential is held at the specific value for up to 20 hours. Then, the static leakage current is obtained as the indicator of the rate of parasitic reactions between the working electrode and the electrolyte. In addition, the cells are conditioned in an environmental chamber, which enables measurement of the kinetics of the parasitic reactions.

The project demonstrated its newly developed high-precision electrochemical measuring system for stability studies by revisiting the corrosion (or anodic dissolution) process of aluminum foils in nonaqueous electrolytes. Figure 27 shows that the measured static leakage current grows roughly exponentially with the applied potential, indicating an ongoing electrochemical oxidation of electrolyte on the carbon-coated aluminum foil. Figure 27b shows that the measured parasitic current increased exponentially with the holding potential, indicating an electrochemical oxidation of a certain species on the aluminum surface. It is the project's hypothesis that this reaction is related to the oxidation of ethylene carbonate. DFT calculations using models representative of current collector's surface basic groups indicate that redox potential can decrease even more than that when the proton is transferred to either hydroxyl (by 1.4 to 2.5 V) or thiol group (by 1 to 2 V) coordinated to aluminum. Larger calculations on either hydroxyl group or a bridging oxygen site on amorphous alumina models similarly indicate that the alumina promotes the deprotonation reaction for the radical cation (EC<sup>+</sup>). It was found that the degradation of aluminum foil at high potentials is a coupled electrochemical-chemical reaction; the electrochemical oxidation of organic solvents at high potentials triggers the chemical corrosion of aluminum foils.

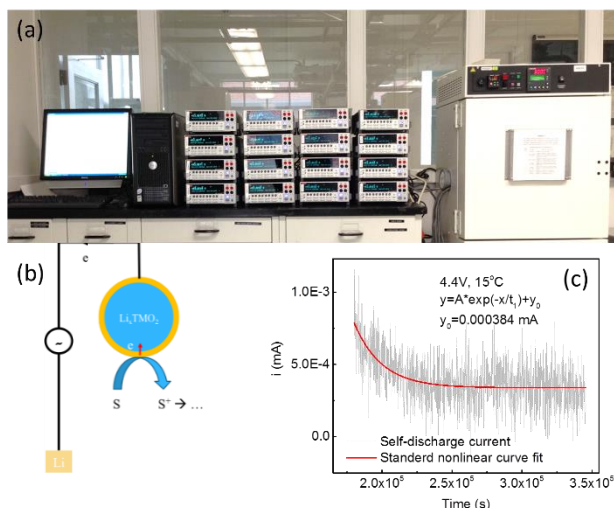


Figure 26. (a) Picture of a 16-channel high precision leakage current measuring system. (b) Schematics showing the connection between the leakage current and the rate of parasitic reactions. (c) A typical current relaxation curve collected to extract the static leakage current.

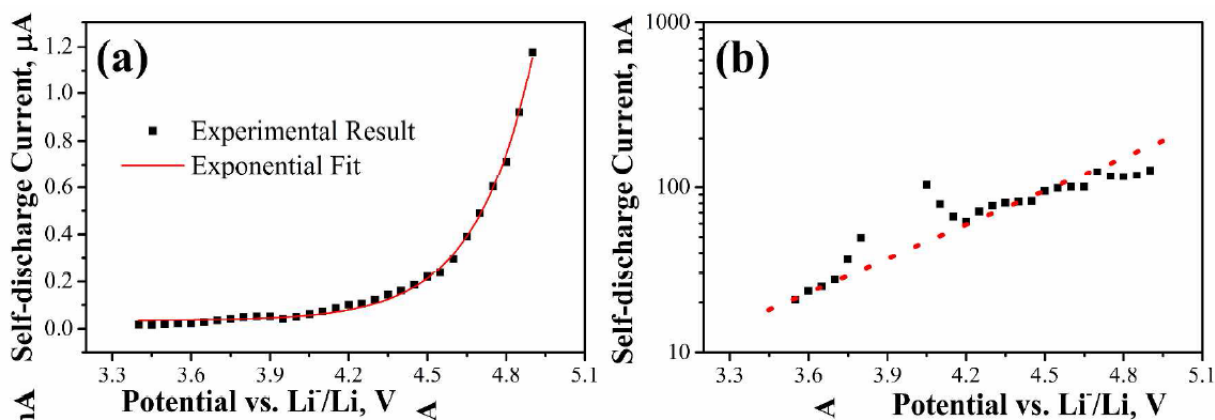


Figure 27. Evolution of the static parasitic current as a function of the holding potential for (a) carbon black cast on aluminum foil, and (b) the bare aluminum foil. The electrolyte used was 1.2 M LiPF<sub>6</sub> in EC/EMC (3:7 by mass).

Experiments done on a three-electrode setup enable identification of electrochemical currents arising solely from the cathode material. To underpin the instabilities of  $\text{LiCoO}_2$  at higher potentials, the first-of-its-kind experiment of *in situ* dissolution of cobalt monitored by a SPRDE-ICP-MS setup is shown in Figure 28. With a stationary probe for coupling to ICP-MS, it is noted that with the current methodology the project can probe the kinetics of intercalation/de-intercalation and kinetics of 3D-TM ions dissolution simultaneously as a function of time and potential. For example, while up to 4.2 V de-intercalation of lithium is already taking place (Figure 27), the project observes significant dissolution of cobalt only above 4.5 V versus  $\text{Li/Li}^+$ , indicative that

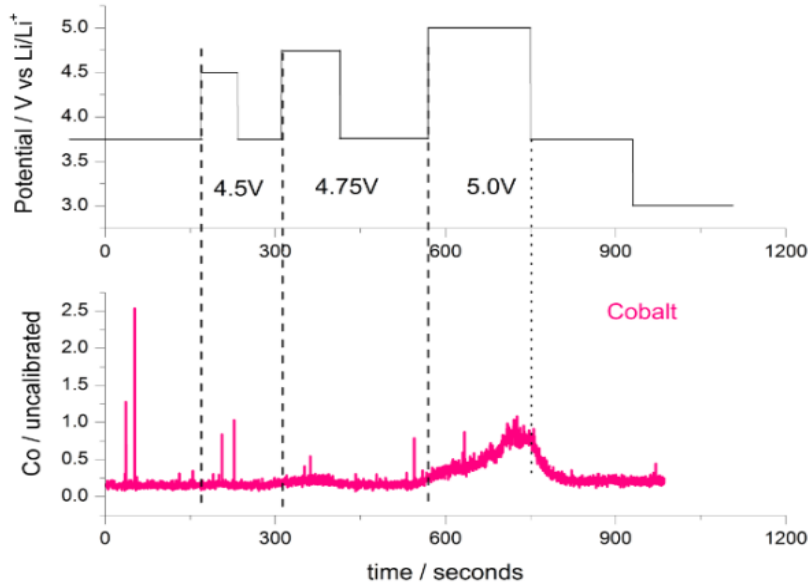


Figure 28. The initial inductively coupled plasma with mass spectrometry (ICP-MS) results of Co dissolution upon electrochemical polarization using a stationary probe rotating disk electrode system. Working electrode:  $\text{LiCoO}_2/\text{C}/\text{PVDF}$ . Electrolyte: 1M  $\text{LiPF}_6$  in EC:EMC (3:7 by mass).

interplay between charging/discharging processes to corresponding cobalt dissolution may occur. Moreover, at high electrode potentials, the time transient profile of cobalt dissolution shows an increase with longer polarization period (Figure 28). This effect can be correlated not only to intrinsic kinetics of dissolution and de-intercalation of  $\text{LiCoO}_2$ , but also from a morphological effect arising from the electrode thickness. Although the results shown in Figure 28 represent a proof of concept, the project emphasizes that these first experiments already demonstrate the power of such methodology in gaining fundamental knowledge on electrochemical interfaces of high energy cathodes, inaccessible by conventional battery testing.

## Task 4.2 – Advanced Li-ion Battery Technology: High-Voltage Electrolyte (Joe Sunstrom and Ron Hendershot, Daikin)

**Project Objective.** The overall project objective is to identify electrolyte formulations, based on fluoro-chemistries, that will allow significantly improved operating voltage, increased durability, and increased energy density of Li-ion batteries at a reasonable cost. The specific objective of the project is to understand the conditions under which the electrolyte degrades, the effect on battery performance, and solutions that can overcome current limitations of the electrolyte. The strategy is to select from a range of available fluorinated chemistries those combinations that provide the highest possible battery voltages, greater than 4.5 V, while keeping incremental battery cost increase as low as possible.

**Project Impact.** An understanding of the failure mechanisms for both state-of-the-art hydrocarbon and fluorocarbon electrolytes as they pertain to various cell chemistries is ultimately valuable in the design of future high-performance batteries. Electrolyte degradation has been a key limiting factor in development of new Li-ion technology. The ability to stop/significantly slow down this degradation opens a whole new level of design for rechargeable batteries.

**Approach.** The evolving composition of the electrolyte in the battery will be examined by a variety of analytical instrumentation to study the gas (GC/MS), liquid chromatography (LC/MS) and solid (TOF-SIMS, TGA/MS, XRD) electrolyte decomposition products during battery operation. In the first year, the team will address the gas composition and kinetics for both hydrocarbon and fluorocarbon as a function of several charge/discharge conditions that include (but are not limited to) electrode composition, operational voltage and current, temperature, and cycle number.

**Out-Year Goals.** Work will progress toward formulating rough mass balances of the both fluorinated and hydrocarbon electrolytes under the performance parameters suggested. Specifically, analysis of the liquid and solid decomposition products will be pursued. Understanding how the mass balance and kinetics change will give information on decomposition pathways and allow for solutions to be formulated to increase battery performance.

### Milestones

1. Establish baseline and review current state-of-the-art. Compile baseline electrochemical and physical property specification for current best practice electrolyte. (In progress)
2. Determination of gas composition. Failure mechanisms are understood, and mitigation strategies/additives are selected for interim cells. (In progress)

## Progress Report

Initial work has been divided into two tasks that progress against the first two milestones: (1) establishing a baseline on knowledge learned from the first DOE funding opportunity, and (2) initiating setup of instruments and samples for gas analysis. Daikin furnished a final set of optimized best guess cells to the DOE to fulfill the previous funding opportunity. The cells were sent to ANL in October and are still on test. The completion of the performance tests will be the final data needed to complete the first milestone. The cells are being tested at 4.5 V and 4.6 V, which is believed to be the performance limit of the current fluorinated electrolyte. For this project, 3 voltages are being considered for evaluation: 4.2 V (both hydrocarbon and fluorocarbon stable), 4.5 V (hydrocarbon unstable, fluorocarbon stable) and 4.6 V (both hydrocarbon and fluorocarbon unstable). Samples of NMC-111/graphite cells have been charged at all three test voltages and have been disassembled while charged to the appropriate test voltage. Measured pieces have been cut and placed into pouches containing both the

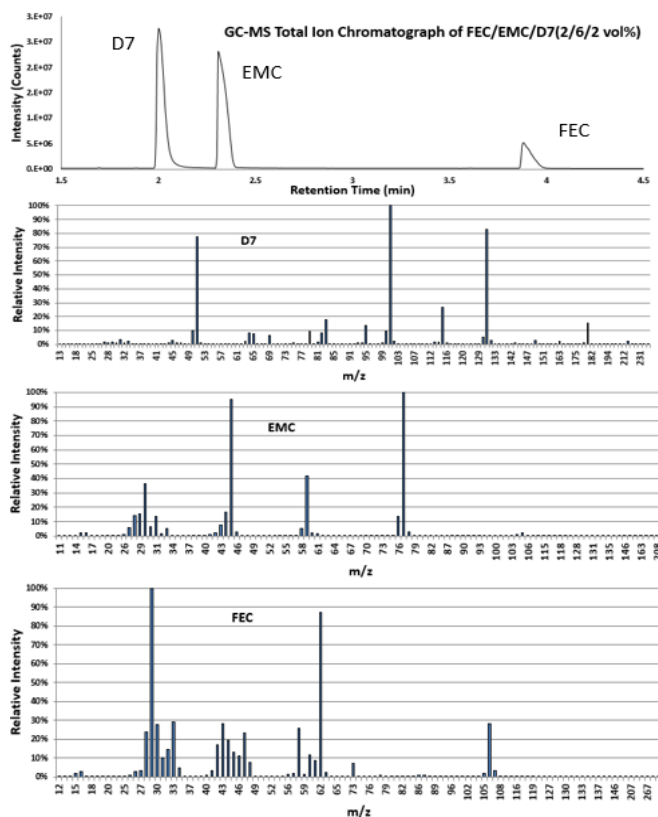


Figure 30. Baseline gas chromatography – mass spectrometry data for baseline fluorinated electrolyte.

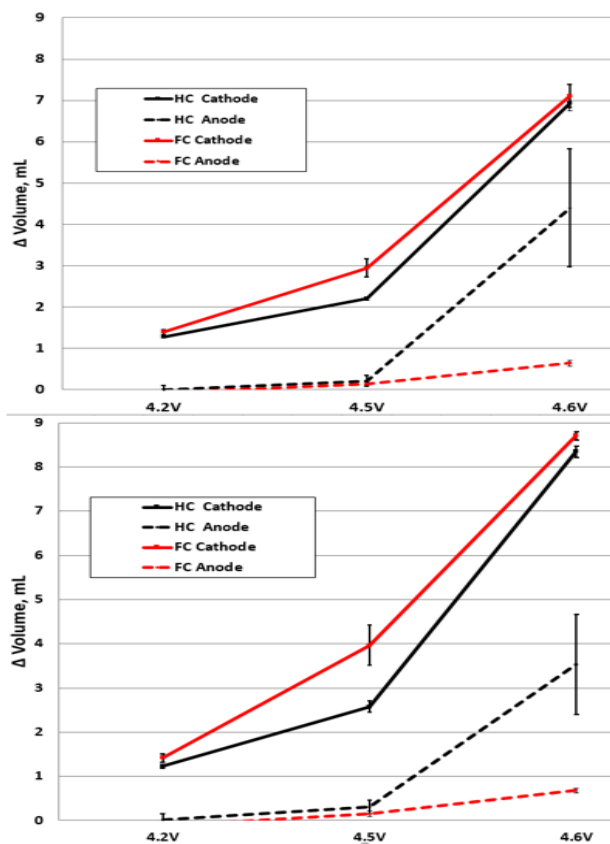


Figure 29. Volume change as function of voltage at 4.2, 4.5 and 4.6 V for both cathode and anode exposed to hydrocarbon and fluorocarbon electrolyte.

hydrocarbon and fluorocarbon control. The pouches are then stored at 60°C. The data collected here establishes gassing baseline for the cell and provides samples for gas analysis. The data are shown in Figure 29 at 3 and 4 weeks. The main result is a significant gassing increase at the anode above 4.5 V.

Significant time this quarter was spent preparing instrumentation, tooling, and procedures to accomplish the gas analysis objectives in the first year. This included design and construction of a fixture for gas sampling from pouch cells, establishment of repeatable procedures, and setup/calibration of GC/MS and LC/MS equipment. In addition, several baseline runs for the existing best practice electrolytes were completed. An example is shown in Figure 30.

## Task 4.3 – Multi-Functional, Self-Healing Polyelectrolyte Gels for Long-Cycle-Life, High-Capacity Sulfur Cathodes in Lithium-Sulfur Batteries (Alex Jen and Jihui Yang, University of Washington)

**Project Objective.** The project objective is to develop self-healing and polysulfide-trapping polyelectrolyte gels containing room-temperature ionic liquid (RTIL) for the Li-S battery system. The battery design will be capable of achieving gravimetric and volumetric energy densities of  $\geq 800$  Wh/kg and  $\geq 1000$  Wh/L, respectively.

**Project Impact.** The Li-S battery system is currently hampered by poor capacity retention, primarily caused by dissolution of polysulfide reaction intermediates in typical organic electrolytes, as well as poor electrical contact between insulating sulfur and the conductive carbon matrix. This project aims to produce a high-capacity, long-cycle-life Li-S battery system by using rational molecular design strategies to address each capacity loss mechanism directly. A long-cycle-life Li-S battery system with the capability of doubling Li-ion energy density would enable production of lighter, longer range EVs at a cost that is affordable to the average U.S. household.

**Approach.** The team will develop Li-S coin cells that utilize self-healing, interpenetrated ionomer gel electrolytes in both the cathode and separator. The team will synthesize necessary starting materials and fabricate components of these gels while testing their relevant electrochemical and mechanical properties. All components will be combined into interpenetrating structures, which will be tested both alone and in cell configurations. Device performance data will be collected and used to further optimize designs of both material and cell, culminating in an optimized Li-S battery design capable of doubling the energy density of traditional Li-ion batteries. During the first year, the team is focusing on (1) synthesis of a variety of precursors for gel electrolytes, (2) fabrication and testing of both baseline materials, and novel materials made from these precursors, and (3) iterative validation and improvement of design principles through both materials and device testing.

**Out-Year Goals.** Work will progress toward developing structure-property relationships for the self-healing, interpenetrated gel ionomer electrolyte and its individual components, as well as successful incorporation of such an electrolyte into a working Li-S cell. The team plans to demonstrate significant improvements in both capacity and retention when using the project's novel materials, as compared to state-of-the-art baseline systems.

**Collaborations.** This project funds work at the University of Washington – Seattle. Dr. Alex Jen (PI) focuses on the design, synthesis, and testing of novel materials, as well as device-based verification of design principles. Dr. Jihui Yang (Co-PI) focuses on optimization of device fabrication and testing, as well as investigation of failure mechanisms in devices using novel materials. Facilities at PNNL in Richland, Washington, will be used for detailed study of device operation.

### Milestones

1. Synthesize organic starting materials, and demonstrate both an ionomer gel electrolyte and a self-healing film based on these materials. (Q3 – In progress)
2. Integrate S/C composites into Li-S coin cells, and cycle them both with an organic electrolyte system and with several novel gel electrolyte systems. (Q4)



## Progress Report

**Facilities.** Equipment and supplies were ordered, and setup of a new facility for small-scale device testing is in progress and expected to be completed next quarter.

**Organic Synthesis.** Chemical synthesis of first-generation novel starting materials (Figure 31) was performed, including PyrTFSIMA and a trivalent physical cross-linker bearing pyrene units. Several starting materials, including ionic liquids, PENDI, and TEGMA were synthesized previously.

**Noncovalent Interactions.** To better understand the reversible intermolecular interactions meant to impart self-healing properties to the project's gel, a series of spectroscopic and electrochemical tests were performed on model pyrene and NDI compounds. Equal concentrations of pyrene and NDI derivatives were mixed together and UV-vis spectra taken of the resulting solutions (Figure 32). A new charge transfer absorption peak at 500 nm was found to emerge upon mixing of the species, ascribed to the complex formed via their  $\pi$ - $\pi$  stacking interaction. This absorption increases linearly with concentration between 0.005 M – 0.03 M in dichloromethane, allowing direct study of interaction strength. CV of both species showed that in the operating range of a sulfur cathode, pyrene has no significant electrochemical activity, while NDI undergoes two reversible reductions. Combining the species in a 1:1 ratio did not appear to introduce any new electrochemical features, although both reductions were shifted by about +0.3V.

**Lithium Metal Cycling in Ionic Liquid.** To investigate the lithium dendrite resistance and interface-forming abilities of RTIL electrolytes, symmetric cells containing a glass fiber separator wetted with electrolyte and sandwiched between two pieces of pristine lithium foil were fabricated and subjected to cyclic stripping/plating at 22°C. Cells with electrolytes containing only the TFSI anion produced large (>100 mV) and unpredictable overpotentials, culminating in cell failure due to excessive voltage (Figure 33a), whereas cells with electrolytes containing only the FSI anion displayed exceptionally low and stable overpotential during stripping/plating after an initial “formation” period (Figure 33b). It was found that “FSI-like” cycling behavior could be produced in electrolytes with greater than 25mol% FSI content. No cells short-circuited at any time during testing, demonstrating the dendrite-inhibiting effect of these electrolytes.

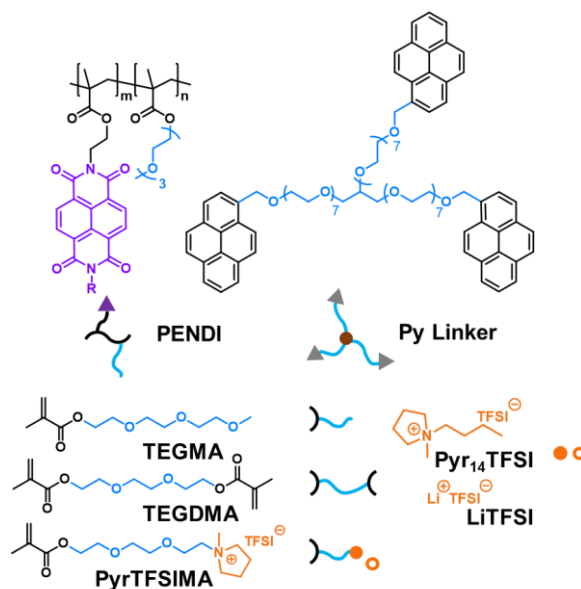


Figure 31. First-generation organic starting materials for novel polyelectrolyte gels, all of which have now been synthesized or acquired commercially.

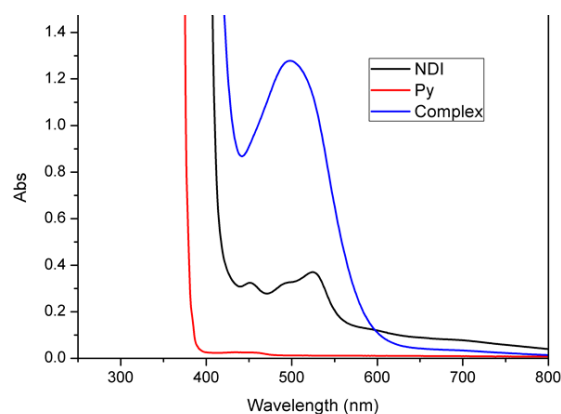
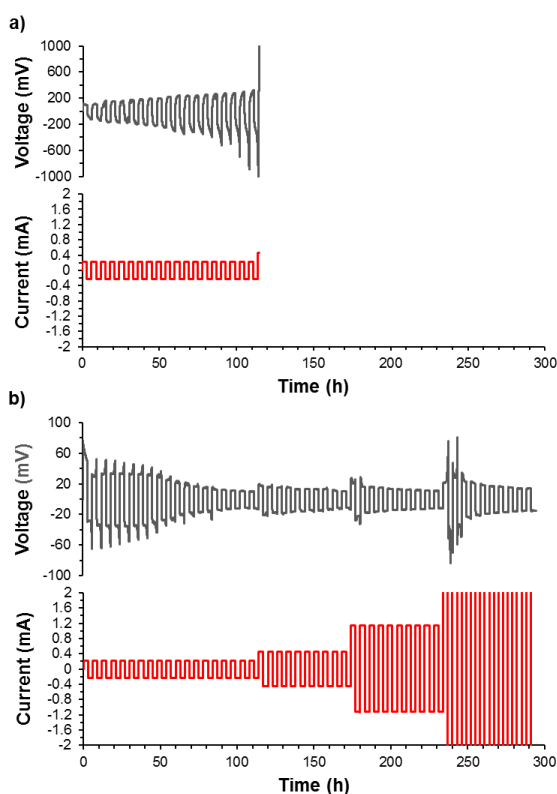


Figure 32. Mixing solutions containing model pyrene and NDI species results in a new absorption peak at 500 nm (visible as a deep red color).

**Baseline Li-S Cell Fabrication.** Several Li-S concept cells were fabricated and cycled at C/10 rate to establish baseline performance. Initial cells containing sulfur particles physically ground with carbon black showed low capacity (< 50% of theoretical); those cells with organic electrolyte manifested a significant overcharge problem, while cells with RTIL electrolyte did not (Figure 34), demonstrating the low solubility of polysulfide intermediates in RTIL. Iterative improvements in electrode fabrication allowed S/C black cells to reach initial capacities in excess of 1200 mAh/g; however, overcharge problems persist with organic electrolyte. To demonstrate the importance of SEI properties on the anode, 1-2 wt%  $\text{LiNO}_3$  was added to the organic electrolyte. This severely reduced or eliminated overcharge during the first cycle, along with increasing initial capacity.

**Synthesis of S/C Composites.** To improve electrical contact and inhibit polysulfide dissolution, sulfur was infiltrated into the pores of ketjen black (0.6:1 S:C weight ratio) via melt diffusion at  $150^\circ\text{C}$ . A significant decrease in specific surface area and pore volume, measured using  $\text{N}_2$  absorption isotherms, confirmed successful infiltration. Further tests on these S/C composites, and cathodes fabricated with them, are in progress.



**Figure 33.** (a) Symmetric cell with TFSI-only room-temperature ionic liquid (RTIL) electrolyte displays high overpotential that quickly grows out of control. (b) FSI-only RTIL electrolyte, with the same pyrrolidinium cation and  $\text{Li}^+$  molar concentration, displays low and continuously decreasing overpotential (note the change in scale), even at increasing current rates.

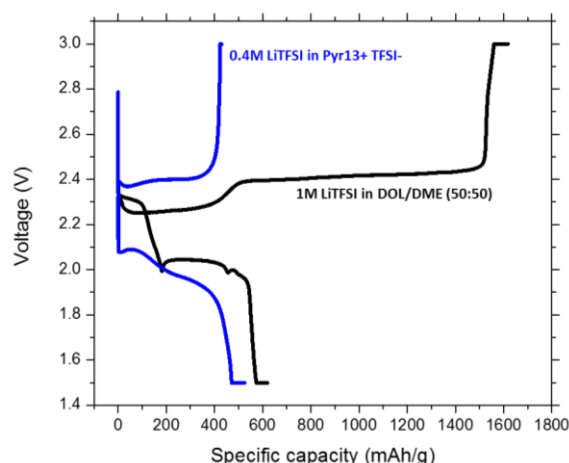


**Figure 34.** Elimination of overcharge (polysulfide redox shuttle) in Li-S cells with room-temperature ionic liquid electrolyte, as opposed to additive-free organic electrolytes, which cause severe overcharge issues.

## Task 4.4 – Development of Ion-Conducting Inorganic Nanofibers and Polymers (Nianqiang (Nick) Wu, West Virginia University; Xiangwu Zhang, North Carolina State University)

**Project Objective.** The project objective is to develop solid-state electrolytes based on the highly-conductive inorganic nanofibrous network in the polymer matrix for lithium batteries.

**Project Impact.** The research team will conduct research and development on solid-state inorganic nanofiber-polymer composite electrolytes that will not only provide higher ionic conductivity, improved mechanical strength, and better stability than the polyethylene oxide polymer electrolyte, but also exhibit better mechanical integrity, easier incorporation, and better compatibility with the Li-metal anode than the planar ceramic membrane counterparts. The proposed inorganic nanofiber-polymer composite electrolytes will enable practical use of high-energy-density, high-power-density Li-metal batteries and Li-S batteries.

**Approach.** Integration of the highly Li<sup>+</sup>-conductive inorganic nanofiber network into the polymer matrix not only provides the continuous Li<sup>+</sup> transport channels, but also kinetically inhibits the crystallization from the amorphous state of polymer electrolyte. The inorganic nanofibers will be fabricated with an electrospinning technique; and the ionic conductivity of inorganic nanofibers will be improved by chemical substitution or doping. Highly ionic-conductive polymers will be developed by cross-linking and/or creation of a block-copolymer structure; and the composition and microstructure of the composite electrolyte will be designed to suppress the lithium dendrite formation.

**Out-Year Goals.** Work will progress toward synthesis of the inorganic nanofibers and the polymer matrix. The goal is to find the optimal synthetic route to achieve the desirable conductivity.

**Collaborations.** This project funds work at West Virginia University (WVU) and North Carolina State University (NCSU). Sujun Kasani (Ph.D. student, WVU), Chaoyi Yan (Ph.D. student, NCSU) and Mahmut Dirican (Postdoctoral Fellow, NCSU) contributed to the project.

### Milestones

1. Attend the kick-off meeting. (Q1– Complete)
2. Delegate tasks and clarify technical aspects among collaborators. (Q1 – Complete)
3. Select the lithium ionic-conductive materials, and develop the doping strategy. (Q1 – Complete)
4. Synthesize the inorganic nanofibers by the electrospinning technique. (Q2 – In progress)
5. Design new ionic-conductive polymers via cross-linking and formation of block-copolymer. (Q1 – In progress)
6. Synthesize the ion-conducting polymers. (Q1 – In progress)

## Progress Report

**Administrative.** Postdoctoral Fellows were recruited and are in the visa application process. Subcontracts were completed in November.

**Synthesis of Inorganic Nanofibers.** To achieve improved ionic conductivities, synergistic effects of molybdenum (Mo) and aluminum (Al) doping on lithium lanthanum zirconium oxide (LLZO) nanofibers were investigated. In the previous study, the ionic conductivity of Mo-doped garnet-type oxide ( $\text{Li}_{6.5}\text{La}_3\text{Zr}_2\text{Mo}_{0.5}\text{O}_{12}$ ) reached  $0.8 \text{ mS/cm}$ .<sup>1</sup> Al doping may further increase the ionic conductivity of  $\text{Li}_{6.5}\text{La}_3\text{Zr}_2\text{Mo}_{0.5}\text{O}_{12}$  due to the stabilization of cubic phase at room temperature. Al-doped nanofibers with different Al concentrations were prepared by electrospinning process, which had the general formula as  $\text{Li}_{6.7-3x}\text{La}_3\text{Al}_x\text{Zr}_{1.85}\text{Mo}_{1.5}\text{O}_{12}$  ( $x=0.05, 0.1, 0.15$ ). Uniform nanofiber mats were obtained by peeling off the as-spun nanofibers from the collector and stored in vacuum dryer for 24 h. The thickness of the nanofiber mats was around 2 mm. As-spun nanofiber samples were calcinated at  $700^\circ\text{C}$  for 1 h, 1.5 h, and 2 h, respectively. The calcination process was performed to decompose the PVP polymer and crystallize the LLAZMO to form stable cubic garnet nanofibers. Different heating times were applied to investigate the morphology and phase evolution of LLAZMO nanofibers. Figure 35 shows the photographs of as-spun precursor nanofibers and calcinated inorganic nanofibers. In future studies, the project will characterize the structure of Al-doped inorganic nanofibers prepared with different calcination parameters, and determine the optimum calcination temperature and time.

### Synthesis of Polymer Matrix.

Precursors and monomers for block co-polymers were synthesized. Two lithium salt-based monomers and one polyethylene oxide (PEO)-based monomer were selected for block co-polymer synthesis: (a) lithium poly[(4-styrenesulfonyl) (trifluoromethanesulfonyl)imide] (LiPSTFSI), (b) lithium poly[(4-styrenesulfonyl) (trifluoromethyl(S-tri-

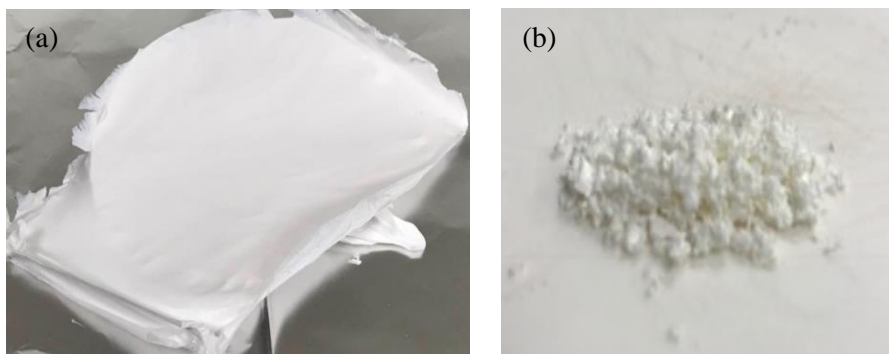


**Figure 35. Photographs of (a) as-spun precursor nanofibers, and (b) calcinated Al-doped inorganic nanofibers.**

fluoromethylsulfonylimino)sulfonyl)imide] (LiPSsTFSI), and (c) methoxy-polyethylene glycol acrylate (MPEGA). Two different block co-polymers, that is, LiPSTFSI-MPEGA-LIPSTFSI (a) and LiPSsTFSI-MPEGA-LiPSsTFSI (b), are being synthesized. For both co-polymers, the lithium salt-based blocks are single-ion conducting, containing highly delocalized polyanions to trap anions inside the polymer structure. These single-ion conducting blocks give relatively higher ionic conductivity and nearly 100%  $\text{Li}^+$  transference number. Compared with LiPSTFSI, LiPSsTFSI has a more delocalized structure due to the stronger electron-withdrawing group ( $=\text{NSO}_2\text{CF}_3$ ). Therefore, the electrochemical performance of LiPSsTFSI-based block co-polymer is expected to be better than that of LiPSTFSI-based copolymer. In this work, both structures are being synthesized for comparison, and the ratio of lithium salt-based block to PEO-based block will be kept the same in both cases. The PEO-based block is used to provide excellent mechanical stability to the resultant triblock polymers.

This quarter, the two-step synthesis of monomer STFSI was accomplished, and the four-step synthesis of monomer SsTFSI was partially completed at Step 3. Fourier transform infrared spectroscopy (FTIR) was used to verify the reaction products. Figure 36 shows the FTIR spectrum of 4-vinylbenzenesulfonyl chloride, which is the product of the first synthesis step of monomer STFSI. The characteristic peaks for 4-vinylbenzenesulfonyl chloride can be determined:  $1591\text{ cm}^{-1}$  for aryl stretching,  $1399\text{ cm}^{-1}$  and  $1170\text{ cm}^{-1}$  for sulfonyl (S=O) stretching, and  $988\text{ cm}^{-1}$  and  $927\text{ cm}^{-1}$  for vinyl (C=C) stretching. The FTIR spectrum in Figure 36 indicates that 4-vinylbenzenesulfonyl chloride has been synthesized successfully. Monomer STFSI has also been synthesized, but the characterization is in progress.

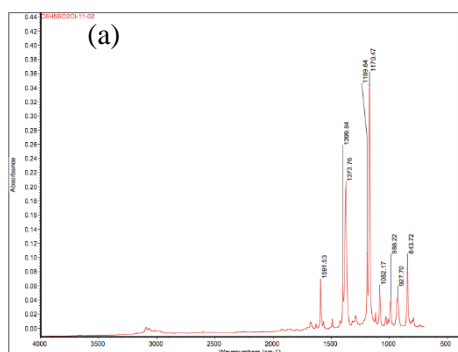


Figure 36. (a) Infrared spectrum. (b) Photograph (pale yellow liquid) of 4-vinylbenzenesulfonyl chloride.

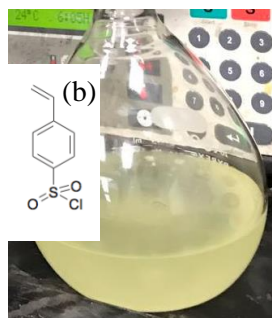


Figure 37 shows the infrared spectrum of 4-vinylbenzenesulfonyl amine, which is the product of the first synthesis step of SsTFSI. Similar to 4-vinylbenzenesulfonyl chloride, characteristic peaks for 4-vinylbenzenesulfonyl amine include  $1541\text{ cm}^{-1}$  for aryl stretching,  $1303\text{ cm}^{-1}$  and  $1162\text{ cm}^{-1}$  for sulfonyl (S=O) stretching, and  $994\text{ cm}^{-1}$  and  $933\text{ cm}^{-1}$  for vinyl (C=C) stretching. The same peak pattern at lower wavenumber range belongs to the 4-vinylbenzenesulfonyl amine structure. Two additional peaks at  $3343$  and  $3262\text{ cm}^{-1}$  in 4-vinylbenzenesulfonyl amine spectrum can be attributed to amine (N-H) stretching.

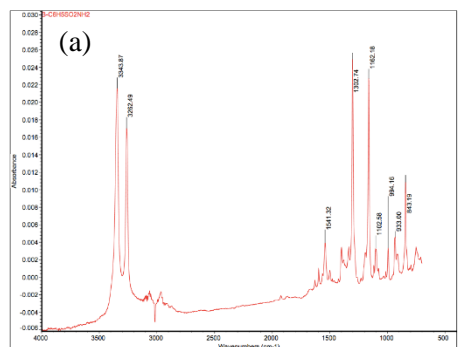


Figure 37. (a) Infrared spectrum. (b) Photograph of 4-vinylbenzenesulfonyl amine.

Figure 38 demonstrates the infrared spectra of the product in the second synthesis step of SsTFSI. If successful, the product of the second step is N-sulfinyltrifluoromethanesulfonamide ( $\text{CF}_3\text{SO}_2\text{N}=\text{S}=\text{O}$ ). However, the synthesis of N-sulfinyltrifluoromethanesulfonamide was not successful initially, without the use of a catalyst. As shown in Figure 38a, there is no clear difference in the infrared spectra of product and reactant even after

a long reaction time of 72 h. Therefore, a second attempt was carried out by adding the catalyst. Obviously, the product shows a different FTIR spectrum as compared with the reactant (Figure 38b). First, the peaks for amine (N-H) groups at  $3279$  and  $3387\text{ cm}^{-1}$  disappeared, indicating that the amine groups were reacted and new functional groups were formed. The peaks at  $1352$  and  $1186\text{ cm}^{-1}$  and those at  $1231$ ,  $1145$ , and  $950\text{ cm}^{-1}$  were attributed to sulfonate (S=O) stretching and fluoride (C-F) stretching, which were similar to those of reactant; the peak at  $1067\text{ cm}^{-1}$  was ascribed to amide (C-N) stretching,<sup>2</sup> indicating that the desired product N-sulfinyltrifluoromethanesulfonamide was obtained. Other additional peaks that appeared in spectrum may be due to induced impurities during reaction. The FTIR spectra in Figures 37 and 38 demonstrate that the first two synthesis steps of monomer SsTFSI were successfully completed. The third and fourth steps are in progress.

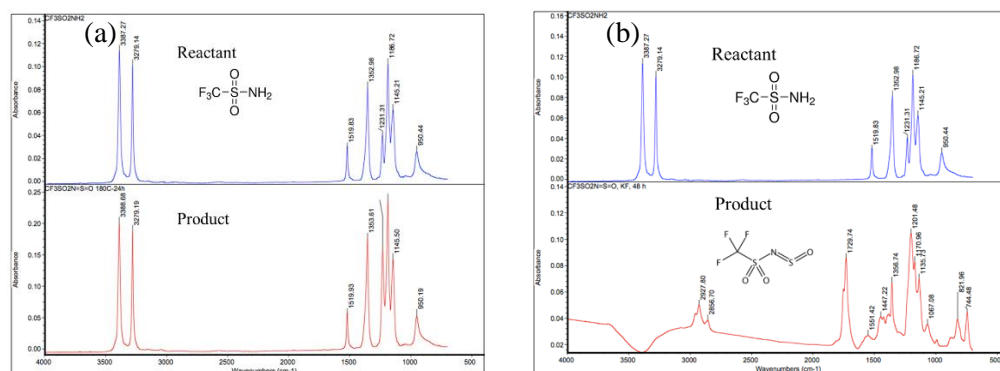


Figure 38. Infrared spectra of N-Sulfinyltrifluoromethanesulfonamide ( $\text{CF}_3\text{SO}_2\text{N}=\text{S}=\text{O}$ ): (a) without catalyst and (b) with catalyst.

- [1] Rettenwander, D., and A. Welzl, L. Cheng, J. Fleig, M. Musso, E. Suard, M. M. Doeff, G. J. Redhammer, and G. Amthauer. "Synthesis, Crystal Chemistry, and Electrochemical Properties of  $\text{Li}_{7-2x}\text{La}_3\text{Zr}_{2-x}\text{Mo}_x\text{O}_{12}$  ( $x = 0.1-0.4$ ): Stabilization of the Cubic Garnet Polymorph via Substitution of  $\text{Zr}^{4+}$  by  $\text{Mo}^{6+}$ ." *Inorganic Chemistry* 54, no. 21 (2015): 10440–10449.
- [2] Roesky, H. W., and G. Holtschneider, and H. H. Giere. "Trifluormethylsulfonylstickstoff-Verbindungen." *Zeitschrift für Naturforschung B* 25, no. 3 (1970): 252–254.

## Task 4.5 – High Conductivity and Flexible Hybrid Solid-State Electrolyte (Eric Wachsman, Liangbing Hu, and Yifei Mo, University of Maryland)

**Project Objective.** The project objective is to develop flexible hybrid electrolyte with garnet nanofibers to achieve the following: (1) flexible, with greater mechanical strength ( $\sim 10$  MPa) and thermal stability than polymer electrolytes; (2) high room temperature ionic conductivity,  $\sim 0.5$  mS/cm; (3) stable interface with lithium metal and effective blocking of lithium dendrites at current densities up to  $3$  mA/cm<sup>2</sup>; and (4) battery performance with Li-S chemistry with an energy density of  $\geq 450$  Wh/kg and ( $\geq 1000$  Wh/L), and maintain  $\geq 80\%$  of capacity up to 500 cycles.

**Project Impact.** Instability and/or high resistance at the interface of lithium metal with various solid electrolytes limit the use of the metallic anode for batteries with high energy density, such as Li-air and Li-S batteries. The critical impact of this endeavor will be focused on developing a new type of solid-state electrolyte (SSE) that is highly conductive, highly flexible, and electrochemically stable. In particular, the new SSE will enable Li-metal anodes with excellent interfacial impedance and blocking of lithium dendrite formation.

**Approach.** The project will synthesize garnet nanofibers, fill the porous region with polymer electrolyte, and characterize the flexible hybrid membrane properties. The flexible hybrid SSE microstructure will be determined using focused ion beam (FIB)/SEM and integrated with electrochemical methods to investigate the properties and stability with Li-metal anode.

**Out-Year Goals.** The project will develop a fundamental understanding of the mechanism of Li-ionic diffusion in garnet nanofibers and their mechanical properties, as well as these properties for hybrid garnet-fiber/polymer hybrids. Work will progress toward the study of the electrode assembly during electrochemical cycling of the anode.

**Collaborations.** This project funds work at University of Maryland, College Park. Dr. Eric D. Wachsman (PI) will focus on optimizing the garnet network to achieve high ionic conductivity and flexibility using FIB/SEM and EIS characterization. Dr. Liangbing Hu (Co-PI) focuses on synthesis of the hybrid electrolyte and test for Li-metal anode with the hybrid electrolyte. Dr. Yifei Mo (Co-PI) will lead efforts on computational modeling of the garnet nanofiber hybrid electrolytes for fundamental mechanistic understanding.

### Milestones

1. Fabricate 4-cm by 4-cm garnet nanofiber membrane. (Q1 – Complete)
2. Synthesize ion-conductive polymers, synthesize ion-insulation polymers, and *in situ* synthesize polymer electrolyte coated garnet nanofibers. (Q2 – In progress)
3. Understand Li-ionic diffusion in garnet nanofibers and its response to mechanical deformation. (Q3 – In progress)
4. Achieve hybrid solid-state electrolyte with a high ionic conductivity ( $\sim 0.5 \times 10^{-3}$  S/cm), high electrochemical stability ( $\sim 4.5$ V), and high mechanical property. (Q4)

## Progress Report

Stoichiometric amounts of chemicals were dissolved in dimethylformamide (DMF). The salt solution and polyvinylpyrrolidone in DMF were mixed at a 1:1 volume ratio to form an electrospinning precursor solution. The electrospinning setup was composed of a syringe pump, a high-voltage power supply, and a drum collector covered with aluminum foil.

After electrospinning, the as-spun fiber membrane was peeled off the collector and placed in an alumina crucible for calcination. The calcination process was conducted in air at 800°C for 4 h to remove polymer and crystallize the fibers. Figure 39 shows the morphology of garnet nanofibers before and after sintering. The as-spun membrane consists of continuous nanofibers with diameters ranging from ~200 to 300 nm. After calcination, the polymer was removed, and garnet nanofibers were crystallized.

PEO-LiTFSI was filled into the garnet nanofiber membrane by repeated wetting and drying to get flexible solid-state electrolyte membrane. The total Li-ion conductivity of flexible solid-state electrolyte was characterized by EIS. Figure 40 shows the Arrhenius plot of the garnet nanofiber electrolyte. Li-ion conductivity was calculated based on the thickness of flexible electrolyte and diameter of stainless electrodes. As reported, Li-ion conductivity of cubic phase LLZO garnet pellet would reach as high as  $10^{-3}$  S/cm, while

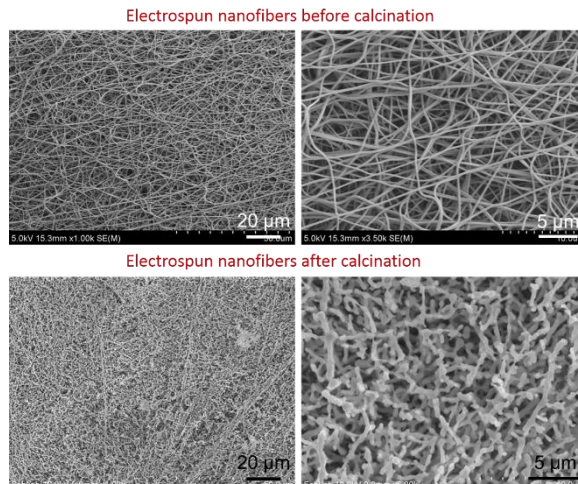


**Figure 39.** Scanning electron microscopy images of garnet nanofibers before (top) and after (bottom) calcination.

lithium salt stuffed PEO is generally in the order of  $10^{-6}$ - $10^{-9}$  S/cm at room temperature. The flexible electrolyte combining conductive cubic LLZO garnet and lithium-PEO could exhibit a reasonably high ionic conductivity of  $2.5 \times 10^{-4}$  S/cm at room temperature.

In addition to electrospinning, a very scalable method was developed to produce large-size garnet nanofiber membranes. Carbon mat template was soaked in a precursor solution and dried in air. After calcination, the project obtained a 4-cm by 4-cm freestanding garnet mat of cubic phase garnet nanofibers (Figure 41). The diffraction peaks match well with those of cubic phase garnet  $\text{Li}_5\text{La}_3\text{Nb}_2\text{O}_{12}$  (JCPDS card 80-0457).

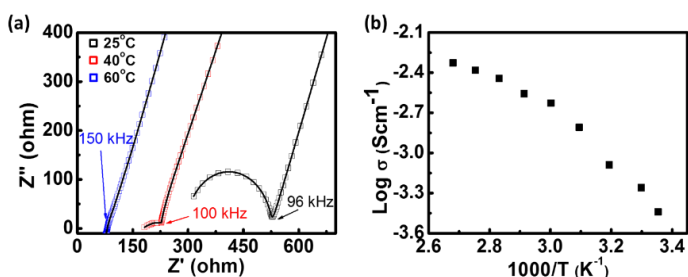


**Figure 40.** (a) Electrochemical impedance spectroscopy profiles of the flexible electrolyte membrane at different temperatures (25°C, 40°C, and 90°C). (b) Arrhenius plot of the flexible electrolyte membrane at elevated temperatures.

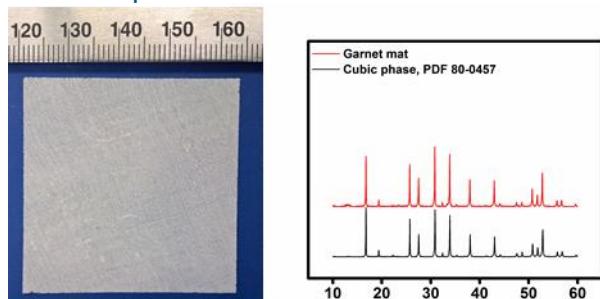


**Figure 41.** Digital photo (left) and X-ray diffraction pattern (right) of 4cm by 4cm conductive garnet textile.



## Patents/Publications/Presentations

### Publication

- Fu, K., et al. “Flexible, Solid-State, Ion-Conducting Membrane with 3D Garnet Nanofiber Networks for Lithium Batteries.” *PNAS* 113 (2016): 7094–7099.

## Task 4.6 – Self-Forming Thin Interphases and Electrodes Enabling 3D Structured High-Energy-Density Batteries (Glenn Amatucci, Rutgers University)

**Project Objective.** The project objective is to develop and implement a novel *in situ* formed lithium-metal-based metal fluoride battery that will enable packaged 10mAh batteries of energy densities  $> 1000$  Wh/L and  $>400$  Wh/kg at 12V.

**Approach.** The project focuses on the coalescence of three main aspects of the baseline technology, corresponding to the three sub-tasks of the project: the self-forming chemistry comprised of electrodes and electrolyte, electrode and electrolyte fabrication, and cell design.

**Impact.** Successful realization of 3D batteries formed *in situ* with a practical approach to large-scale fabrication would address some of the DOE EV performance goals, including: (1) areal capacity increase, (2) improved rates, and (3) designs to enable high-voltage unit cells.

### Milestones

All milestones are in progress, without any major scientific hurdles.

### Progress Report

**Project Functionality.** The project is fully functional with the staff, characterization equipment, and deposition system operational. New cycler has been ordered, received, and incorporated into the project specific work flow. Appropriate shadow masks for Q1-Q3 studies have been burned (in-house) and are in use. Shadow masks for Q3-Q4 are being burned (in-house).

**Bi-Ion Conductor Development.** A systematic process is in place for fabrication and characterization of the bi-ion glass conductors that will carry on throughout this project to achieve ionic conductivity of  $> 1 \times 10^{-4}$  S/cm prior to *in situ* formation. More than 20 compositions and 80 cells were deposited this quarter. After deposition, the compositions were characterized by (1) EIS to extract the ionic conductivity, (2) a combination of stepped and linear sweep voltammetry to investigate the electrochemical stability, and (3) XRD to investigate nano-crystallinity. Dopants were identified to increase conductivity from  $1 \times 10^{-8}$  S/cm to  $1 \times 10^{-5}$  S/cm, showing a progressive path to the  $1 \times 10^{-4}$  S/cm that the project expects to achieve on schedule. In addition, all except one composition exhibited electrochemical stability to breakdown in excess of 6 V with no increase of interfacial impedance.

**Positive and Negative Current Collectors Development.** This project focuses on identification of best source material to allow high flux and high quality reactive current collectors and to identify current collectors that have the highest initial and post-formation electronic conductivity. Initial compositions were identified to proceed with the first full cell fabrication.

## Task 4.7 – Dual Function Solid-State Battery with Self-Forming, Self-Healing Electrolyte and Separator (Esther Takeuchi, Stony Brook University)

**Project Objective.** The project objective is to demonstrate a solid-state rechargeable battery based on a Li-metal anode and iodine cathode with a self-forming, self-healing electrolyte and separator. The resulting rechargeable self-assembled metal/iodine solid state battery will provide an energy density of  $\geq 560$  Wh/kg and  $\geq 1536$  Wh/kg.

**Project Impact.** This program will enable demonstration of the proposed rechargeable battery with improved power capability, high energy density, and a self-forming, self-healing solid-state electrolyte / separator. Technical insight will be gained regarding improved conductivity of the solid lithium iodide (LiI) based electrolyte, power capability of the proposed system, the self-healing nature of the LiI layer, the nature of the electrode-electrolyte interfaces, and feasibility of the system to reach the EV Everywhere Grand Challenge targets.

**Approach.** The proposed concept is a dual function rechargeable solid-state battery utilizing LiI combined with silver iodide (AgI) as the electrolyte with lithium metal (and small quantities of silver metal) as the anode and iodine as the cathode with a self-forming, self-healing separator/electrolyte. The battery will be assembled in the discharged state where the anode and cathode will be created during the first formation (charge) step. Initially, silver ion ( $\text{Ag}^+$ ) will diffuse toward the negative electrode and be reduced to silver metal ( $\text{Ag}^0$ ), and iodine ion ( $\text{I}^-$ ) will be oxidized to elemental iodine ( $\text{I}_2$ ) at the cathode side. As the formation of the battery continues, lithium ion ( $\text{Li}^+$ ) will form a Li-metal layer at the anode, with generation of iodine at the cathode. LiI will remain and serve as both the separator and electrolyte.

**Out-Year Goals.** This is a multiyear program where the effort is divided into three major tasks.

- Year 1 involves electrolyte preparation and characterization including preparation of solid state electrolytes and conductivity measurements.
- Year 2 will focus on cell construction and testing including both *in situ* and *ex situ* analysis.
- Year 3 will focus on cell characterization. Under the program, cycle life, efficiency, energy density, and the functional capacity of cells will be determined.

**Collaborations.** This project collaborates with Amy Marschilok and Kenneth Takeuchi of Stony Brook University.

### Milestones

1. Reagents procured; composition, purity, and water content verified. (Q1 – Complete)
2. Develop methodology for AC impedance measurement as a function of temperature. (Q2 – Complete)
3. Identify the four most conductive silver-containing LiI solid electrolytes for further study. (Q3)
4. At least one electrolyte with conductivity  $\geq 10^{-3}$  S/cm. (Q4)

**Reagents.** The reagents needed for the study of the solid electrolytes were obtained commercially and carefully characterized. XRD patterns were recorded for the as received materials, Figure 42. Analysis of the diffraction patterns showed that the AgI sample was a majority  $\beta$ -AgI phase with a small contribution from  $\gamma$ -AgI. Lithium iodide diffraction patterns showed that the majority phase was LiI.

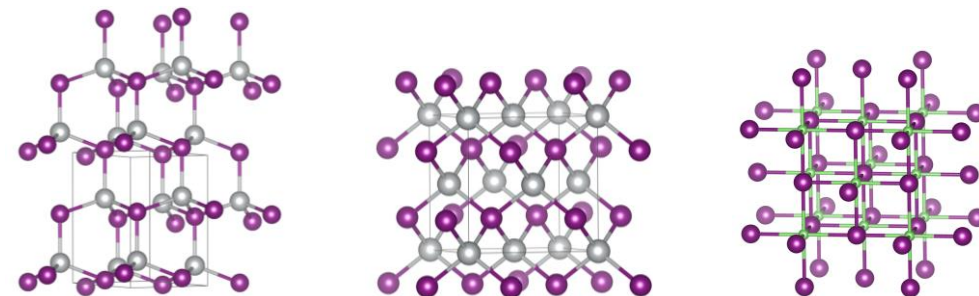


Figure 42. Structures of AgI  $\beta$ -phase (left), AgI  $\gamma$ -phase (center), and LiI (right).

**Resistance Measurements.** The development of the methodology to measure resistance of the solids was initiated to generate reproducible data. The method selected for the measurements was EIS as a function of temperature. Every set of measurements was conducted in triplicate. The results of a typical experiment showing the Nyquist plots as a function of the temperature for AgI are shown in Figure 43. Note that three samples were measured at each temperature, and all three sets of data are plotted in Figure 43, showing good reproducibility. The EIS data were analyzed where the data were fitted to an equivalent circuit, Figure 44. Use of the equivalent circuit fits allowed quantitative analysis of the data. The values of the circuit elements were determined from the equivalent circuit fits. The results for AgI and LiI conductivity as a function of temperature are shown in Figure 45. The conductivity results obtained from the series of measurements align with prior literature.

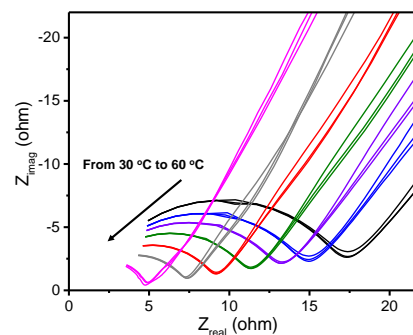


Figure 43. Electrochemical impedance spectroscopy for silver iodide as a function of temperature.

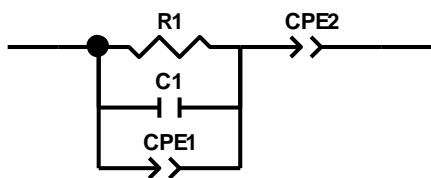


Figure 44. Equivalent circuit used for data analysis.

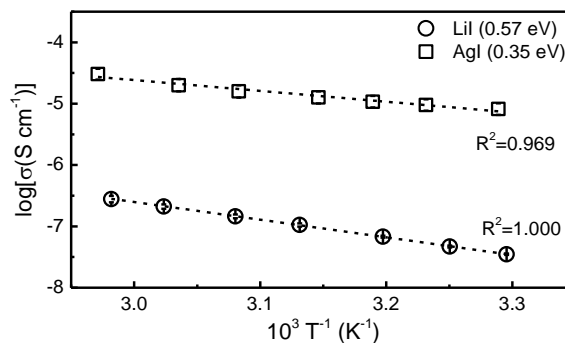


Figure 45. Resistance as a function of temperature.

## Patents/Publications/Presentations

### Patent

- Patent disclosure on Dual Function Solid State Cell concept filed with Stony Brook University Technology Transfer Office.

## TASK 5 – DIAGNOSTICS

### Summary and Highlights

To meet the goals of VTO-Multi Year Program Plan and develop lower-cost, abuse-tolerant batteries with higher energy density, higher power, better low-temperature operation and longer lifetimes suitable for the next-generation of HEVs, PHEVs and EVs, there is a strong need to identify and understand structure-property-electrochemical performance relationships in materials, life-limiting and performance-limiting processes, and various failure modes to guide battery development activities and scale-up efforts. In the pursuit of batteries with high energy density, high cell operating voltages and demanding cycling requirements lead to unprecedented chemical and mechanical instabilities in cell components. Successful implementation of newer materials such as silicon anode and high-voltage cathodes also requires better understanding of fundamental processes, especially those at the solid/electrolyte interface of both anode and cathode.

This task takes on these challenges by combining model system, *ex situ*, *in situ*, and *operando* approaches with an array of state-of-the-art analytical and computational tools. Four subtasks are tackling the chemical processes and reactions at the electrode/electrolyte interface. Researchers at LBNL use *in situ* and *ex situ* vibrational spectroscopy, far- and near-field scanning probe spectroscopy and laser-induced breakdown spectroscopy (LIBS) to understand the composition, structure, and formation/degradation mechanisms of the SEI at silicon anode and high-voltage cathodes. The University of California – San Diego (UCSD) combines STEM/EELS, XPS and *ab initio* computation for surface and interface characterization and identification of instability causes at both electrodes. At Cambridge, nuclear magnetic resonance (NMR) is being used to identify major SEI components, their spatial proximity and how they change with cycling. Subtasks at BNL and PNNL focus on the understanding of fading mechanisms in electrode materials, with the help of synchrotron-based X-ray techniques (diffraction and hard/soft X-ray absorption) at BNL and high-resolution transmission electron microscopy (HRTEM) and spectroscopy techniques at PNNL. At LBNL, model systems of electrode materials with well-defined physical attributes are being developed and used for advanced diagnostic and mechanistic studies at both bulk and single-crystal levels. These controlled studies remove the ambiguity in correlating material's physical properties and reaction mechanisms to performance and stability, which is critical for further optimization. The final subtask takes advantage of the user facilities at ANL that bring together X-ray and neutron diffraction, X-ray absorption, emission and scattering, HRTEM, Raman spectroscopy, and theory to look into the structural, electrochemical, and chemical mechanisms in the complex electrode/electrolyte systems. The diagnostics team not only produces a wealth of knowledge key to developing next-generation batteries, it also advances analytical techniques and instrumentation that have a far-reaching effect on material and device development in a variety of fields.

**Highlights.** The highlights this quarter are as follows:

- LBNL (Kostecki's group) demonstrated that the existence of the reconstruction rock-salt layer on NMC-532 surface improves the cell performance by inhibiting impedance growth during cycling.
- PNNL (Wang's Group) reported that Al<sub>2</sub>O<sub>3</sub> coating layer suppresses manganese reduction at the interface and its dissolution into the electrolyte, leading to overall reduced side reactions between LMR cathode and the electrolyte.

## Task 5.1 – Model System Diagnostics for High-Energy Cathode Development (Guoying Chen, Lawrence Berkeley National Laboratory)

**Project Objective.** This project will use a rational, non-empirical approach to design and synthesize next-generation high-energy, high-voltage cathode materials. Combining a suite of advanced diagnostic techniques with model cathode materials and model electrode/electrolyte interfaces, the project will perform systematic studies to achieve the following goals: (1) obtain new insights into solid-state chemistry, particularly cationic and/or anionic redox activities during charge and discharge of high-capacity Li-TM oxides, (2) gain fundamental understanding on cathode/electrolyte interfacial chemistry and charge transfer process as a function of operating voltage, (3) reveal performance- and stability-limiting properties and processes in high-energy, high-voltage cathodes, and (4) develop strategies to mitigate the structural and interfacial instabilities.

**Project Impact.** The project will improve the commercial viability of next-generation high-energy cathode materials. The findings will enable more stable high-voltage cycling of existing Li-TM oxides as well as development of novel high-capacity cathode materials for advanced Li-ion batteries.

**Approach.** Prepare crystal samples of Li-stoichiometric and Li-excess TM oxides with well-defined physical attributes. Perform advanced diagnostic and mechanistic studies at both bulk and single-crystal levels. Global properties and performance of the samples will be established from the bulk analyses, while the single-crystal-based studies will utilize time- and spatial-resolved analytical techniques to probe the material redox transformation process and failure mechanisms under battery operating conditions.

**Out-Year Goals.** Obtain fundamental knowledge on performance-limiting physical properties, phase transition mechanisms, parasitic reactions, and transport processes that prevent cathode materials from delivering higher capacities and achieving more stable cycling at high voltages. Develop approaches to mitigate cathode structural and interfacial instabilities during high-voltage operation. Design and synthesize optimized Li-TM oxide cathodes as well as novel high-energy electrode materials.

**Collaborations.** This project collaborates with the following: G. Ceder, K. Persson, M. Doeff and P. Ross (LBNL); V. Srinivasan (ANL); Simon Mun (GIST); Y. Liu (SSRL); J. Guo (ALS); C. Wang (PNNL); C. Grey (Cambridge); and A. Huq and J. Nanda (ORNL).

### Milestones

1. Synthesize model Li-TM oxide cathode materials with several different chemical compositions and/or morphologies. (December 2016 – Complete)
2. Investigate the bulk activities of TM and oxygen redox centers in Li-TM oxides as a function of state of charge and temperature. (March 2017 – On schedule)
3. *Go/No-Go*: Investigate synthesis methods for preparing single crystals of Li-excess TM oxides with previously reported reversible oxygen redox activities. *No-Go* if high-quality crystals of the oxide cannot be made. (June 2017 – On schedule)
4. Determine the activities of lattice oxygen and TM on particle surface and the impact of cathode chemistry and surface facet. (September 2017 – On schedule)

## Progress Report

Recently, it has been shown that some Li-excess TM oxides are capable of cycling more than one Li<sup>+</sup> per formula unit and delivering much higher capacities through the participation of both TM and oxygen redox centers. One such example is Li<sub>1.3</sub>Nb<sub>0.3</sub>Mn<sub>0.4</sub>O<sub>2</sub>, which was reported by Yabuuchi et al. to deliver a specific energy up to 950 Wh/kg at 60°C. As manganese is the only redox active TM capable of producing ~120 mAh/g with the Mn<sup>3+</sup>/Mn<sup>4+</sup> reaction, the mechanism for the extra capacity, the possible involvement of bulk oxygen redox and its reversibility in long-term cycling, are not understood. This quarter, a series of uniform micron-sized crystals of Li-rich niobium/tantalum manganese oxides with a formula of Li<sub>1.4-x</sub>Nb<sub>0.4-x</sub>Mn<sub>0.2+2x</sub>O<sub>2</sub> ( $x = 0.1, 0.2, M = \text{Nb}, \text{Nb}_{0.5}\text{Ta}_{0.5}$  and Ta) was synthesized by a molten salt method. In a typical synthesis procedure, stoichiometric amounts of Li<sub>2</sub>CO<sub>3</sub>, Nb<sub>2</sub>O<sub>5</sub>/Ta<sub>2</sub>O<sub>5</sub>, and Mn<sub>2</sub>O<sub>3</sub> were used as precursors. To compensate the loss of lithium at elevated temperature, 10% excess of Li<sub>2</sub>CO<sub>3</sub> was used. The precursors were mixed in a small amount of ethanol/acetone and ball-milled in a zirconia jar for 12 h. The resulting powder was then mixed with the KCl flux (m.p. = 771°C) in an R value of 2.5 or 5 (R is defined as the molar ratio between the flux and the total TMs) and further grinded for 15 minutes. The mixture was transferred into an alumina crucible covered with a lid, heated in a tube furnace at 950°C under argon atmosphere for 12 h, and then cooled to room temperature. The ramping rate was 4°C/min for both heating and cooling.

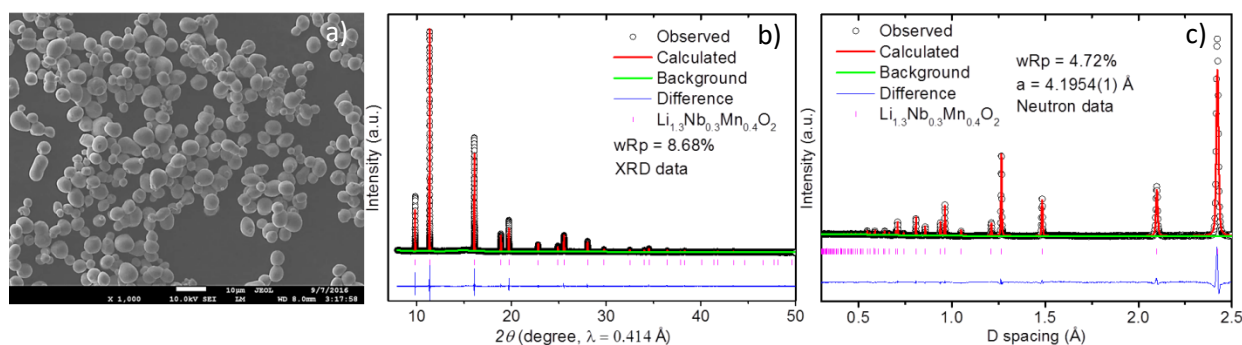


**Figure 46. (a) Scanning electron microscopy image. (b-c) Rietveld refinements of synchrotron X-ray diffraction and neutron patterns of Li<sub>1.3</sub>Nb<sub>0.3</sub>Mn<sub>0.4</sub>O<sub>2</sub> crystal sample.**

Figure 46 shows the morphology and structural refinement results of both XRD and neutron patterns of the Li<sub>1.3</sub>Nb<sub>0.3</sub>Mn<sub>0.4</sub>O<sub>2</sub> sample. The particles are uniform large spheres with an average size of 5 μm (Figure 46a). Joint synchrotron X-ray and neutron Rietveld refinements (Figure 46b-c) confirmed the cation-disordered rock-salt structure with a space group of *Fm* $\bar{3}$ *m* and a lattice parameter of 4.1954(1) Å. No oxygen vacancy was found in the pristine sample. Delithiated Li<sub>x</sub>Nb<sub>0.3</sub>Mn<sub>0.4</sub>O<sub>2</sub> samples were prepared by chemical oxidation in a NO<sub>2</sub>BF<sub>4</sub> solution in acetonitrile, with the lithium content ( $x$ ) controlled by the mole ratio between the oxide and the oxidizing agent. Figure 47a shows the synchrotron XRD patterns of the series with various lithium content of  $0 < x \leq 1.3$ , collected at beamline 11 at APS. With decreasing  $x$ , the cell dimension reduces while the rock-salt crystal structure maintains. Two separate regions, a single-phase region with  $0.9 < x \leq 1.3$  and a two-phase region with  $0 < x < 0.9$ , were found, suggesting involvement of distinctively different redox activities. Detailed structural refinements are under way.

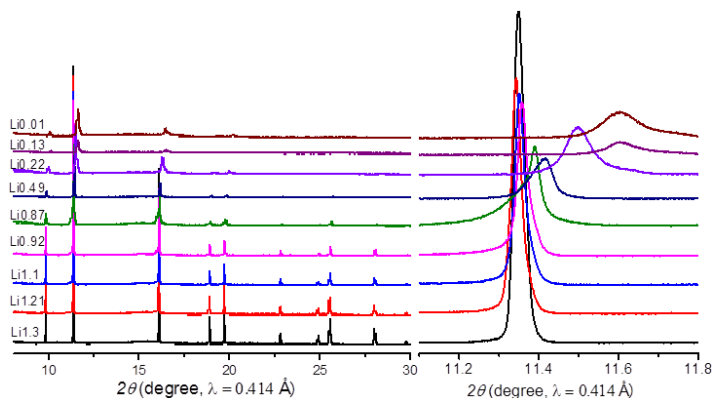


**Figure 47. Synchrotron X-ray diffraction patterns of chemically delithiated Li<sub>x</sub>Nb<sub>0.3</sub>Mn<sub>0.4</sub>O<sub>2</sub> ( $0 < x \leq 1.3$ ) crystal samples.**



## Patents/Publications/Presentations

### Publications

- Kuppam, S., and A. K. Shukla, D. Membreno, D. Nordlund, and G. Chen. “Revealing Anisotropic Spinel Formation on Pristine Li- and Mn-Rich Layered Oxide Surface and Its Impact on Cathode Performance.” *Advanced Energy Materials* 7 (2017): 1602010. doi: 10.1002/aenm.201602010.
- Kuppam, S., and Y. Xu, Y. Liu, and G. Chen. “Phase Transformation Mechanism in Lithium Manganese Nickel Oxide Revealed by Single-Crystal Hard X-ray Microscopy.” *Nature Communications*, in press.

### Presentations

- 2016 Bay Area Battery Summit, Menlo Park, California (November 2016): “Advanced High-Energy Cathode Materials for Lithium-Ion Batteries”; W.-H. Kan, S. Kuppam, and G. Chen.
- 2016 PRIME, Honolulu (October 2016): “Single-Crystal Based Diagnostics for Li-Ion Battery Cathode Development”; S. Kuppam, A. K. Shukla, and G. Chen.
- 2016 PRIME, Honolulu (October 2016): “A New Anion Receptor for Improved Interface between the Lithium- and Manganese-Rich Layered Oxide Cathode and the Electrolyte”; Y. Ma, Y. Zhou, G. Yin, F. Lin, and G. Chen.

## Task 5.2 – Interfacial Processes – Diagnostics (Robert Kostecki, Lawrence Berkeley National Laboratory)

**Project Objective.** This collaborative project involves developing and applying advanced experimental methodologies to study and understand the mechanism of operation and degradation of high-capacity NMC materials for Li-ion cells for PHEV and EV applications. The main objective is to apply *in situ* and *ex situ* far- and near-field optical multifunctional probes to obtain detailed insight into the active material structure and the physicochemical phenomena at electrode/electrolyte interfaces of stoichiometric NMCs with high nickel contents such as 622 and 523 compositions materials at a spatial resolution that corresponds to the size of basic chemical or structural building blocks. The primary goal of these studies is to unveil the structure and reactivity at hidden or buried interfaces and interphases that determine material, composite electrode, and full-cell electrochemical performance and failure modes.

**Project Impact.** Instability and/or high resistance at the interface of high-voltage Li-ion cathodes limits electrochemical performance of high-energy density batteries. A better understanding of the underlying principles that govern these phenomena is inextricably linked with successful implementation of high-energy-density materials such as silicon and high-voltage cathodes in Li-ion cells for PHEVs and EVs. The proposed work constitutes an integral part of the concerted effort within the BMR Program and it supports development of new cathode materials for high-energy Li-ion cells.

**Approach.** The pristine and cycled NMC powders and electrodes will be probed using a variety of surface- and bulk-sensitive techniques, including FTIR, attenuated total reflection (ATR)-FTIR, near-field infrared and Raman spectroscopy and microscopy, and scanning probe microscopy to identify and characterize changes in materials structure and composition. Novel *in situ/ex situ* far- and near-field optical multifunctional probes in combination with standard electrochemical and analytical techniques are developed to unveil the structure and reactivity at interfaces and interphases that determine materials electrochemical performance and failure modes.

**Out-Year Goals.** Determine the degradation mechanism(s) of high-voltage cathodes; propose and test effective remedies to intrinsic interfacial instability of these materials and composite electrodes.

**Collaborations.** NMC materials and composite electrodes tested under different cycling regimes by M. Doeff (LBNL) and C. Ban (NREL) will be studied. The diagnostic studies will be carried out in sync with differential electrochemical mass spectrometry analysis by B. McCloskey (LBNL) and other diagnosticians in the BMR program. He will also work closely with V. Battaglia (LBNL) to obtain samples from full-cell cycling experiments.

### Milestones

1. Determine relationship between surface reconstruction and aging/cycling of in NMC powders/electrodes. (December 2016 – Complete)
2. Complete *in situ* atomic force microscopy (AFM) characterization of interfacial activity of the model NMC material in organic carbonate electrolytes. (Q3 – On schedule)
3. Determine composition of surface film and its effect on electrochemical performance of NMC electrodes. (Q3 – On schedule)
4. Determine relationship between surface reconstruction, film formation, and metal dissolution in NMC electrodes. (Q4 – On schedule)

## Progress Report

The project analyzed the relationship between the reconstruction layer on the surface of Ni-rich NMC (Ni:Mn:Co=5:3:2) particles and its electrochemical properties. For this purpose, an artificial reconstructed surface layer was produced by storing the NMC powder for 10 days in 1M LiPF<sub>6</sub> in EC/DEC 1:2 electrolyte at 60°C. The NMC powder was then washed and sonicated in DEC, and dried in vacuum. The resultant surface rock-salt layer is expected to have a similar thickness as the one that evolves from electrochemical charging and discharging, as reported by Lin et al.<sup>1</sup> The pristine (NMC) powder and the powder with a surface reconstruction layer (NMC/R) were then used to prepare composite electrodes for electrochemical tests in a standard coin cell configuration.

After 200 charge-discharge cycles at 0.5 C between 2.0-4.7 V, both the NMC and NMC/R cells show similar capacity retention ca. 61% of the original discharge capacity (Figure 48a). Interestingly, NMC/R electrode showed consistently lower polarization than pristine NMC (Figure 48b-d). The polarization difference between NMC and NMC/R is about 0.2 V for discharging and 0.1 V for charging at 50% SOC for 200<sup>th</sup> cycle. This demonstrates that the existence of the reconstruction layer improves cell performance by inhibiting impedance growth during cycling.

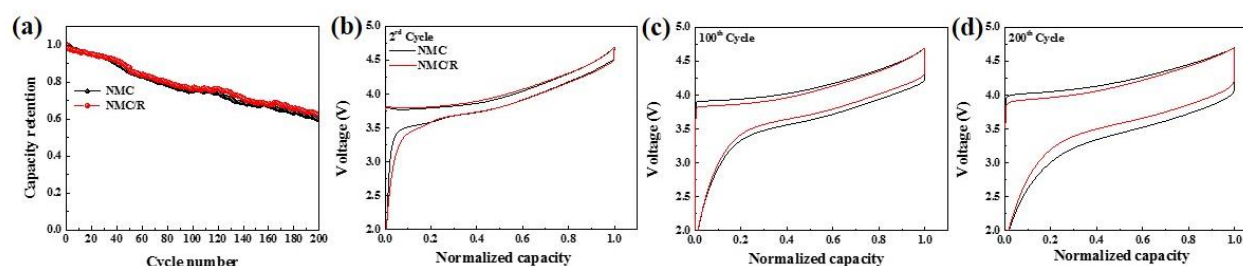


**Figure 48. (a) NMC and NMC/R electrodes capacity retention. (b-d) Charge discharge voltage profiles.**

To clearly identify possible origins of impedance growth, EIS was employed at selected cycles (Figure 49a-b). The high-frequency semi-circle can be assigned to the contact resistance ( $R_s$ ), that is, electronic resistance between the current collector, conductive additive, and active material.  $R_s$  is highly related to the electron percolation in the composite electrode. The mid-frequency semi-circle can be assigned to charge transfer resistance ( $R_{ct}$ ) at the interface between the active material and electrolyte. Those resistances can be obtained by fitting the spectra using an adequate equivalent circuit model (Figure 49c-d). Both electrode materials show similar trends with  $R_{ct}$  variations that continuously increase over 90 cycles. However,  $R_s$  for the pristine NMC electrode is not only higher, it grows substantially during cycling;  $R_s$  for the NMC/R electrode is relatively low, and remains constant during cycling.

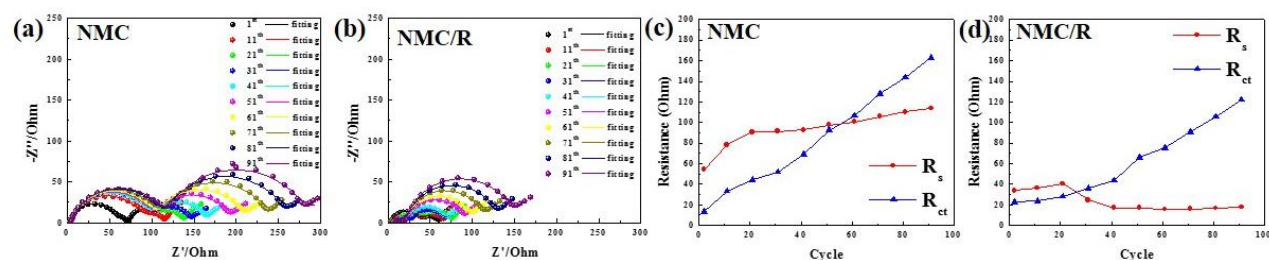


**Figure 49. Nyquist plots of coin cells with NMC (a) and NMC/R (b) cathodes.  $R_s$  and  $R_{ct}$  extracted from the impedance data for NMC (c) and NMC/R (d) electrodes.**

Lin et al.<sup>1</sup> demonstrated that reconstruction layer at NMC surface has lower valence state of the TM than in the bulk. Earlier work<sup>2</sup> inferred the electrolyte decomposition mechanism that relates to the catalysis effect at high-charge-state TM surface. Thus, lower interfacial activity toward the electrolyte of MeO-rich surfaces may inhibit electrolyte decomposition and slow accumulation of reaction products, which are mainly responsible for creating ionic and electronic barriers in the composite electrode.

[1] Lin, F., et al. *Nat. Commun.* 5 (2014).

[2] Jarry, A. et al. *J. Am. Chem. Soc.* 137 (2015): 3533-3539.

## Task 5.3 – Advanced *In Situ* Diagnostic Techniques for Battery Materials (Xiao-Qing Yang and Seongmin Bak, Brookhaven National Laboratory)

**Project Objective.** The primary project objective is to develop new advanced *in situ* material characterization techniques and to apply these techniques to support development of new cathode and anode materials for the next generation of Li-ion batteries for PHEVs. To meet the challenges of powering the PHEV, Li-ion batteries with high energy and power density, low cost, good abuse tolerance, and long calendar and cycle life must be developed.

**Project Impact.** The VTO Multi Year Program Plan describes the goals for battery: “Specifically, lower-cost, abuse-tolerant batteries with higher energy density, higher power, better low-temperature operation, and longer lifetimes are needed for the development of the next-generation of HEVs, PHEVs, and EVs.” The knowledge gained from diagnostic studies through this project will help U.S. industries develop new materials and processes for new generation Li-ion batteries in the effort to reach these VTO goals.

**Approach.** This project will use the combined synchrotron-based *in situ* X-ray techniques (XRD, and hard and soft XAS) with other imaging and spectroscopic tools such as HRTEM and MS to study the mechanisms governing the performance of electrode materials and provide guidance for new material and new technology development regarding Li-ion battery systems.

**Out-Year Goals.** Complete the first-stage development of diagnostic technique to study kinetic property of advanced Li-ion electrode materials using time-resolved XRD and XAS (TR-XRD, TR-XAS) combined with STEM imaging and TXM. Apply this technique to study the structural changes of new cathode materials including various NCM and high-voltage spinel materials during high-rate cycling.

**Collaborations.** The BNL team will work closely with material synthesis groups at ANL (Drs. Thackeray and Amine) for the high-energy composite; and at PNNL for the Si-based anode materials. Such interaction between the diagnostic team at BNL and synthesis groups of these other BMR members will catalyze innovative design and synthesis of advanced cathode and anode materials. The project will also collaborate with industrial partners at GM and Johnson Controls, as well as with international collaborators.

### Milestones

1. Complete the structure studies of  $\text{Li}_2\text{Ru}_{0.5}\text{Mn}_{0.5}\text{O}_3$ , as a model compound for Li- and Mn- rich (LMR) high-energy-density cathode materials using pair distribution function (PDF) to correlate the voltage and capacity fading with micro-structural defects in this type of materials. (Q1 – Complete)
2. Complete the structure studies  $\text{Li}_2\text{Ru}_{0.5}\text{Mn}_{0.5}\text{O}_3$ , as a model compound for LMR high-energy-density cathode materials using STEM to correlate the voltage and capacity fading with micro-structural defects in this type of materials. (Q2 – In progress)
3. Complete the XRD and XAS studies of  $\text{Li}_2\text{Ru}_{0.5}\text{Mn}_{0.5}\text{O}_3$  cathode material samples with different cycle history (charge and discharge limit and cycle numbers). (Q3 – In progress)
4. Complete the structure studies of  $\text{Li}_{1.2}\text{Ni}_{0.15}\text{Co}_{0.1}\text{Mn}_{0.55}\text{O}_2$  for LMR high-energy-density cathode materials using STEM to correlate the voltage and capacity fading with micro-structural defects in this type of material. (Q4 – In progress)

## Progress Report

The first milestone was completed this quarter. BNL has been focused on the structure studies of  $\text{Li}_2\text{Ru}_{0.5}\text{Mn}_{0.5}\text{O}_3$ , as a model compound for LMR high-energy-density cathode materials using PDF to correlate the voltage and capacity fading with micro-structural defects. Figure 50a shows that PDF peaks correspond to characteristic bond distances, while the amplitude of the peak is relating to the coordination number. Using  $\text{LiNiO}_2$  as an example, the first peak (in red) is mainly from TM-oxygen bond, and the peak position corresponds to the TM-oxygen bond length. The second peak (in blue) is mainly from TM-TM bond. The PDF data for pristine state and “OCV-1V-3V” state are shown in Figure 50b, providing structural information in the scale of around 50 Å. In the short-range region (Figure 50c), which covers from 1.6 Å to around 20 Å, the two data sets are almost identical. This indicates that at the scale of a unit cell dimension, the pristine state and “OCV-1V-3V” state have very similar atomic arrangements, suggesting their crystal structures are basically the same. However, when it comes to long-range data sets, as shown in Figure 50d, there is obvious difference between these two states. The pristine state still exhibits well-defined structural features at R value as high as 50 Å. However, for “OCV-1V-3V” state, these structural features are gradually lost when R is greater than 35 Å, indicating that the coherently scattering domain is on the scale of several nanometers.

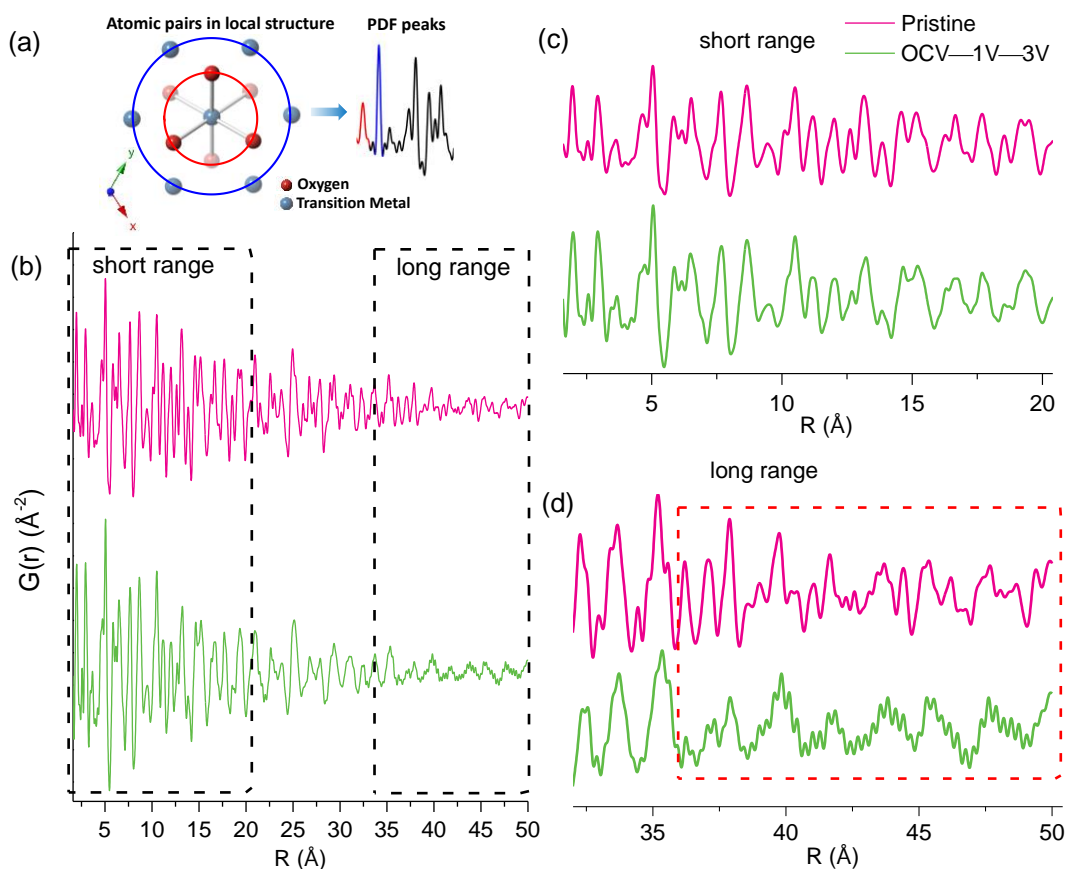


**Figure 50.** (a) Illustration of pair distribution function (PDF) showing that peaks correspond to characteristic bond lengths. (b) *Ex situ* PDF data of pristine sample and “OCV-1V-3V” sample. (c) Zoomed in data on the short-range region of *ex situ* PDF data. (d) Zoomed in data on the long-range region of *ex situ* PDF data.

## Patents/Publications/Presentations

### Publications

- Xu, Yahong, and Enyuan Hu, Feifei Yang, Jeff Corbett, Zhihong Sun, Yingchun Lyue, Xiqian Yu, Yijin Liu, Xiao-Qing Yang, and Hong Li. “Structural Integrity—Searching the Key Factor to Suppress the Voltage Fade of Li-Rich Layered Cathode Materials Through 3D X-Ray Imaging and Spectroscopy Techniques.” *Nano Energy* 28 (2016): 164–171. doi: 10.1016/j.nanoen.2016.08.039.
- Xu, Jing, and Enyuan Hu, Dennis Nordlund, Apurva Mehta, Steven N. Ehrlich, Xiao-Qing Yang, and Wei Tong.\* “Understanding the Degradation Mechanism of Lithium Nickel Oxide Cathode for Li-Ion Batteries.” *ACS Appl. Mater. and Interfaces* 8, No. 46 (2016): 31677–31683. Web publication date: 1 Nov 2016. doi: 10.1021/acsami.6b11111.

## Task 5.4 – Nuclear Magnetic Resonance and Magnetic Resonance Imaging Studies of Solid Electrolyte Interphase, Dendrites, and Electrode Structure (Clare Grey, Cambridge University)

**Project Objective.** The growth of a stable SEI on most electrode materials is key to long-term capacity retention of a working Li-ion battery. On anodes such as silicon, this is particularly critical because the continual expansion and contraction of this intermetallic upon alloying with lithium exposes fresh, reactive surfaces that result in further electrolyte decomposition and SEI growth. This project will perform a detailed multinuclear NMR study of the SEI that forms on silicon, where thick SEIs typically grow and where SEI stability is a key aspect hindering commercialization of this technology. The focus will be to determine how additives (for example, fluoroethylene carbonate, or FEC) and charging parameters (for example, voltage) influence the composition and stability of the SEI. Fundamental studies of SEI structure *in operando* will be complemented by a synthetic program aimed at preparing new silicon coatings based on phosphazene (P-N) elastomeric polymers to increase CE. Further, the nature of the SEI is one factor that appears to control the type of lithium microstructures that form on lithium metal during cycling. To test this hypothesis, the project will use magnetic resonance imaging (MRI) to investigate lithium dendrite versus moss formation in different electrolytes as a function of salt concentration and with different additives. Finally, it will compare lithium and sodium metal anode chemistries to determine the composition, morphology, and stability of local structures that form on sodiating anodes such as tin and hard carbons.

**Project Impact.** The first impact of this project will be a molecular-level understanding of how factors such as applied voltage and electrolyte additives modify the SEI that forms on silicon anodes. The insight gained from these studies will guide the design of new P-N coatings for silicon. A rationally designed surface coating has the potential to improve SEI stability, and thus increase CE for silicon and beyond. A description of how SEI composition influences lithium microstructures will provide the foundation to mitigate dendrite formation during cycling that currently limits the safety of many promising electrode materials. These approaches will be extended to study Na-ion battery electrodes to provide an understanding of how to chemically manipulate both electrodes as well as the electrolyte to avoid adverse failure mechanisms in next-generation batteries.

**Out-Year Goals.** The project goals are to (a) determine the effect of voltage and additives (for example, FEC) on the composition of the silicon SEI; (b) synthesize and test new inorganic coatings to increase the CE seen on cycling silicon; (c) identify correlations between SEI structure and thickness and Li-metal dendrite formation; and (d) determine the local and long-range structures formed on cycling sodium anode materials and compare with lithium. To facilitate these goals, the project will prepare  $^{13}\text{C}$ -enriched FEC for  $^{13}\text{C}$  NMR multinuclear studies to investigate the SEI that forms on silicon during cycling. It will synthesize new P-N polymers for coating silicon nanoparticles and probe changes in performance in the presence of these coatings. In addition, the project will use MRI to correlate lithium dendrite formation with the nature of the SEI. Finally, it will apply the methods developed to study lithium chemistries to investigate sodium electrodes.

**Collaborations.** This project collaborates with B. Lucht (U Rhode Island); J. Cabana, (University of Illinois – Chicago); Y. Shirley Meng (UCSD), S. Whittingham (SUNY – Binghamton); P. Bruce (St. Andrews); S. Hoffman and A. Morris (Cambridge); and P. Shearing (University College London).

### Milestones

1. Synthesis of  $^{13}\text{C}$  FEC. (Q1 – Complete)
2. Preparation of P-N coatings on silicon; Develop *in situ*  $^{19}\text{F}$  NMR studies of FEC. (Q2 – In progress)
3. Multinuclear NMR studies of SEI coatings on silicon with FEC. (Q3 – In progress)
4. Testing of P-N coatings; MRI/dendrite studies of two ionic liquids. (Q4 – In progress)



## Progress Report

The project has investigated a series of different layered sodium cathode materials, focusing on questions such as how does cation substitution of nominally inert ions such as magnesium and lithium affect the structural transformations that occur at high voltages (when most sodium ions are removed), and how does sodium mobility change in these phases? An in-depth investigation of the effect of manganese doping on electrochemical performance and structural stability of  $\text{Na}_{2/3}\text{MnO}_2$  with a P2 layer stacking was performed by comparing three compositions:  $\text{Na}_{2/3}\text{Mn}_{1-y}\text{Mg}_y\text{O}_2$  ( $y = 0.0, 0.05, 0.1$ ). Manganese substitution leads to smoother electrochemistry, with fewer distinct electrochemical processes, improved rate performance, and better capacity retention (Figure 51).

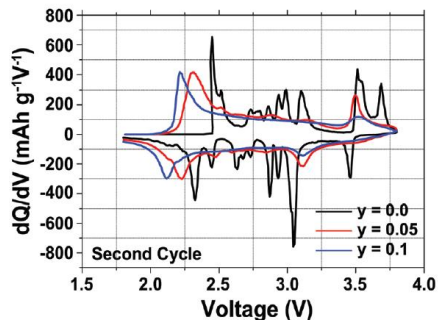


**Figure 51.** Differential capacity versus voltage plots of the  $\text{Na}_{2/3}\text{Mn}_{1-y}\text{Mg}_y\text{O}_2$  ( $y = 0.0, 0.05, 0.1$ ) compositions.

The improved electrochemistry upon manganese substitution was attributed to more gradual structural changes upon charge and discharge, as observed with synchrotron, powder X-ray, and neutron diffraction. Manganese doping reduces the number of  $\text{Mn}^{3+}$  Jahn-Teller centers and delays the high-voltage phase transition that occurs in P2- $\text{Na}_{2/3}\text{MnO}_2$ . The local structure was investigated using  $^{23}\text{Na}$  ssNMR spectroscopy. The ssNMR data provides direct evidence for fewer oxygen layer shearing events, leading to a stabilized P2 phase, and an enhanced  $\text{Na}^+$  ion mobility up to 3.8 V vs.  $\text{Na}^+/\text{Na}$  upon manganese doping. By comparing the  $^{23}\text{Na}$  NMR spectra of the  $x = 0, 0.05$  and  $0.1$  phases (Figure 52), it is clear that much less complex spectra with fewer resonances are observed on manganese substitution. For example, the  $y = 0.10$  sample contains only a single resonance for sodium contents of between 0.67 and 0.4, consistent with rapid  $\text{Na}^+$  mobility in between the layers. A weak signal centered at around 1100 ppm forms due to the OP4 phase, which contains alternating octahedral and prismatic environments for sodium in the Na-metal layers. The relative concentration of this phase (formed by layer shearing) decreases with increasing manganese content. The  $y = 0.05$  Mg-doped phase exhibits one of the best rate performances reported to date for Na-ion cathodes with a P2 structure, with a reversible capacity of  $106 \text{ mAh g}^{-1}$  at the very high discharge rate of  $5000 \text{ mA g}^{-1}$ . In addition, its structure is highly reversible, and stable cycling is obtained between 1.5 and 4.0 V versus  $\text{Na}^+/\text{Na}$ , with a capacity of approximately  $140 \text{ mAh g}^{-1}$  retained after 50 cycles at a rate of  $1000 \text{ mA g}^{-1}$ .

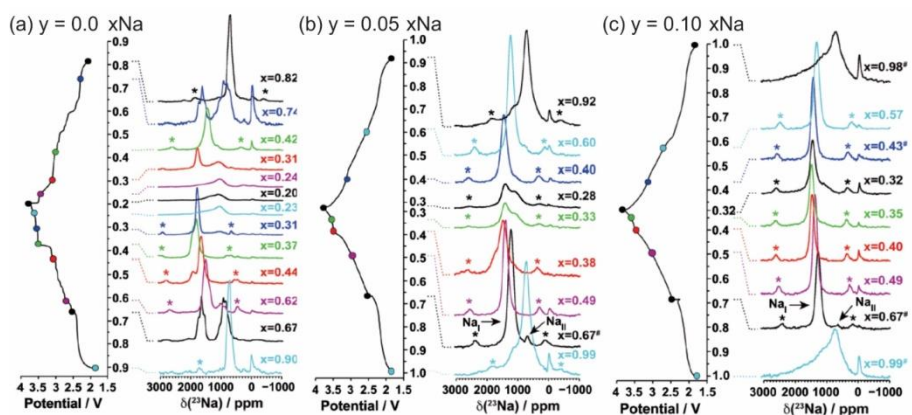


**Figure 52.** *Ex situ*  $^{23}\text{Na}$  magic angle spinning solid-state nuclear magnetic resonance (NMR) spectra collected on cells stopped at different points along the first electrochemical charge/discharge cycle of  $\text{Na}_{2/3}\text{Mn}_{1-y}\text{Mg}_y\text{O}_2$ , where  $y = 0.0, 0.05, 0.1$  for (a), (b), and (c), respectively. Spectra are scaled according to number of scans collected during the experiment, amount of sample in the rotor, and NMR signal decay obtained from  $T_2$  relaxation time measurements. Hashes indicate samples for which a lack of experimental data prevents proper scaling of the spectrum. Asterisks indicate spinning sidebands.

This study was complemented by  $^{23}\text{Na}$  NMR investigations of local structure and electro-chemistry of P2- $\text{Na}_x[\text{Li}_y\text{Ni}_z\text{Mn}_{1-y-z}]\text{O}_2$  ( $x, y, z \leq 1$ ); direct evidence for rapid  $\text{Na}^+$  mobility in these phases was obtained.

## Patents/Publications/Presentations

### Publications

- Clément, R. J., and D. S. Middlemiss, I. D. Seymour, A. J. Ilott, and C. P. Grey. “Insights into the Nature and Evolution upon Electrochemical Cycling of Planar Defects in the Beta-NaMnO<sub>2</sub> Na-Ion Battery Cathode: An NMR and First-Principles Density Functional Theory Approach.” *Chem. Mater.* 28 (2016): 8228–8239.
- Ilott, A. J., and M. Mohammadi, H. J. Chang, C. P. Grey, and A. Jerschow. “Real-time 3D Imaging of Microstructure Growth in Battery Cells Using Indirect MRI.” *Proc. Nat. Ac. Sci. USA* 113 (2016): 10779–10784.
- Clément, R. J., and J. Billaud, A. R. Armstrong, G. Singh, T. Rojo, P. G. Bruce, and C. P. Grey. “Structurally Stable Mg-Doped P2-Na<sub>2/3</sub>Mn<sub>1-y</sub>Mg<sub>y</sub>O<sub>2</sub> Sodium-Ion Battery Cathodes with High Rate Performance: Insights from Electrochemical, NMR and Diffraction Studies.” *Energy Environ. Sci.* 9 (2016): 3240–3251.
- Michan, A. L., and B. S. Parimalam, M. Leskes, R. N. Kerber, T. Yoon, C. P. Grey, and B. L. Lucht. “Fluoroethylene Carbonate and Vinylene Carbonate Reduction: Understanding Lithium-Ion Battery Electrolyte Additives and Solid Electrolyte Interphase Formation.” *Chem. Mater.* 28 (2016): 8149–8159 doi: 10.1021/acs.chemmater.6b02282 (2016).

### Presentations

- University of Lancaster, Chemistry Department Opening and Lecture (October 2016).
- École Polytechnique Fédérale de Lausanne (EPFL), Chemistry Department and Marvel Centre Distinguished Lecture, Switzerland (October 2016).
- Materials for Tomorrow Conference, Chalmers University, Sweden (November 2016).
- CHAINS: Chemistry as Innovating Science 2016, Netherlands (December 2016).

## Task 5.5 – Optimization of Ion Transport in High-Energy Composite Cathodes (Shirley Meng, University of California – San Diego)

**Project Objective.** This project aims to probe and control the atomic-level kinetic processes that govern the performance limitations (rate capability and voltage stability) in a class of high-energy composite electrodes. A systematic study with a powerful suite of analytical tools [including atomic resolution STEM (a-STEM) and EELS, neutron, XPS and first principles (FP) computation] will elucidate approaches to optimize ion transport. Ultimately, this will hone in on the optimum bulk compositions and surface characteristics to improve the mechanistic rate and cycling performance of high-energy composite electrodes. Moreover, it aims to develop the large-scale synthesis efforts to produce materials with consistent performance. The surface-sensitive characterization tools will be extended to diagnose various silicon anode types.

**Project Impact.** If successful, this research will provide a major breakthrough in commercial applications of the class of high-energy-density cathode material for Li-ion batteries. Additionally, it will provide in-depth understanding of the role of surface modifications and bulk substitution in the high-voltage composite materials. The diagnostic tools developed here can also be leveraged to study a wide variety of cathode and anode materials for rechargeable batteries.

**Approach.** This unique approach combines STEM/EELS, XPS, and *ab initio* computation as diagnostic tools for surface and interface characterization. This allows for rapid identification of surface interphases that provide surface instability or stability in various types of electrode materials including both high-voltage cathodes and low-voltage anodes. Neutron enables the characterization of bulk material properties to enhance and further optimize high-energy electrode materials.

**Out-Year Goals.** The goal is to control and optimize Li-ion transport, TM migration, and oxygen activity in the high-energy composite cathodes and to optimize electrode/electrolyte interface in silicon anodes so that their power performance and cycle life can be significantly improved.

**Collaborations.** This work funds collaborations on EELS (Miaofang Chi, ORNL); molecular layer deposition (MLD, Chunmei Ban, NREL); neutron diffraction (Ken An, ORNL); soft XAS (Marca Doeff, LBNL); and XPS, TOF-SIMS characterization (Keith Stevenson, UT Austin). It supports collaborative work with Zhaoping Liu and Yonggao Xia at Ningbo Institute of Materials Technology and Engineering in China.

### Milestones

1. Complete efforts on probing the surface TM oxidation state and oxygen activities of Li-rich layered oxide. (December 2016 – Complete)
2. Quantify structural change and its correlation with oxygen activities in Li-rich layered oxide during electrochemical cycling. (December 2016 – Complete)

## Progress Report

### Probing the Surface Transition Metal Oxidation State and Oxygen Activities of Li-Rich Layered Oxides

To study the structure and chemistry differences between bulk and surface from the atomic level, STEM/EELS data were collected from the Li-rich electrode ( $\text{Li}_{7/6}\text{Ni}_{1/6}\text{Co}_{1/6}\text{Mn}_{1/2}\text{O}_2$ ) after one cycle, as shown in Figure 53. Similar to previous observations, a defect spinel structure that is different from the layered structure in bulk

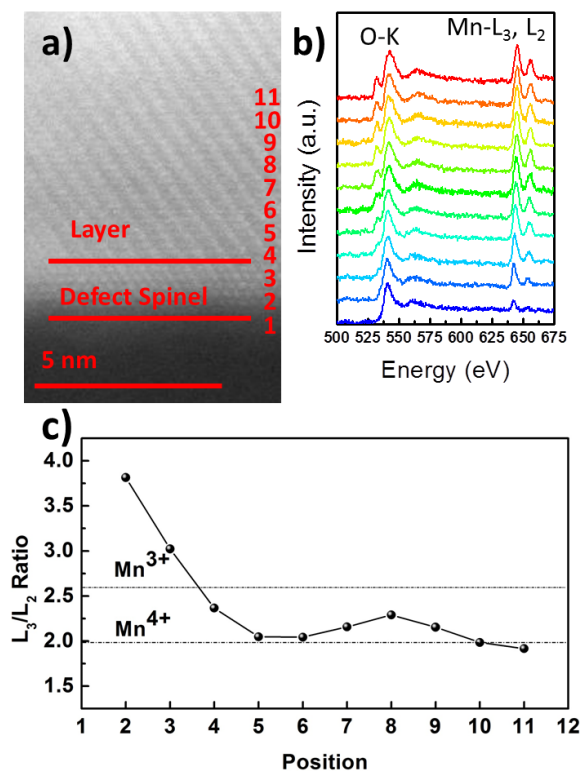


**Figure 53.** (a) Aberration corrected high-angle annular dark field (HAADF) scanning transmission electron microscopy image. (b) Spatially resolved O K-edge and Mn L-edge electron energy loss spectroscopy (EELS) spectra. (c) Mn L<sub>3</sub>/L<sub>2</sub> ratio fit results from the EELS spectra.

consumptions upon cycling. In this project, alternative electrolytes and binders have been investigated to improve the SEI stability and therefore enhance the silicon electrochemical performance. Room-temperature ionic liquids (IL) have attracted much attention due to their low volatilities, low vapor pressures, thermal stabilities, high-voltage ability windows, and sufficient ionic conductivities. On the other hand, previous works have reported Na-CMC and PAA polymer binders are of great interest compared to PVDF because they improve the electrode integrity. In this work, the effect of CMC and PAA binders on the electrochemical performance of silicon cycled in EMIFSI-LiFSI electrolyte have been studied. Figure 54 shows the initial charge and discharge voltage profiles of the silicon electrode cycled in IL with two binders within the voltage range of 0.05-1 V at C/20. In the first cycle, the charge capacities are 3533 and 3660 mAh/g and the CEs are 70% and 72.8% for the CMC and PAA binders, respectively. The surface and interfacial characterization of these electrodes at various cycle numbers are under way using STEM, SEM, and XPS techniques to study the SEI morphology and chemistry evolution.

formed on the surface regions (less than 2 nm) due to TM migration from the TM layer to the neighboring lithium layer. Spatially resolved EELS (see Figure 53b) was also performed using a step size of ~6 Å from surface to bulk. The data points are aligned with the STEM image to specify where the specific spectrum was taken. The Oxygen K-edge pre-peak, aligned to the onset energy of 532 eV, is associated with the hybridization states between TM 3d and oxygen 2p orbitals in the octahedral unit. There is no oxygen pre-peak detected in the spectra obtained in the surface region. From surface to bulk, the intensity of the pre-peaks increases gradually. Manganese L-edge EELS was also collected from the identical area. Previous studies have shown that the L<sub>3</sub>/L<sub>2</sub> ratio is sensitive to the valence state of manganese. In the detailed L<sub>3</sub>/L<sub>2</sub> ratio analysis shown in Figure 53c, it is going to lower manganese oxidation state within a ~ 2 nm region from the surface, which is consistent with the XPS result in the last report. The generation of the reduced manganese can be a direct consequence of the formation of a large number of oxygen vacancies, which once again proves oxygen participates in the electrochemical cycling.

### Investigating the Effect of Binders of Silicon Anode Using a Bis(fluorosulfonyl)imide-Based Ionic Liquid

Silicon electrodes suffer from unstable SEI formation, which results in continuous Li<sup>+</sup> and electrolyte

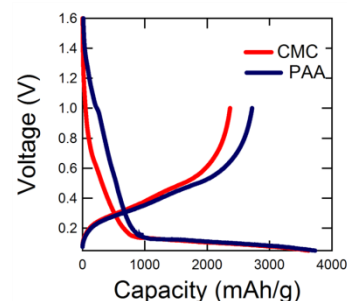


**Figure 54.** First charge and discharge profiles of silicon with CMC and PAA binders.

## Patents/Publications/Presentations

### Publication

- Qiu, B., and M. Zhang, Y. Xia, Z. Liu, and Y. S. Meng. “Understanding and Controlling Anionic Electrochemical Activity in High-Capacity Oxides for Next Generation Li-Ion Batteries.” *Chem. Mater.*, accepted.

### Presentation

- 2016 MRS Fall Meeting, Boston (2016): “Minimize the Voltage Degradation in Li-rich Layered Oxide Cathode Materials by Morphology Control”; M. Zhang, H. D. Liu, C. Fang, and Y. S. Meng.

**Task 5.6 – *In Situ* Diagnostics of Coupled Electrochemical-Mechanical Properties of Solid Electrolyte Interphases on Lithium Metal Rechargeable Batteries**  
(Xingcheng Xiao, General Motors; Brian W. Sheldon, Brown University; Yue Qi, Michigan State University; and Y.T. Cheng, University of Kentucky)

**Project Objective.** The project objective is to develop a comprehensive set of *in situ* diagnostic techniques combined with atomic/continuum modeling schemes to investigate and understand the coupled mechanical/chemical degradation of the SEI layer/lithium system during lithium cycling. The goal of this understanding is to develop a new coating design strategy to achieve high cycle efficiency/dendrite free and extend the cycle life of high-energy-density batteries with lithium as the anode for EV application.

**Project Impact.** The fundamental understanding of the coupled mechanical/chemical degradation of the SEI layer during lithium cycling will enable the project to identify the desirable mechanical properties on SEI/lithium as a system and the specific transport properties that enable the homogenous lithium stripping/plating while avoiding the mossy structure. Furthermore, it will allow the project to develop a highly impactful strategy to protect lithium metal and achieve dendrite-free high cycle efficiency, which can dramatically increase the energy density of lithium batteries for EV applications.

**Approach.** Different *in situ* techniques, including AFM, nanoindenter, dilatometer, and stress-sensor, will be developed to investigate the mechanical compatibility between SEI and soft lithium and the relationship between surface morphology and current density distribution that results in an inhomogeneous lithium plating/stripping process. Multiple strategies will be developed to tailor the mechanical and transport properties of SEI and to properly engineer the protective coating/lithium interface.

**Out-Year Goals.** The project will first develop a lithium film model-system with well-controlled thickness, roughness, and textures for different *in situ* diagnostic tool and cycle performance tests. Then, a comprehensive set of *in situ* diagnostic tools will be adapted from the previous work to characterize the mechanical behavior of both SEI and lithium electrodes. In parallel, the advanced electrochemical characterization and postmortem analysis will be used to characterize the electrochemical performance, composition, and microstructure of the SEI and lithium.

**Collaborations.** Prof. Huajian Gao (Brown University) and Dr. Peng Lu (GM) will be the key researchers involved in continuum simulation and postmortem analysis. Dr. Chongmin Wang (PNNL), Dr. Wangli Yang (LBNL) and Dr. Jie Xiao will be collaborators on advanced *in situ* analysis and electrolyte additives.

### Milestones

1. Lithium film electrodes with controlled thickness and roughness developed. (December 2016 – Complete)
2. Composition map of representative SEI as a function of current density and capacity established. (March 2017 – Complete)
3. The results from different tools correlated with SEI microstructure, transport properties, and cycle performance. (June 2017)
4. *Go/No-Go*: Decision based on information obtained from *in situ* and *ex situ* experiments demonstrated to be complementary and coherent. (September 2017)

## Progress Report

**Established Capability for Deposited, Well-Controlled Lithium Thin-Film Electrode.** A key challenge associated with identifying the governing failure modes is the lack of a well-controlled system that can enable a quantitative assessment of the coupled mechanical and chemical behavior of the SEI layer. Investigating SEI/lithium system in an electrochemical environment is particularly difficult because the SEI is extremely thin, lithium is very soft, and both are air/moisture sensitive. The unique PVD system integrated with glovebox (as shown in Figure 55) at GM enables us to make Li-film electrodes on a current collector by depositing lithium. In addition, a well-controlled protective coating can be directly deposited on lithium afterwards.



Figure 55. PVD system integrated with glovebox for making lithium thin-film electrode and protective coatings.

**Established *In Situ* Nanoindentation to Investigate the Mechanical Properties of Lithium Metal.** The project used a G200 nanoindentation system installed in an argon-filled glovebox. As shown in Figure 56a, the load corresponding to the same depth increases with the value of  $\dot{F}/F$  for constant strain rate-controlled nanoindentation tests. The creep penetration depth during the holding period increases with the loading rate. As with viscoelastic materials, “noses” appeared at the initial part of the unloading curves. Elastic recovery during unloading is only few tens of nanometers. Therefore, the indentation deformation is mainly plastic.

The load-displacement (L-D) curves of the loading rate-controlled and indentation strain rate-controlled nanoindentation shows rate-dependent characteristics. Combined with an iterative finite element (FE) modeling procedure, the viscoplastic constitutive law of lithium is determined as follows,

$$\sigma_f = 0.0042 \varepsilon_p^{0.23} \left[ 1 + \left( \frac{\dot{\varepsilon}_p}{0.30} \right)^{0.54} \right]$$

where  $\sigma_f$  is the flow stress,  $\varepsilon_p$  is the plastic strain and  $\dot{\varepsilon}_p$  is the plastic strain rate. In addition, FE modeling results showed that elastic modulus, on the order of several gigapascals, has a negligible influence on the nanoindentation response of lithium at ambient temperature (Figure 57). Therefore, the elastic modulus may not be as important as the viscoplastic properties of lithium in the mechanical design of Li-metal electrodes.

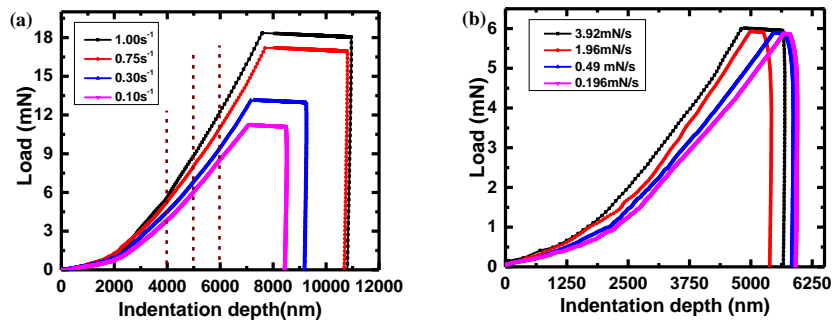


Figure 56. (a) Typical L-D curves with different indentation strain rates ( $\dot{F}/F$ ). (b) Typical L-D curves with different loading rates ( $\dot{F}$ ).

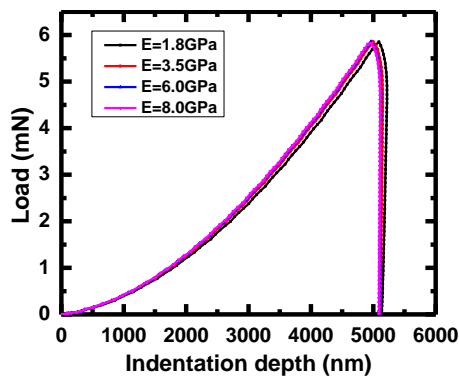


Figure 57. The effect of elastic modulus on the L-D curves. The L-D curves with  $E \geq 3.5$  GPa nearly overlap with each other.

## Patents/Publications/Presentations

### Publication

- Wang, Y., and Y.-T. Cheng. “A Nanoindentation Study of the Viscoplastic Behavior of Pure Lithium.” *Scripta Materialia* 130 (2017): 191–195.



## Task 5.7 – Microscopy Investigation on the Fading Mechanism of Electrode Materials (Chongmin Wang, Pacific Northwest National Laboratory)

**Project Objective.** The objective will be using a combination of *ex situ*, *in situ*, and *operando* high-resolution TEM and spectroscopy to probe the fading mechanism of layer structured cathode under high-voltage operating condition. To complement the high-resolution TEM study, *in situ* liquid cell SIMS and atom probe tomography (APT) will also be used to gain structural and chemical evolution of electrodes and correlate the structural and chemical evolution with battery performance.

**Project Impact.** The proposed characterization work focused on atomic level structural and chemical analysis and direct correlation with battery fading properties. The work can be directly used to guide the designing of electrode materials with tailored microstructure and chemistry for enhanced properties of increasing the energy density of Li-ion batteries and accelerate market acceptance of EV, especially for PHEV required by the EV Everywhere Grand Challenge.

**Approach.** This project will use the unique *ex situ* and *in situ* TEM methods to probe the structure of Li-ion batteries, especially a biasing liquid electrochemical cell that uses a real electrolyte in a nano-battery configuration. It will also use various microscopic techniques, including *ex situ*, *in situ*, and especially the *operando* TEM system, to study the fading mechanism of electrode materials in batteries. This project will be closely integrated with other research and development efforts on high-capacity cathode and anode projects in the BMR Program to: (1) discover the origins of voltage and capacity fading in high-capacity layered cathodes, and (2) provide guidance for overcoming barriers to long cycle stability of electrode materials.

**Out-Year-Goals.** This project has the following out-year goals:

- Multi-scale (ranging from atomic-scale to meso-scale) *ex situ/in situ* and *operando* TEM investigation of failure mechanisms for energy-storage materials and devices. Atomic-level *in situ* TEM and STEM imaging to help develop fundamental understanding of electrochemical energy-storage processes and kinetics of electrodes.
- Extended the *in situ* TEM capability for energy storage technology beyond lithium ions, such as Li-S, Li-air, Li-metal, sodium ions, and multi-valence ions

**Collaborations.** This project collaborates with Michael M. Thackeray and Jason Croy (ANL); Guoying Chen (LBNL); Jagjit Nanda (ORNL); Chunmei Ban (NREL); Khalil Amine (ANL); Donghai Wang (Penn State), Arumugam Manthiram (UT Austin), Wei Tong (LBNL), Gao Liu (LBNL); Yi Cui (Stanford); Jason Zhang (PNNL); Jun Liu (PNNL); Xingcheng Xiao (GM), Shirley Meng (UCSD), and Stan Whittingham (SUNY – Binghamton).

### Milestones

1. Void formation mechanism and its correlation with ionic mobility in the lattice upon high-voltage cycling; exploring lattice stability with dopant such as tin, silicon, and phosphorous. (March 2017 – In progress)
2. Atomic-level identification of the behavior of nickel, manganese, cobalt, and aluminum in the NCM and NCA when cycled at high voltage; correlate with fading mechanism. (June 2017)
3. Environmental TEM (ETEM) studies of the nickel segregation characteristics, and correlation with materials processing temperature. (September 2017)

## Progress Report

Although it has been observed that ALD- $\text{Al}_2\text{O}_3$  coating of cathode particle can significantly improve battery performance, the exact functioning mechanism of such a thin layer of coating, in terms of surface chemistry between cathode and electrolyte, is not sufficiently understood.

The advanced STEM and spectroscopy techniques, X-ray EDS and EELS have been used to probe the functioning mechanism of ALD- $\text{Al}_2\text{O}_3$  coating layer on LMR cathode ( $\text{Li}_{1.2}\text{Ni}_{0.2}\text{Mn}_{0.6}\text{O}_2$ ). For the first time, it is directly visualized that the  $\text{Al}_2\text{O}_3$  coating layer suppresses the cathode/electrolyte side reactions. The battery cycling that induced severe manganese reduction that frequently occurred on uncoated cathode particle surface was significantly suppressed following the  $\text{Al}_2\text{O}_3$  coating, therefore resulting in well-preserved particle surface and stabilized surface EELS structure.

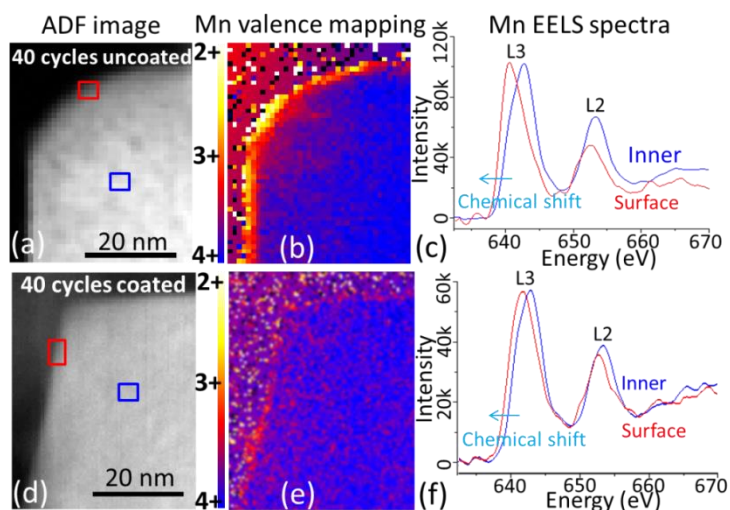


**Figure 58.** Scanning transmission electron microscopy – electron energy loss spectroscopy (STEM–EELS) analysis valence mapping of the 40 cycles and its correlation with the  $\text{Al}_2\text{O}_3$  coating layer. (a–c) Uncoated samples. (d–f) Coated samples. (a) Annular dark field (ADF) image. (b) Estimated manganese valence state map based on EELS chemical shift. (c) Manganese EELS spectra from surface and inner region in (a). (d) ADF image. (e) Estimated manganese valence state map from EELS chemical shift. (f) Manganese EELS spectra from surface and inner region in (d).

Battery cycling induced surface manganese reduction was perceived as one of the most important causes of cathode material degradation. Previous reports consistently showed that surface corrosion and surface layer structure transformation were closely related to manganese cation valence reduction in layered Mn-based cathode materials, because reduced manganese cations (such as  $\text{Mn}^{2+}$ ) are believed to have higher mobility and can be easily dissolved into electrolyte. Moreover, the well-known Jahn-Teller effect will occur and destabilize the structure when manganese average valence state is reduced to  $3+$ . Therefore, the stability of LMR cathode is heavily depended on manganese valence state. Thus, the manganese valence state and its spatial distribution on both uncoated and coated particle upon battery cycling were probed using STEM-EELS. Previous studies have established two methods can be used to estimate manganese valence state using EELS. One is through measuring Mn-L edge onset energy shift (that is, chemical shift). The other is by calculating manganese  $L_3/L_2$  ratio. In this work, chemical shift was used to estimate manganese valence state, because it is more reliable due to its relative insensitivity to sample thickness as well as the reliable processing protocol. In this case, manganese chemical shift was estimated by measuring  $L_3$  edge peak positions, because bulk EELS peak onset can be modified by the top and bottom surface layers, misleading the chemical shift measurement. Figure 58b/e show the measured manganese valence states for the uncoated and coated particles after 40 cycles, respectively. A distinctive difference can be seen on the spatial distribution of manganese valence between uncoated and coated particles. For the uncoated particle, the  $\text{Mn}^{2+}$  is uniquely located at the outmost surface of particle followed by a thick  $\text{Mn}^{3+}$  layer. In contrast, for the  $\text{Al}_2\text{O}_3$  coated particle, manganese reduction only occurred in a very thin surface layer and the valence states are well above  $3+$ . Further, the EELS spectra acquired from surface and inner part of both uncoated and coated samples also support the mapping results (Figure 58c/f), where the chemical shift and manganese  $L_3/L_2$  ratio are distinctively different for the coated and uncoated samples. The spatial mapping of manganese valence distribution and its apparent correlation with the  $\text{Al}_2\text{O}_3$  coating layer clearly indicate that  $\text{Al}_2\text{O}_3$  coating suppresses reduction of manganese at the cathode/electrolyte interface, therefore mitigating the dissolution of the manganese into the electrolyte.

## Patents/Publications/Presentations

### Publications

- Shen, Chenfei, and Mingyuan Ge, Langli Luo, Xin Fang, Yihang Liu, Anyi Zhang, Jiepeng Rong, Chongmin Wang, and Chongwu Zhou. “*In Situ* and *Ex Situ* TEM Study of Lithiation Behaviors of Porous Silicon Nanostructures.” *Sci. Rep.* 6 (2016): 31334.
- Lee, Eungje, and Joel Blauwkamp, Fernando C. Castro, Jinsong Wu, Vinayak P. Dravid, Pengfei Yan, Chongmin Wang, Soo Kim, Christopher Wolverton, Roy Benedek, Fulya Dogan, Joong Sun Park, Jason R. Croy, and Michael M. Thackeray. “Exploring Lithium-Cobalt-Nickel Oxide Spinel Electrodes for  $\geq 3.5$  V Li-Ion Cells.” *ACS Appl. Mater. Interfaces* 8 (2016): 27720–27729.

### Presentation

- 2016 MRS Fall Meeting, Boston (November 28, 2016): “Direct *In Situ* TEM Atomic Level Observation of Intercalation to Conversion of  $\text{WO}_3$  upon Li, Na, and Ca Ions Insertion.” Chongmin Wang, Yingge Du, He Yang, and Scott X. Mao.

## Task 5.8 – Characterization and Computational Modeling of Structurally Integrated Electrodes (Michael M. Thackeray and Jason R. Croy, Argonne National Laboratory)

**Project Objective.** The primary project objective is to explore the fundamental, atomic-scale processes that are most relevant to the challenges of next-generation, energy-storage technologies, in particular, high-capacity, structurally integrated electrode materials. A deeper understanding of these materials relies on novel and challenging experiments that are only possible through unique facilities and resources. The goal is to capitalize on a broad range of facilities to advance the field through cutting-edge science, collaborations, and multi-disciplinary efforts to characterize and model structurally integrated electrode systems, notably those with both layered and spinel character.

**Project Impact.** This project capitalizes on and exploits DOE user facilities and other accessible national and international facilities (including skilled and trained personnel) to produce knowledge to advance Li-ion battery materials. Specifically, furthering the understanding of structure-electrochemical property relationships and degradation mechanisms will contribute significantly to meeting the near- to long-term goals of PHEV and EV battery technologies.

**Approach.** A wide array of characterization techniques including X-ray and neutron diffraction, X-ray absorption, emission and scattering, HRTEM, Raman spectroscopy, and theory will be brought together to focus on challenging experimental problems. Combined, these resources promise an unparalleled look into the structural, electrochemical, and chemical mechanisms at play in novel, complex electrode/electrolyte systems being explored at ANL.

**Out-Year Goals.** The out-year goals are as follows:

- Gain new, fundamental insights into complex structures and degradation mechanisms of high-capacity composite cathode materials from novel, probing experiments carried out at user facilities and beyond.
- Investigate structure-property relationships that will provide insight into the design of improved cathode materials.
- Use knowledge and understanding gained from this project to develop and scale up advanced cathode materials in practical Li-ion prototype cells.

**Collaborators.** This project collaborates with the following: J. R. Croy, A. Gutierrez, R. Benedek, and F. Dogan (CSE, ANL); M. Balasubramanian and Y. Ren (APS, ANL); Ashfia Huq (spallation neutron source, SNS, ORNL); V. Dravid and C. Wolverton (Northwestern University), and Chongmin Wang (PNNL).

### Milestones

1. Characterize bulk and surface properties of structurally integrated electrode materials using the DOE User Facilities at Argonne (APS, EMC, and ALCF) and facilities elsewhere (for example, the SNS at ORNL), The EMSL at PNNL, and the NUANCE characterization center at Northwestern University. (September 2017 – In progress)
2. Use complementary theoretical approaches to further the understanding of structural and electrochemical properties of LS electrodes and protective surface layers. (September 2016 – In progress)
3. Analysis, interpretation, and dissemination of collected data for publication and presentation. (September 2017 – In progress)

## Progress Report

The structural integration of a spinel component into a layered electrode structure or a two-component LL system has been demonstrated in model compounds such as  $x\text{Li}_2\text{MnO}_3 \cdot \text{Li}_{1-x}\text{M}_2\text{-xO}_4$  (LS) and  $x[\text{Li}_2\text{MnO}_3 \cdot \text{LiMO}_2] \cdot (1-x)\text{LiM}_2\text{O}_4$  (LLS), where M is typically a TM ion, and that these materials have advantages over conventional layered electrode materials.<sup>1</sup> They can be simply prepared by reducing the amount of lithium in the precursor materials normally used to synthesize stoichiometric layered or LL structures. For example, reducing the lithium content of a stoichiometric  $0.5\text{Li}_2\text{MnO}_3 \cdot 0.5\text{LiMn}_{0.5}\text{Ni}_{0.5}\text{O}_2$  compound (alternatively,  $\text{Li}_{1.5}\text{Mn}_{0.75}\text{Ni}_{0.25}\text{O}_{2.5}$ ), in which the Mn:Ni ratio is 3:1, drives the composition towards the  $\text{LiMn}_{1.5}\text{Ni}_{0.5}\text{O}_4$  spinel apex of the phase diagram, following the LLS tie-line in Figure 59, while maintaining a constant Mn:Ni (3:1) ratio.<sup>2</sup> Note that this is a special case that has been observed experimentally and that the term ‘layered-layered-spinel’ is used for convenience because it describes the compositions of all compounds within this phase space. A question that remains unanswered is: At what lithium deficiency do the TM ions start diffusing into the Li-rich layers during synthesis to provide spinel (or spinel-like) character to predominantly layered structures with complex cation arrangements?

In an attempt to better understand the structural complexity of LLS materials, a series of compounds was prepared by reducing the lithium content in  $0.25\text{Li}_2\text{MnO}_3 \cdot 0.75\text{Li}(\text{Ni}_{0.375}\text{Mn}_{0.375}\text{Co}_{0.25})\text{O}_2$  by various amounts and analyzed by combined Rietveld refinement analyses of neutron and synchrotron XRD data. For simplicity, the normalized composition and formula,  $\text{Li}_{1.25-x}(\text{Ni}_{0.28}\text{Mn}_{0.53}\text{Co}_{0.19})\text{O}_{2.25-\delta}$  ( $0 \leq x \leq 0.25$ ), is used for this discussion.

For  $0 \leq x \leq 0.075$ , both neutron and XRD patterns could be indexed to compounds with either monoclinic symmetry ( $C2/m$ ), denoted M-phase or, if the weak ordering peaks associated with the M-phase were ignored, to trigonal symmetry ( $R-3m$ ), denoted L-phase. For  $x = 0.1$ , the XRD pattern showed additional peaks that were tentatively assigned to a spinel component with cubic symmetry, denoted S-phase. These initial refinements and attempts to use a two-phase model to refine both layered and spinel components have not provided conclusive results. The analyses are continuing; HRTEM studies are being planned to gather more insight into the structural composition of these complex electrode materials.

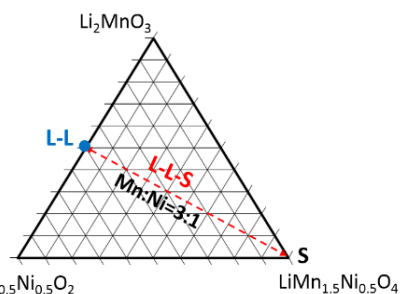


Figure 59. The compositional phase space of a layered (L)-layered (L)-spinel (S) system.  $\text{Li}_2\text{MnO}_3 \cdot \text{LiNi}_{0.5}\text{Mn}_{0.5}\text{O}_2 \cdot \text{LiNi}_{0.5}\text{Mn}_{1.5}\text{O}_4$ .

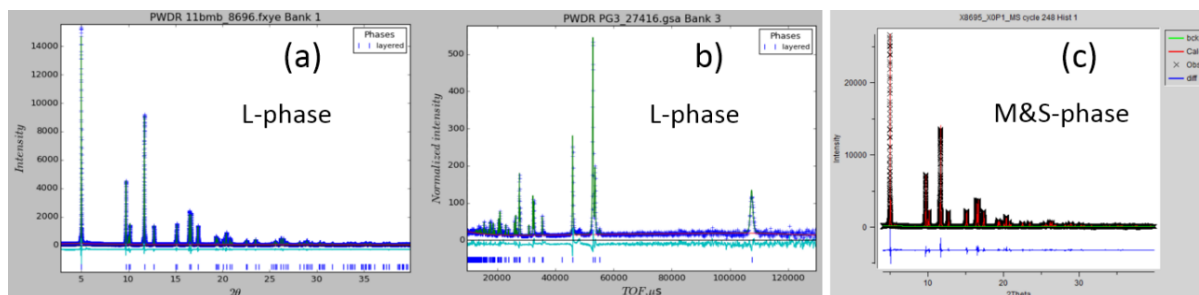


Figure 60. Rietveld refinement results of (a) synchrotron X-ray and (b) neutron diffraction of the  $x = 0.75$  sample. (c) Synchrotron X-ray diffraction of the  $x = 1.0$  sample.

- [1] Long, B. R., and J. R. Croy, J. S. Park, J. Wen, D. J. Miller, and M. M. Thackeray. *J. Electrochem. Soc.* 161., no. 14 (2014): A2160.
- [2] Park, S.-H., and S.-H. Kang, C. S. Johnson, K. Amine, and M. M. Thackeray. *Electrochem. Commun.* 9 (2007): 262.

## TASK 6 – MODELING ADVANCED ELECTRODE MATERIALS

### Summary and Highlights

Achieving the performance, life, and cost targets outlined in the EV Everywhere Grand Challenge will require moving to next generation chemistries, such as higher capacity Li-ion intercalation cathodes, silicon and other alloy-based anodes, Li-metal anode, and sulfur cathodes. However, numerous problems plague the development of these systems, from material-level challenges in ensuring reversibility to electrode-level issues in accommodating volume changes, to cell-level challenges in preventing cross talk between the electrodes. In this task, a mathematical perspective is applied to these challenges to provide an understanding of the underlying phenomenon and to suggest solutions that can be implemented by the material synthesis and electrode architecture groups.

The effort spans multiple length scales from *ab initio* methods to continuum-scale techniques. Models are combined with experiments, and extensive collaborations are established with experimental groups to ensure that the predictions match reality. Efforts are also focused on obtaining the parameters needed for the models, either from lower-length scale methods or from experiments. Projects also emphasize pushing the boundaries of the modeling techniques used to ensure that the task stays at the cutting edge.

In the area of intercalation cathodes, the effort is focused on understanding the working principles of the high nickel layered materials with an aim of understanding structural changes and the associated changes in transport properties. In addition, focus is paid to the assembling of porous electrodes with particles to predict the conduction behavior and developing tools to measure electronic conduction. In this quarter, the theory effort on understating and devising safety strategies has moved to examining the role of dopants to inhibit oxygen loss. In addition, the efforts to rationally design new disordered cathode materials continue with a deeper understanding this quarter on the origin of cation disorder. Finally, the conductivity probe method previously developed to examine anisotropic conduction in battery electrodes has been extended to a flexible design, and results suggest that the conductivity measurements are largely consistent with the rigid probe.

In the area of silicon anodes, the effort is in trying to understand the interfacial instability and suggest ways to improve the cyclability of the system. A new project has also started this year to examine the mechanical aspects of SEI cracking. Work this quarter has examined the stability of SEIs based on calculating the discontinuity in the electrical potential at the interface. In addition, work on the cracking of the SEI has looked at the effect at multiple length scales.

In the area of lithium metal anodes, the focus is on understanding how materials can be designed to prevent dendrite growth at high current densities using continuum modeling approaches. The results are used to guide materials development by providing the properties needed to prevent dendrites, while also achieving the energy and power goals. In this quarter, the models have examined the initial state of lithium on the propensity for dendrite formation and have concluded that an initially relaxed state of lithium is more representative of experimental data, contrasting previous literature models.

## Task 6.1 – Predicting and Understanding Novel Electrode Materials from First Principles (Kristin Persson, Lawrence Berkeley National Laboratory)

**Project Objective.** This project supports VTO programmatic goals by developing next-generation, high-energy cathode materials and enabling stable cathode operation at high voltages through target particle morphology design, functional coatings, and rational design of electrolytes. The end-of-project goals include: (1) novel disordered, high-rate Li-excess cathodes, (2) new fundamental understanding of the cathode/electrolyte interface and the factors that control the interfacial chemistry and interfacial impedance, (3) critical surface and coating design and optimization strategies that will improve cycling of Li-ion battery cathodes, and finally (4) understanding of the factors that govern stability in nonaqueous electrolytes for Li-ion and Li-S systems.

**Project Impact.** To enhance the performance of Li-ion systems, improvements on the cathode and the electrolyte side are needed. This project is aimed to result in an improved understanding of the atomistic mechanisms underlying the surface behavior and performance of the Li-ion cathode materials with the ultimate goal being to suggest strategies, such as coatings, surface protection, and particle morphology design. Furthermore, fundamental studies of electrolyte stability, as a function of solvent and salt concentrations, and components will be conducted.

**Out-Year Goals.** Stable interfaces will be determined by focusing initially on degradation mechanisms related to the release of surface oxygen at high charge. Tuning particle morphology and coating materials—both of crystalline as well as amorphous structure—will be explored using the Materials Project. For the electrolyte development, the work will be aimed toward understanding the atomistic interactions underlying the performance of lithium electrolytes specifically elucidating the solvation structure (as a function of salt concentration) and its impact on the stability of the different liquid constituent species.

**Collaborations.** This project is highly collaborative between BMR PIs G. Chen (LBNL), G. Ceder (LBNL) and V. Srinivasan (ANL). Cathode design and synthesis will be performed by Chen and Ceder, surface design by Persson, and electrolyte design and testing by Persson and Srinivasan.

### Milestones

1. Provide matrix of surface candidate dopants based on literature search and practical considerations. (December 2016 – Complete)
2. Benchmark calculations of amorphous coating materials, that is,  $\text{Al}_2\text{O}_3/\text{SiO}_2$ . (March 2017 – In progress)
3. Present first screening of surface dopants. (May 2017 – In progress)
4. *Go/No-Go*: New strategies are identified. Stop this approach if facet stabilization cannot be achieved. (May 2017 – In progress)
5. Two electrolyte benchmark formulations for Li-S and Li-ion are evaluated from stability and diffusion. (September 2017 – In progress)

## Progress Report

The current BMR project is aimed toward the study of surface stability of the Li-excess layered materials using first-principles calculations. The previous work showed that the end member  $\text{Li}_2\text{MnO}_3$  is rendered unstable toward oxygen release for low amounts of lithium removal. The project continues to study mitigation strategies to inhibit spontaneous oxygen evolution to improve the cycling performance and rate behavior of this class of materials. Figure 61 shows the charge evolution of nearby cations as oxygen is removed.

To mitigate oxygen release, lithium excess cathodes may be protected through post-synthesis processes such as surface doping or surface coating. Hence, the project is first focusing on investigation of surface dopants, with the assumption that stable dopants will substitute on the TM or lithium sites. Two commonly used dopants are chromium and nickel. Figure 62 shows the effects of

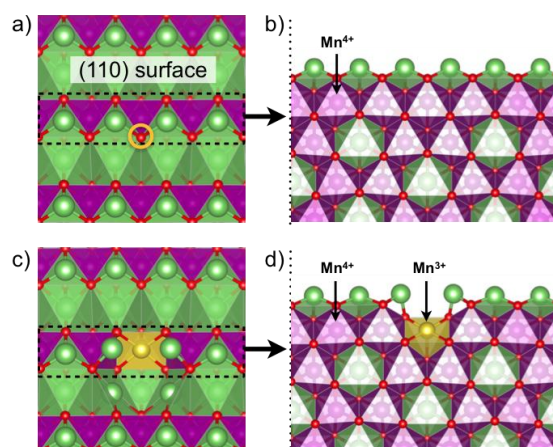


**Figure 61.** Spontaneous oxygen evolution and its impact on the nearest cation. For instance, surface  $\text{Mn}^{4+}$  (purple octahedral site) to  $\text{Mn}^{3+}$  (yellow site) by first oxygen evolution (yellow site in c/d).

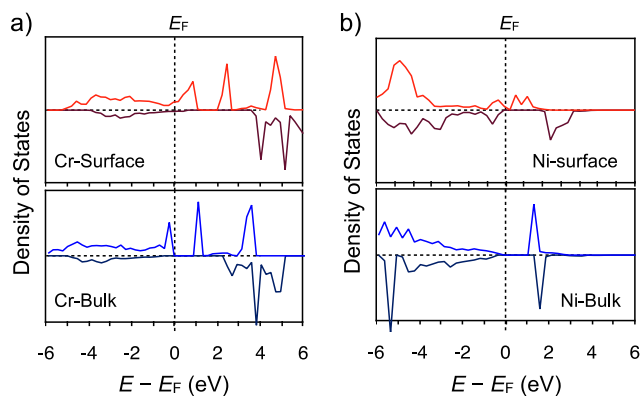


**Figure 62.** The d-orbital density of state (DOS) of the defect site in the surface (top) and at the bulk (bottom). Cr defect prefers the surface as reflected by the bulk versus surface DOS behavior (a). Ni shows the opposite behavior (b).

surface and bulk doping with chromium and nickel through first-principles electronic structure calculations for the (010) surface as compared to the bulk. Chromium and nickel have similar average coordination numbers and cation radiuses, such that the cation radiuses of chromium and nickel are 6.45% smaller and 6.45% larger than manganese ( $0.62 \text{ \AA}$ ), respectively. However, the electronic structures of the dopants are dissimilar. Bulk chromium defects increase the total energy of the system owing to a peak in the occupied density of state (Figure 62a). In contrast, a surface chromium defect shows less impact on the total energy of the system as compared to the bulk case. Bulk nickel defect prefers the bulk as compared to the surface, as presented in Figure 62b, which agrees well with common knowledge in these layered materials.

## Patents/Publications/Presentations

### Presentation

- 2016 MRS Fall Meeting, Boston (November 30, 2016): “Surface Morphology and Surface Stability against Oxygen Loss of the Li-Excess Layered Cathode Material”; Yongwoo Shin and Kristin A. Persson.



## Task 6.2 – Addressing Heterogeneity in Electrode Fabrication Processes (Dean Wheeler and Brian Mazzeo, Brigham Young University)

**Project Objective.** The project goal is to better understand connections between fabrication conditions and undesired heterogeneity of thin-film electrodes by means of new nondestructive inspection techniques and computer models. Two nondestructive inspection techniques will be developed or improved to characterize electrochemical and mechanical uniformity of the electrodes. The first tool will be a flexible contact probe on a polymer substrate for rapidly measuring local electrical conductivity across electrodes of any geometry. The second tool will be a new acoustic probe that measures local elasticity and density of the composite film. These two prototyping efforts will be tied together by a particle-based microstructure model that allows prediction and correlation of electrode conductive and mechanical properties with fabrication conditions.

**Project Impact.** This work will result in new diagnostic and modeling tools for rapidly and conveniently interrogating how well homogeneity has been maintained in electrodes during fabrication and in subsequent cycling. Real-time measurement of heterogeneity will enable manufacturer quality control improvements. The measurement and modeling tools will further enable researchers to compare different electrodes, improve formulations and processes, and anticipate cell performance of new designs.

**Out-Year Goals.** This project was initiated October 2016 and concludes September 2018. Overall goals by fiscal year are as follows:

- **2017.** Fabricate first-generation flexible conductivity probe and proof-of-concept of acoustic probe; improve microstructure model to match experiment.
- **2018.** Integrate flex probe with test fixtures suitable for assessment of large or continuous samples; demonstrate measurement of localized ionic conductivity.

**Collaborations.** Ram Subbaraman (Bosch), Daniel Abraham (ANL), Steve Harris (LBNL), Bryant Polzin (ANL), and Karim Zaghib (HQ) have provided battery materials for analysis. Other collaborations and the transfer of this technology to interested parties are being pursued.

### Milestones

1. Complete flex probe prototype and demonstrate that measurements match those for the previous rigid probe. (December 2017 – Complete)
2. Integrate the flex probe with existing high-precision positioning system and make measurements on 3 different electrode materials. (Q2 – In progress)
3. Demonstrate that the dynamic particle packing (DPP) model can predict effective conductivities that match experiment for 3 different electrode materials. (Q3)
4. Complete prototype of localized acoustic probe and associated model. *Go/No-Go*: Determine whether to continue developing the acoustic method by assessing sensitivity to film stiffness. (Q4)

## Progress Report

**Milestone 1 (Complete).** The first milestone was to demonstrate that the micro-flex-line probe ( $\mu$ FLP), which is the flexible variant of the micro-N-line probe ( $\mu$ NLP), obtains valid measurements of electrode-film electronic conductivity. Specifically, the flex probe results are to be compared to those obtained for the previously validated  $\mu$ NLP. Figure 63 shows a side-by-side comparison of the geometry of the completed  $\mu$ NLP and the  $\mu$ FLP probes. In this case  $N = 6$ ; that is, there are 6 parallel lines on the devices, 4 of which are used for any particular electrical measurement.

The design and materials used to construct the  $\mu$ FLP were iterated and improved to increase reliability of the measurements. Nevertheless, this should still be considered the first-generation design; further improvements are anticipated. For this report, the primary test material used is an anode provided by an undisclosed commercial battery manufacturer.

To obtain the results found in Table 1, tests were performed as follows. Using a  $\mu$ NLP, an electrical sample of the electrode film was collected in 9 independent locations and used with the inversion model to obtain average conductivity with 95% confidence interval. The process was then repeated on the same sample using the  $\mu$ FLP.

**Table 1. Experimental conductivity results (with 95% confidence intervals) from using  $\mu$ NLP and  $\mu$ FLP on the same electrode sample.**

	Rigid probe	Flex probe
Conductivity (mS/cm)	1421 $\pm$ 33	1496 $\pm$ 182

These results show that the  $\mu$ FLP measures conductivity that is largely consistent with measurements of the rigid probe, though the significance level is not as high as ultimately desired. Through these and other results there are indications of a modest bias of the flex probe toward measuring larger conductivity values than does the rigid probe. This may be caused by a small amount of current leakage between lines on the flex probe. Work will continue on the flex probe to confirm this hypothesis and reduce the problem so as to improve accuracy relative to other methods. It is anticipated that as the flexible probe becomes a more mature technology as a result of this project, it will allow conductivity measurements on thin-film electrodes in new geometries.

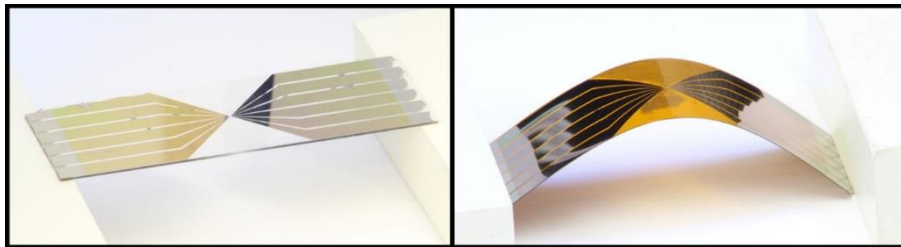


**Figure 63. Side-by-side comparison of the rigid micro-N-line probe consisting of metal deposited on a glass substrate (left), and the flexible micro-flex-line probe consisting of metal deposited on a polyimide substrate (right).**

## Patents/Publications/Presentations

No publications were made this quarter, though several are in preparation. Additionally, two presentations were made in October 2016 based on previous EERE-funded work:

- 2016 PRIME / ECS, Honolulu (October 2016): “A Predictive Model of Lithium-Ion Electrode Fabrication, Including Mixing, Coating, Drying, and Calendering”; M. Mehdi Forouzan, Anthony Gillespie, Nicholas Lewis, Brian A. Mazzeo, and Dean R. Wheeler.
- 2016 PRIME / ECS, Honolulu (October 2016): “Correlation of Local Conductivity to Microstructure for Li-Ion Battery Electrodes by Use of a Contact Probe and SEM/FIB”; John E. Vogel, William Lange, Derek Clement, Brian A. Mazzeo, and Dean R. Wheeler.

## Task 6.3 – Understanding and Strategies for Controlled Interfacial Phenomena in Lithium-Ion Batteries and Beyond (Perla Balbuena, Jorge Seminario, and Partha Mukherjee, Texas A&M University)

**Project Objective.** The project objective is to evaluate and characterize interfacial phenomena in lithiated silicon and lithium metal anodes and to develop guidelines for potential solutions leading to controlled reactivity at electrode/electrolyte interfaces of rechargeable batteries using advanced modeling techniques based on first-principles.

**Project Impact.** Understanding SEI growth on constantly evolving silicon surfaces and on highly reactive Li-metal surfaces is expected to define the electrolyte properties required in high performance cells. Strategies to control the silicon anode instability and pulverization issues and the well-known safety and short effective lifetimes of Li-metal anodes will be developed by tuning the electrolyte composition, structure, dynamic, and stability, as well as that of the electrode morphology and interactions with the electrolyte, on the basis of multiple characterizations of interfacial phenomena.

**Approach.** A comprehensive multiscale modeling approach including first-principles *ab initio* static and dynamics, classical molecular dynamics, and coarse-grained mesoscopic models will focus on the roles of the electrolyte chemical, structural, and dynamical properties and of the electrode micro- and nanostructure on the formation and evolution of the SEI layer and associated electrochemical performance on silicon and on Li-metal anodes.

**Out-Year Goals.** Work will progress toward characterizing lithiation and SEI formation at silicon surfaces as well as the subsequent cracking and reforming events under the most realistic modeling conditions. Similarly, with electrolyte effects on reactivity and dendrite formation in Li-metal surfaces. The project aims to capture how the chemistry of the various components of the electrolyte (mainly liquids but also solid polymers and gels) affects the main issues that influence the electrode performance.

**Collaborations.** This project funds work at Texas A&M University (TAMU). Dr. Chunmei Ban (NREL), Dr. Xiaolin Li (PNNL), and Dr. Kevin Leung (Sandia National Laboratories, SNL) may also contribute.

### Milestones

- Characterize SEI nucleation and modes of cracking as functions of SEI composition on lithiated silicon nanoparticles. (Q1)
- Identify and quantify Li-ion transport mechanisms through SEI blocks. (Q2)
- Evaluate and quantify the relative influence of mechanical and chemical degradation interplay in silicon active particles. (Q3)
- Characterize SEI growth as a function of SEI composition. Compare the SEI rate growth with experimental trends in the literature and from collaborators; if there is any disagreement, revise respective modeling approach. (Q4)

## Progress Report

A  $\text{Li}_{16}\text{Si}_{16}$  (1 nm) cluster was initially lithiated in vacuum from  $\text{LiSi}$  to  $\text{Li}_{3.5}\text{Si}$ . Then a  $\text{LiSi}$  cluster was sequentially lithiated in presence of the electrolyte. Two electrolyte compositions were employed: ethylene carbonate (EC) +  $\text{LiPF}_6$  and only EC. The process was followed with *ab initio* molecular dynamics (AIMD) simulations. During lithiation, simultaneous formation of the SEI layer was detected. Figure 64a shows a snapshot of the lithiated silicon cluster surrounded by fragments of the decomposition of EC and the formation of  $\text{LiF}$ , whereas only organic fragments are found in absence of  $\text{LiPF}_6$  (Figure 64b/c). The different SEI layer formed induces different volume changes of the cluster. An expansion of  $\sim 300\%$  is found for the only-organic SEI and of 219% when  $\text{LiF}$  is formed. This result illustrates the effect of the inorganic phase on controlling the volume expansion. However, in both cases, the majority of the added lithium ended up incorporated to the SEI layer instead of stored in the  $\text{Li}_x\text{Si}_y$  alloy, suggesting that the excessively small cluster size is less appropriate for lithium storage.

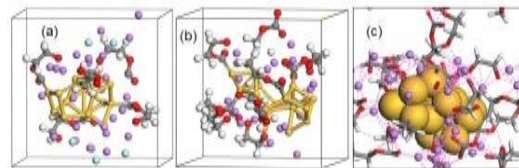


**Figure 64. Effect of electrolyte composition on lithiation and SEI formation in a silicon cluster. (a) EC/ $\text{LiPF}_6$ . (b) EC only. (c) Same as (b) with enlarged silicon atoms. Si (yellow), Li (purple), O (red), C (grey), H (white), F (light blue).**

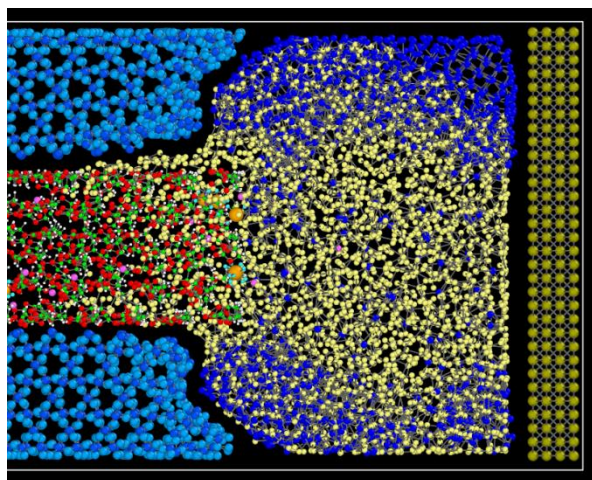


**Figure 65. Snapshot of a classical molecular dynamics simulation of a model silicon anode after a constant electric field of  $1 \text{ V/\AA}$  is applied. The model anode is in a larger cell containing also the electrolyte phase and the cathode. The charge is simulated by applying a constant potential to the cell. Si (blue), Li (yellow), Li (electrolyte, pink), C (green), H (white), O (red), P (orange), F (light blue).**

Classical molecular dynamics simulations were used to study the swelling, alloying, and amorphization of a silicon nanocrystal anode in a full nanobattery model during the first charge. A dissolved salt of  $\text{LiPF}_6$  in EC was chosen as the electrolyte solution and  $\text{LiCoO}_2$  as cathode. External electric fields were applied to emulate the charging, causing the migration of the lithium ions from the cathode to the anode, by drifting through the electrolyte solution, thus converting pristine silicon gradually into  $\text{Li}_{14}\text{Si}_5$  when fully lithiated. The volume of the anode increases with the amorphization of the silicon as the external field is applied by creating a layer of  $\text{Li}_x\text{Si}_y$  alloy between the electrolyte and the silicon nanocrystal. It is found that the drift velocity of lithium ions is greater than their velocity in the pure nanocrystal structure. This model allowed the evaluation of mechanical changes in the electrode during the first charge. Current efforts are oriented to adding the SEI and determining changes in volume and structure occurring during lithiation and delithiation.

In addition, a mesoscopic random lattice spring model coupled with solid-state diffusion of lithium in active particles, and SEI formation was developed to model fracture in the active material along with SEI film growth. The model solves the Li-induced mechanics interaction (that is, stress generation) in active particles and captures microcrack formation and propagation. The lithium diffusion induced stress deforms the spring elements. Fracture occurs when the strain energy in a spring exceeds the fracture energy threshold; consequently, these springs are removed from the network. The effect of fracture on diffusion inside the active material is incorporated by diffusion coefficients modified using a damage parameter. The cracks provide additional sites for lithium intercalation electrochemical reaction as well as SEI reaction. It was found that peripheral (surface) cracks form easily during delithiation and central cracks (close to active material center) during lithiation. The surface cracks provide extra area for intercalation and SEI reaction, while isolated central cracks only hinder diffusion of lithium ions inside the active material.

## Task 6.4 – First Principles Modeling of SEI Formation on Bare and Surface/Additive Modified Silicon Anode (Perla Balbuena, Texas A&M University)

**Project Objective.** This project aims to develop fundamental understanding of the molecular processes that lead to formation of an SEI layer due to electrolyte decomposition on silicon anodes, and to use such new knowledge in a rational selection of additives and/or coatings. The focus is on SEI layer formation and evolution during cycling and subsequent effects on capacity fade through two concatenated problems: (1) SEI layers formed on lithiated silicon surfaces, and (2) SEI layers formed on coated surfaces. Key issues being addressed include the dynamic evolution of the system and electron transfer through solid-liquid interfaces.

**Project Impact.** Finding the correspondence between electrolyte molecular properties and SEI formation mechanism, structure, and properties will allow identification of new/improved additives. Studies of SEI layer formation on modified surfaces will allow identification of effective coatings able to overcome the intrinsic deficiencies of SEI layers on bare surfaces.

**Approach.** Investigating the SEI layer formed on modified silicon surfaces involves the following: (1) analysis of the interfacial structure and properties of specific coating(s) deposited over the silicon anode surface, (2) characterization of the corresponding surface properties before and after lithiation, especially how such modified surfaces may interact with electrolyte systems (solvent/salt/additive), and (3) what SEI layer structure, composition, and properties may result from such interaction. This study will allow identification of effective additives and coatings able to overcome the intrinsic deficiencies of SEI layers on bare surfaces. Once the SEI layer is formed on bare or modified surfaces, it is exposed to cycling effects that influence its overall structure (including the anode), chemical, and mechanical stability.

**Out-Year Goals.** Elucidating SEI nucleation and electron transfer mechanisms leading to growth processes using a molecular level approach will help establish their relationship with capacity fading, which will lead to revisiting additive and/or coating design.

**Collaborations.** Work with Chunmei Ban (NREL) consists in modeling the deposition-reaction of alucone coating on silicon surfaces and their reactivity. Reduction of solvents and additives on silicon surfaces were studied in collaboration with K. Leung and S. Rempe, from SNL. This project collaborates with Professor Jorge Seminario (TAMU) on electron and ion transfer reactions and with Dr. Partha Mukherjee (TAMU) focusing on development of a multi-scale model to describe SEI growth on silicon anodes.

### Milestones

1. Determining matching and chemistry of solid-solid interfaces including possible cracking effects. Further force-field development and test for solid-liquid interfaces. (In progress)
2. Perform further computational studies on SEI formed in alucone coating including some experimental tests by Chunmei Ban and Clare Grey. (In progress)

## Progress Report

**Stability of Growing Solid-Solid Interfaces.** At the onset of nucleation of new phases, one important property is the mechanical stability of the interface between the growing nuclei and the support. One possible test

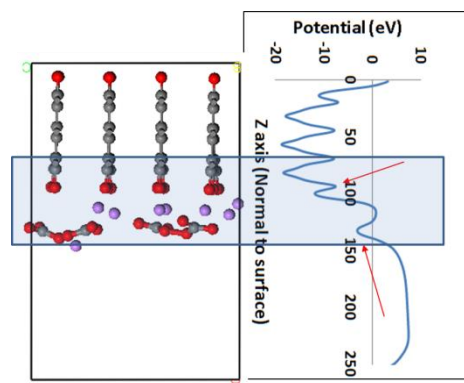


**Figure 66.** (left) Nucleation of  $\text{Li}_2\text{CO}_3$  over graphite electrode. Lithium ions interact with adsorbed oxygen atoms at the graphite edge. (right) Electrostatic potential (eV) of the nucleating phase on the solid electrode. Note the discontinuity at the interface (highlighted).

includes evaluation of electrostatic potential of the system, including the support phase in contact with the nucleating phase. At the interface, there is a discontinuity in this potential, the magnitude of which is an indicator of the degree of instability of the interface. The TAMU team has computed this indicator for various relevant interfaces as nucleation advances. The interfacial electrostatic potential is illustrated in Figure 66 for the nucleation of  $\text{Li}_2\text{CO}_3$  over a graphite surface. Initially,  $\text{CO}_3$  radical anions, products of decomposition of the solvent, are adsorbed on the graphite edges, and generate the sites where nucleation of  $\text{Li}_2\text{CO}_3$  may take place. The potential shown at the top corresponds to that of the electrode surface; the first red arrow points to the potential of the exposed graphite edges. After that, there is clear discontinuity in the potential, which corresponds to incipient nucleation of the  $\text{Li}_2\text{CO}_3$  phase. The difference between the two peaks shown with the red arrows is the indicator of the stability of the interface. As the difference reduces, the interface is more stable. The idea can be extended to evaluate nucleation of a heterogeneous film on the electrode. K. Leung (SNL) has modeled grain boundaries in a

LiF film coating a Li-metal surface. It was found that a substantial over-potential is needed to insert a lithium atom ( $\text{Li}^+ + e^-$ ) into the grain boundary core regions. As shown previously by this team, such lithium atoms can carry an undesirable electric current and degrade the electron-blocking passivation function of SEI films; therefore, it is important that they are minimized.

**Li-Ion Transport Through SEI Layer.** Rempe’s group (SNL) is using non-polarizable force fields to study  $\text{Li}^+$  ion transport in SEI layers. They focus on the well-known component of SEI layers, di-lithium ethylene dicarbonate ( $\text{Li}_2\text{-EDC}$ ). For fluids like EC, the Gaussian behavior of the “self” part of the van Hove function

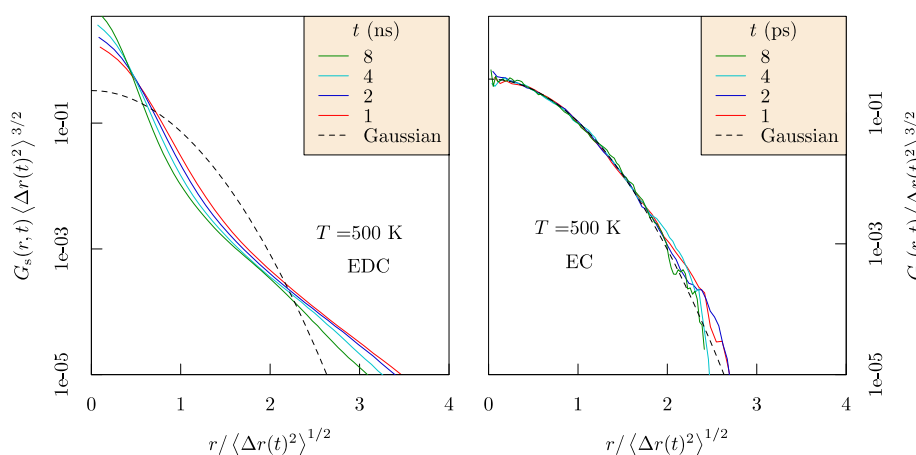


**Figure 67.** Gaussian fit to the “self” part of van Hove function suggests  $\text{Li}_2\text{EDC}$  (left) is crystalline compared to pure EC (right). Correlations are calculated for ps compared to ns in the  $\text{Li}_2\text{EDC}$  case.

obtained from molecular dynamics (MD) simulations is exact (Figure 67, right). The non-Gaussian behavior of the “self” part in SEI layers further confirms that the SEI layer is glassy. To understand transport properties in this glassy SEI layer, the group next will use mode-coupling theory on the “self” part.

## Patents/Publications/Presentations

### Publications

- Leung, K., and F. A. Soto, K. Hankins, P. B. Balbuena, and K. L. Harrison. “Stability of Solid Electrolyte Interphase Components on Reactive Anode Surfaces.” *J. Phys. Chem. C* 120 (2016): 6302–6313.
- Kumar, N., and J. M. Seminario. “Lithium-Ion Model Behavior in an Ethylene Carbonate Electrolyte Using Molecular Dynamics.” *J. Phys. Chem. C* 120 (2016): 16322–16332.
- Chaudhari, M., and J. Nair, L. Pratt, F. A. Soto, P. B. Balbuena, and S. Rempe. “Scaling Atomic Partial Charges of Carbonate Solvents for Lithium ion (Li+) Solvation and Diffusion.” *J. Chem. Theor. Comp.* 12 (2016): 5709–5718.
- Soto, F. A., and P. B. Balbuena. “Elucidating Oligomer-Surface and Oligomer-Oligomer Interactions at a Lithiated Silicon Surface.” *Electrochim. Acta* 220 (2016): 312–321.
- Soto, F. A., and J. M. Martinez de la Hoz, J. M. Seminario, and P. B. Balbuena. “Modeling Solid-Electrolyte Interfacial Phenomena in Silicon Anodes.” *Curr. Op. Chem. Eng.* 13 (2016): 179–185.



## Task 6.5 – A Combined Experimental and Modeling Approach for the Design of High Current Efficiency Silicon Electrodes (Xingcheng Xiao, General Motors; Yue Qi, Michigan State University)

**Project Objective.** The use of high-capacity, Si-based electrode has been hampered by its mechanical degradation due to large-volume expansion/contraction during cycling. Nanostructured silicon can effectively avoid silicon cracking/fracture. Unfortunately, the high surface-to-volume ratio in nanostructures leads to an unacceptable amount of SEI formation and growth, and thereby low current/CE and short life. Based on mechanics models, the project demonstrates that artificial SEI coating can be mechanically stable despite the volume change in silicon, if the material properties, thickness of SEI, and the size/shape of silicon are optimized. Therefore, the project objective is to develop an integrated modeling and experimental approach to understand, design, and make coated silicon anode structures with high current efficiency and stability.

**Project Impact.** The validated model will ultimately be used to guide synthesis of surface coatings and optimization of silicon size/geometry that can mitigate SEI breakdown. The optimized structures will eventually enable a negative electrode with a 10x improvement in capacity (compared to graphite), while providing > 99.99% CE; this could significantly improve the energy/power density of current Li-ion batteries.

**Out-Year Goals.** The out-year goal is to develop a well-validated mechanics model that directly imports material properties either measured from experiments or computed from atomic simulations. The predicted SEI induced stress evolution and other critical phenomena will be validated against *in situ* experiments in a simplified thin-film system. This comparison will also allow fundamental understanding of mechanical and chemical stability of artificial SEI in electrochemical environments and correlation between CE and the dynamic process of SEI evolution. Thus, the size and geometry of coated silicon nanostructures can be optimized to mitigate SEI breakdown, providing high current efficiency.

**Collaborations.** This project engages in collaboration with LBNL, PNNL, and NREL.

### Milestones

1. Identify critical mechanical and electrochemical properties of the SEI coating that can enable high current efficiency. (December 2015 – Complete)
2. Design a practically useful silicon electrode where degradation of the SEI layer is minimized during lithiation and delithiation. (March 2016 – Complete)
3. Construct an artificial SEI design map for silicon electrodes, based on critical mechanical and transport properties of desirable SEI for a given silicon architecture. (June 2016 – Complete)
4. Validated design guidance on how to combine the SEI coating with a variety of silicon nano/microstructures. *Go/No-Go*: Decision based on whether the modeling guided electrode design can lead to high CE > 99.9%. (September 2016 – Complete; Go)

## Progress Report

**Further Elaborated the Failure Mechanism of SEI Layer on Silicon Electrode.** Two possible explanations for this, depicted in Figure 68, are based on a bilayer SEI structure that has been detected with a variety of methods. One possibility is that the crack only runs through the top organic layer and does not reach the interface of SEI and silicon to cause further SEI formation. Another possible explanation is that the cracks run all the way to the SEI/Si interface, but that filling only occurs at the bottom of the crack with much denser inorganic compounds as the potential is low. Further investigation of these possibilities is needed.

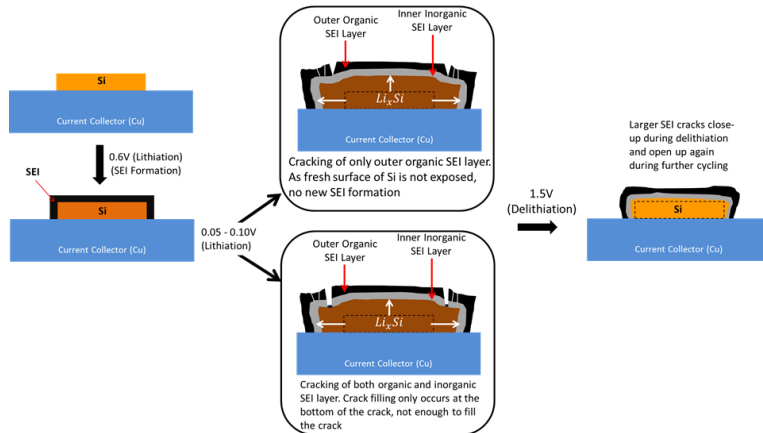


**Figure 68. Schematic showing deformation of patterned silicon island during cycling, and the resulting impact of volume changes on SEI formation and failure.**

modulus, yield stress and interfacial shear strength. After 50 cycles, a bump is formed in the cycled silicon island due to plastic localization. Mechanical failure of the electrode such as surface cracking or delamination could be induced by this geometric instability. While the present study uses a sliding silicon island as a model, the results suggest that ratcheting induced failure is generic to rechargeable Li-ion batteries and any electrochemical systems with concentration dependent mechanical properties subject to large number of cycles.

**Lithium Diffusion Through Mixed LiF/SiO<sub>2</sub>.** Reactive MD simulations were performed to investigate the effect of composite coating on LiF. Previously, the project demonstrated that lithium diffuses very fast through the SiO<sub>2</sub> coating by lithiating it first (Figure 70b), and LiF acts as a barrier for lithium diffusion (Figure 70d). For a SiO<sub>2</sub>-LiF mixed coating (50 vol% for each phase), lithium diffusion through the composite coating is almost as slow as that in LiF coating. Lithiation of SiO<sub>2</sub> was observed, but few lithium atoms were able to diffuse through. One possible reason is that lithiated SiO<sub>2</sub> in the composite coating was under large compressive stress, as the LiF phase prevented its volume expansion. Therefore, lithium diffusion through the SiO<sub>2</sub> is hindered dramatically.

**Ratcheting Induced by Concentration Dependent Properties.** Mechanical properties of lithiated silicon have been found to be dependent on lithium concentration, such as elastic modulus, yield stress, and interfacial shear strength of Li<sub>x</sub>Si/Cu interface. Finite element simulations and theoretical analysis have been conducted to demonstrate that the concentration dependence of these mechanical properties can result in plastic ratcheting of silicon electrodes upon lithiation/delithiation cycles. Figure 69 shows that a silicon island electrode on current collector gradually shrinks with increasing cycle number, which is directly attributed to the concentration dependent

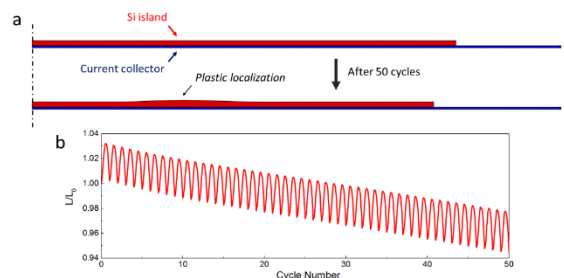


**Figure 69. (a) Finite element model of a sliding silicon island electrode on a current collector; (b) Length change of the silicon island versus cycle number.**

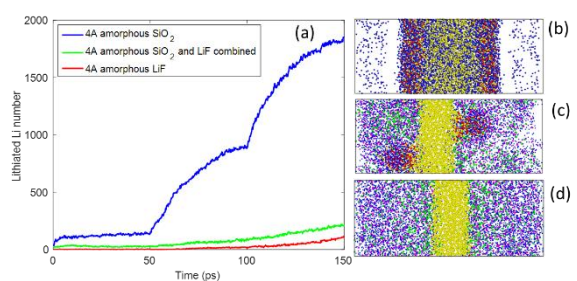


**Figure 70. (a) The number of lithium atoms reached silicon thin film after 150ps molecular dynamic simulations, and the corresponding structure of silicon initially coated with (b) SiO<sub>2</sub>, (c) SiO<sub>2</sub>-LiF, and (d) LiF.**

## Patents/Publications/Presentations

### Publication

- Verbrugge, M., and X. Xiao, Q. Zhang, M. Balogh, K. Raghunathan, and D. Baker. “Fabrication and Characterization of Lithium-Silicon Thick-Film Electrodes for High-Energy-Density Batteries.” *J. Elec. Soc.* 164, no. 2 (2017): A156–A167.

### Presentation

- Society of Engineering Science Annual Meeting, University of Maryland, College Park (October 4, 2016): “Mechanical Degradation and Optimization of Solid Electrolyte Interphases in Li-Ion Batteries”; Brian W. Sheldon.

## Task 6.6 – Electrode Materials Design and Failure Prediction (Venkat Srinivasan, Argonne National Laboratory)

**Project Objective.** The project goal is to develop a continuum-based mathematical model to (1) investigate the impact of mechanical stress on the growth of dendritic protrusions and (2) elucidate the competition between transport and mechanical means for preventing dendrite growth. Effectiveness of protective layers in preventing the growth of dendritic protrusions will also be studied. The focus will be to develop a microscale model that can capture the mechanical stresses and transport processes within lithium metal and adjacent electrolyte/protective layer. Impact of surface energy on growth of dendrites will be investigated. Possibility of plastic deformation within lithium metal and/or solid electrolyte material will also be elucidated along with its effect on propagation of dendrites. Propensity of fracture within the SEI layer (or the protective layer) and its impact on dendrite growth will be explored.

**Project Impact.** The next-generation Li-ion batteries are expected to use Li-metal based anodes, which offer low reduction potential and superior specific capacity. The biggest drawback preventing widespread usage of Li-metal anodes is the formation of dendrites over multiple cycles during operation at higher current densities. Insight gained from this project will provide guidance in designing solid polymer electrolytes (or protective layers) that prevent the growth of dendrites on lithium metal.

**Out-Year Goals.** At the end of this project, a mathematical model will be developed that can capture the mechanical stress field, concentration, and potential profiles around a dendritic protrusion. This model will allow estimation of the propensity for growth of such a protrusion and provide guidance in the design of solid polymer electrolytes (or protective layers) for the prevention of lithium dendrites.

### Milestones

1. Develop mathematical model to understand the proper stress state that exists within lithium metal and adjacent electrolyte during electrochemical deposition of lithium. (December 2016 – Complete)
2. Develop mathematical models to investigate and capture possibility of plastic deformation within lithium metal. Impact of plasticity on effective exchange current density will also be explored. (March 2017 – In progress)
3. Combine the impact of elasto-plastic stress evolution with transport of lithium within the electrode-electrolyte system. If unsuccessful in combining both elastic and plastic deformation with the transport process, consider only elastic deformation of lithium and electrolyte. (June 2017)
4. Report on the electrolyte shear modulus required for successful prevention of dendrites. The coupled mechanics and transport framework will be used to analyze the Li-electrolyte system. (September 2017)

## Progress Report

**Develop Mathematical Model to Understand the Proper Stress State that Exists Within Lithium Metal and Adjacent Electrolyte During Electrochemical Deposition of Lithium.** It has been observed in several experiments that dendrite growth in lithium metal can be prevented to some extent by the application of mechanical stress. However, how the stress field prevents the growth of dendrites has not been studied extensively. Newman et al. have published two articles investigating the stress state and subsequent deformation of lithium metal and the adjacent electrolyte phase (*JES* 2005: A396; *JES* 2014: A1350), in which they considered lithium electrodes in a pre-stressed state. They found that prevention of dendrite growth by mechanical means is only possible by using electrolytes with shear modulus at least two times larger than that of lithium metal. The pre-stressed condition led to severe dendrite growth even during operation at extremely low current densities, which is inconsistent with typical experimental observations that show no dendrite growth at lower current densities. The present study assumed that the lithium metal begins in a relaxed state. A schematic diagram of the pre-stressed and relaxed condition is shown in Figure 71.

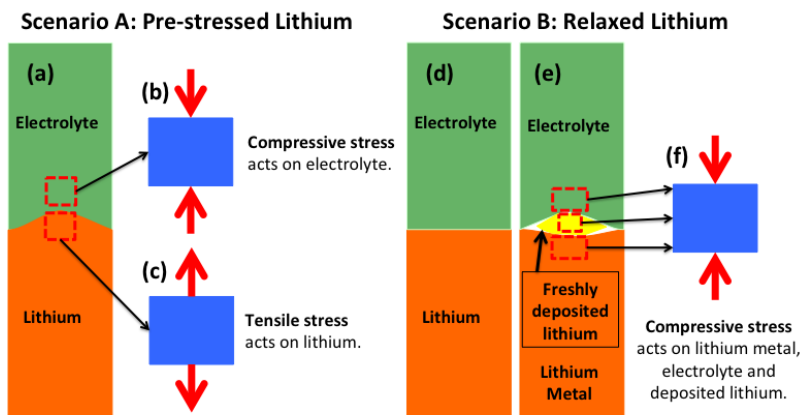


Figure 71. (a-c) According to the pre-stressed lithium scenario, tensile stresses act within lithium metal, and compressive stresses act inside electrolyte. (d-f) Relaxed lithium assumes stress-free condition for lithium metal and electrolyte. During operation, when fresh lithium gets deposited, bulk lithium metal, electrolyte, and the newly deposited lithium experience compression.

Detailed simulations have been conducted to estimate the deformation and stress generation in a Li-metal protrusion and adjacent electrolyte for different shear modulus of the electrolyte phase. An electrochemical potential term was defined that incorporates the impact of mechanical stress and surface tension into the effective exchange current density. Figure 72a-c demonstrates that during operation at low current density, initially relaxed lithium does not lead to any dendrite growth, whereas the pre-stressed lithium leads to severe dendrite formation, which is not typically observed experimentally. Hence, for all subsequent analysis, lithium metal in an initially relaxed condition will be considered. The development and use of this model satisfies the first quarter milestone.

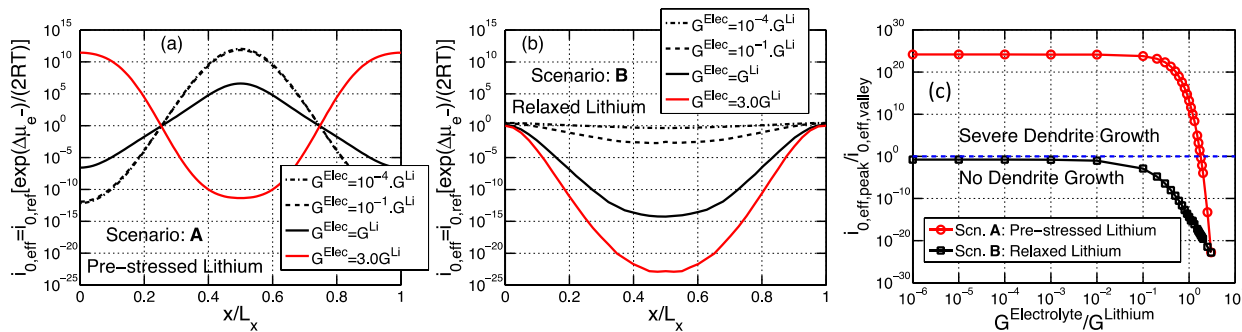


Figure 72. (a-b) Variation in effective exchange current density around the dendritic protrusion. If the current at the peak is greater than that at the valley, dendrites grow. (a) For pre-stressed lithium. (b) For initially relaxed lithium. (c) Ratio of the effective exchange current density at the protrusion peak over that at the valley. For initially relaxed lithium, dendrite growth never occurs at low current operation.

### Patents/Publications/Presentations

- Barai, P., and K. Higa, and V. Srinivasan. “Effect of Initial State of Lithium on the Propensity for Dendrite Formation: A Theoretical Study.” *J. Elec. Soc.* 164, no. 2 (2017): A180–A189.

## Task 6.7 – First Principles Calculations of Existing and Novel Electrode Materials (Gerbrand Ceder, Lawrence Berkeley National Laboratory)

**Project Objective.** Develop very high-capacity, layered cathodes with high structural stability ( $> 250$  mAh/g) and high surface stability. Clarify the role that Li-excess and cation disorder play in capacity and structural stability. Develop predictive modeling of oxygen charge transfer and oxygen loss, and find ways to make oxygen redox beneficial in terms of increase capacity. Develop materials with engineered surface passivation that does not lead to impedance increase.

**Project Impact.** The project will lead to insight in how Li-excess materials work and ultimately to higher capacity cathode materials for Li-ion batteries. The project will help in the design of high-capacity cathode materials that are tolerant to TM migration.

**Out-Year Goals.** Higher capacity Li-ion cathode materials, and novel chemistries for higher energy density storage devices. Guide the field in the search for higher energy density Li-ion materials.

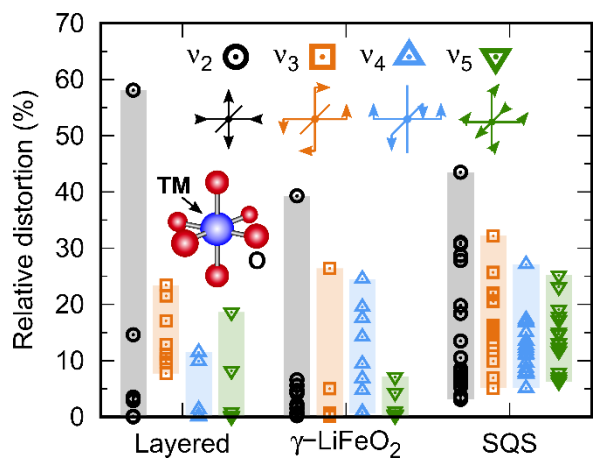
**Collaborations.** This project collaborates with the following: K. Persson (LBNL), C. Grey (Cambridge), V. Srinivasan (ANL), and G. Chen (LBNL).

### Milestones

1. Computational approach to predict cation disorder and synthesis temperature. (Q1 – Complete)
2. Comparison of electronic structure modeling with experimental spectra (for example, XAS, XPS, or EELS). (Q2 – On target)
3. Use modeling to come up with a new cation-disordered material. (Q3 – On target)
4. Demonstrate reduced surface oxygen loss by surface modification of a disordered cathode material using DEMS or TEM. (Q4 – On target)

## Progress Report

Cation-disordered Li-TM oxides have recently emerged as a new class of high-energy-density cathode materials for Li-ion batteries. The compositions of conventional layered cathodes are limited to few TM species (manganese, nickel, and cobalt). In contrast, cation-disordered compositions containing additionally titanium, vanadium, chromium, iron, zirconium, niobium, and molybdenum have been reported. Apart from this



increased design space, cation disorder might also be beneficial for the material stability, as disordered structures undergo smaller volume changes upon lithium extraction than layered structures. However, owing to the large number of possible constituents, it is practically infeasible to scan all possible compositions for stability, and thus concrete design guidelines are required. The project recently demonstrated that high-throughput computations allow for the systematic screening of select composition spaces,<sup>1</sup> but a qualitative understanding of the origin of cation disorder is desirable.

According to the Hume-Rothery rules, a species is likely soluble in a metal if the atomic sizes are within about 15%.

The project finds that, in Li-TM oxides, similar cation radii are also a requirement for stable cation-disordered structures, but this alone is insufficient criterion. Even small ionic radius differences give rise to distortions of the octahedral TM sites that affect the stability. Figure 73 shows the magnitude of the maximal TM site distortions in ordered LiTMO<sub>2</sub> ground state structures and special quasi-random structures for all first- and second-row TMs except manganese and technetium. The site distortions are

**Figure 73.** Maximal transition metal site distortion relative to the original bond lengths in ordered LiTMO<sub>2</sub> ground state structures and in cation-disordered LiTMO<sub>2</sub> structures. Contribution of the four symmetry-breaking normal modes,  $v_2$  through  $v_5$ , to the site distortions are shown.

decomposed in contributions from the four symmetry-breaking normal modes of the octahedral point group. As seen in the figure, disordered structures generally exhibit distortions in all four modes, whereas distortions of types  $v_2$  and  $v_5$  are small in most ordered structures. Depending on the electronic configuration of the TM species, these additional distortions may give rise to large energy penalties. In fact, it can be shown that only TM cations with  $d^0$  configuration are insensitive with respect to the mode of distortion. Consequently, in compositions containing at least one  $d^0$  TM species (Ti<sup>4+</sup>, Nb<sup>5+</sup>, Mo<sup>6+</sup>, etc.), sites occupied by the  $d^0$  species may absorb the distortions required to stabilize the structure (Figure 74). This conceptual understanding moves the project one step closer to the rational design of new cation-disordered cathode materials for Li-ion batteries.

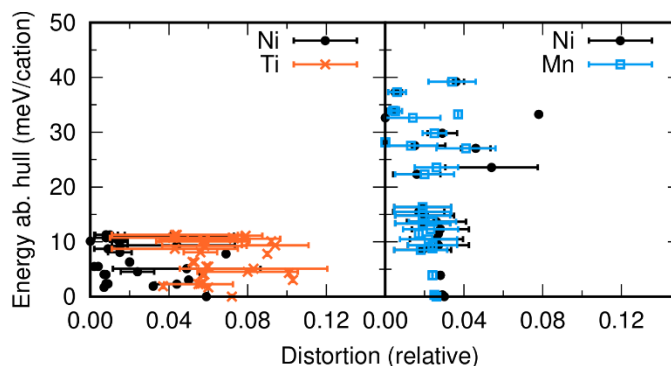


**Figure 74.** Energy and relative transition metal (TM) site distortion in LiNi<sub>0.5</sub>Ti<sub>0.5</sub>O<sub>2</sub> and LiMn<sub>0.5</sub>Ni<sub>0.5</sub>O<sub>2</sub>. Each data point corresponds to a single atomic structure. The error bars indicate the range of distortions for all sites of one TM species within that structure.

[1] A. Urban, I. Matts, A. Abdellahi, and G. Ceder, *Adv. Energy Mater.* 6 (2016): 1600488.



## TASK 7 – METALLIC LITHIUM AND SOLID ELECTROLYTES

### Summary and Highlights

The use of a metallic lithium anode is required to realize dramatic improvements in energy density, vehicle range, and cost requirements for batteries based on high energy intercalation and conversion cathodes. For a long lifetime and safety, it is essential that no lithium capacity is lost to either physical isolation from roughening, dendrites, or delamination processes, or to chemical isolation from side reactions. Adding excess lithium to compensate for such losses effectively negates the high-energy density for lithium in the first place. Furthermore, dendrites formed through the separator or electrolyte create short circuit and failure. Preventing these reactions, shorts, and gradual roughening of the lithium is the challenge posed for this Task.

For success, a much deeper analysis of the degradation processes is needed, so that both the electrolytes and lithium anode can be engineered to fulfill the target level of performance for EV, namely 1000 cycles and a 15-year lifetime, with adequate pulse power. Projecting the performance required in terms of just the lithium anode, this requires a high rate of lithium deposition and stripping reactions, specifically about 20 - 40  $\mu\text{m}$  lithium per cycle, with pulse rates up to 10 and 20 nm/s (15mA/cm<sup>2</sup>) charge and discharge, respectively, at > 99.99% CE. Viewed another way, lithium cycling must achieve a cumulative plating of 7000 hours at sustained 1 mA/cm<sup>2</sup> current density. Only a few thin-film batteries with a Lipon glass electrolyte have plated lithium to an excess of 1Ah/cm<sup>2</sup> cumulative capacity. Most batteries, with liquid, polymer, or ceramic electrolytes are not even close to this goal, yet promising advances have been made in this Task over the last two years.

This Task takes a broad look at this challenge for both solid-state batteries and batteries continuing to use liquid electrolytes with the lithium anode. For the liquid electrolyte batteries, PNNL researchers are examining the use of dual lithium salts and other organic additives to the typical carbonate electrolytes to impede lithium corrosion and dendrite formation at both the lithium and graphite anodes. If successful, this is the simplest approach to implement. At Stanford, novel artificial SEI coatings are applied to the lithium surface and appear to suppress roughening and lengthen cycle life. New activities for liquid electrolyte batteries include a program at the University of Pittsburgh (U Pitt) that is providing a porous foam host for the lithium metal.

For solid electrolyte batteries, several programs have advanced the use of the garnet Li<sub>7</sub>La<sub>3</sub>Zr<sub>2</sub>O<sub>12</sub> (LLZO) family of crystalline electrolytes due to their outstanding conductivity and stability with lithium. Key advances from programs at the Universities of Maryland, Michigan, and Texas have shown new processing of the LLZO that ensures a very low area specific resistance (ASR) (< 10 ohm) attributed to the Li/LLZO interface and also good wetting of the lithium to the electrolyte. It is anticipated that this may allow higher current densities without dendrites, but sustained cycling is needed for further validation. The LLZO/lithium interface is being characterized mechanically by a joint investigation (ORNL, University of Michigan, and Michigan Technological University) to shed light on what flaws may lead to shorts, as well as changes in the lithium defect and grain structure that evolve during cycling. Further, a new program at ANL is probing the interface reactions between lithium and various single crystal and model compound membranes. Alternate solid electrolytes include ceramic/polymer composites. In one program, a low loading of LLZO fiber was incorporated in polymer matrix (U Michigan); a second program features high loading of ceramic particles for a high shear modulus (ORNL). Understanding Li<sup>+</sup> motion across the ceramic-polymer interface represents a gap in understanding of ion transport. Other new solid electrolytes will be introduced into several programs over coming quarters and years.

Most studies are favoring symmetric Li-Li cell tests, but work is expanding to include full cells with a battery cathode, including sulfur and NMC, typically constructed as a hybrid battery with both liquid and solid electrolytes. These cells generally incorporate an excess of lithium, but a few programs are starting to effectively limit the lithium inventory. This is essential to demonstrating efficient cycling. Each project involves a collaborative team of experts with the experimental and modeling skills needed to address the challenging materials studies of this dynamic electrochemical system.

**Highlights.** The highlights for this quarter are as follows:

- Full batteries using LLZO electrolyte membranes were demonstrated for Li-S and for Li-NMC. In each demonstration, a liquid or gel electrolyte was used to fill the porous cathode structure and provide a contact to the LLZO membrane. (7.2, 7.4, 7.7)
- LiF was used to stabilize the LLZO solid electrolyte against moisture and CO<sub>2</sub> in the air. In a Li-S battery, this solid electrolyte blocked the shuttle reaction, reduced interface resistance, and improved the CE. (7.7)
- Dual salts using LiPF<sub>6</sub> and LiBOB in carbonate solvents help to form a superior SEI on the lithium anode that improves cycling stability at high current density. (7.6)

## Task 7.1 – Mechanical Properties at the Protected Lithium Interface (Nancy Dudney, Oak Ridge National Laboratory; Erik Herbert, Michigan Technological University)

**Project Objective.** This project will develop the understanding of the Li-metal SEI through state-of-the-art mechanical methods, including nanoindentation, lap shear, and acoustic pulse studies, each coupled with electrochemical cycling. The goal is to provide the critical information that will enable transformative insights into the complex coupling between the microstructure, its defects, and the mechanical behavior of Li-metal anodes.

**Project Impact.** Instability and/or high resistance at the interface of lithium metal with various solid electrolytes limit the use of the metallic anode for batteries with high-energy-density batteries, such as Li-air and Li-S. The critical impact of this endeavor will be a much deeper analysis of the degradation, so that materials can be engineered to fulfill the target level of performance for EV batteries, namely 1000 cycles and 15-year lifetime, with adequate pulse power.

**Approach.** Mechanical properties studies through state-of-the-art nanoindentation techniques will be used to probe the surface properties of the solid electrolyte and the changes to the lithium that result from prolonged electrodeposition and dissolution at the interface. An understanding of the degradation processes will guide future electrolyte and anode designs for robust performance. In the first years, the team will address the two critical and poorly understood aspects of the protected Li-metal anode assembly: (1) the mechanical properties of the solid electrolyte, and (2) the morphology of the cycled lithium metal.

**Out-Year Goals.** Work will progress toward study of the electrode assembly during electrochemical cycling of the anode. The project hopes to capture the formation and annealing of vacancies and other defects in the lithium and correlate this with the properties of the solid electrolyte and the interface.

**Collaborations.** This project funds work at ORNL, Michigan Technological University, and University of Michigan. Asma Sharafi (U Michigan, Ph. D. student) and Dr. Robert Schmidt (ORNL) also contribute to the project. Steve Visco (PolyPlus) will serve as a technical advisor.

### Milestones

1. Characterize *in situ* changes in lithium anode from a single stripping and plating half cycle. (March 2017 – In progress)
2. Measure the Li-LLZO interface strength as a function of surface treatment using the Instron and EIS capability. (June 2017 – Initiated equipment setup)
3. Determine the physical properties of electrolyte failures, the nature of material reduction or lithium incursion/pileup, using indentation and X-ray tomography. Samples obtained from other Task 7 projects. (September 2017 – In progress)
4. Examine lithium anode *in situ* during extended electrochemical plating, stripping, and relaxation to assess defect formation and annealing. (September 2017)

## Progress Report

**Performed First Attempts at Characterizing the Mechanical Properties of Lithium Films Post Electrochemical Cycling.** Initial attempts at characterizing the mechanical properties of lithium films post electrochemical cycling were unsuccessful. Significant roughening or reaction occurred during the prolonged plating. The figure shows the lithium, initially 2- $\mu\text{m}$  thick, after plating to 5  $\mu\text{m}$ . Contact was made to the outer edge of the lithium only, to protect the center area for nanoindentation. While the center is still silver in appearance, the surface was irregular. Future procedures are being developed around an *in situ* electrochemical cycling cell that will allow plating and stripping of the lithium to be performed while a flat punch indenter tip is continuously held in contact with the free surface of the film.



Figure 75. Performed first attempts at characterizing mechanical properties of lithium films post electrochemical cycling.

### Quantifying Elastic Anisotropy Effects in Lithium Films as a Function of Film Thickness.

Elastic modulus measurements from 20- and 5- $\mu\text{m}$  thick films (course and fine grained, respectively) indicate the films have different texture. Figure 76a shows the elastic modulus from 30 measurements in a relatively coarse-grained 20- $\mu\text{m}$  thick film. The range in elastic modulus from 5 to 9 GPa correlates well to the expected value of 8.9 in 110 type directions. Figure 76b, on the other hand, shows the elastic modulus from 35 measurements in a more fine-grained 5- $\mu\text{m}$  thick film. The range in elastic modulus from 9 to 18 GPa suggests the thinner film has less texture, as the data show a broad mixture of elastic moduli ranging from 110 and 111 type directions (111 is expected to be approximately 23 GPa). These observations are consistent with lithium's shear anisotropy factor of 9.3 and previously published measurements of lithium's elastic constants. Continuing efforts will be made to quantify the plastic anisotropy as well.

### Assessed Homogeneity in the Mechanical Properties of the Solid Electrolyte LLZO as a Function of Grain Size.

High-speed nanoindentation experiments were performed in LLZO to assess changes in the hardness and elastic modulus as a function of grain size. Results from 300 measurements indicate no significant difference in mechanical properties of LLZO that has been annealed for 1 hour versus 50 (50 hours produce grains on the order of 25  $\mu\text{m}$ ). However, when the indentation depth is decreased from 500 to 100 nm, the ratio of modulus to hardness shifts to a slightly lower value. Assuming this result is not a sample preparation artifact, it suggests the near surface region will accommodate strain somewhat more elastically than the bulk. The depth dependence and grain size independence will be corroborated with additional experiments in specimens that have been thermally etched to reveal the grain boundaries.

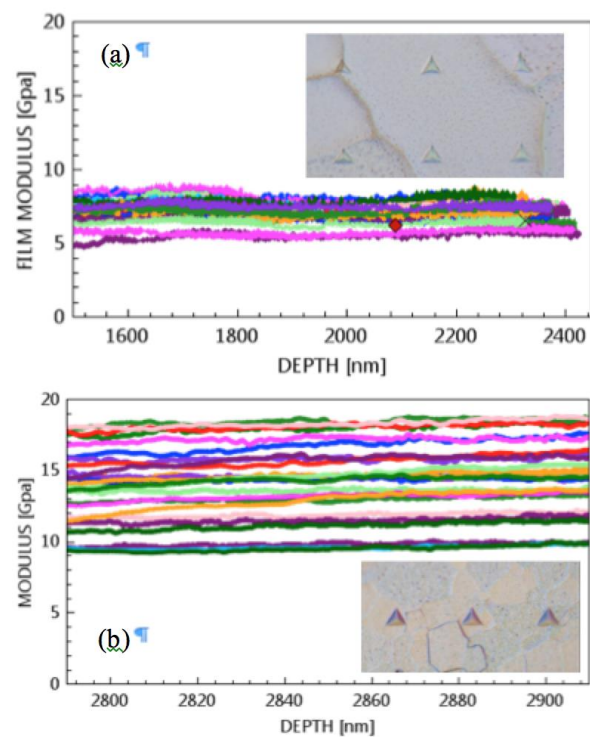


Figure 76. (a) 20- $\mu\text{m}$  thick lithium film. (b) 5- $\mu\text{m}$  thick lithium film. The residual hardness impressions are approximately 11  $\mu\text{m}$  along each face.

## Task 7.2 – Solid Electrolytes for Solid-State and Lithium–Sulfur Batteries (Jeff Sakamoto, University of Michigan)

**Project Objective.** *Enable advanced Li-ion solid-state and lithium-sulfur EV batteries using LLZO solid-electrolyte membrane technology.* Owing to its combination of fast ion conductivity, stability, and high elastic modulus, LLZO exhibits promise as an advanced solid-state electrolyte. To demonstrate relevance in EV battery technology, several objectives must be met. First, LLZO membranes must withstand current densities approaching  $\sim 1$  mA/cm<sup>2</sup> (commensurate with EV battery charging and discharging rates). Second, low ASR between lithium and LLZO must be achieved to obtain cell impedance comparable to conventional Li-ion technology ( $\sim 10$  Ohms/cm<sup>2</sup>). Third, low ASR and stability between LLZO and sulfur cathodes must be demonstrated.

**Project Impact.** The expected outcomes will: (1) enable Li-metal protection, (2) augment DOE access to fast ion conductors and/or hybrid electrolytes, (3) mitigate Li-polysulfide dissolution and deleterious passivation of Li-metal anodes, and (4) prevent dendrite formation. Demonstrating these aspects could enable Li-S batteries with unprecedented end-of-life, cell-level performance:  $> 500$  Wh/kg,  $> 1080$  Wh/l,  $> 1000$  cycles, and lasting  $> 15$  years.

**Approach.** This effort will focus on the promising new electrolyte known as LLZO (Li<sub>7</sub>La<sub>3</sub>Zr<sub>2</sub>O<sub>12</sub>). LLZO is the first bulk-scale ceramic electrolyte to simultaneously exhibit the favorable combination of high conductivity ( $\sim 1$  mS/cm at 298K), high shear modulus (61 GPa) to suppress lithium dendrite penetration, and apparent electrochemical stability (0-6 V versus Li/Li<sup>+</sup>). While these attributes are encouraging, additional R&D is needed to demonstrate that LLZO can tolerate current densities in excess of 1mA/cm<sup>2</sup>, thereby establishing its relevance for PHEV/EV applications. This project hypothesizes that defects and the polycrystalline nature of realistic LLZO membranes can limit the critical current density. However, the relative importance of the many possible defect types (porosity, grain boundaries, interfaces, and surface and bulk impurities), and the mechanisms by which they impact current density, have not been identified. Using experience with the synthesis and processing of LLZO (Sakamoto and Wolfenstine), combined with sophisticated materials characterization (Nanda), this project will precisely control atomic and microstructural defects and correlate their concentration with the critical current density. These data will inform multi-scale computation models (Siegel and Monroe), which will isolate and quantify the role(s) that each defect plays in controlling the current density. By bridging the knowledge gap between composition, structure, and performance, this project will determine if LLZO can achieve the current densities required for vehicle applications.

**Collaborations.** This project collaborates with Don Siegel (U Michigan, atomistic modeling), Chuck Monroe (U Michigan, continuum scale modeling), Jagjit Nanda (ORNL, sulfur chemical and electrochemical spectroscopy), and Jeff Wolfenstine (ARL, AFM).

### Milestones

1. Establish processes to control the defects (microstructural and atomic-scale) that govern the critical current density (CCD) to achieve a CCD of  $> 1$  mA/cm<sup>2</sup>. (Q1 – Complete)
2. Assess initial performance of Li-LLZO-liquid-S+carbon cells. (Q2 – Complete)
3. Extended cycling of hybrid Li-LLZO-liquid-S+carbon cells. (Q3)
4. Evaluate CCD, based on the dominant defects identified in years 1 and 2, as a function of Q, temp, and pressure. Characterize the CE. (Q4)
5. Cycling Li-LLZO-liquid-state-of-the-art Li-ion cathode to demonstrate hybrid electrolyte concept can cycle at  $\geq 1$  mA/cm<sup>2</sup>. (Q4)

## Progress Report

Enabling Li-metal anodes and S-C composite cathodes is a primary goal of this work. The milestone for this quarter entailed characterizing the beginning of life performance of hybrid Li-LLZO-liquid-S+carbon cells. LLZO membranes were fabricated at U Michigan, integrated with Li-metal anodes, and sent to ORNL for assembly in hybrid cells. Baseline, state-of-the-art all-liquid cells were also fabricated and cycled for comparison. From this study, several goals were achieved. First, while the all-liquid cell cycling performance was hindered by auxiliary chemical reactions during charging (forced termination due to auxiliary reaction after 10 cycles), the hybrid cells maintained high CE (~ 100 %) over 30 cycles. The project believes physical isolation of the lithium anode from the S+liquid electrolyte prevents auxiliary chemical reactions, thus improving cycling in preliminary tests. Second, these data demonstrate that the interposition of a solid electrolyte between lithium and a state-of-the-art electrolyte is feasible. Despite a relatively thick LLZO membrane (~ 0.75 mm) and a solid Li-LLZO interface, the hybrid cell cycled reasonably well. Furthermore, the S-C composite cathode fabrication as well as the liquid electrolyte volume are not fully optimized yet. The project expects better capacity retention and cycle life in the next round of results.

Taken together, these three aspects demonstrate promise in enabling hybrid Li-LLZO-liquid-S+carbon cells and support the successful completion of Milestone 2.1.

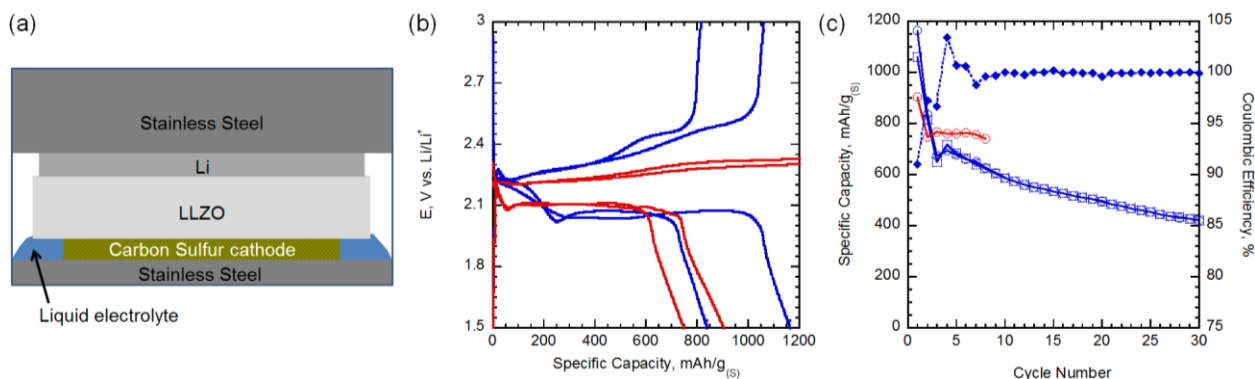


Figure 77. First-generation Li-LLZO-Sulfur+carbon cells. By wt.; 46% S, 37% KJB, 8.5% PVDF, and 8.5% Super P. Cycled at 0.06 mA/cm<sup>2</sup> in 1M LiTFSI, DOL:DME. Electrodes were ~30- to 35- $\mu$ m thick; 0.8 mg<sub>(S)</sub>/cm<sup>2</sup> loading. (a) Schematic diagram of test cell. LLZO membrane physically isolated lithium from the liquid electrolyte. (b) First two cycles comparing a typical all-liquid cell (red) and hybrid cell (blue data). Specific capacities normalized by grams S. (c) Sulfur specific capacity versus cycle number, and Coulombic efficiency versus cycle number. All-liquid cell (red), hybrid cell (blue) data.

## Patents/Publications/Presentations

### Publications

- Smith, S., and T. Thompson, J. Sakamoto, J. L. Allen, D. R. Baker, and J. Wolfenstine. “Electrical, Mechanical, and Chemical Behavior of Li<sub>1.2</sub>Zr<sub>1.9</sub>Sr<sub>0.1</sub>(PO<sub>4</sub>)<sub>3</sub>.” *Solid State Ionics* 300 (2017): 38–45.
- Cheng, Eric Jianfeng, and Asma Sharafi, and Jeff Sakamoto. “Intergranular Li Metal Propagation Through polycrystalline Li<sub>6.25</sub>Al<sub>0.25</sub>La<sub>3</sub>Zr<sub>2</sub>O<sub>12</sub> Ceramic Electrolyte.” *Electrochimica Acta* (2016).

### Presentations

- University of Michigan, Ann Arbor: “Cubic Li<sub>7</sub>La<sub>3</sub>Zr<sub>2</sub>O<sub>12</sub> as a Solid Electrolyte and LiCoPO<sub>4</sub> as a High Voltage Cathode”; Jeff Wolfenstine.
- Plug Volt Webinar: “Stability of Li<sub>7</sub>La<sub>3</sub>Zr<sub>2</sub>O<sub>12</sub> Garnet Solid-State Electrolyte Against Metallic Lithium”; Asma Sharafi. Invited speaker.

## Task 7.3 – Composite Electrolytes to Stabilize Metallic Lithium Anodes (Nancy Dudney and Frank Delnick, Oak Ridge National Laboratory)

**Project Objective.** Prepare composites of representative polymer and ceramic electrolyte materials to achieve thin membranes that have the unique combination of electrochemical and mechanical properties required to stabilize the metallic lithium anode while providing for good power performance and long cycle life. Understand the Li-ion transport at the interface between polymer and ceramic solid electrolytes, which is critical to the effective conductivity of the composite membrane. Identify key features of the composite composition, architecture, and fabrication that optimize the performance. Fabricate thin electrolyte membranes to use with a thin metallic lithium anode to provide good power performance and long cycle life.

**Project Impact.** A stable lithium anode is critical to achieve high energy density with excellent safety, lifetime, and cycling efficiency. This study will identify the key design strategies that should be used to prepare composite electrolytes to meet the challenging combination of physical, chemical, and manufacturing requirements to protect and stabilize the Li-metal anode for advanced batteries. By utilizing well characterized and controlled component phases, the design rules developed for the composite structures will be generally applicable toward substitution of alternative and improved solid electrolyte component phases as they become available. Success in this project will enable these specific DOE technical targets: 500-700 Wh/kg, 3000-5000 deep discharge cycles, and robust operation.

**Approach.** This project seeks to develop practical solid electrolytes that will provide stable and long-lived protection for the Li-metal anode. Current electrolytes all have serious challenges when used alone: oxide ceramics are brittle, sulfide ceramics are air sensitive, polymers are too resistive and soft, and many electrolytes react with lithium. Composites provide a clear route to address these issues. This project does not seek discovery of new electrolytes; rather, the goal is to study combinations of current well-known electrolytes. The project emphasizes investigation of polymer-ceramic interfaces formed as bilayers and as simple composite mixtures where the effects of the interface properties can be readily isolated. In general, the ceramic phase is several orders of magnitude more conductive than the polymer electrolyte, and interfaces can contribute an additional source of resistance. Using finite element simulations as a guide, composites with promising compositions and architectures are fabricated and evaluated for Li-transport properties using AC impedance and DC cycling with lithium in symmetric or half cells. General design rules will be determined that can be widely applied to other combinations of solid electrolytes.

**Out-Year Goal.** The out-year goal is to use advanced manufacturing processes where the architecture of the composite membrane can be developed and tailored to maximize performance and cost-effective manufacturing.

**Collaborations.** Collaborators at ORNL include Dr. A. Samuthira Pandian (synthesis, testing), Dr. Sergiy Kalnaus (modeling), and Dr. Jihua Chen (microscopy). Electrolyte powders are obtained from Ohara corporation and Prof. Sakamoto (U Michigan).

### Milestones

1. For spray-coated composites with high ceramic loading, vary the salt, plasticizer, and ceramic content to achieve facile ion transport across phase boundaries and  $10^{-5}$  S/cm. (Q2 – In progress)
2. Assess the lithium/electrolyte interface resistance. Adjust the composition or add a barrier coating to reduce the ASR and passivate the interface. (Q3 – In progress)
3. Fabricate a full battery using aqueous spray coating for both the composite electrolyte and cathode incorporating a protected Li-metal anode. Demonstrate lithium cyclability. (Q4 – Stretch goal)

## Progress Report

Composite electrolyte membranes of a PEO-based polymer with dispersed Ohara Nasicon glass-ceramic powders were spray coated from an aqueous slurry, following earlier reports. The effects of plasticizers, co-plasticizers, and a wider range of salt and ceramic content were investigated to further inform the understanding of the ion transport between the ceramic and polymer phases within the composite.

To date it appears that maximum ionic conductivity is achieved by vapor adsorption of DMC into the melt formed composite. To the sprayed composite, TEGDME has been added to the slurry, as this is likely more stable in contact with lithium than DMC. While the TEGDME enhances the conductivity of the composite, it is still below the conductivity of the plasticized polymer electrolyte without the Ohara particles (Figure 78). For each of these composites, the Ohara particles constitute 50 vol% of the composite. It is interesting that the TEGDME appears to inhibit the adsorption of DMC vapor, which occurs readily for the glyme-free composites. Various levels of co-plasticizers are being investigated.

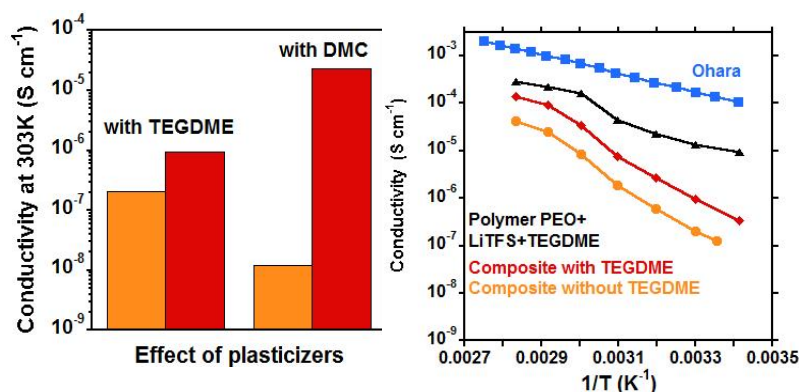


Figure 78. (left) Room-temperature conductivity comparing the composites with (red) and without (orange) plasticizers. TEGDME is added to the spray coat and DMC to the melt samples. (right) Arrhenius results for the spray-coated electrolytes are shown along with those for the single-phase Ohara (blue) and polymer (black) electrolytes.

Because it is difficult to ensure a dense composite with the very high ceramic particle loading used in this study, composites were formed with less ceramic to minimize the effect of particle agglomeration and jamming. These results, in Figure 79 (left), confirm that even a small amount of Ohara strongly reduces the conductivity. One hypothesis is that the ceramic powder scavenges the TEGDME from the polymer matrix. Considering further the balance of lithium ions and coordinating ethyl oxygens, higher salt concentrations are dissolved into the PEO. Figure 79 (right) shows the result of doubling the salt content greatly reduces the conductivity.

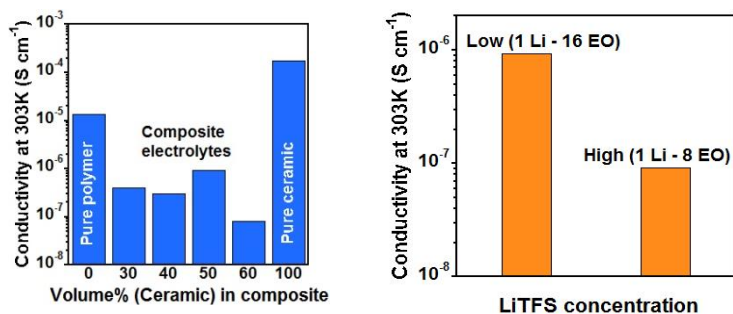


Figure 79. (left) Room temperature conductivity of the spray-coated composite with different amounts of the Ohara ceramic. The conductivity was recorded after heating the composite to 80°C and cooling. (right) Similar results for composites formed with different concentrations of dissolved lithium triflate salt.

Galvanostatic and impedance tests of nickel/composite-electrolyte/lithium samples are being used to confirm the transference number for lithium transport and investigate the interface stability and resistance. This will be described in the next report.



## Patents/Publications/Presentations/Presentations

### Presentation

- 2016 PRIME, Honolulu (October 2016): “Composite Polymer-Ceramic Electrolyte for High Energy Lithium Secondary Batteries”; Amaresh Samuthira Pandian, Frank Delnick, and Nancy Dudney.

## Task 7.4 – Overcoming Interfacial Impedance in Solid-State Batteries (Eric Wachsman, Liangbing Hu, and Yifei Mo, University of Maryland College Park)

**Project Objective.** The project objective is to develop a multifaceted and integrated (experimental and computational) approach to solve the key issue in solid-state, Li-ion batteries (SSLIBs), interfacial impedance, with a focus on garnet-based SSEs, the knowledge of which can be applied to other SSE chemistries. The focus is to develop methods to decrease the impedance across interfaces with the solid electrolyte, and ultimately demonstrate a high power/energy density battery employing the best of these methods.

**Project Impact.** Garnet electrolytes have shown great promise for safer and high-energy-density batteries. The success of the proposed research can lead to dramatic progress on development of SSLIBs based on garnet electrolytes. Regarding fundamental science, the project methodology by combining computations and experiments can lead to an understanding of the thermodynamics, kinetics and structural stability, and evolution of SSLIBs with the garnet electrolytes. Due to the ceramic nature of garnet electrolyte, being brittle and hard, garnet electrolyte particles intrinsically lead to poor contacts among themselves or with electrode materials. A fundamental understanding at the nanoscale and through computations, especially with interface layers, can guide design improvements and eventually lead to commercial use of such technologies.

**Approach.** SSLIB interfaces are typically planar, resulting in high impedance due to low specific surface area, and attempts to make 3D high surface area interfaces can also result in high impedance due to poor contact (for example, pores) at the electrode-electrolyte interface that hinders ion transport or degrades due to expansion/contraction with voltage cycling. This project will experimentally and computationally determine the interfacial structure-impedance relationship in SSLIBs to obtain fundamental insight into design parameters to overcome this issue. Furthermore, it will investigate interfacial modification (layers between SSE and electrode) to see if it can extend these structure-property relationships to higher performance.

**Collaborations.** This project is in collaboration with Dr. Venkataraman Thangadurai on garnet synthesis. It will collaborate with Dr. Leonid A. Bendersky (Leader, Materials for Energy Storage Program at NIST) and use neutron scattering to investigate the lithium profile across the bilayer interface with different charge-discharge rates. The project is in collaboration with Dr. Kang Xu, ARL, with preparation of perfluoropolyether (PFPE) electrolyte.

### Milestones

1. Fabricate and test SSLiBs with Li-NMC Chemistry. (December 2016 – Complete)
2. Fabricate and test SSLiBs with Li-S Chemistry. (Q2 – Initiated)
3. Develop models to investigate interfacial transport for Li-S and Li-NMC SSLiBs. (Q3)
4. Achieve full cell (Li-S or Li-NMC) performance of 350-450 Wh/kg and 200 cycles. (Q4)

## Progress Report

**Preparation of Bi-Layered Garnet Scaffold.** To achieve the proposed energy density of garnet SSE-based full battery, a unique bi-layered garnet scaffold design composed of a thin, high density electrolyte layer and second thick, but highly porous electrolyte layer serving as an electrode support is being used. The bilayer was prepared by sintering laminated tape-cast electrolyte layers. The structure of the sintered bilayer garnet electrolyte scaffold is shown in Figure 80a. The dense electrolyte layer and porous electrode layer are 20  $\mu\text{m}$  and 120  $\mu\text{m}$  from the SEM image, respectively.

**Assembling NMC Cathode/Garnet Scaffold/Lithiated Carbon Nanotube Full Battery.** A commercial NMC cathode of 10  $\text{mg}/\text{cm}^2$  active material loading was used to achieve the proposed energy density. The NMC cathode was placed on the dense side of the electrolyte bilayer scaffold. A thin layer of soft gel polymer was inserted between the NMC cathode and garnet electrolyte to provide sufficient contact. Carbon nanotubes (CNTs) were infiltrated into the porous side to coat the open surface area of the garnet grains throughout the pore structure to act as high surface area anode current collector, as shown in Figure 80b.

**Battery Performance.** Figure 80c shows the CV results of the full battery. Lithium was successfully infiltrated into the porous structure to make an anode with controlled potential. The CV test shows that there is an oxidation peak around 4.2 V, which is the charging voltage plateau characteristic for NMC. The reduction peak is around 3.4 V, corresponding for the discharge plateau. No other reaction current can be observed in the CV test. The full battery composed of NMC cathode and bi-layer garnet scaffold thus shows stable cycling performance.

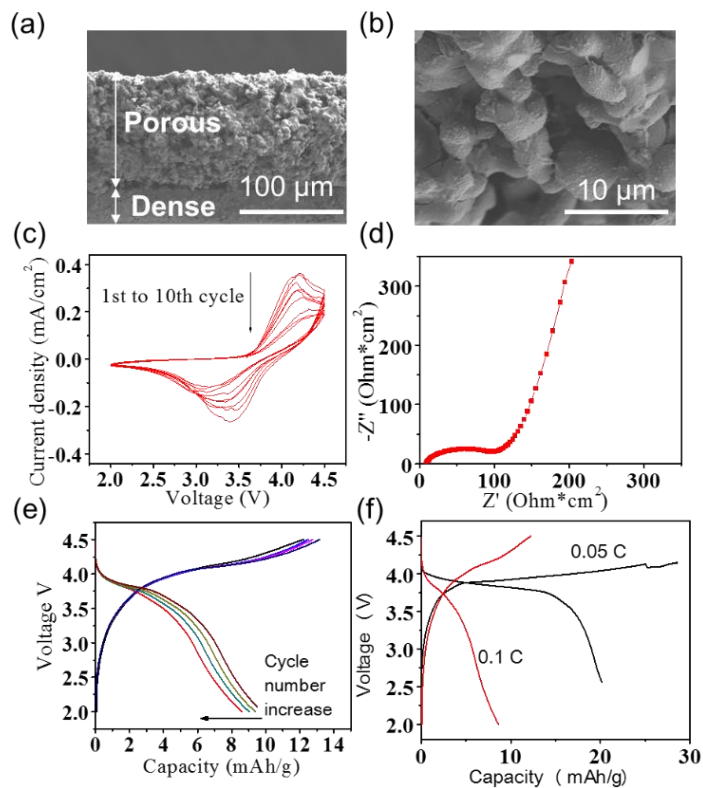


**Figure 80. Characterization of bi-layer garnet and performance of NMC battery.** (a) Cross sectional scanning electron microscopy (SEM) image of bi-layer garnet. (b) SEM of garnet grains coated with carbon nanotube (CNT). (c) Cyclic voltammetry of the NMC battery with CNT anode. (d). Electrochemical impedance spectroscopy of the NMC battery with CNT anode after lithiation. (e) Cycling performance of the NMC battery at 0.1 C rate. (f) Rate test of the NMC battery at 0.1C and 0.05 C rates.

Impedance plot of the battery using lithiated CNTs as the anode is shown in Figure 80d. The total resistance is about 120  $\text{Ohm}\cdot\text{cm}^2$ , which is about the same as the gel interfacial resistance reported previously. It proves that the bi-layer garnet scaffold and CNT anode have good interfacial contact after lithiation. Figure 80e-f shows the charging and discharging performance of the battery. The voltage profiles at 0.1 C rate (1 C = 190  $\text{mA}/\text{g}$ ) are shown in Figure 80e. The trend of the curves looks similar to that of a battery with liquid electrolyte; however, the discharge capacity is lower than the reported capacity of the commercial NMC cathode. Possible reasons could be utilization of active material in the thick and dense cathode. Figure 80f compares cycling performance at different C rates. Much higher capacity can be achieved at slower C rate (0.05 C).

## Patents/Publications/Presentations

### Presentations

- Bunsen-Kolloquium: Solid-State Batteries II, Frankfurt, Germany (November 2016): “Computation-Guided Design of Interfaces in All-Solid-State Li-Ion Batteries”; Y. F. Mo. Invited keynote speaker.
- 2016 MRS Fall Meeting, Boston (December 2016): “First Principles Study of Solid Electrolyte-Electrode Interfaces in All-Solid-State Li-Ion Batteries”; Y. Z. Zhu,\* X. F. He, and Y. F. Mo.
- 2016 MRS Fall Meeting, Boston (November 27 – December 2, 2016): “All-Solid-State Li-Ion Batteries for Transformational Energy Storage”; E. D. Wachsman. Invited speaker.
- 2016 MRS Fall Meeting, Boston (November 27 – December 2, 2016): “Overcoming Interfacial Impedance in Solid State Batteries”; E. D. Wachsman. Invited speaker.

## Task 7.5 – Nanoscale Interfacial Engineering for Stable Lithium-Metal Anodes (Yi Cui, Stanford University)

**Project Objective.** This study aims to render Li-metal anode with high capacity and reliability by developing chemically and mechanically stable interfacial layers between lithium metal and electrolytes, which is essential to couple with sulfur cathode for high-energy, Li-S batteries. With the nanoscale interfacial engineering approach, various kinds of advanced thin films will be introduced to overcome issues related to dendritic growth, reactive surface, and virtually “infinite” volume expansion of Li-metal anode.

**Project Impact.** Cycling life and stability of Li-metal anode will be dramatically increased. The success of this project, together with breakthroughs of sulfur cathode, will significantly increase the specific capacity of lithium batteries and decrease cost as well, therefore stimulating the popularity of EVs.

**Out-Year Goals.** Along with suppressing dendrite growth, the cycle life, CE, and current density of Li-metal anode will be greatly improved (that is, no dendrite growth for current density up to 3.0 mA/cm<sup>2</sup>, with CE greater than 99.5%) by choosing the appropriate interfacial nanomaterial along with rational electrode material design.

### Milestones

1. Rational design of composite artificial SEI for the stabilization of 3D nanoporous Li-metal anode. (December 2016 – Complete)

## Progress Report

In recognition of the problems associated with the “hostless” nature of lithium metal, the project has successfully introduced stable hosts for metallic lithium.<sup>1-3</sup> The approach resulted in 3D porous lithium, which reduced the effective current density and the degree of interface fluctuation during cycling, leading to more uniform lithium deposition with greatly improved cycling stability. Engineering the SEI on porous lithium electrodes is the next step needed to further improve the cycling efficiency. Thus, the project proposes the rational design of an artificial SEI layer, composed of  $\text{Cu}_3\text{N}$  nanoparticles in styrene butadiene rubber matrix ( $\text{Cu}_3\text{N} + \text{SBR}$ ).<sup>4</sup> This composite artificial SEI can simultaneously possess high mechanical strength due to the densely packed inorganic nanoparticles, good flexibility due to the polymeric binder matrix, and importantly, high Li-ion conductivity owing to the conversion of  $\text{Cu}_3\text{N}$  to ion-conducting  $\text{Li}_3\text{N}$  in the presence of lithium.

The CE of the artificial SEI protected anode was first measured on copper foil. At a current density of  $1 \text{ mA cm}^{-2}$  in carbonate electrolyte (1 M lithium hexafluorophosphate in 1:1 ethylene carbonate/diethyl carbonate with 10 wt% fluoroethylene carbonate additive), the CE of bare copper started at around 95% and quickly decayed to merely 70% within 50 stripping/plating cycles due to the growth of lithium dendrites and the continuous breakdown/repair of SEI (Figure 81a). Surprisingly, the artificial SEI protected copper demonstrated a much-improved CE of  $\approx 97.4\%$  averaged between the 20th and 70th cycles and such high efficiency performance can sustain for more than 100 cycles. In addition, the overpotential increase due to the existence of the artificial SEI was minimal (Figure 1a-inset) because of its relatively high ionic conductivity. Since the effective current density can be significantly reduced on porous Li-metal anodes, CE at a lower current density of  $0.25 \text{ mA cm}^{-2}$  was also studied to better resemble the real working condition of the artificial SEI protected porous lithium. With reduced current density, the CE increased to as high as  $\approx 98\%$ , which was stable for at least 150 cycles (Figure 81b).

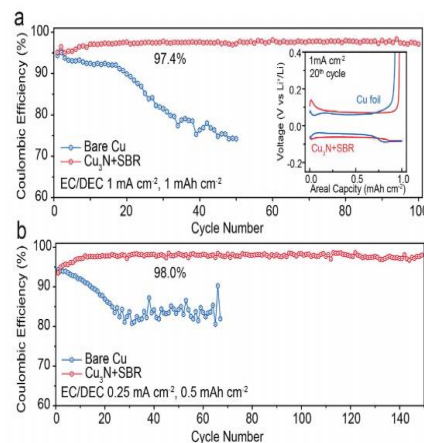


**Figure 81. CE of artificial SEI protected Cu foil and bare Cu foil at a current density of (a)  $1 \text{ mA cm}^{-2}$  (cycling capacity  $1 \text{ mAh cm}^{-2}$ ; Inset: the corresponding voltage profiles at the 20<sup>th</sup> cycle) and (b)  $0.25 \text{ mA cm}^{-2}$  (cycling capacity  $0.5 \text{ mAh cm}^{-2}$ ).**

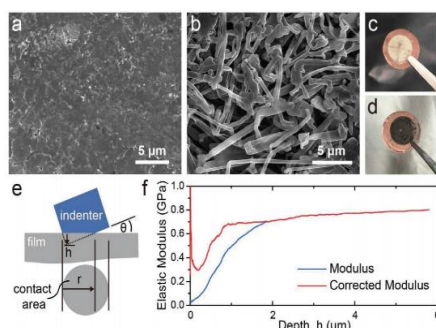


**Figure 82. Top-view scanning electron microscopy images and corresponding digital photographs of lithium deposition after five cycles on (a/c) artificial SEI protected Cu and (b/d) bare Cu foil. (e) Configuration of nano-indentation measurements. (f) Elastic modulus versus depth for indentation test.**

The morphology of lithium deposition after cycling was also studied (Figure 82). After five galvanostatic plating/stripping cycles at a current density of  $0.5 \text{ mA cm}^{-2}$  and a capacity of  $0.5 \text{ mAh cm}^{-2}$ , no observable dendrites on copper foil protected by the artificial SEI, while excessive wire-shaped lithium with a diameter around  $1\text{--}2 \mu\text{m}$  has already formed on the bare copper counterpart. The color of the lithium deposit on the protected copper foil remained silver and shiny, similar to that of pristine lithium metal. However, dark gray lithium was observed for deposition directly on bare copper. The dendrite suppression mechanism can be attributed by the more uniform Li-ion flux across the ion-conducting artificial SEI and its good mechanical property. Accordingly, the elastic modulus of the artificial SEI was measured via nanoindentation with proper mathematical corrections based on the contact model. The elastic modulus was measured on the order of 1 GPa, which can be considered sufficient in suppressing lithium dendrite formation.

## Patents/Publications/Presentations

### Publications

- Lin, D., and Y. Liu, Z. Liang, H.-W. Lee, J. Sun, H. Wang, K. Yan, J. Xie, and Y. Cui. *Nat. Nanotechnol.* 11 (2016): 626.
- Liu, Y., and D. Lin, Z. Liang, J. Zhao, K. Yan, and Y. Cui. *Nat. Commun.* 7 (2016): 10992.
- Liang, Z., and D. Lin, J. Zhao, Z. Lu, Y. Liu, C. Liu, Y. Lu, H. Wang, K. Yan, X. Tao, and Y. Cui. *Proc. Natl. Acad. Sci. U.S.A.* 113 (2016): 2862.
- Liu, Y., and D. Lin, P. Y. Yuen, K. Liu, J. Xie, R. H. Dauskardt, and Y. Cui. *Adv. Mater.* doi: 10.1002/adma.201605531.

## Task 7.6 – Lithium Dendrite Suppression for Lithium-Ion Batteries (Wu Xu and Ji-Guang Zhang, Pacific Northwest National Laboratory)

**Project Objective.** The project objective is to enable lithium metal to be used as an effective anode in rechargeable Li-metal batteries for long cycle life at a reasonably high current density. The investigation will focus on the effects of various lithium salts, additives, and carbonate-based electrolyte formulations on Li-anode morphology, lithium CE, and battery performances in terms of long-term cycling stability at room temperature and elevated temperatures and at various current density conditions, rate capability, and low-temperature discharge behavior. The surface layers on lithium anode and cathode will be systematically analyzed. The properties of solvates of cation-solvent molecules will also be calculated to help explain the obtained battery performances.

**PROJECT IMPACT.** Lithium metal is an ideal anode material for rechargeable batteries. Unfortunately, dendritic lithium growth and limited CE during lithium deposition/stripping inherent in these batteries have prevented practical applications. This work will explore new electrolyte additives that can lead to dendrite-free lithium deposition with high CE. The success of this work will increase energy density of Li-metal batteries and accelerate market acceptance of EVs, especially for PHEVs required by the EV Everywhere Grand Challenge.

**Out-Year Goals.** The long-term goal of the proposed work is to enable lithium and Li-ion batteries with > 120 Wh/kg (for PHEVs), 1000 deep-discharge cycles, 10-year calendar life, improved abuse tolerance, and less than 20% capacity fade over a 10-year period.

**Collaborations.** This project collaborates with the following: Bryant Polzin (ANL) on NMC electrodes, and Chongmin Wang (PNNL) on Characterization by TEM/SEM.

### Milestones

1. Verify formation of a transient high Li<sup>+</sup>-concentration electrolyte layer during fast discharging by direct microscopic observation. (Q1 – In progress)
2. Identify effects of dual-salt electrolytes on Li-metal protection during fast charging. (Q2 - Complete)
3. Identify new electrolytes that are stable with both lithium and high-voltage cathode. (Q3).
4. Increase the CE of lithium cycling in the new electrolyte to be more than 99%. (Q4).



## Progress Report

This quarter, the effect and the mechanism of the additive X (that is,  $\text{LiPF}_6$ ) in the  $\text{LiTFSI-LiBOB}$  dual-salt electrolyte on the protection of Li-metal anode and the performances of  $\text{Li||NMC}$  cells during fast charging were further investigated. The lowest unoccupied molecular orbital (LUMO) energies of the lithium salts and solvents studied in this work demonstrate that the reduction voltage decreases in the following order:  $\text{LiBOB} \gg \text{LiTFSI} > \sim\text{LiPF}_6 \gg \text{EC} > \text{EMC}$  (Figure 83a).  $\text{LiBOB}$  could be easily reduced to form an SEI layer on the Li-metal surface and dictates the morphology of lithium during the deposition process. CV analysis is consistent with the LUMO energies, demonstrating that  $\text{LiBOB}$  in the pure and the  $\text{LiTFSI-LiBOB}$  dual-salt electrolytes shows a reduction peak with an onset potential of ca. 1.1 V versus  $\text{Li/Li}^+$ , while the onset reduction potentials for pure  $\text{LiTFSI}$  and  $\text{LiPF}_6$  electrolytes are hard to find. The addition of  $\text{LiPF}_6$  additive in the dual-salt electrolyte greatly suppresses the reduction peak at 1.1 V for  $\text{LiBOB}$ , probably due to the superior SEI layer formed. The XPS and EDS results are also in good agreement with the calculated LUMO energies.

Based on the electrochemical performance and post-mortem analysis, a functioning mechanism of  $\text{LiPF}_6$  additive in  $\text{LiTFSI-LiBOB}$  dual-salt electrolyte has been proposed (Figure 83b). On one hand, the

$\text{LiPF}_6$  additive plays an important role in stabilizing the aluminum current collector and maintaining good electrical contact between the active material and aluminum. On the other hand, a small amount of  $\text{LiPF}_6$  in the  $\text{LiTFSI-LiBOB}$  dual-salt electrolyte significantly alters the nature of the SEI layer formed on the Li-metal anode. The decomposition products of  $\text{LiPF}_6$ , that is,  $\text{PF}_5$  and  $\text{POF}_3$ , act as catalysts and induce the formation of polycarbonates and polyethers from the ring-opening polymerization of EC molecules. The SEI layer formed on lithium metal in the  $\text{LiPF}_6$ -added dual-salt electrolyte is highly conductive and can minimize electrode polarization. It can also prevent the accumulation of isolated/“dead” lithium during each deposition/stripping cycle. In addition, the polycarbonates and polyethers formed in the SEI layer are flexible, can efficiently cover the Li-metal surface, reduce the side reactions, hold the isolated/“dead” lithium particles tightly, and adhere to the bulk lithium anode, thus preventing the separation of the SEI layer from the bulk lithium metal. Therefore, the utilization of lithium metal initiates at the surface and slowly propagates inward. More importantly, there is no internal short circuit occurring at a charge current density, even up to  $5.25 \text{ mA cm}^{-2}$ . The high charging capability and the excellent cycle life validate the  $\text{LiPF}_6$ -added  $\text{LiTFSI-LiBOB}$  dual-salt electrolyte as an appealing functional electrolyte for high-performance Li-metal batteries.

The effect of lithium amount during each deposition/stripping cycle (that is, the lithium areal capacity) on the stability of Li-metal anode and the cycling performance of the Li-metal battery has also been studied. NMC cathodes with different areal capacities (from  $\sim 1.0$  to  $\sim 4.0 \text{ mAh cm}^{-2}$  with an interval of  $\sim 0.5 \text{ mAh cm}^{-2}$ ) were used to represent the lithium areal capacity to be used in each deposition/stripping cycle. Preliminary cycling data show that the capacities of all  $\text{Li||NMC}$  cells with different NMC areal loadings can be well maintained for at least 50 cycles; seemingly, the usage of lithium amount in each cycle does not affect the cycling stability of the Li-metal cells. More detailed results will be reported next quarter.

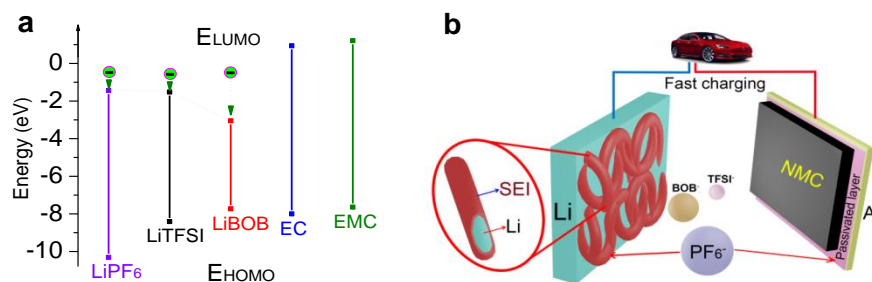


**Figure 83.** (a) Highest occupied molecular orbital (HOMO) and lowest unoccupied molecular orbital (LUMO) energies of lithium salts ( $\text{LiPF}_6$ ,  $\text{LiTFSI}$ ,  $\text{LiBOB}$ ) and solvents ( $\text{EC}$ ,  $\text{EMC}$ ). The vertical lines indicate the electrochemical stability window of related lithium salts and solvents. (b) Schematic illustration demonstrating that  $\text{LiPF}_6$  additive in  $\text{LiTFSI-LiBOB}$  dual-salt electrolyte improves the stability of the Al current collector and the Li-metal anode.

## Patents/Publications/Presentations

### Publication

- Zheng, J., and M. H. Engelhard, D. Mei, S. Jiao, B. J. Polzin, J.-G. Zhang,\* and W. Xu.\* “Electrolyte Additive Enabled Fast Charging and Stable Cycling Lithium Metal Batteries.” Revised manuscript under review.

### Presentations

- 2016 PRIME, Honolulu (October 3, 2016): “CsPF<sub>6</sub> and Propylene Carbonate in Conventional LiPF<sub>6</sub>/Carbonate Electrolytes for Enhanced Lithium-Ion Battery Performances in Wide Temperature Range”; W. Xu, H. Xiang, J. Zheng, Q. Li, J.-G. Zhang, D. Mei, P. Yan, R. Cao, P. Bhattacharya, S. D. Burton, M. H. Engelhard, M. E. Bowden, Z. Zhu, C. Wang, S. Jiao, S. S. Cartmell, A. V. Cresce, K. Xu, and B. Polzin. Invited talk.
- 2016 PRIME, Honolulu (October 4, 2016): “Optimization of Dual-Salt Electrolytes for Rechargeable Lithium Metal Batteries”; S. Jiao, J. Zheng, H. Xiang, P. Shi, D. Mei, Q. Li, S. S. Cartmell, J.-G. Zhang, and W. Xu. Oral presentation.

## Task 7.7 – Lithium Batteries with Higher Capacity and Voltage (John B. Goodenough, University of Texas – Austin)

**Project Objective.** The project objective is to develop an electrochemically stable alkali-metal anode that can avoid the SEI layer formation and the alkali-metal dendrites during charge/discharge. To achieve the goal, a thin and elastic solid electrolyte membrane with a Fermi energy above that of metallic lithium and an ionic conductivity  $\sigma > 10^{-4} \text{ S cm}^{-1}$  will be tested in contact with alkali-metal surface. The interface between the alkali-metal and the electrolyte membrane should be free from liquid electrolyte, have a low impedance for alkali-metal transport and plating, and keep a good mechanical contact during electrochemical reactions.

**Project Impact.** An alkali-metal anode (lithium or sodium) would increase the energy density for a given cathode by providing a higher cell voltage. However, lithium is not used as the anode in today's commercial Li-ion batteries because electrochemical dendrite formation can induce a cell short-circuit and critical safety hazards. This project aims to find a way to avoid the formation of alkali-metal dendrites and to develop an electrochemical cell with dendrite-free alkali-metal anode. Therefore, once realized, the project will have a significant impact by an energy-density increase and battery safety; it will enable a commercial Li-metal rechargeable battery of increased cycle life.

**Approach.** The project will design, make, and test cells. The key approach is to introduce a solid-solid contact between an alkali metal and a solid electrolyte membrane. Where SEI formation occurs, the creation of new anode surface at dendrites with each cycle causes capacity fade and a shortened cycle life. To avoid the SEI formation, a thin and elastic solid electrolyte membrane would be introduced, or the solid electrolyte should not be reduced by, but should be wet by, a metallic alkali-ion anode.

**Out-Year Goals.** The out-year goal is to develop coin cells that are safe and low-cost with a long cycle life at a voltage  $V > 3.0 \text{ V}$ .

**Collaborations.** This project collaborates with A. Manthiram at UT Austin, and Karim Zaghib at HQ.

### Milestones

1. Demonstrate the cycle life and capacity of a Li-S cell. (Q1 – Complete)
2. Demonstrate a high-voltage cell containing the glass electrolyte. (Q2)
3. Demonstrate a new battery concept. (Q3)
4. Test energy density, cycle life, rate of charge/discharge of the new battery concept. (Q4)

## Progress Report

$\text{Li}_7\text{La}_3\text{Zr}_2\text{O}_{12}$  (LLZO) garnet electrolytes, which have a Li-ion conductivity of  $10^{-3} \text{ S cm}^{-1}$  at  $25^\circ\text{C}$  and better stability versus lithium metal than the other ceramic electrolytes, face two great challenges: (1) a large interfacial resistance for Li-ion transfer and (2) lithium-dendrite penetration along grain boundaries. The origin of the large interfacial resistance is related to the garnet instability at room temperature. The grains of garnet electrolyte react with moisture and carbon dioxide in air to form  $\text{LiOH}$  and  $\text{Li}_2\text{CO}_3$  on the surface of the LLZO grains. Both  $\text{LiOH}$  and  $\text{Li}_2\text{CO}_3$  are Li-ion insulators, which leads to a large grain-boundary resistance of the garnet electrolyte and the lithium/garnet interface also has a large impedance. The project used LiF to increase stability of the garnet electrolyte  $\text{Li}_{6.5}\text{La}_3\text{Zr}_{1.5}\text{Ta}_{0.5}\text{O}_{12}$  (LLZT) against moisture and carbon dioxide in air; the grain-boundary and interfacial resistances were reduced significantly, which makes LLZT a possible solid electrolyte in Li-S batteries.

To demonstrate the advantages of the LiF modification that decreases the interfacial resistance, Li-S cells with a LLZT and a LLZT–2LiF solid electrolyte were assembled. The solid electrolyte can efficiently block the polysulfide shuttle, which is a severe problem in Li-S batteries. The total resistance of the cells with LLZT and LLZT–2LiF in Figure 84a were  $1000$  and  $2620 \text{ } \Omega \text{ cm}^{-2}$ , respectively. The cells with LLZT and LLZT–LiF display well-defined discharge/charge plateaus and low overpotentials. The cell with LLZT–2LiF exhibited a much lower gap ( $0.34 \text{ V}$ ) between charge and discharge voltages than that with LLZT ( $0.59 \text{ V}$ ) at the current density of  $200 \text{ } \mu\text{A cm}^{-2}$ . The much-reduced interfacial resistance allows the cells to be cycled at high current densities. As shown in Figure 1c, discharge capacities of  $1137$ ,  $1074$ , and  $1042 \text{ mAh g}^{-1}$  can be obtained at the rates of  $100$ ,  $200$  and  $300 \text{ } \mu\text{A cm}^{-2}$ , respectively. Notably, since the polysulfide shuttle can be completely blocked by the solid electrolyte, the hybrid cells assembled also exhibit a stable cyclability at  $200 \text{ } \mu\text{A cm}^{-2}$ . The reversible capacity stabilized at  $988 \text{ mAh g}^{-1}$  after 100 cycles with the retention of  $93\%$  of the stabilized capacity in the second cycle (Figure 84d). Furthermore, the CE maintains almost  $100\%$  over the subsequent 100 cycles, which is much higher than the L-S cell without garnet in Figure 85, indicating that the solid electrolyte can successfully block the polysulfide shuttle during the whole cycling processes.

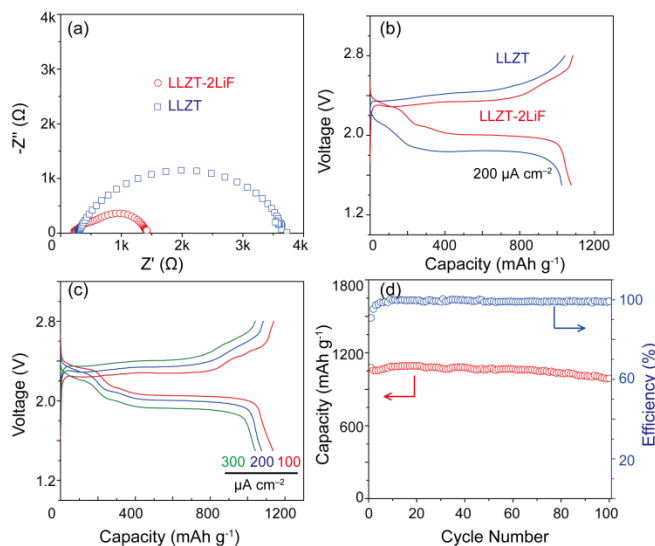


**Figure 84.** (a) The impedance plots of a Li-S battery. (b) Charge and discharge voltage profiles of a Li-S battery with LLZT and LLZT–2LiF as a separator. (c) Charge and discharge voltage profiles of a Li-S battery with LLZT–2LiF at different current densities. (d) Capacity retention and cycling efficiency of the Li-S battery.

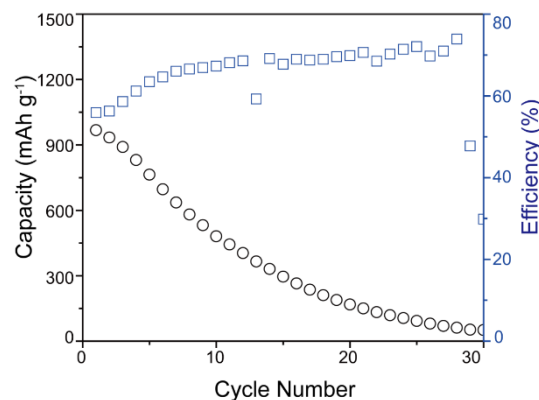


**Figure 85.** Cycling stability and CE of the Li-S cell without solid electrolyte nor  $\text{LiNO}_3$  additive.

## Task 7.8 – Advancing Solid-State Interfaces in Li-ion Batteries (Nenad Markovic and Larry A. Curtiss, Argonne National Laboratory)

**Project Objective.** The project objectives are multifaceted, including: (1) development of a new mechanically and chemically stable Li-selective solid “membrane” capable of protecting the metal lithium anode during the discharge process in commercially available liquid electrolytes (hereafter denoted as a  $S_{Li}$ - $S_M$ - $E_L$  system); and (2) development of a mechanically/chemically stable and Li-ion conductive ( $\geq 2 \times 10^{-4}$  S/cm at 298K) solid electrolyte for a solid-state battery encompassing a metal lithium anode and nonflammable solid electrolyte that can operate at cathode potentials  $> 5$  V (denoted as a  $S_{Li}$ - $S_{EL}$ - $S_C$  system).

**Project Impact.** Protective organic and inorganic compounds can enhance stability of interface, improve Li-ion interfacial transport, minimize dendrite formation, and increase safety in Li-ion batteries.

**Approach.** The project proposes to develop and use interdisciplinary, atomic-/molecular-level insight obtained from integrating both experimental- and computational-based methodologies to define the landscape of parameters that control interfacial properties for a new generation of the Li-ion solid-solid battery systems. The strategy will involve transferring knowledge gained from well-characterized thin-film materials to real-world materials. This strategy forms a closed loop wherein the knowledge gained from model systems is used to design more complex, real-world materials and vice-versa. The work will focus on utilizing existing in-house synthesis and characterization methods to enable rapid transition from fundamental science to realistic cells.

**Out-Year Goals.** The out-year goals are to use and develop the physical and chemical synthesis methods for design of solid-solid interfaces with unique chemical/mechanical/conductivity properties of  $S_{Li}$ - $S_M$ - $E_L$  and  $S_{Li}$ - $S_{EL}$ - $S_C$  systems. The proposed work will develop and exploit a variety of *ex situ* and *in situ* experimental optical and surface sensitive techniques and electrochemical methods to explore and explain bulk and interfacial properties of the selected materials. The results will serve to unravel many of puzzling bulk and interfacial properties of  $S_{Li}$ - $S_M$ - $E_L$  and  $S_{Li}$ - $S_{EL}$ - $S_C$  materials.

**Collaborations.** This project funds work at ANL and UCI (Prof. Amin Salehi). It will establish collaboration with Jeff Sakamoto at U Michigan (co-PI for Task 7.1: Mechanical Properties and the Protected Lithium Interfaces).

### Milestones

1. Development of new synthesis and characterization methods for controlled deposition of lithium on well-defined  $SrTiO_3$  single crystals. (Q1 – In progress)
2. Use UHV-based experimental techniques in combination with computational methods to investigate parameters that control interaction of lithium anode with individual components of  $Li_{6.5}La_3Zr_{1.5}M_{0.5}O_2$  ( $M = Nb, Ta$ ) and  $Li_2CO_3$  “membrane.” (Q2)
3. Design and develop *in situ* evaluation of stability of both  $Li_2CO_3$  “membrane” (ICP-MS) and selected organic electrolytes during charge-discharge processes (DEMS). (Q3)
4. Investigate the CE of as well as the charge-discharge cyclability for selected  $S_{Li}$ - $S_M$ - $E_L$  and  $S_{Li}$ - $S_{EL}$ - $S_C$  systems. (Q4)

## Progress Report

Conditions for controlled lithium deposition (Magnetron Sputtering Method; *lithium film* ~ 2-nm thick) on SrTiO<sub>3</sub> (STO) single crystal substrate are established (*lithium sputtering* ~ 30 min at 100°C). Transfer of the Li-STO system without air-born contamination allowed exploration of the lithium interaction with oxygen and the corresponding cations at atomic and molecular levels. As summarized in Figures 86 and 87, XPS results reveal that lithium interaction with near-surface oxygen (interfacial formation of Li<sub>2</sub>O in Figure 86) leads to reduction of Ti<sup>4+</sup> to Ti<sup>3+</sup> and Ti<sup>2+</sup>.

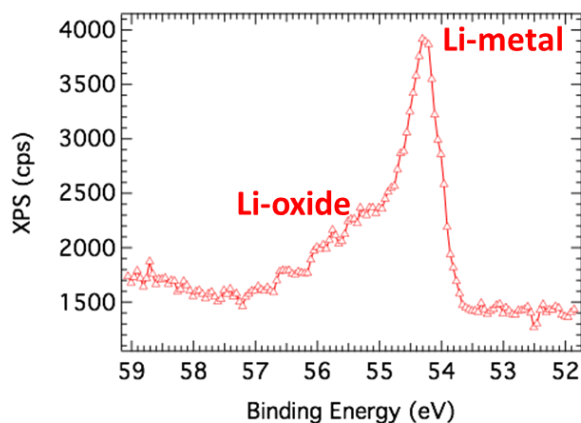


Figure 86. X-ray photoelectron spectroscopy results for 1s lithium peak to establish Li-O interaction.

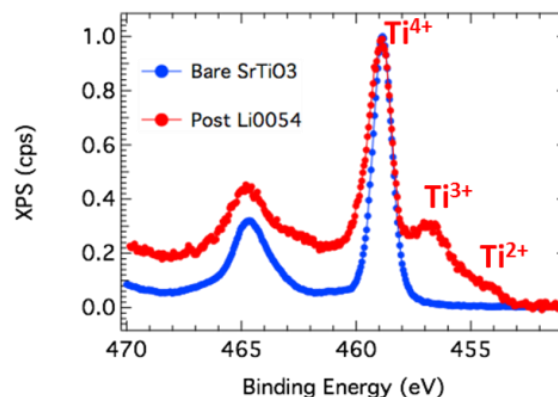


Figure 87. X-ray photoelectron spectroscopy results for titanium 2p peaks to track valence state of titanium.

To confirm experimentally established chemical transformations and to understand important details associated with interaction of lithium with STO, the project applies DFT calculations capable of providing thermodynamic and kinetic insights for the Li<sub>2</sub>O formation and the concomitant change in the valence state of strontium and titanium. Indeed, the project found that the thermodynamically favorable pathway for the observed instability is Li-induced titanium oxide reduction. The importance of experimental and computational results goes well beyond the model Li-STO systems, and will be used in the future for understanding instability of Li/Li<sub>0.5</sub>La<sub>3</sub>Zr<sub>1.5</sub>M<sub>0.5</sub>O<sub>2</sub> (M = Nb) interfaces.

Initial information for the S<sub>Li</sub>-S<sub>M</sub>-E<sub>L</sub> system is also obtained by utilizing a science-based approach, which includes a combination of experimental and computational methods. Thus far, the project has learned how to synthesize the Li<sub>2</sub>CO<sub>3</sub> coating for the Li/Li<sub>2</sub>CO<sub>3</sub> interface and which computational methods will be required to explore lithium migration through Li<sub>2</sub>CO<sub>3</sub> to the lithium surface (see Figure 88) as well as how lithium transport through Li<sub>2</sub>CO<sub>3</sub> may compete with other species present in the system.

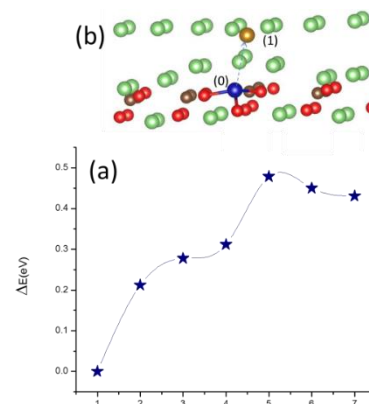


Figure 88. (a) Density functional theory calculated reaction path for lithium migration from Li<sub>2</sub>CO<sub>3</sub> to the Li(100) surface. (b) Illustration showing migration of one lithium (blue) across the interface.

## Task 7.9 – Engineering Approaches to Dendrite-Free Lithium Anodes (Prashant Kumta, University of Pittsburgh)

**Project Objective.** This project will yield Li-metal anodes with specific capacity  $\geq 2000$  mAh/g ( $\geq 10$  mAh/cm<sup>2</sup>),  $\sim 1000$  cycles, CE loss  $\leq 0.01\%$ , and CE  $\geq 99.99\%$  with superior rate capability. The goal is to (1) systematically characterize different approaches for generation of dendrite-free Li-metal anodes while also providing an understanding of the scientific underpinnings, and (2) evaluate the microstructure and electrochemical performance of the dendrite free Li-metal anodes. Generation of high-performance, dendrite free Li-metal anodes will successfully demonstrate generation of novel sulfur cathodes, affording the fabrication of Li-S batteries meeting the targeted gravimetric energy densities  $\geq 350$  Wh/kg and  $\geq 750$  Wh/l with a cost target \$125/kWh and cycle life of at least 1000 cycles for meeting the EV Everywhere Grand Challenge blueprint.

**Project Impact.** Dendrite formation in electrochemical systems occurs due to inhomogeneous current densities coupled with local diffusion gradients, surface roughness, and kinetic roughening. Lithium dendrite formation and growth are, however, not well-understood; adding to the complexity is the SEI formation. Control and elimination of Li-metal dendrite formation is a veritable challenge. If overcome, it would render the universal adoption of Li-anode batteries (LABs) for stationary and mobile applications. The current proposal is a scientific study of novel approaches to address dendrite formation in LABs, electrolyte decomposition, and associated cell failure. Development of dendrite-free, high-performance lithium anodes will enable the use of Li-free cathodes, opening up myriad possibilities pushing the envelope in terms of cathode capacity and battery energy density.

**Out-Year Goals.** This multi-year project comprises three major phases to be successfully completed in three years:

- Phase 1 (year 1) – Synthesis, characterization and scale up of suitable PF (porous foams) for use as current collectors for lithium anodes and Li-ion conductor (LIC) materials to prepare multilayer porous foams (MPFs).
- Phase 2 (year 2) – Development of Li-rich structurally isomorphous alloy (SIA) anodes, and generation of composite multilayer anodes (CMAs).
- Phase-3 (year 3) – Advanced high-energy-density, high-rate, extremely cyclable cell development.

**Collaborations.** The project will involve collaboration with Dr. Moni Kanchan Datta (U Pitt) and Dr. Oleg I. Velikokhatnyi (U Pitt) as co-PIs, and Dr. Prashanth Jampani Hanumantha (U Pitt) as senior research personnel. In addition, collaborations will be undertaken with Dr. D. Krishnan Achary (U Pitt) for solid-state nuclear magnetic resonance (MAS-NMR) characterization.

### Milestones

1. Delegate tasks and convene the technical aspects between partners. (October 2016 – Complete)
2. Determine electrode and cell design parameters for achieving the targeted energy density. (October 2016 – Complete)
3. Identify and synthesize materials with high electronic conductivity, electrochemical stability that can be generated as porous architectures. (Q3)
4. Prepare doped LIC with improved ionic conductivity for coating of PFs to prepare MPFs. (Q4)

Reaction coordinate

## Progress Report

Phase 1 was aimed at developing PF materials and MPFs with the target of reducing orthogonal lithium nucleation and growth. Figure 89 shows improvement in CE achieved by use of Gen-1 MPF used as a current collector in a cell consisting of a lithium counter electrode. Lithium was plated (at  $1\text{mA}/\text{cm}^2$ ) and deplated (to 1V) repeatedly onto the MPF current collector, and CE was calculated using the difference in capacities of plating/deplating. It can be seen that the novel MPF current collector displayed superior CE as compared to a conventional copper current collector, indirectly indicating that the MPF aided in the reduction of dendritic structure formation. The use of composite polymer electrolytes (CPEs), shown in Figure 90, with high mechanical strength (200-350% higher tensile strength) and interfacial characteristics resulted in the stabilization of Li-metal anodes when tested in symmetric Li-metal cells (stable CE of 99.88% observed over 80 cycles during plating/ deplating of  $12\text{mAh}/\text{cm}^2$  lithium at  $3\text{mA}/\text{cm}^2$ ). Further, Figure 91 shows the preliminary results demonstrating successful use of Li-SIA electrodes in preventing dendrite formation, even when tested at very high current densities of  $\sim 16\text{mA}/\text{cm}^2$ . More detailed studies and results of SIA systems will be discussed and provided in later reports.

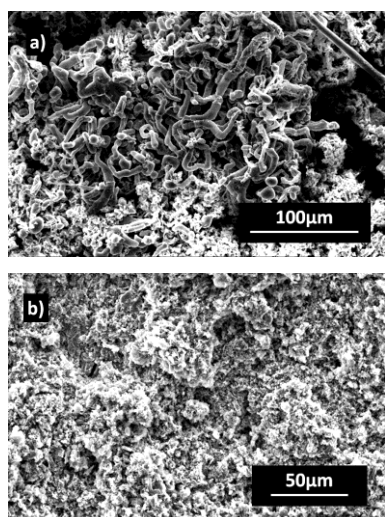


Figure 91. Scanning electron microscopy images of the morphology of (a) lithium electrode and (b) lithium structurally isomorphous alloy (Li-SIA) electrode cycled at high current density  $\sim 1\text{A}/\text{g}$  (30 cycles). A clear absence of dendritic structures observed in the Li-SIA electrode.

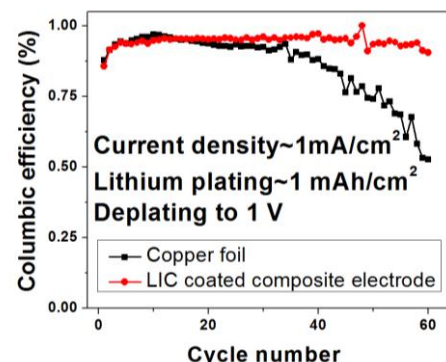


Figure 89. Significant improvement in Coulombic efficiency of lithium afforded by use of multilayer porous foams.

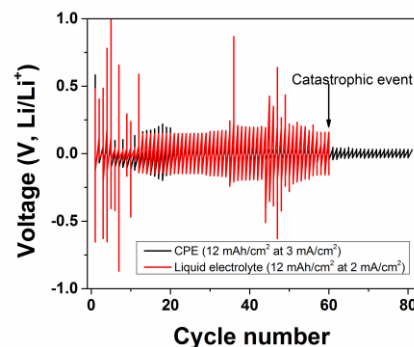


Figure 90. Voltage hysteresis plot of composite polymer electrolytes (black) showing superior Coulombic efficiency and stability as compared to commercial separators with liquid electrolyte (red).

## Patents/Publications/Presentations

### Publication

- ECS, 230<sup>th</sup> Meeting, Honolulu (October 2016): “Engineering Approaches to Dendrite Prevention in Lithium Anode Based Batteries”; P. H. Jampani, B. Gattu, M. K. Datta, P. M. Shanthi, and P. N. Kumta.



## TASK 8 – LITHIUM–SULFUR BATTERIES

### Summary and Highlights

Advances in Li-ion technology have been stymied by challenges involved in developing high reversible capacity cathodes and stable anodes. Hence, there is a critical need for development of alternate battery technologies with superior energy densities and cycling capabilities. In this regard, Li-S batteries have been identified as the next flagship technology, holding much promise due to the attractive theoretical specific energy densities of 2,567 Wh/kg. In addition, realization of the high theoretical specific capacity of 1,675 mAh/g corresponding to formation of Li<sub>2</sub>S using earth-abundant sulfur renders the system highly promising compared to other available cathode systems. Thus, the research focus has shifted to developing Li-S batteries. This system, however, suffers from major drawbacks, as elucidated below:

- Limited inherent electronic conductivity of sulfur and sulfur-compound based cathodes;
- Volumetric expansion and contraction of both the sulfur cathode and lithium anode;
- Soluble polysulfide formation/dissolution and sluggish kinetics of subsequent conversion of polysulfides to Li<sub>2</sub>S, resulting in poor cycling life;
- Particle fracture and delamination as a result of the repeated volumetric expansion and contraction;
- Irreversible loss of lithium at the sulfur cathode, resulting in poor CE; and
- High diffusivity of polysulfides in the electrolyte, resulting in plating at the anode and consequent loss of driving force for lithium diffusion (that is, drop in cell voltage).

These major issues cause sulfur loss from the cathode, leading to mechanical disintegration. Additionally, surface passivation of anode and cathode systems results in a decrease in the overall specific capacity and CE upon cycling. Consequently, the battery becomes inactive within the first few charge-discharge cycles. Achievement of stable high capacity in Li-S batteries requires execution of fundamental studies to understand the degradation mechanisms in conjunction with engineered solutions. This Task addresses both aspects with execution of esoteric, fundamental *in situ* XAS and *in situ* electron paramagnetic resonance (EPR) studies juxtaposed with innovative applied research comprising use of suitable additives, coatings, and exploration of composite morphologies as well as engineered strategies. Both ANL and LBNL use X-ray based techniques to study phase evolution and loss of CE in S- and S-Se based electrodes, primarily by the former during lithiation/delithiation while understanding polysulfide formation in sulfur and oligomeric PEO solvent by the latter, respectively. Work from PNNL, U Pitt, and Stanford demonstrates high areal capacity electrodes in excess of 4 mAh/cm<sup>2</sup>. Following loading studies reported this quarter, PNNL performed *in situ* EPR to study reaction pathways mediated by sulfur radical formation. Coating/encapsulation approaches adopted by U Pitt and Stanford comprise flexible sulfur wire (FSW) electrodes coated with Li-ion conductors by U Pitt, and TiS<sub>2</sub> encapsulation of Li<sub>2</sub>S in the latter, both ensuring polysulfide retention at sulfur cathodes. BNL work on the other hand, has focused on benchmarking of pouch cell testing by optimization of the voltage window and study of additives such as LiI and LiNO<sub>3</sub>. *Ab initio* studies at Stanford and U Pitt involve calculation of binding energies, diffusion coefficients, ionic conductivities and reaction pathways determination, augmenting the experimental results. Similarly, AIMD simulations performed at TAMU reveal multiple details regarding electrolyte decomposition reactions and the role of soluble polysulfides (PS) on such reactions. Using kinetic Monte Carlo (KMC) simulations, electrode morphology evolution and mesostructured transport interaction studies were also executed. Studies over the last quarter at PNNL suggest that proper control of electrode porosity/thickness is essential for obtaining high-energy Li-S batteries. Porosity shows strong dependence on calendaring pressure because of low tap densities of electrode components such as sulfur and carbon. Increasing the calendaring-pressure from 0.2 to 1.5 ton (T) leads to quick decrease of electrode porosity, resulting in improvement of electrode volumetric energy density. Measured electrode volumetric energy density increased from 650 Wh L<sup>-1</sup> for as-cast electrode (120 μm thick) to 1300 Wh L<sup>-1</sup> for electrode compressed to 60 μm.

Additionally, Penn State has shown the use of dimethyl disulfide as a functional co-solvent, demonstrating its ability to show an alternate electrochemical reaction pathway for sulfur cathodes by the formation of dimethyl polysulfides and lithium organosulfides as intermediates and reduction products.

Each of these projects has a collaborative team of experts with the required skill set needed to address the EV Everywhere Grand Challenge of 350 Wh/kg and 750 Wh/l, and cycle life of at least 1000 cycles.

**Highlights.** This Task reports the following project highlights for this quarter:

- Studies at PNNL (Jun Liu, Dongping Lu) suggest that proper control of electrode porosity/thickness is essential for obtaining high-energy Li-S batteries. Porosity shows strong dependence on calendaring pressure because of low tap densities of electrode components such as sulfur and carbon. Increasing the calendaring pressure from 0.2 to 1.5 ton (T) leads to quick decrease of electrode porosity, resulting in improvement of electrode volumetric energy density. Measured electrode volumetric energy density increased from 650 Wh L<sup>-1</sup> for as-cast electrode (120- $\mu$ m thick) to 1300 Wh L<sup>-1</sup> for electrode compressed to 60  $\mu$ m.
- Dimethyl disulfide as a functional co-solvent has been demonstrated (Donghai Wang, PSU) to show an alternate electrochemical reaction pathway for sulfur cathodes by the formation of dimethyl polysulfides and lithium organosulfides as intermediates and reduction products.

## Task 8.1 – New Lamination and Doping Concepts for Enhanced Lithium–Sulfur Battery Performance (Prashant N. Kumta, University of Pittsburgh)

**Project Objective.** The project objective is to successfully demonstrate generation of novel sulfur cathodes for Li-S batteries meeting targeted gravimetric energy densities  $\geq 350$  Wh/kg and  $\geq 750$  Wh/l with a cost target \$125/kWh and cycle life of at least 1000 cycles for meeting the EV Everywhere Grand Challenge blueprint. The proposed approach will yield sulfur cathodes with specific capacity  $\geq 1400$  mAh/g, at  $\geq 2.2$  V, generating  $\sim 460$  Wh/kg energy density higher than the target. Full cells meeting required deliverables will also be made.

**Project Impact.** Identifying new laminated S-cathode-based systems displaying higher gravimetric and volumetric energy densities than conventional Li-ion batteries will likely result in new commercial battery systems that are more robust, capable of delivering better energy and power densities, and more lightweight than current Li-ion battery packs. Strategies and configurations based on new LIC-coated sulfur cathodes will also lead to more compact battery designs for the same energy and power density specifications as current Li-ion systems. Commercialization of these new S-cathode-based Li-ion battery packs will represent, fundamentally, a major hallmark contribution of the DOE VTO and battery community.

**Out-Year Goals.** This multi-year project comprises three phases to be successfully completed in three years:

- Phase 1 (year 1) – Synthesis, characterization, and scale up of suitable LIC matrix materials and multilayer composite sulfur cathodes. (Complete)
- Phase 2 (year 2) – Development of LIC-coated sulfur nanoparticles, scale up of high-capacity engineered LIC-coated multilayer composite electrodes, and doping strategies for improving electronic conductivity.
- Phase 3 (year 3) – Advanced high-energy-density, high-rate, extremely cyclable cell development.

**Collaborations.** The project collaborates with the following members with the corresponding expertise: Dr. Spandan Maiti (U Pitt) for mechanical stability and multi-scale modeling; Dr. A. Manivannan (NETL) for XPS for surface characterization; and Dr. D. Krishnan Achary (U Pitt) for solid-state MAS-NMR characterization.

### Milestones

1. Preparing doped LIC with improved ionic conductivity. (January 2016 – Complete)
2. Identification of dopants and doping sulfur with suitably identified dopants with enhanced electronic properties. (April 2016 – Complete)
3. Developing organic and inorganic Complex Framework Networks (CFN) as effective polysulfide traps. (July 2016 – Complete)
4. Application of ceramic filler incorporated CPEs to improve specific capacity of commercial sulfur to  $\sim 812$  mAh/g for over 100 cycling. (October 2016 – Complete)
5. Design and engineering of high-capacity, LIC-coated sulfur nanoparticles. (January 2017 – Complete)
6. Development of sulfur composite products (SCPs) with very high sulfur loadings of  $\sim 18$  mg/cm<sup>2</sup>. (January 2017 – Complete)
7. Synthesis of vertically aligned CNT (VACNT) and LIC coated nanosulfur based composite materials. (In progress)
8. Optimize doping composition and thickness to maximize capacity, rate capability, and cycling stability. (In progress)

## Progress Report

Phase 2 concluded with successful demonstration of improved ionic conductivity of LIC, achieved by effective doping, altering the sulfur electronic structure by suitable dopants, and designing effective methods for coating LICs onto sulfur cathodes. Phase 1 involved replacement of commercial separator with LIC and successful demonstration of prevention of polysulfide dissolution. Generation of integrated doped nanoparticulate sulfur with VACNT-LIC generated composite electrodes, business value analysis, and fabrication of the desired 4 mAh full cell are the main aims of Phase 3. This quarter, the project worked on developing SCPs with very high sulfur loadings of  $\sim 18 \text{ mg/cm}^2$  and developing simple engineering strategies to coat LIC onto individual

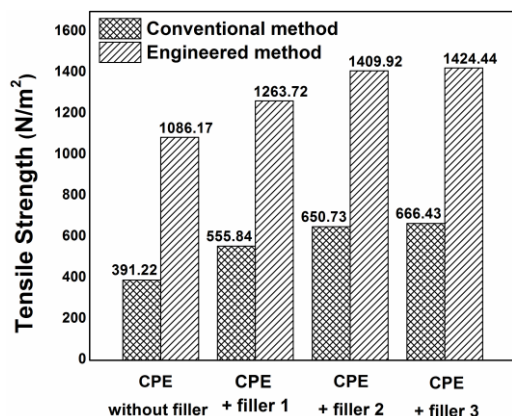
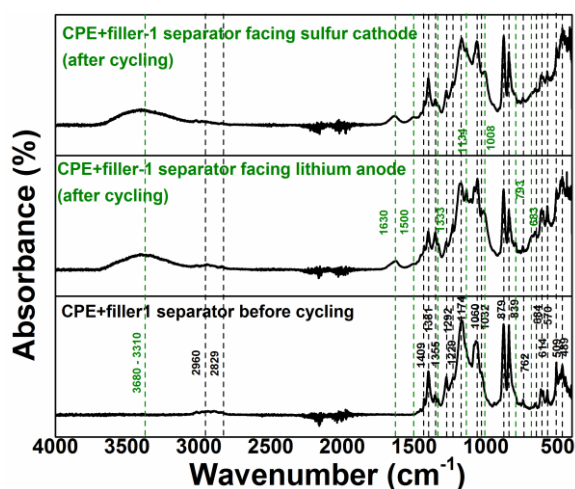


**Figure 92:** Mechanical behavior of composite polymer electrolyte showing superior strength of engineered synthesis method.

sulfur nanoparticles. Work also involved conducting a comprehensive study of the physical and chemical properties of the CPEs developed last quarter, which when tested against commercial sulfur cathodes demonstrated very stable capacity of  $\sim 812 \text{ mAh/g}$  after 100 cycles with minimal fade rate of  $0.012\%/cycle$ . Mechanical property analysis showed that the CPEs displayed two- to three-fold improvement in tensile strength as compared to counterparts synthesized using the conventional technique (Figure 92). The CPEs also showed excellent chemical stability with minimal modification to the polymer backbone after cycling confirmed by FTIR spectroscopy (Figure 93a) and good flame resistance properties as compared to commercial battery separators (Figure 93b).



**b**

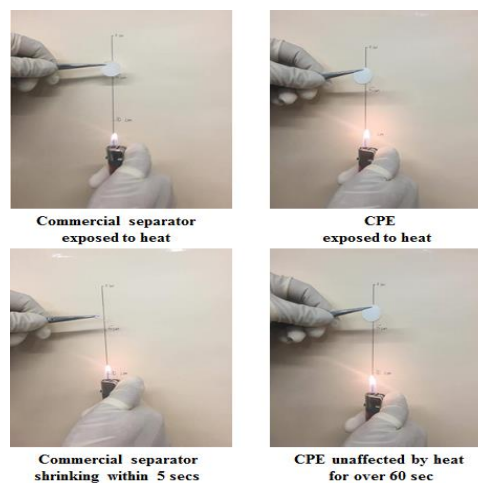


**Figure 93.** (a) Fourier transform infrared spectra of composite polymer electrolyte (CPE) after cycling. (b) Flammability test result of the CPE.

## Patents/Publications/Presentations

### Publications

- Jampani, P. H., and B. Gattu, P. M. Shanthi, S. S. Damle, Z. Basson, R. Bandi, M. K. Datta, S. K. Park, and P. N. Kumta. “Flexible Sulfur Wires (Flex-SWs) – A Versatile Platform for Lithium-Sulfur Batteries.” *Electrochim. Acta* 212 (2016) 286–293.
- Shanthi, P. M., and P. H. Jampani, B. Gattu, M. Sweeney, M. K. Datta, and P. N. Kumta. “Nanoporous Non-Carbonized Metal Organic Frameworks (MOFs): Effective Sulfur Hosts for High Performance Li-S Batteries.” *Electrochim. Acta* (2017): In press. doi: <http://dx.doi.org/10.1016/j.electacta.2017.01.115>.

## Task 8.2 – Simulations and X-Ray Spectroscopy of Lithium–Sulfur Chemistry (Nitash Balsara, Lawrence Berkeley National Laboratory)

**Project Objective.** Li-S cells are attractive targets for energy storage applications, as their theoretical specific energy of 2600 Wh/kg is much greater than the theoretical specific energy of current Li-ion batteries. Unfortunately, the cycle-life of Li-S cells is limited due to migration of species generated at the sulfur cathode. These species, collectively known as polysulfides, can transform spontaneously, depending on the environment, and it has thus proven difficult to determine the nature of redox reactions that occur at the sulfur electrode. The project objective is to use XAS to track species formation and consumption during charge-discharge reactions in a Li-S cell. Molecular simulations will be used to obtain X-ray spectroscopy signatures of different polysulfide species, and to determine reaction pathways and diffusion in the sulfur cathode. The long-term objective is to use mechanistic information to build high specific energy lithium-sulfur cells.

**Project Impact.** Enabling rechargeable Li-S cells has potential to change the landscape of rechargeable batteries for large-scale applications beyond personal electronics due to: (1) high specific energy, (2) simplicity and low cost of cathode (the most expensive component of Li-ion batteries), and (3) earth abundance of sulfur. The proposed diagnostic approach also has significant potential impact, as it represents a new path for determining the species that form during charge-discharge reactions in a battery electrode.

**Out-Year Goals.** The out-year goals are as follows:

- **Year 1.** Simulations of sulfur and PSL in oligomeric PEO solvent. Prediction of X-ray spectroscopy signatures of PSL/PEO mixtures. Measurement of X-ray spectroscopy signatures of PSL/PEO mixtures.
- **Year 2.** Use comparisons between theory and experiment to refine simulation parameters. Determine speciation in PSL/PEO mixtures without resorting to ad hoc assumptions.
- **Year 3.** Build an all-solid lithium-sulfur cell that enables measurement of X-ray spectra *in situ*. Conduct simulations of reduction of sulfur cathode.
- **Year 4.** Use comparisons between theory and experiment to determine the mechanism of sulfur reduction and Li<sub>2</sub>S oxidation in all-solid Li-S cell. Use this information to build Li-S cells with improved life-time.

**Collaborations.** This project collaborates with Tsu-Chien Weng, Dimosthenis Sokaras, and Dennis Nordlund at SSRL, SLAC National Accelerator Laboratory in Stanford, California.

### Milestones

1. Continue *in situ* XAS and other spectroscopies to determine reaction products as a function of charge/discharge rate. (December 2016 – Complete)
2. Theoretical prediction of polysulfide solution composition based on thermodynamic calculations of polysulfide and disproportionation reaction Gibbs free energy. (February 2017)
3. Employ carbon confinement strategies and demonstrate improved cycle life relative to all solid Li-S cells with unconfined sulfur. (June 2017 – On Schedule)
4. Perform *in situ* XAS on Li-S cells containing perfluoropolyether electrolytes; determine reaction products in absence of polysulfide dissolution. (September 2017 – On schedule)

## Progress Report

The first milestone is complete, and a publication describing the results has been accepted. Impregnating sulfur into microporous carbon has shown improved cycling life of Li-S batteries; however, knowing exactly where sulfur resides is challenging, both from a design perspective and from microscopy characterization techniques. Through extensive computer simulations, it was found that liquid sulfur will preferentially and spontaneously intercalate into porous carbon (< 2 nm) due to the formation of a quasi-liquid phase with enhanced binding enthalpy that persists well below the freezing point. Therefore, sulfur will preferentially fill the pores in the carbon shell first before getting inside the carbon nanospheres. Figure 94d shows that for a 30-wt% sulfur loading, only amorphous sulfur is observed within the shell, while 60-wt% sulfur loading started to have crystalline sulfur inside the shell. Extensive computational calculation reveals a decreased 1s core electron binding due to additional (semi-metallic) screening from the delocalized electron cloud on graphene, which results in a 0.3 eV red shift in the XAS spectrum for sulfur at the sulfur/carbon interface compared to the bulk sulfur absorption. This red-shift is consistent with experimental XAS measurement of 30-wt% loading sample with sulfur reside within the carbon shell.

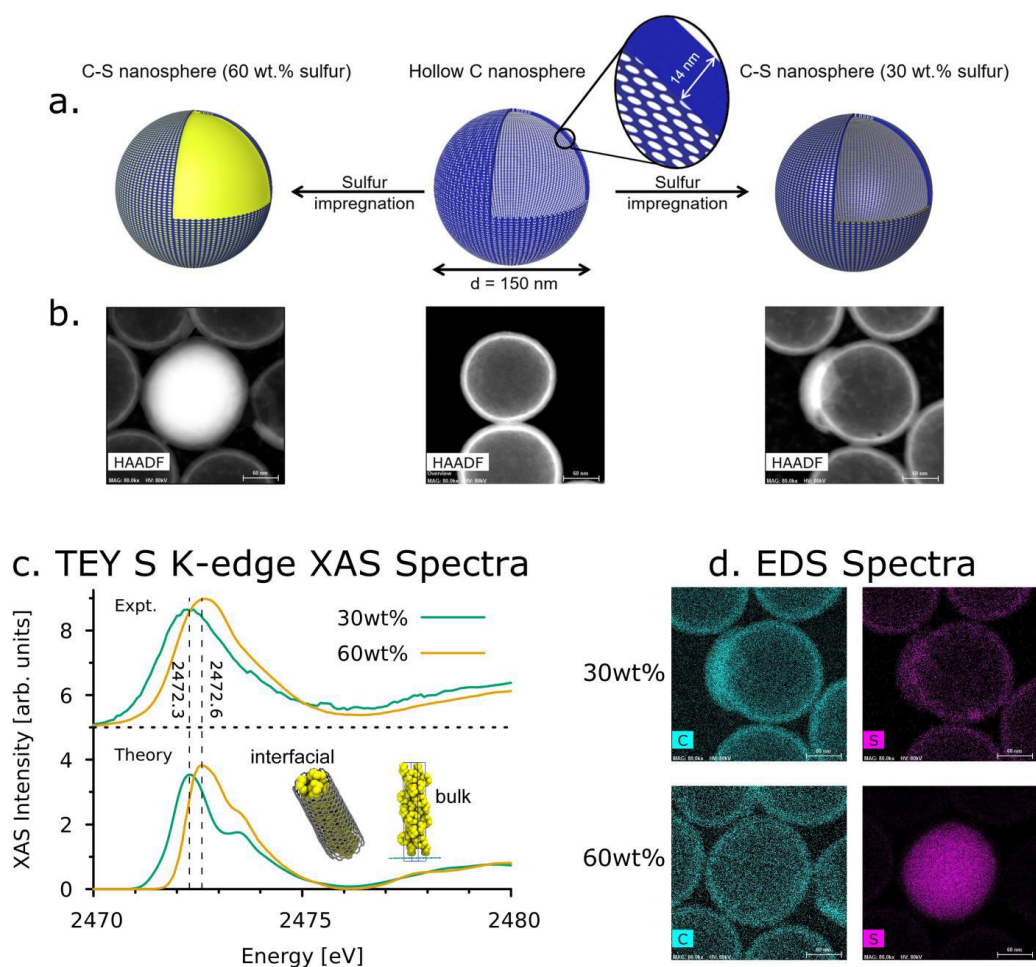


**Figure 94. Structure of C-S nanospheres.** (a) Schematic of the 60 wt% (left) and 30 wt% (right) carbon nanosphere morphology. (b) Simulated high-angle dark-field images. (c) Simulated (bottom) and measured X-ray absorption spectra of 30 wt% (green) and 60 wt% (orange) loaded carbon nanoshells. Dashed vertical lines indicate the positions of peak maximum. Bottom insets: Models used when calculating the X-ray absorption spectroscopy of the 30-wt% and 60-wt% nanoshells, respectively. (d) Energy dispersive X-ray spectra of nanoshells at the carbon and sulfur edges.

## Patents/Publications/Presentations

### Publications

- Wujcik, K. H., and D. R. Wang, T. A. Pascal, D. Prendergast, and N. P. Balsara. “*In Situ* X-Ray Absorption Spectroscopy Studies of Discharge Reactions in a Thick Cathode of a Lithium Sulfur Battery.” *Journal of Electrochemical Society* 164 (2017): A18–A27. doi: 10.1149/2.1441614jes.
- Pascal, T. A., and K. H. Wujcik, D. R. Wang, N. P. Balsara, and D. Prendergast. “Thermodynamic Origins of the Solvent-Dependent Stability of Lithium Polysulfides from First Principles.” *Physical Chemistry Chemical Physics* 19 (2017): 1441–1448. doi: 10.1039/C6CP06889H.
- Wujcik, K. H., and D. R. Wang, A. Teran, E. Nasybulin, T. Pascal, D. Prendergast, and N. Balsara. “Determination of Redox Reaction Mechanisms in Lithium Sulfur Batteries.” Invited review book chapter in *Advances in Electrochemical Science and Engineering*, Wiley-VCH. Accepted 2016.
- Pascal, T. A., and I. Villaluenga, K. Wujcik, D. Devaux, X. Jiang, D. R. Wang, N. Balsara, and D. Prendergast. “Liquid Sulfur Impregnation of Microporous Carbon Accelerated by Nanoscale Interfacial Effects.” *Nano Letters*, in press, 2017.



## Task 8.3 – Novel Chemistry: Lithium Selenium and Selenium Sulfur Couple (Khalil Amine, Argonne National Laboratory)

**Project Objective.** The project objective is to develop a novel  $S_xSe_y$  cathode material for rechargeable lithium batteries with high energy density and long life, as well as low cost and high safety.

**Project Impact.** Development of a new battery chemistry is promising to support the goal of PHEV and EV applications.

**Approach.** The dissolution of lithium polysulfides in nonaqueous electrolytes has been the major contribution to the low energy efficiency and short life of Li/S batteries. In addition, the insulating characteristics of both end members during charge/discharge (S and  $Li_2S$ ) limit their rate capacity. To overcome this problem, sulfur or  $Li_2S$  are generally impregnated in a carbon conducting matrix for better electronic conductivity. However, this makes it difficult to increase the loading density of practical electrodes. It is proposed here to solve the above barriers using the following approaches: (1) partially replace sulfur with selenium and (2) nano-confine the  $S_xSe_y$  in a nanoporous conductive matrix.

**Out-Year Goals.** When this new cathode is optimized, the following result can be achieved:

- A cell with nominal voltage of 2 V and energy density of 600 Wh/kg.
- A battery capable of operating for 500 cycles with low capacity fade.

**Collaborations.** This project engages in collaboration with the following: Professor Chunsheng Wang of University of Maryland, Dr. Yang Ren and Dr. Chengjun Sun of APS at ANL, and Dr. Luis Estevez at PNNL.

### Milestones

1. Investigating the impact of fluorinated solvents for Se-S systems. (December 2016 – Complete)
2. Investigating the effect of the pore volume of carbon matrix on high loading Se-S systems. (In progress)
3. Investigating the effect of the pore size and specific surface area of carbon matrix on high loading Se-S systems. (Q2)
4. Exploration of novel electrolytes for high loading Se-S systems. (Q3)
5. Synthesis of Se-S/carbon composites with high loading such as 7 wt% and high performance. (Q4)

## Progress Report

In late fiscal year 2016, an electrolyte based on fluorinated solvents (ANL-1) was explored to improve the electrochemical performance of Se-S systems. As shown in Figure 95, the DME-based electrolyte shows multi-discharge plateaus, indicating formation of highly soluble polysulfides/polyselenides species; only one long discharge plateau related to solid-state lithiation/de-lithiation process was observed in the ANL-1 based electrolytes. The solubility test showed that the polysulfides (for example,  $\text{Li}_2\text{S}_6$ ) can be dissolved well in the DME solvent, while no dissolution takes place in the ANL-1 solvent. This result further confirms that there is no soluble polysulfides/polyselenides dissolution in the ANL-1 solvent.

Since the dissolution issue seems to be mitigated using a novel ANL-1 electrolyte, future efforts will focus on the cathode part. Most reported Se and Se-S loadings in the electrodes are less than 50 wt%, which does not take full advantage of the high electronic conductivity of selenium, making them less competitive with the long-term developed Li/S battery. Moving to Se and Se-S systems with high loading is crucial, but present many challenges. With respect to the high loading ratio, the pore volume of the conductive host materials may play an important role. Figure 96a shows the estimated pore volume needed for different sulfur or selenium loading when considering the volume changes from S (Se) to  $\text{Li}_2\text{S}$  ( $\text{Li}_2\text{Se}$ ). High pore volume is necessary for high loading Se-S systems. A new batch of porous carbon material (denoted as PC-1) was recently developed, which has a specific surface area of  $1446 \text{ m}^2/\text{g}$  and a main pore size of 39 nm, with an ultra-high pore volume of  $6 \text{ cc/g}$ . A Se/PC-1 composite with 90 wt% Se loading was then synthesized using melt-diffusion strategy. However, its XRD pattern shows a lot of crystalline Se formation in the composite (Figure 96c), which could affect in a negative way the battery performance. This means that high pore volume cannot guarantee high electrochemical performance for high loading of Se-S. Future study will focus on the synthesis of porous carbon with a pore size of 2-10 nm and a high pore volume of over  $3 \text{ cc/g}$  to enable high loading of selenium-sulfur.

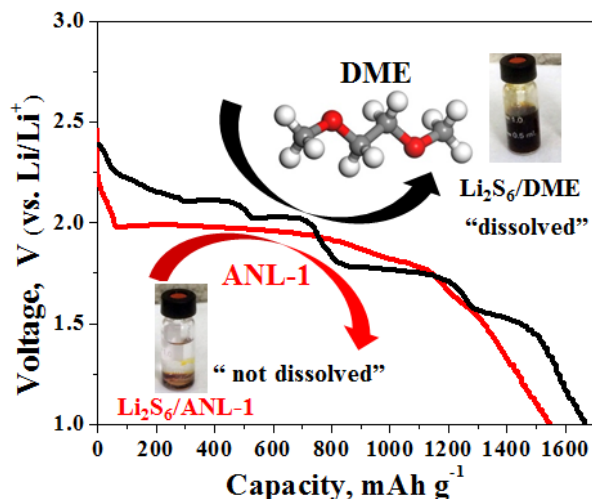


Figure 95. Schematic for the voltage profile and polysulfides solubility test of Li/Se-S cell in two different electrolytes.

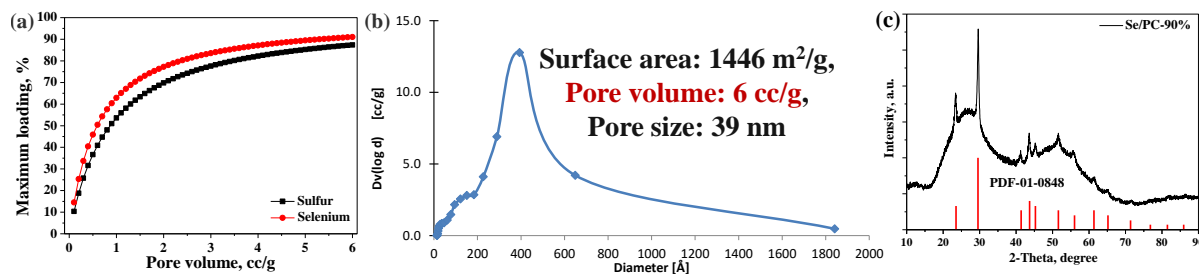


Figure 96. (a) Estimated maximum sulfur and selenium loading versus pore volume of carbon materials. (b) Pore size distribution of a newly developed carbon material for high-loading Se-S system. (c) X-ray diffraction pattern showing crystalline selenium formation in the composite.

## Patents/Publications/Presentations

### Publication

- Xu, Gui-Liang, and Jianzhao Liu, Zonghai Chen, and Khalil Amine. “Selenium and Selenium-Sulfur Chemistry for Rechargeable Lithium Batteries: Interplay of Cathode Structures, Electrolytes, and Interfaces.” Submitted to *ACS Energy Letters*, 2016, under revision.

## Task 8.4 – Multi-Functional Cathode Additives for Lithium–Sulfur Battery Technology (Hong Gan, Brookhaven National Laboratory; and Co-PI Esther Takeuchi, Brookhaven National Laboratory and Stony Brook University)

**Project Objective.** Develop a low-cost battery technology for PEV application utilizing Li-S electrochemical system by incorporating multi-functional cathode additives (MFCA), consistent with the long-term goals of the DOE EV Everywhere Grand Challenge.

**Project Impact.** The Li-S battery system has gained significant interest due to its low material cost potential (35% cathode cost reduction over Li-ion) and its attractive 2.8x (volumetric) to 6.4x (gravimetric) higher theoretical energy density compared to conventional Li-ion benchmark systems. Commercialization of this technology requires overcoming several technical challenges. This effort will focus on improving cathode energy density, power capability, and cycling stability by introducing MFCA. The primary deliverable is to identify and characterize the best MFCA for Li-S cell technology development.

**Approach.** TM sulfides are evaluated as cathode additives in sulfur cathode due to their high electronic conductivity. Electrochemically active additives are also selected for this investigation to further improve energy density of the sulfur cell system. In the first year, the project established individual baseline sulfur and TM sulfide coin cell performances, and demonstrated strong interactions between sulfur and various MFCA within the hybrid electrode. During the second year, the project identified  $\text{TiS}_2$  as the best MFCA candidate and demonstrated the particle size/BET surface area effect on Li-S cell electrochemical performance. In addition, sulfur electrode binder and carbon additives were optimized to achieve high sulfur loading up to  $10 \text{ mg/cm}^2$  with good mechanical integrity. This year, the project targets to achieve optimized Li-S cell electrochemical performance by incorporating  $\text{TiS}_2$  additive into the cathode formulation with new binder and new carbon additive. Electrode preparation process conditions and cell design factors will also be examined. The cell activation and cycling conditions will be defined, and 4 mAh sample cells will be built for DOE evaluation.

**Out-Year Goals.** This is a multi-year project comprised of two major phases to be completed in three years. Phase 1 was successfully completed during year 2, with selection of  $\text{TiS}_2$  as the leading MFCA. Entering Phase 2, the project has completed binder and carbon selection. In the third year, tasks include cathode formulation optimization, process optimization, cell design optimization, cell activation, and testing optimization. At the end, the project will build 4 mAh sample cells for DOE testing. The mechanistic studies of MFCA and sulfur interaction will continue throughout the year to advance fundamental understanding of the system.

**Collaborations.** This project collaborates with Dong Su, Xiao Tong, and Yu-chen Karen Chen-Wiegart at BNL and with Amy Marschilok and Kenneth Takeuchi at Stony Brook University.

### Milestones

1. Cathode formulation and process optimization with  $\text{TiS}_2$ . (Q1 – Complete)
2. Cathode loading/density effect and power optimization. (Q2 – In progress)
3. Cell design and cell activation procedure development. (Q3 – On Schedule)
4. 4 mAh cell samples preparation and confirmation study. (Q4 – On schedule)

## Progress Report

Last year, new binders and new carbon additives were identified that allowed the project to achieve good electrode mechanical integrity and obtain electrode with sulfur loading up to 10 mg/cm<sup>2</sup>. In these studies, metal sulfide was not part of the formulation. This quarter, TiS<sub>2</sub> is introduced to the formulation study.

**Sulfur Electrode with TiS<sub>2</sub> Formulation.** The cathode formulation optimization was executed using the previously identified binders and carbons, in combination with TiS<sub>2</sub> additive. In the experimental design, either part of the carbon in the formulation is replaced by TiS<sub>2</sub> (Table 2; see Groups 1-3), or part of the S:C composite is replaced by TiS<sub>2</sub> (Table 2; see Groups 1, 4, and 5). To optimize the Li-S cell energy density, cell discharge data are compared at component level and at the electrode level. Figure 97 shows the sulfur utilization of first discharge for all 5 group’s cells under C/20 discharge rate. Except Group 3 cells, the presence of TiS<sub>2</sub> significantly improves the sulfur electrode discharge efficiency from ~41% (Group 1) to up to ~65% (Groups 4 and 5), consistent with the project’s previous observation. Considering the variation in sulfur content in each cathode formulation, cell discharge capacities at various C-rates are normalized against total electrode weight, as shown in Figure 98. Although Group 5 formulation may still exhibit slightly higher sulfur utilization, at a practical level, Group 4 formulation results in high energy density at the total cathode level. Therefore, Group 4 formulation is selected for additional process optimization.

**Table 2. Formulation design.**

Group	Cathode Formulation (wt%)			
	Sulfur	Carbon	TiS <sub>2</sub>	Binder
1	62.0	30.0	0.0	8.0
2	62.0	25.4	4.6	8.0
3	62.0	20.7	9.3	8.0
4	56.0	27.0	9.0	8.0
5	50.0	24.2	17.8	8.0

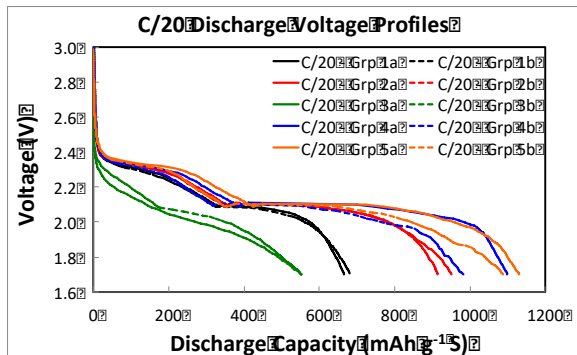


Figure 97. TiS<sub>2</sub> effect on sulfur utilization.

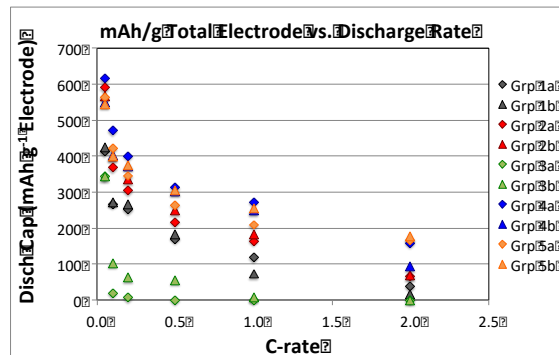


Figure 98. Energy density at electrode level.

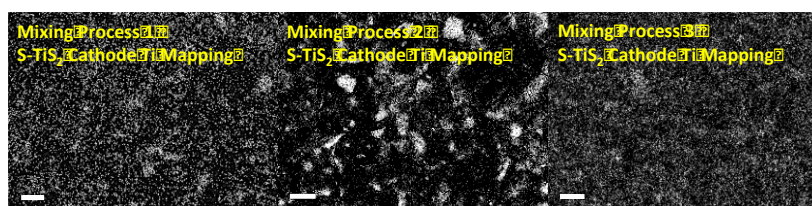


Figure 99. Slurry mixing process methods versus  $\text{TiS}_2$  distribution (energy dispersive spectroscopy) within coated cathode.

**Slurry Preparation Process Evaluation.** The cathode slurry process is found to be critical to achieve uniform  $\text{TiS}_2$  particles distribution and high sulfur loading. Using Group 4 formulation (Table 2), three slurry-mixing processes were evaluated. Mixing Process 1 results in uniform  $\text{TiS}_2$  distribution within the coated

electrode (Figure 99), but it is difficult to obtain high sulfur loading electrode without cracking during bending test. Mixing Process 2 affords high sulfur loading electrode with no cracking, but shows no uniform  $\text{TiS}_2$  distribution (Figure 99). Mixing Process 3 yields uniform  $\text{TiS}_2$  distribution (Figure 99) and achieves high sulfur loading electrode with good mechanical integrity. Tape test also exhibited more material weight loss for electrodes from Process 1 than that from Processes 2 and 3. Based on consideration of achieving uniform  $\text{TiS}_2$  distribution, ability to coat the electrode with high sulfur loading ( $> 6 \text{ mg/cm}^2$ ), and good mechanical integrity, Mixing Process 3 is chosen for further optimization.

## Patents/Publications/Presentations

### Patent

- Gan, Hong, and Ke Sun. “Electrochemically Active Interlayers for Lithium Ion Batteries.” Provisional patent application, S.N. 62/413,583, filed October 27, 2016.

### Publication

- Sun, Ke, and Hellen Liu, and Hong Gan. “Cathode Loading Effect on Sulfur Utilization in Lithium-Sulfur Battery.” *J. Electrochem. En. Conv. Stor.* 13, no. 2 (October 4, 2016): 021002.

### Presentations

- University of New Hampshire, Durham, New Hampshire (October 28, 2016): “Multi-Functional Cathode Additives for Li-S Battery Technology”; Hong Gan. Invited.
- 5th Annual Early Career Researcher Symposium (ECRS), BNL, Long Island, New York (December 13, 2016): “*In Operando* Multi-Modal Synchrotron Investigation for Structural and Chemical Evolution of  $\text{CuS}$  Additive in Li-S Battery”; Chonghang Zhao (with Ke Sun, Garth Williams, Jianming Bai, Eric Dooryhee, Juergen Thieme, Yu-chen Karen Chen-Wiegart, and Hong Gan).

## Task 8.5 – Development of High-Energy Lithium–Sulfur Batteries (Jun Liu and Dongping Lu, Pacific Northwest National Laboratory)

**Project Objective.** The project objective is to develop high-energy, low-cost Li-S batteries with long lifespan. All proposed work will employ thick sulfur cathode ( $\geq 2$  mAh/cm<sup>2</sup> of sulfur) at a relevant scale for practical applications. The diffusion process of soluble polysulfide out of thick cathode will be revisited to investigate cell failure mechanism at different cycling. Alternative anode will be explored to address the lithium anode issue. The fundamental reaction mechanism of polysulfide under the electrical field will be explored by applying advanced characterization techniques to accelerate development of Li-S battery technology.

**Project Impact.** The theoretical specific energy of Li-S batteries is ~2300 Wh/kg, which is almost three times higher than that of state-of-the-art Li-ion batteries. The major challenge for Li-S batteries is polysulfide shuttle reactions, which initiate a series of chain reactions that significantly shorten battery life. The proposed work will design novel approaches to enable Li-S battery technology and accelerate market acceptance of long-range EVs required by the EV Everywhere Grand Challenge.

**Out-Year Goals.** This project has the following out-year goals:

- Fabricate Li-S pouch cells with thick electrodes to understand sulfur chemistry/electrochemistry in the environments similar to the real application.
- Leverage the Li-metal protection project funded by the DOE and PNNL advanced characterization facilities to accelerate development of Li-S battery technology.
- Develop Li-S batteries with a specific energy of 400 Wh/kg at cell level, 1000 deep-discharge cycles, improved abuse tolerance, and less than 20% capacity fade over a 10-year period to accelerate commercialization of electrical vehicles.

**Collaborations.** This project engages in collaboration with the following:

- Dr. Xiao-Qing Yang (LBNL) – *In situ* characterization
- Dr. Deyang Qu (University of Wisconsin – Milwaukee) – Electrolyte Analysis
- Dr. Xingcheng Xiao (GM) – Materials testing
- Dr. Jim De Yoreo (PNNL) – *In situ* characterization

### Milestones

1. Study thick sulfur electrode ( $\geq 4$  mg/cm<sup>2</sup>) with controlled porosity/thickness; demonstrate 80% capacity retention for 200 cycles. (Q1 – Complete)
2. Investigate electrolyte and additive degradation mechanism with thick sulfur electrode. (Q2 – In progress)
3. Identify approaches to minimize quick capacity drop and efficiency fluctuation occurring in thick sulfur electrode during initial cycles. (Q3 – In progress)
4. Complete pouch cell assembly and testing by using optimized high energy cathode and electrolyte/additives. (Q4 – In progress)

## Progress Report

New approaches for the preparation of high-loading sulfur cathodes were reported last year. Dense and high-loading sulfur electrodes required for high-energy-density Li-S battery system have been prepared, but they still suffer from low sulfur utilization rate and limited cycle life. This quarter, effects of electrode porosity on the electrode energy density, cell cycling stability, lithium anode interface, and electrolyte/sulfur ratio were investigated using high-loading sulfur electrodes.

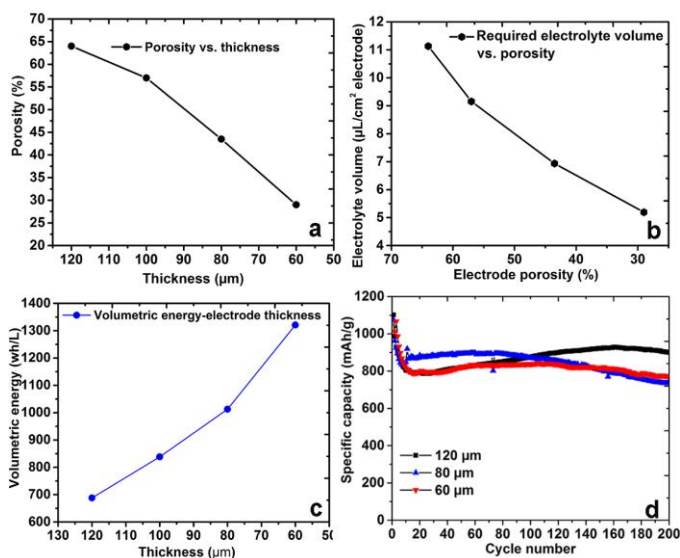


**Figure 100.** (a) Dependence of electrode porosity on thickness. (b) Calculated electrolyte amount for electrodes with different porosities. (c) Dependence of volumetric energy density on electrode thickness. (d) Cycling stability of electrodes at different thicknesses.

Thick sulfur electrodes with mass loading of  $4 \text{ mg cm}^{-2}$  were prepared by slurry coating method and calendered at different pressure to reach different thickness and porosity. The electrode porosity shows strong dependence on calendering pressure because of low tap densities of the electrode components such as sulfur and carbon. Increasing calendering-pressure from 0.2 to 1.5 ton (T) leads to quick decrease of electrode porosity from original ca. 64% to ca. 29% (Figure 100a). A direct benefit of reducing electrode porosity is the significant improvement of electrode volumetric energy density, which is one of the most important parameters for practical applications. Figure 100c shows dependence of electrode volumetric energy densities on thicknesses. The measured electrode volumetric energy density is only  $650 \text{ Wh L}^{-1}$  for as-cast electrode (120- $\mu\text{m}$  thick). For electrode compressed to 60  $\mu\text{m}$ , the corresponding energy density was improved significantly to  $1300 \text{ Wh L}^{-1}$ . These results suggest that proper control of electrode porosity/thickness is essential for high-energy Li-S batteries. The other significant benefit of controlling electrode porosity is reduction of electrolyte amount needed for full electrode wetting. For thick and porous electrode, extra volume of electrolyte is required for full electrode wetting, which enables high sulfur utilization rate but in turn greatly sacrifices system gravimetric energy density. Figure 100b shows the relationship of electrode porosity and calculated electrolyte amount, assuming that all the pores of both electrode and separator are filled with electrolyte. More than 11  $\mu\text{L}$  electrolyte is required for pristine electrode, while only 4.7  $\mu\text{L}$  is needed for the 60- $\mu\text{m}$  compressed electrode. Figure 100d compares electrode cycling stability at different thicknesses using 0.15M  $\text{Li}_2\text{S}_6$  as electrolyte additive. The electrode without calendering (120  $\mu\text{m}$ ) shows promising cycling stability with 83% capacity retention after 200 cycles. Remarkable results are also demonstrated for the calendered electrodes (80- $\mu\text{m}$  and 60- $\mu\text{m}$  thick), as shown in Figure 100d. Detailed morphology study on both sulfur cathode and lithium anode indicates that synergistic effects of the dense sulfur cathode, enhanced electrolyte penetration, and suppressed lithium anode corrosion contribute to the improved performance of Li-S battery.



## Patents/Publications/Presentations

### Patent

- Lu, D., and Q. Li, J. Liu, J. Xiao, J. Zhang, J. Liu, and G. Graff. Additives to Enhance Electrode Wetting and Performance and Methods of Making Electrodes Comprising the Same. Patent application: #30459-E CIP.

### Publication

- Lu, D., and Q. Li, J. Liu, J. Zheng, Y. Wang, S. Ferrara, S. Chen, J. Xiao, J. Zhang, and J. Liu. “Enabling High Capacity and High Energy Density Cathode for Lithium-Sulfur Batteries.” Submitted for publication.

## Task 8.6 – Nanostructured Design of Sulfur Cathodes for High-Energy Lithium–Sulfur Batteries (Yi Cui, Stanford University)

**Project Objective.** The charge capacity limitations of conventional TM oxide cathodes are overcome by designing optimized nano-architected sulfur cathodes.

This study aims to enable sulfur cathodes with high capacity and long cycle life by developing sulfur cathodes from the perspective of nanostructured materials design, which will be used to combine with Li-metal anodes to generate high-energy Li-S batteries. Novel sulfur nanostructures as well as multifunctional coatings will be designed and fabricated to overcome issues related to volume expansion, polysulfide dissolution, and the insulating nature of sulfur.

**Project Impact.** The capacity and the cycling stability of sulfur cathode will be dramatically increased. This project's success will make Li-S batteries to power EVs and decrease the high cost of batteries.

**Out-Year Goals.** The cycle life, capacity retention, and capacity loading of sulfur cathodes will be greatly improved (200 cycles with 80% capacity retention,  $> 0.3 \text{ mAh/cm}^2$  capacity loading) by optimizing material design, synthesis, and electrode assembly.

**Collaborations.** This project engages in collaboration with the following:

- BMR PIs
- SLAC: *In situ* X-ray, Dr. Michael Toney
- Stanford: Professor Nix, mechanics; Professor Bao, materials

### Milestones

1. Investigate Li-ion diffusion mechanism in different types of metal sulfides. (October 2016 – Complete)
2. Identify initial activation energy barrier of  $\text{Li}_2\text{S}$  on various metal sulfides. (December 2016 – Complete)

## Progress Report

To understand the role of metal sulfides in catalytic decomposition of  $\text{Li}_2\text{S}$ , the project systematically investigated the effect of six kinds of metal sulfides including  $\text{VS}_2$ ,  $\text{CoS}_2$ ,  $\text{TiS}_2$ ,  $\text{FeS}$ ,  $\text{SnS}_2$ , and  $\text{Ni}_3\text{S}_2$  on tuning the decomposition energy barrier. According to simulation of electronic band structures (Figure 101),  $\text{Ni}_3\text{S}_2$ ,  $\text{FeS}$ , and  $\text{CoS}_2$  are metallic materials, while  $\text{VS}_2$  and  $\text{TiS}_2$  are semi-metallic; this means they are all materials with good electrical conductivities, while  $\text{SnS}_2$  is a semiconductor with a band gap of 2.2 eV. Carbon material (a graphene/carbon nanotube hybrid (G/CNT)) was chosen for comparison. The cathode consists of a commercial  $\text{Li}_2\text{S}$  cathode material mixed uniformly with various metal sulfides, carbon black, and polyvinylidene fluoride (PVDF) binder. Coin cells were assembled with lithium metal as anode and reference electrode. The initial charge voltage profiles were used to clearly show the activation barrier (Figure 102a). The G/CNT- $\text{Li}_2\text{S}$  cathode without the addition of metal sulfide exhibits a high potential barrier at about 3.41 V in the initial charging process, indicating a sluggish activation process with high charge-transfer resistance. The  $\text{SnS}_2$ - $\text{Li}_2\text{S}$  cathode shows a clear voltage jump with a potential barrier of 3.53 V during the activation process due to the semiconducting nature of  $\text{SnS}_2$ . The charge voltage plateaus after the short voltage jump represent the phase conversion reaction from  $\text{Li}_2\text{S}$  to low-order LiPSs, high-order LiPSs, and sulfur. A similar charging phenomenon is observed for  $\text{Ni}_3\text{S}_2$ - $\text{Li}_2\text{S}$  and  $\text{FeS}$ - $\text{Li}_2\text{S}$  electrodes with high potential barriers of 3.47 and 3.25 V, even though both are metallic. However, addition of  $\text{CoS}_2$ ,  $\text{VS}_2$ , and  $\text{TiS}_2$  significantly reduces the height of the potential barrier to 3.01, 2.91 and 2.88 V, respectively (Figure 102a). The lower potential barrier and longer voltage plateau of the  $\text{CoS}_2$ ,  $\text{VS}_2$ , and  $\text{TiS}_2$  based electrodes compared to other metal sulfides indicate improved conductivity and reduced charge-transfer resistance.

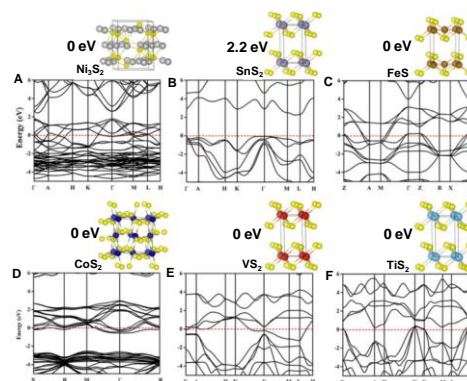


**Figure 101.** Crystal structures and calculated band structures for bulk phases of (a)  $\text{Ni}_3\text{S}_2$ , (b)  $\text{SnS}_2$ , (c)  $\text{FeS}$ , (d)  $\text{CoS}_2$ , (e)  $\text{VS}_2$ , and (f)  $\text{TiS}_2$ . The red dashed lines mark the Fermi energy level.

To attain an in-depth understanding of the function of these metal sulfides, the group used the climbing-image nudged elastic band (CI-NEB) method to calculate the barrier for  $\text{Li}_2\text{S}$  decomposition to evaluate the delithiation

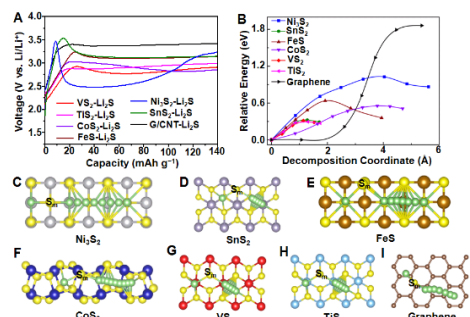


**Figure 102.** (a) First-cycle charge voltage profiles of  $\text{Ni}_3\text{S}_2$ - $\text{Li}_2\text{S}$ ,  $\text{SnS}_2$ - $\text{Li}_2\text{S}$ ,  $\text{FeS}$ - $\text{Li}_2\text{S}$ ,  $\text{CoS}_2$ - $\text{Li}_2\text{S}$ ,  $\text{VS}_2$ - $\text{Li}_2\text{S}$ ,  $\text{TiS}_2$ - $\text{Li}_2\text{S}$ , and G/CNT- $\text{Li}_2\text{S}$  electrodes. (b) Energy profiles for the decomposition of  $\text{Li}_2\text{S}$  cluster on  $\text{Ni}_3\text{S}_2$ ,  $\text{SnS}_2$ ,  $\text{FeS}$ ,  $\text{CoS}_2$ ,  $\text{VS}_2$ ,  $\text{TiS}_2$ , and graphene. Top view schematic representations of the corresponding decomposition pathways for (c)  $\text{Ni}_3\text{S}_2$ , (d)  $\text{SnS}_2$ , (e)  $\text{FeS}$ , (f)  $\text{CoS}_2$ , (g)  $\text{VS}_2$ , (h)  $\text{TiS}_2$  and (i) graphene. Here, green, yellow, grey, purple, brown, blue, red, cyan, and beige balls symbolize lithium, sulfur, nickel, tin, iron, cobalt, vanadium, titanium, and carbon atoms, respectively.  $\text{S}_m$  represents the sulfur atom in the  $\text{Li}_2\text{S}$  cluster.

reaction kinetics on the surface of different metal sulfides. Here, the group considered the decomposition process from an intact  $\text{Li}_2\text{S}$  molecule into a  $\text{LiS}$  cluster and a single lithium ion ( $\text{Li}_2\text{S} \rightarrow \text{LiS} + \text{Li}^+ + \text{e}^-$ ). The main evolution is composed of the lithium ion moving far away from the sulfur atom in the  $\text{Li}_2\text{S}$  molecule, which is accompanied by breaking of the Li-S bond. The energy profiles for the decomposition processes on different sulfides are shown in Figure 200b. The  $\text{Ni}_3\text{S}_2$  decomposition barrier is as high as 1.03 eV, much larger than the other five cases, and is consistent with the large initial voltage barrier for  $\text{Ni}_3\text{S}_2$  added  $\text{Li}_2\text{S}$  cathode. The barriers for  $\text{FeS}$ ,  $\text{CoS}_2$ ,  $\text{VS}_2$ , and  $\text{TiS}_2$  are 0.63, 0.56, 0.31, and 0.30 eV, respectively, and qualitatively agree with the voltage magnitudes measured experimentally. For  $\text{SnS}_2$ , the calculated barrier for decomposition is as low as 0.32 eV, but experimentally exhibits a very large initial charge potential. This can be probably attributed to the insulating nature of  $\text{SnS}_2$  and the electron-ion recombination process, which is the rate-determining step for the delithiation process, but not the lithium decomposition process. Figure 200c-h illustrates the decomposition pathway for one lithium ion departing from the  $\text{LiS}$  cluster on the surface of six kinds of sulfides. It can be clearly seen that the decomposition

process is associated with the binding between the isolated lithium ion and the sulfur in sulfides. This is the dominant reason that the sulfide anchor can induce a lower decomposition barrier compared with carbon materials. For graphene, the chemical interaction between the lithium ion and carbon is much weaker, and therefore, the decomposition process should have a very large activation energy barrier (Figure 200i; 1.81 eV according to simulation).

## Task 8.7 – Addressing Internal “Shuttle” Effect: Electrolyte Design and Cathode Morphology Evolution in Lithium-Sulfur Batteries (Perla Balbuena, Texas A&M University)

**Project Objective.** The project objective is to overcome the Li-metal anode deterioration issues through advanced Li-anode protection/stabilization strategies including (1) *in situ* chemical formation of a protective passivation layer and (2) alleviation of the “aggressiveness” of the environment at the anode by minimizing the polysulfide shuttle with advanced cathode structure design.

**Project Impact.** Through formulation of alternative electrolyte chemistries as well as design, fabrication, and test of improved cathode architectures, it is expected that this project will deliver Li/S cells operating for 500 cycles at efficiency greater than 80%.

**Approach.** A mesoscale model including different realizations of electrode mesoporous structures generated based on a stochastic reconstruction method will allow virtual screening of the cathode microstructural features and the corresponding effects on electronic/ionic conductivity and morphological evolution. Interfacial reactions at the anode due to the presence of polysulfide species will be characterized with *ab initio* methods. For the cathode interfacial reactions, data and detailed structural and energetic information obtained from atomistic-level studies will be used in a mesoscopic-level analysis. A novel sonochemical fabrication method is expected to generate controlled cathode mesoporous structures that will be tested along with new electrolyte formulations based on the knowledge gained from the mesoscale and atomistic modeling efforts.

**Out-Year Goals.** By determining reasons for successes or failures of specific electrolyte chemistries, and assessing relative effects of composite cathode microstructure and internal shuttle chemistry versus that of electrolyte chemistry on cell performance, expected results are : (1) develop an improved understanding of the Li/S chemistry and ways to control it; (2) develop electrolyte formulations able to stabilize the lithium anode; (3) develop new composite cathode microstructures with enhanced cathode performance; and (4) develop a Li/S cell operating for 500 cycles at an efficiency greater than 80%.

**Collaborations.** This is a collaborative work combining first-principles modeling (Perla Balbuena, TAMU), mesoscopic level modeling (Partha Mukherjee, TAMU), and synthesis, fabrication, and test of Li/S materials and cells (Vilas Pol, Purdue University).

### Milestones

1. Complete electrochemical modeling of cell performance with electrolyte and cathode properties. (Q1 – Complete)
2. Complete development of stable electrolytes. (In progress)
3. Produce 3-5 grams of C/S composite material.
4. Complete the scale-up of cathode composites, cell construction, and testing.

## Progress Report

**Characterization of SEI Nucleation and Growth at the PS/Lithium Interface.** The project showed that AIMD study of the reactions at the surface of lithium metal demonstrated the effects of concentrated electrolyte solutions on the first coordination shell of the lithium ion, where a mixed shell composed of salt anion, PS anion, and solvent is present. The importance of these differences in comparison to the low salt concentration is that as the lithium ion travels near to the surface, electron transfer reduces first the PS anion and salt anion and then the solvent. Thus, the work of desolvation needed for lithium plating depends strongly on the composition of the first shell and also on the degree of reduction. Thus, for concentrated solutions the work for desolvation will be lower than in diluted solutions because the salt anion decomposes first. Moreover, the simultaneous reduction of the lithium ion and decomposition of the salt and PS anions modify the type of precursors for dendrite formation.

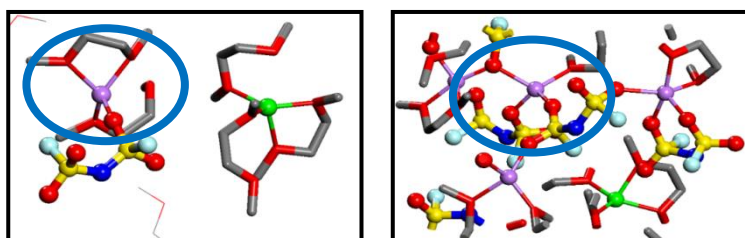


Figure 103. First coordination shell of a lithium ion (purple) surrounded by DME molecules (left) at 1M LiFSI concentration, and solvated by salt anions and DME molecules at 4M LiFSI concentration (right). Camacho Forero, Smith, Balbuena, *JPCC*, 2017. O (red), C (grey), S (yellow), N (blue).

In presence of PS species, the reactions become much more complex. In collaboration with M. Vijayakumar at PNNL, DFT and AIMD simulations were used to explain XPS results and identify SEI products at the lithium anode surface due to PS shuttle effects. The main findings include (1) confirmation of the earlier prediction of  $\text{Li}_2\text{S}$  deposition at the Li-metal surface, and (2) identification of an intermediate  $\text{LiS}_5$  species as a reduction product at the anode surface. Such product explains the ratio of S neutral to S monoanion of 4 and the increase of  $\text{Li}_2\text{S}$  concentration observed in the *in situ* XPS results. In addition, a variety of products of the decomposition of the TFSI anion predicted by AIMD simulations was found in the observed XPS peaks. The complexity of the SEI layer in this model experiment was further elucidated. Moreover, it was demonstrated that this type of combined experimental-theoretical study could be extremely useful for elucidating behavior of complex battery materials. A manuscript has been submitted for publication.

**Charge Transport in Solid Discharge Products.** Based on the results from atomistic/molecular simulations, a mesoscopic electrochemical model was extended to evaluate the full cell performance considering mass transport and physicochemical interplays in the anode.

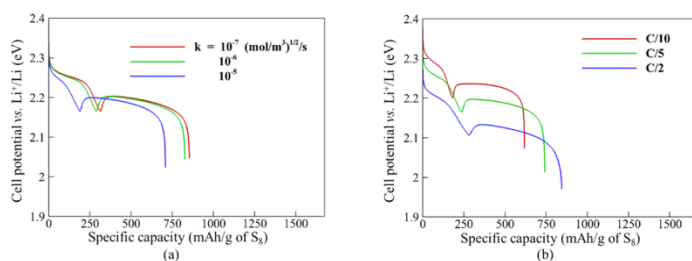


Figure 104. Cell performance is affected by chemical reactions in the anode side: (a) effect of chemical reaction kinetics; and (b) effect of discharge rate.

Figure 104a reports the cell performance at C/5 rate, at various rate constants for the PS reduction at the anode. The model involves co-precipitation of  $\text{Li}_2\text{S}_2$ , thus capacity is limited to  $\sim 800$  mAh/g of S. Increasing the rate constant, more sulfur is consumed and limits cell capacity. The V decreases due to less active material undergoing electrochemical reduction, which results in concentration overpotential. Figure 104b shows the discharge rate on cell performance. The higher C rate mitigates the capacity loss caused by PS reduction at the anode. The terminal V on Figure 104b is related to C-rate of operation and hence decreases as C-rate is increased.

Although the chemical reaction rate does not depend on current, the amount of electrochemical reactions scales linearly with operating current density. Thence, at lower C-rates, a larger fraction of dissolved PS undergoes chemical reduction instead of electrochemical one. At high C-rate, PSs are consumed very fast in the cathode side, which leads to fewer PSs transferred to the anode side. The terminal V on Figure 104b is related to C-rate of operation and hence decreases as C-rate is increased.

## Patents/Publications/Presentations

### Publications

- Camacho-Forero, Luis E., and Taylor W. Smith, and Perla B. Balbuena. “Effects of High and Low Salt Concentration in Electrolytes at Lithium-Metal Anode Surfaces.” *J. Phys. Chem. C* 121, no. 1 (2017): 182–194.
- Liu, Zhixiao, and Perla B. Balbuena, and Partha P. Mukherjee. “Revealing Charge Transport Mechanisms in  $\text{Li}_2\text{S}_2$  for Li-Sulfur Batteries.” *J. Phys. Chem. Lett.*, under review.
- Liu, Zhixiao, and Partha P. Mukherjee. “Mesoscale Elucidation of Surface Passivation in the Li-Sulfur Battery Cathode.” *ACS Applied Materials & Interfaces*, under review.
- Nandasiri, M. J., and L. E. Camacho-Forero, A. M. Schwarz, V. Sutthanandan, S. Thevuthasan, P. B. Balbuena, K. T. Mueller, and M. Vijayakumar. “*In Situ* Chemical Imaging of SEI Layer Evolution in Li-S Batteries Using X-ray Photoelectron Spectroscopy.” Submitted.

## Task 8.8 – Investigation of Sulfur Reaction Mechanisms (Deyang Qu, University of Wisconsin Milwaukee; Xiao-Qing Yang, Brookhaven National Laboratory)

**Project Objective.** With the advantages of the unique analytical assay developed in 2016, the primary objectives are to further conduct focused fundamental research on the mechanism for Li-S batteries, investigate the kinetics for the sulfur redox reaction, develop electrolytes and additives suitable for Li-S chemistry, and optimize the sulfur electrode and cell designs. In these objectives, special attention will be paid to the investigation of the redox reaction of sulfur cathode, the management for the solubility of polysulfide ions, the formation of SEI layer and dead lithium on the surface of lithium anode, the rechargeability of lithium anode in the solution containing polysulfide, and the exploration of electrode and cell designs. Through such investigations, the Li-S chemistry will be studied systematically, and the scientific understanding of the reaction mechanism can be well utilized to guide the system engineering design.

**Project Impact.** The unique *in situ* electrochemical high-performance liquid chromatography (HPLC)/MS technique will identify the soluble polysulfides real-time during the charge/discharge of a Li-S battery; thus, the mechanism can be revealed in detail. The results of the project will guide development of sulfur cathode and Li-S designs.

**Approach.** This project will use *in situ* electrochemical-MS, electrochemical-HPLC/MS, XPS, SEM, and XRD to study electrochemical reactions associated with sulfur electrodes. Electrochemical techniques such as AC impedance, rotation ring disk electrode, and galvanostat will be used to study the electrode process kinetics. The project is developing an *in situ* electrochemical optical method to investigate the surface of lithium anode during the cycling of a Li-S cell.

**Out-Year Goals.** The out-year goal is to establish tools to investigate the interaction between dissolved sulfur and polysulfide ions with lithium anode, exploring the additives which can migrate such interaction. In addition, gain further understanding of the chemical behaviors of the polysulfide in the electrolyte and propose a valid mechanism for the Li-S reaction.

**Collaborations.** The PI, Deyang Qu, is the Johnson Control Endowed Chair Professor; thus, the University of Wisconsin – Milwaukee and BNL team have close collaboration with Johnson Controls' scientists and engineers. This collaboration enables the team to validate the outcomes of fundamental research in pilot-scale cells. This team has been closely working with top scientists on new material synthesis at ANL, LBNL, and PNNL, with U.S. industrial collaborators at GM, Duracell, and Johnson Control as well as international collaborators in Japan and South Korea. These collaborations will be strengthened and expanded to give this project a vision on both today's state-of-the-art technology and tomorrow's technology in development, with feedback from the material designer and synthesizers upstream, as well as from industrial end users downstream.

### Milestones

1. Complete design and validation of the *in situ* electrochemical – microscopic cell for *in situ* investigation of lithium anode during cycling. (December 2016 – Complete)
2. Complete study of interaction between dissolved elemental sulfur and polysulfide ions with both the electrolytes and lithium anode. (Q2)
3. Complete investigation of chemical equilibriums among dissolved polysulfide ions during the course of discharge and recharge of Li-S batteries. (Q3)



## Progress Report

This quarter, the project continued to take advantage of the reliable HPLC-MS analytical technique developed last year for investigation of the chemical and electrochemical reactions of elemental sulfur and polysulfide ions with metallic lithium anode in the Li-S battery electrolytes. The stability of the SEI on the lithium electrode in Li-S batteries was studied using a newly designed *in situ* electrochemical optical cell.

Due to the nonpolar nature of elemental sulfur ( $S_8$ ), the solubility of  $S_8$  in a nonaqueous electrolyte is relatively low compared to the solubility of polysulfide ions. For example, the saturated concentration of sulfur in dimethyl sulfoxide (DMSO) electrolyte is around 2 mM, and the concentration of polysulfide ions in a similar electrolyte can be as high as a few hundred mM. Because of the low concentration of sulfur in the electrolyte, little attention has been paid to the potential interaction between dissolved sulfur in the electrolyte and the lithium anode. Figure 105 shows an image of various sulfur-containing electrolytes after exposure to lithium. The formation of polysulfide ions is evident by the color change of many of the electrolytes.

An *in situ* air-tight cell was designed as shown in Figure 106. The cell can be assembled in an argon-filled glove-box for each observation. A Keyence VHX-2000 optical microscope was used to observe the dendrite formation on the lithium disk in the two-electrode cell. During observation, the cell was operated under various electrochemical conditions.

The examples in Figure 106a-f show the surface images of a lithium working electrode at the various stages of charge and discharge under galvanostatic condition.

The *in situ* cell will be used to investigate the mechanism of interaction between dissolved sulfur and polysulfides with lithium anode in a Li-S cell. The surface conditions can be observed real-time.



**Figure 105.** DME-based electrolytes with elemental sulfur contacted with lithium metal at different times.

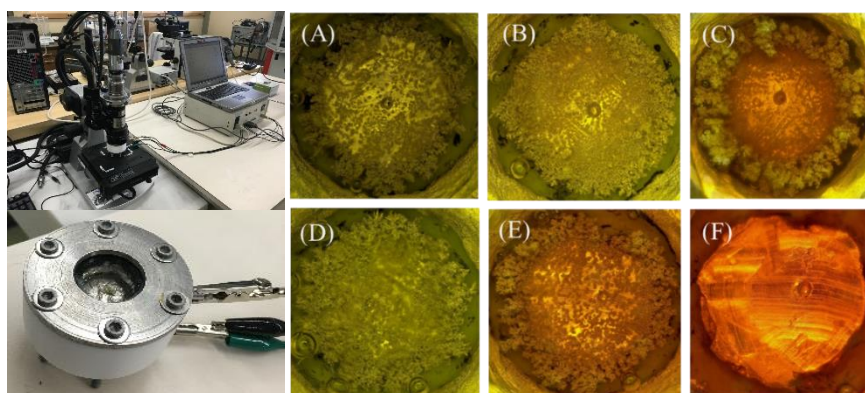
From top to bottom:

electrolytes with sulfur and without Li metal, electrolytes with sulfur and Li metal for 1 day, electrolytes with sulfur with Li metal for 2 days, electrolytes with sulfur with Li metal for 4 days, and electrolytes with sulfur with Li metal for 8 days.

From left to right:

LiTFS/DME electrolyte, LiTFSi/DME electrolyte, LiDFOB/DME electrolyte, LiBOB/DME electrolyte, LiBF<sub>4</sub>/DME electrolyte, LiPF<sub>6</sub>/DME electrolyte, LiClO<sub>4</sub>/DME electrolyte, LiTFSi/DME/DOL electrolyte.

**Figure 106.** *In situ* electrochemical optical cell (left bottom). Full set up (left top). Example photos at various stages of galvanostatic charge (a-f).



## Task 8.9 – Statically and Dynamically Stable Lithium–Sulfur Batteries (Arumugam Manthiram, University of Texas – Austin)

**Project Objective.** The project objective is to develop statically and dynamically stable Li-S batteries by integrating polysulfide-filter-coated separators with a protected Li-metal anode through additives or a modified  $\text{Li}_2\text{S}$  cathode with little or no charge barrier during first charge. The project includes demonstration of electrochemically stable cells with sulfur capacities of  $> 1,000 \text{ mA h g}^{-1}$  and cycle life in excess of 500 cycles (dynamic stability) along with positive storage properties (static stability) at  $> 70 \text{ wt\%}$  sulfur content and  $\sim 5 \text{ mg cm}^{-2}$  loading.

**Project Impact.** The combination of polysulfide-filter (PS-filter)-coated separator, Li-metal-protection additives, and  $\text{Li}_2\text{S}$  cathode modifications offers a viable approach to overcome the persistent problems of Li-S batteries. This project is systematically integrating the basic science understanding gained in its laboratory of these three aspects to develop the Li-S technology as the next-generation power source for EVs. The project targets demonstrating cells with sulfur capacities of over  $1,000 \text{ mA h g}^{-1}$  and cycle life in excess of 500 cycles along with good storage properties at high sulfur content and loading that will make the Li-S technology superior to the present-day Li-ion technology in terms of cost and cell performance.

**Approach.** Electrochemical stability of the Li-S cells is improved by three complementary approaches. (1) The first approach focuses on establishment of an electrochemically stable cathode environment by employing PS-filter-coated separators. The PS-filter coatings aim to suppress the severe polysulfide diffusion and improve the redox capability of Li-S cells with high-sulfur loadings. The study includes an understanding of materials characteristics, fabrication parameters, electrochemical properties, and battery performance of the PS-filter-coated separators. (2) The second approach focuses on electrode engineering from two aspects. First, investigation of a Li-metal anode with coating- and additive-supporting approaches is aimed at improving the safety of Li-S cells. Second, research on activated- $\text{Li}_2\text{S}$  cathode with little or no charge-barrier will promote performance and safety of the C- $\text{Li}_2\text{S}$  cells. (3) Integration of the first two approaches would create statically and dynamically stable Li-S batteries for EVs.

**Out-Year Goals.** The overall goal is to develop statically and dynamically stable Li-S batteries with custom cathode and stabilized anode active materials and establish a firm fundamental understanding. Specifically, the optimization of the electrochemical and engineering parameters of PS-filter-coated separators aims at comprehensively investigating different coating materials and their corresponding coating techniques for realizing various high-performance custom separators. The developed PS-filter-coated separators can be coupled with pure sulfur cathodes with high-sulfur loading and content. Multi-functional PS-filter-coated separators, high-loading sulfur cathodes, stabilized-Li-metal anodes, activated- $\text{Li}_2\text{S}$  cathodes, and novel cell design are anticipated to provide an in-depth understanding of the Li-S battery chemistry and to realize statically and dynamically stable Li-S batteries.

**Collaborations.** This project collaborates with ORNL.

### Milestones

1. Analyze and improve dynamic electrochemical performances of Li-S cells. (Q1 – Complete)
2. Analyze and improve static electrochemical performances of Li-S cells. (Q2 – In progress)
3. Increase the sulfur loading of the cells. (Q3 – In progress)
4. *Go/No-Go*: Fabricate cells with high sulfur content/loading and good electrochemical stability. (Q4)

## Progress Report

This quarter, the project has completed the long-term dynamic electrochemical performance improvements of Li-S batteries by employing PS-filter-coated separators in the cells. Four carbon materials with unique morphologies were selected as coating materials: spherical carbons, CNFs, CNTs, and graphene. The carbon materials were coated onto a polypropylene membrane (Celgard 2500) to form the PS-filter-coated separators. As a reference, the Celgard membrane with a thickness of 25  $\mu\text{m}$  weighs 1.0  $\text{mg cm}^{-2}$ . Pure sulfur cathodes with a sulfur loading of 4.0  $\text{mg cm}^{-2}$  and a sulfur content of 70 to 80 wt% were used in the cells. The electrochemical analysis demonstrates that the Li-S cells with the PS-filter-coated separators show great improvements in dynamic electrochemical performances and high-loading capabilities. The enhanced dynamic performances include a high electrochemical utilization of sulfur at 80%, a high areal capacity of above 4.0  $\text{mA h cm}^{-2}$ , a high sulfur loading of 4  $\text{mg cm}^{-2}$ , and a high sulfur content of 70 to 80 wt%. The cells display long-term cyclability for 500 cycles with a low capacity-fade rate (Figure 107). These results successfully complete the first milestone.

According to the team long-term cycling performances, the PS-filter-coated separators that give the best cell performance and offer great potential for building high-loading sulfur cathode systems are those with the following three coatings: (1) porous spherical carbon – single-walled carbon nanotube (SWCNT) coatings (Figure 107a), (2) layer-by-layer (LBL) CNF coatings (Figure 107b), and (3) LBL CNT coatings (Figure 107c).

The spherical carbon – SWCNT-coated separators were prepared by vacuum-filtrating the spherical carbon – SWCNT mixtures onto polypropylene membranes. All examined 8 carbon coatings were controlled with the same low mass-loading of 0.1  $\text{mg cm}^{-2}$ . The dynamic performances of the cells employing the porous spherical carbon coatings (for example, microporous carbon (MPC), Ketjen (KJ) Black, activated charcoal, and activated carbon) are better than the targeted sulfur capacities (1,000  $\text{mA h g}^{-1}$ ) and cycle life (500 cycles). The outstanding cycling performance results from the porous coating layer forming polysulfide traps and functioning as an additional current collector to reutilize/reactivate the trapped active material during long-term cell cycling.

Besides studying the effect of coating materials, nonporous CNFs and CNTs were used to study the effect of a layered-coating morphology on improving dynamic performances of the Li-S cells. The cells fabricated with the thin-film LBL CNF-coated separators display a high peak capacity of 1,329  $\text{mA h g}^{-1}$  (areal capacity: 4.3  $\text{mA h cm}^{-2}$ ) at C/10 rate and a high reversible capacity of 529  $\text{mA h g}^{-1}$  after 500 cycles. The use of light weight LBL CNT coating could further reduce coating mass to 0.04  $\text{mg cm}^{-2}$  with a thickness of 8  $\mu\text{m}$ . With the highly conductive CNT as the coating material, the cells cycle well at a higher sulfur content of 80 wt% at C/5 rate for 500 cycles.

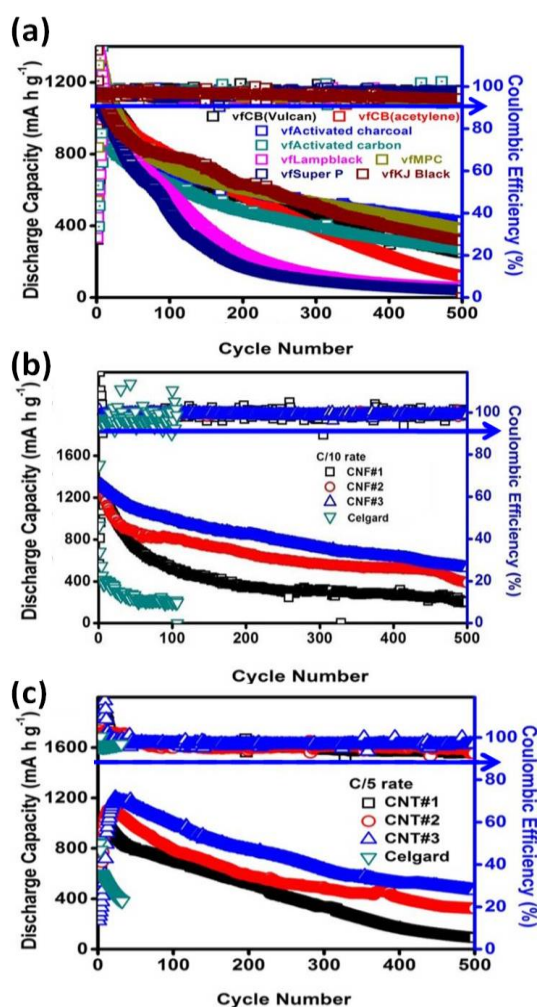


**Figure 107.** Dynamic cycling performance of the cells fabricated with (a) spherical carbon – single-walled carbon nanotube (SWCNT)-coated separators, (b) layer-by-layer (LBL) carbon nanofiber (CNF)-coated separators, and (c) LBL CNT-coated separators.

## Patents/Publications/Presentations

### Publications

- Chung, S.-H., and C.-H. Chang, and A. Manthiram. “Hierarchical Sulfur Electrodes as a Testing Platform for Understanding the High-loading Capability of Li-S Batteries.” *Journal of Power Sources* 334 (2016): 179–190.
- Luo, L., and S.-H. Chung, and A. Manthiram. “Trifunctional Multi-walled Carbon Nanotubes/Polyethylene Glycol (MWCNT/PEG) – Coated Separator through a Layer-by-Layer Coating Strategy for High-Energy Li-S Batteries.” *Journal of Materials Chemistry A*, 4 (2016): 16805–16811.
- Chung, S.-H., and C.-H. Chang, and A. Manthiram. “A Carbon-Cotton Cathode with Ultrahigh-Loading Capability for Statically and Dynamically Stable Lithium-Sulfur Batteries.” *ACS Nano*, 10 (2016): 10462–10470.
- Chang, C.-H., and S.-H. Chung, and A. Manthiram. “Highly Flexible, Freestanding Tandem Sulfur Cathodes for Foldable Li-S Batteries with High Areal Capacity.” *Materials Horizons*, in press.

### Presentations

- Lee Hsun Lecture Award on Materials Science, Institute of Metal Research, Shenyang, China, (October 19, 2016): “Next-Generation Battery Materials and Technologies for Electrical Energy Storage”; A. Manthiram. Invited.
- International Union of Materials Research Society – 17<sup>th</sup> International Conference in Asia (IUMRS-ICA 2016), Qingdao, China, (October 20-24, 2016): “Tailored Carbon Materials for Overcoming Critical Issues in Rechargeable Batteries”; A. Manthiram. Invited.
- National Synchrotron Radiation Center, Hsinchu, Taiwan (October 31, 2016): “Role of Materials Chemistry in Electrical Energy Storage”; A. Manthiram. Invited.
- Applied Science Center, Academia Sinica, Taipei, Taiwan (November 3, 2016): “Next-Generation Battery Chemistries: Materials Challenges and Prospects”; A. Manthiram. Invited.
- Distinguished Lecture at Colorado School of Mines and NREL, Golden, Colorado (November 14, 2016): “Electrical Energy Storage: Next-Generation Battery Chemistries”; A. Manthiram. Invited.
- ISAEST-11, Chennai, India (December 8-10, 2016): “Next-Generation Battery Chemistries: Challenges and Prospect”; A. Manthiram. Invited.

## Task 8.10 – Electrochemically Responsive, Self-Formed, Lithium-Ion Conductors for High-Performance Lithium-Metal Anodes (Donghai Wang, Pennsylvania State University)

**Project Objective.** The project objective is to develop and deliver an electrochemically responsive self-formed hybrid Li-ion conductor as a protective layer for Li-metal anodes, enabling Li-metal anodes to cycle with a high efficiency of ~ 99.7% at high electrode capacity ( $>6$  mAh/cm<sup>2</sup>) and high current density ( $> 2$  mA/cm<sup>2</sup>) for over 500 cycles. The project will also demonstrate prototype ~300 mAh Li-S battery cells with energy densities of ~200 Wh/kg and ~ 80% capacity retention for ~ 300 cycles at ~ 80% depth of discharge using Li-metal anodes with this protective layer.

**Project Impact.** This project aims to develop a new hybrid Li-ion conductor that enables safe and high-performance lithium metal anodes. The use of these high-performance Li-metal anodes in turn enables Li-S batteries with high energy density and long cycling life. Such anodes can also lead to a 50% increase in the energy density of conventional Li-ion batteries with lithium metal oxide cathodes. Meeting the technical targets will potentially develop a new high-energy-density lithium battery, promote increased adoption of EVs and PHEVs, and reduce petroleum consumption in the transportation sector by helping battery-powered vehicles become accepted by consumers as a reliable source of transportation.

**Approach.** The novel multiphase organo-Li<sub>x</sub>S<sub>y</sub> or organo-Li<sub>x</sub>P<sub>y</sub>S<sub>z</sub> hybrid ion conductors with tunable multifunctional organic components and controlled Li<sub>x</sub>S<sub>y</sub> and Li<sub>x</sub>P<sub>y</sub>S<sub>z</sub> inorganic components will be designed and prepared, and thus enable safe use of lithium metal with high CE. In the first year, the team will develop the organo-Li<sub>x</sub>S<sub>y</sub> lithium protection layers with tuned functionality: (1) finding appropriate composition and (2) developing appropriate synthesis and fabrication methods.

**Out-Year Goals.** Work will progress toward the development of organo-Li<sub>x</sub>S<sub>y</sub> lithium protection layers with tuned functionality. Characterization, performance, and compatibility tests on materials and systems. Twelve baseline 300 mAh pouch cells using standard Li-metal anodes and high-performance carbon-sulfur cathodes will be delivered for independent verification.

### Milestones

1. Development of the first-generation of organo-Li<sub>x</sub>S<sub>y</sub> lithium protection layers with tuned functionality. Conduct characterization and performance tests on the materials. (December 2016 – Completed)
2. Deliver 12 baseline ~ 300 mAh Li-S cells for independent verification. (Q2 – In Progress)
3. Optimize organo-Li<sub>x</sub>S<sub>y</sub> protective layer and demonstrate lithium anodes cycling with ~ 98.5% CE for ~ 200 cycles. (Q3)
4. Demonstrate lithium anodes with optimized organo-Li<sub>x</sub>S<sub>y</sub> protective layer and ~ 99% CE for ~ 200 cycles. (Q4)

## Progress Report

Dimethyl disulfide as a functional co-solvent has been demonstrated to show an alternate electrochemical reaction pathway for sulfur cathodes by the formation of dimethyl polysulfides and lithium organosulfides as intermediates and reduction products. The project's studies show that this new pathway not only provides high capacity, but also enables excellent capacity retention through a built-in automatic discharge shutoff mechanism by tuning carbon/sulfur ratio in sulfur cathodes to reduce unfavorable  $\text{Li}_2\text{S}$  formation. Furthermore, this new electrolyte system is also found to enable high capacity of high-sulfur-loading cathodes with low electrolyte/sulfur (E/S) ratios, such as a stable specific capacity of around  $1000 \text{ mAh g}^{-1}$  using a low electrolyte amount (that is, E/S ratio of  $5 \text{ mL g}^{-1}$ ) and high sulfur-loading ( $4 \text{ mg cm}^{-2}$ ) cathodes (Figure 108).

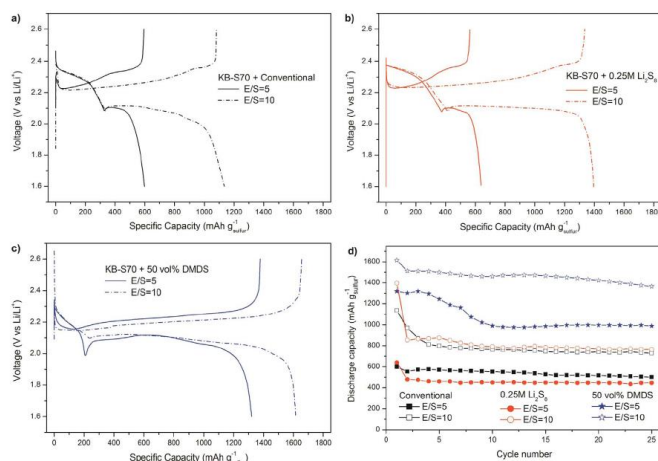


**Figure 108.** Initial discharge-charge profiles of KB-S70 cathodes in (a) conventional, (b) 0.25 M polysulfide-containing, and (c) 50 vol% dimethyl disulfide (DMDS)-containing electrolytes with electrolyte/sulfur ratios of 5 and 10  $\text{mL g}^{-1}$  at a current density of  $0.2 \text{ mA cm}^{-2}$ , with (d) their corresponding cycling performance.

For protection of the Li-metal anode, appropriate compositions for organo- $\text{Li}_x\text{S}_y$  lithium protection layers have been found. The SCPs, which contain the sulfur chains and organic units, are the suitable candidate for the fabrication of organo- $\text{Li}_x\text{S}_y$  lithium protection layers. The effect of sulfur contents in the SCPs on cycling performance of Li-metal anode was investigated. 2 wt% SCPs were added into the electrolyte, which was 1 M LiTFSI (lithium bis(trifluoromethanesulfonyl)imide) and 1 wt%  $\text{LiNO}_3$  in the dioxolane/dimethoxyethane (DOL/DME = 1:1, V/V). As shown in Figure 109, the

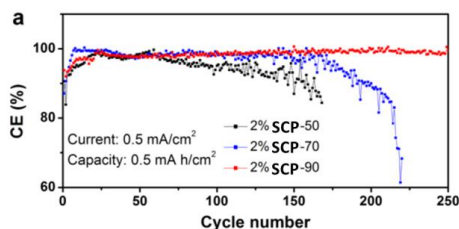


**Figure 109.** Cycling performance of 2 wt% sulfur-containing polymers with different sulfur contents as additives. (a) PSD containing different sulfur contents. (b) PST containing different sulfur contents.

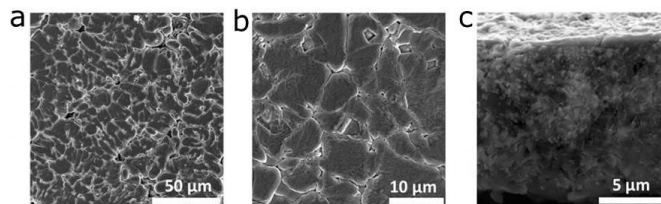


**Figure 110.** Morphologies of lithium metal deposited onto stainless steel substrate. Scanning electron microscopy images of lithium metal deposited onto bare stainless steel substrate in the electrolyte with the addition of 8 wt% the sulfur composite product (SCP)-90.

SCPs with 90 wt% sulfur exhibited the best cycling performance, and the cycling stability dropped with the decrease of sulfur content in the SCPs. The morphologies of the deposited lithium metal using SCP as additives show (Figure 110) that dense and dendrite-free lithium film was deposited on the substrate, and the pancake-like lithium film was continuous and uniform. The cross-section view confirmed that the deposited lithium grew very compact, and no obvious dendritic lithium can be observed in the surface and interior of the lithium film.

## Patents/Publications/Presentations

### Publication

- Chen, S. R., and Y. Gao, Z. X. Yu, M. L. Gordin, J. X. Song, and D. H. Wang. “High Capacity of Lithium-Sulfur Batteries at Low Electrolyte/Sulfur Ratio Enabled by an Organosulfide Containing Electrolyte.” *Nano Energy* 31 (2017): 418.

## TASK 9 – LITHIUM–AIR BATTERIES

### Summary and Highlights

High-density energy storage systems are critical for EVs required by the EV Everywhere Grand Challenge. Conventional Li-ion batteries still cannot fully satisfy the ever-increasing needs because of their limited energy density, high cost, and safety concerns. As an alternative, the rechargeable lithium-oxygen (Li-O<sub>2</sub>) battery has the potential to be used for long-range EVs. The practical energy density of a Li-O<sub>2</sub> battery is expected to be ~ 800 Wh kg<sup>-1</sup>. The advantages of Li-O<sub>2</sub> batteries come from their open structure; that is, they can absorb the active cathode material (oxygen) from the surrounding environment instead of carrying it within the batteries. However, the open structure of Li-O<sub>2</sub> batteries also leads to several disadvantages. The energy density of Li-O<sub>2</sub> batteries will be much lower if oxygen has to be provided by an onboard container. Although significant progress has been made in recent years on fundamental properties of Li-O<sub>2</sub> batteries, research in this field is still in an early stage, and many barriers must be overcome before practical applications. The barriers include:

- Instability of electrolytes—The superoxide species generated during discharge or O<sub>2</sub> reduction process is highly reactive with electrolyte and other components in the battery. Electrolyte decomposition during charge or O<sub>2</sub> evolution process is also significant due to high over-potentials.
- Instability of air electrode (dominated by carbonaceous materials) and other battery components (such as separators and binders) during charge/discharge processes in an O-rich environment.
- Limited cyclability of the battery associated with instability of the electrolyte and other battery components.
- Low energy efficiency associated with large over-potential and poor cyclability of Li-O<sub>2</sub> batteries.
- Low power rate capability due to electrode blocking by the reaction products.
- Absence of a low-cost, high-efficiency oxygen supply system (such as oxygen selective membrane).

The main goal of this Task is to provide a better understanding on the fundamental reaction mechanisms of Li-O<sub>2</sub> batteries and identify the required components (especially electrolytes and electrodes) for stable operation of Li-O<sub>2</sub> batteries. PNNL researchers will investigate stable electrolytes and oxygen evolution reaction (OER) catalysts to reduce the charging overvoltage of Li-O<sub>2</sub> batteries and improve their cycling stability. New electrolytes will be combined with stable air electrodes to ensure their stability during Li-O<sub>2</sub> reaction. Considering the difficulties in maintaining the stability of conventional liquid electrolyte, the Liox team will explore use of a nonvolatile, inorganic molten salt comprising nitrate anions and operating Li-O<sub>2</sub> cells at elevated temperature (> 80°C). It is expected that these Li-O<sub>2</sub> cells will have a long cycle life, low over potential, and improved robustness under ambient air compared to current Li-air batteries. At ANL, new cathode materials and electrolytes for Li-air batteries will be developed for Li-O<sub>2</sub> batteries with long cycle life, high capacity, and high efficiency. The state-of-the-art characterization techniques and computational methodologies will be used to understand the charge and discharge chemistries. The University of Massachusetts/BNL team will investigate the root causes of the major obstacles of the air cathode in the Li-air batteries. Special attention will be paid to optimization of high-surface carbon material used in the gas diffusion electrode, catalysts, electrolyte, and additives stable in Li-air system and with capability to dissolve lithium oxide and peroxide. Success of this project will establish a solid foundation for further development of Li-O<sub>2</sub> batteries toward their practical applications for long-range EVs. The fundamental understanding and breakthrough in Li-O<sub>2</sub> batteries may also provide insight on improving performance of Li-S batteries and other energy storage systems based on chemical conversion processes.

**Highlight.** The highlights for this quarter are as follows:

- The ANL team developed a new electrode based on unique hollow graphene nanocages (HGN) matrix with nano-Pt catalyst that can reduce the charge voltage to below 3.2 V.
- The PNNL team investigated effect of temperature on performance of Li-O<sub>2</sub> batteries. The discharge capacities of the Li-O<sub>2</sub> cells exhibit a surprise increase from 3545 to 17716 mAh g<sup>-1</sup> when temperature decreased from 20°C to -20°C.



## Task 9.1 – Rechargeable Lithium-Air Batteries (Ji-Guang Zhang and Wu Xu, Pacific Northwest National Laboratory)

**Project Objective.** The project objective is to develop rechargeable Li-O<sub>2</sub> batteries with long-term cycling stability. The FY 2017 objective is to stabilize Li-metal anode in Li-O<sub>2</sub> batteries and to investigate the temperature effect on oxygen reduction reaction (ORR) and OER processes of the Li-O<sub>2</sub> chemistry.

**Project Impact.** Li-air batteries have a theoretical specific energy that is more than five times that of state-of-the-art Li-ion batteries and are potential candidates for use in next-generation, long-range EVs. Unfortunately, the poor cycling stability and low CE of Li-air batteries have prevented their practical application. This work will explore a new electrolyte and electrode that could lead to long cyclability and high CEs in Li-air batteries that can be used in the next-generation EVs required by the EV Everywhere Grand Challenge.

**Out-Year-Goals.** The long-term goal of the proposed work is to enable rechargeable Li-air batteries with a specific energy of 800 Wh/kg at cell level, 1000 deep-discharge cycles, improved abuse tolerance, and less than 20% capacity fade over a 10-year period to accelerate commercialization of long-range EVs.

**Collaborations.** This project collaborates with Chongmin Wang of PNNL on characterization of cycled air electrodes by TEM/SEM.

### Milestones

1. Investigate temperature effect on ORR and OER of Li-O<sub>2</sub> batteries. (Q1 – Complete)
2. Identify factors that affect stability of Li-metal anode in Li-O<sub>2</sub> batteries. (Q2 – In progress)
3. Develop surface coating or electrolyte additive to stabilize Li-metal anode and improve cycle life of Li-O<sub>2</sub> battery. (Q4)

## Progress Report

This quarter, the effect of temperature on the discharge behavior of aprotic Li-O<sub>2</sub> batteries based on simple CNT air electrodes was investigated. The electrolyte was 0.1 M LiClO<sub>4</sub>-DME due to its low viscosity and low freezing temperature, and the discharge current density was 0.1 mA cm<sup>-2</sup>. As shown in Figure 111, the discharge capacity of the Li-O<sub>2</sub> battery is significantly affected by the environmental temperature. The discharge capacities of the above Li-O<sub>2</sub> cells are 17716, 12491, 2930, 3250, 3545, 5029, and 7492 mAh g<sup>-1</sup> at -20, -10, 0, 10, 20, 30, and 40 °C, respectively. In the temperature range of 0 to 40 °C, the discharge capacity decreases with the decrease in temperature. However, in the temperature range of 0 to -20 °C, the discharge capacity increases significantly with the decreasing temperature. Although the voltage polarization during initial discharge increases with the decreasing temperature, Li-O<sub>2</sub> batteries cycled at two temperatures below 0 °C (that is, -10 °C and -20 °C) exhibit extremely high discharge capacity as compared to those obtained at 40 °C. The XRD patterns of the discharge products indicate that the reaction product was dominated by Li<sub>2</sub>O<sub>2</sub>. However, the morphologies of these Li<sub>2</sub>O<sub>2</sub> particles are largely different, as shown in Figure 112. The results indicate that decreasing temperature leads to formation of smaller discharge products. More interestingly, at temperatures below 0 °C, Li<sub>2</sub>O<sub>2</sub> was also found inside the glass fiber separators and on the surface of Li-metal anode facing toward the air electrode.

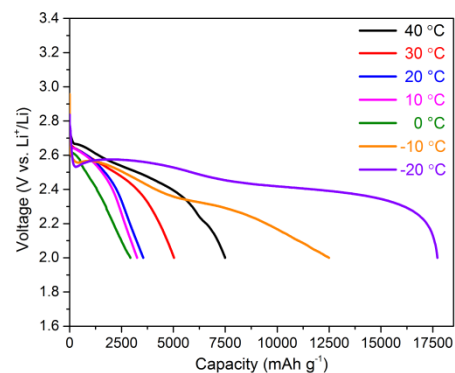


**Figure 111.** Discharge curves of Li-O<sub>2</sub> cells using carbon nanotube air electrodes and 1 M LiClO<sub>4</sub>-DME electrolyte cycled at various temperatures (from 40 °C to -20 °C) and at a discharge current density of 0.1 mA cm<sup>-2</sup>.

The electron EPR and NMR tests on the thermal stability of KO<sub>2</sub> solutions at different temperatures indicate that the lifetime of superoxide radical anions increases exponentially with decreasing temperature. In contrast, the computational calculations indicate that the kinetic rate of ORR increases exponentially with increasing temperature. The simulations after combining the two factors—the lifetime of

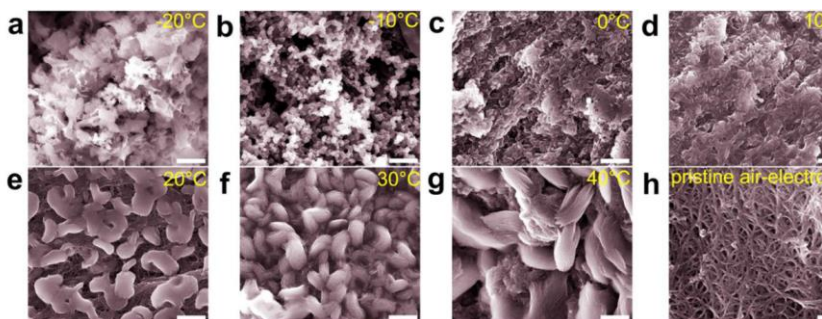


**Figure 112.** Morphological images of the discharged products on the carbon nanotube (CNT)-based air electrodes after discharge at various temperatures (a-g) and the pristine CNTs air electrode (h).

superoxide radical anions and the kinetic rate of ORR—indicate that the lifetime of superoxide radical anions dominates the discharge behavior of the Li-O<sub>2</sub> battery at temperatures below 0 °C and the kinetic rate of ORR controls the discharge behavior of the Li-O<sub>2</sub> battery in temperatures above 0 °C. At temperatures below 0 °C, the superoxide radical anions generated at the air electrode surface during ORR will dissolve into the electrolyte, and move away from the air electrode and even through the glass fiber separator to reach the surface of the Li-metal anode because of their significantly increased lifetime. Therefore, more ORR can occur, and an extremely high discharge capacity results. More analysis and the manuscript preparation are under way.

## Patents/Publications/Presentations

### Presentation

- 2016 MRS Fall Meeting, Boston (December 1, 2016): “Electrochemically Formed Ultrafine Metal Oxide Nano-Catalysts for High-Performance Lithium-Oxygen Batteries”; B. Liu, P. Yan, W. Xu, J. Zheng, Y. He, L. Luo, M. E. Bowden, C. Wang, and J.-G. Zhang.

## Task 9.2 – Efficient Rechargeable Li/O<sub>2</sub> Batteries Utilizing Stable Inorganic Molten Salt Electrolytes (Vincent Giordani, Liox)

**Project Objective.** The project objective is to develop high specific energy, rechargeable Li-air batteries having lower overpotential and improved robustness under ambient air compared to current Li-air batteries.

**Project Impact.** If successful, this project will solve particularly intractable problems relating to air electrode efficiency, stability, and tolerance to the ambient environment. Furthermore, these solutions may translate into reduced complexity in the design of a Li-air stack and system, which in turn may improve prospects for use of Li-air batteries in EVs. Additionally, the project will provide materials and technical concepts relevant for development of other medium temperature molten salt lithium battery systems of high specific energy, which may also have attractive features for EVs.

**Approach.** The technical approach involves replacing traditional organic and aqueous electrolytes with a non-volatile, inorganic molten salt comprising nitrate anions and operating the cell at elevated temperature (> 80°C). The research methodology includes powerful *in situ* spectroscopic techniques coupled to electrochemical measurements (for example, electrochemical MS) designed to provide quantitative information about the nature of chemical and electrochemical reactions occurring in the air electrode.

**Out-Year-Goals.** The long-term goal of this project is to develop Li-air batteries comprising inorganic molten salt electrolytes and protected lithium anodes that demonstrate high (> 500 Wh/kg) specific energy and efficient cyclability in ambient air. By the end of the project, it is anticipated that problems hindering use of both the lithium anode and air electrode will be overcome due to materials advances and strategies enabled within the intermediate (> 80°C) operating temperature range of the system under development.

**Collaborations.** This project funds work at Liox Power, Inc.; LBNL (Prof. Bryan McCloskey: analysis of air electrode and electrolyte); and California Institute of Technology (Prof. Julia Greer: design of air electrode materials and structures).

### Milestones

1. Demonstrate discharge specific energy and energy density  $\geq 500$  Wh/Kg and  $\geq 800$  Wh/L, respectively, based on air electrode mass and volume. (Q1 – Complete)
2. Scale-up downselected cell components for 4 mAh and 10 mAh cells. (Q2 – In progress)
3. Demonstrate  $\geq 10$  cycles at  $\geq 90\%$  round-trip energy efficiency in laboratory-scale Li-air cells comprising a molten nitrate electrolyte and protected lithium electrode. (Q3)
4. Fabricate and test 4 and 10 mAh cells. (Q4)

## Progress Report

This quarter, the O<sub>2</sub> cathode discharge specific energy and energy density were evaluated. Typically, composite cathodes comprising Super P carbon black, PTFE binder, and LiNO<sub>3</sub>-KNO<sub>3</sub> eutectic weighed 4 mg (all components minus the mesh current collector), while thickness was 100 microns. Mass ratio between carbon, binder, and electrolyte was 78/2/20 wt%, respectively. Li/O<sub>2</sub> cells were discharged to 2.5 V, at 0.32 mA/cm<sup>2</sup> ( $A_{cathode} = 0.785 \text{ cm}^2$ ), and at 150°C. With a discharge capacity of 335 Ah/kg, or 170 Ah/L, of air electrode (carbon + binder + eutectic, Figure 113a), the calculated corresponding discharge specific energy and energy density at  $E_{disch.} \approx 2.7 \text{ V}$  were 900 Wh/Kg and 460 Wh/L, respectively.

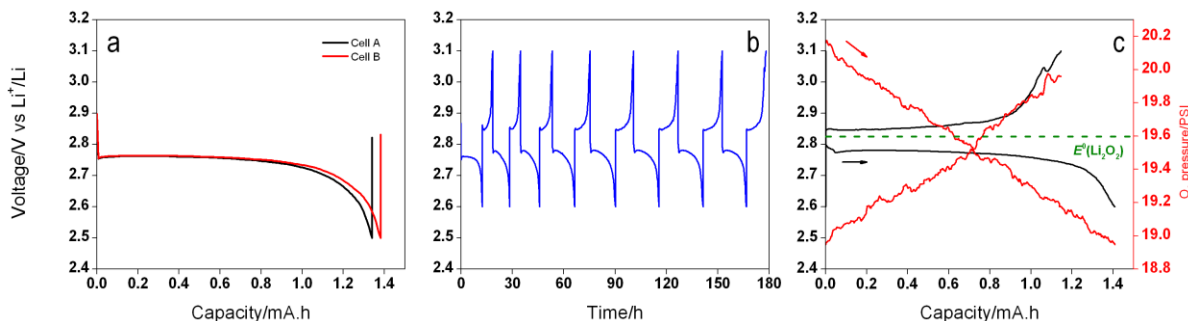


Figure 113. (a) Galvanostatic discharge curves for Li/O<sub>2</sub> cell containing a LiNO<sub>3</sub>-KNO<sub>3</sub> electrolyte and a carbon-based air electrode ( $T = 150^{\circ}\text{C}$ ,  $\text{PO}_2 = 1.4 \text{ atm}$ ,  $j = 0.32 \text{ mA/cm}^2$ ). (b) Cycling profile of a molten nitrate Li/O<sub>2</sub> cell containing a carbon-free air electrode ( $T = 150^{\circ}\text{C}$ ,  $j = 0.13 \text{ mA/cm}^2$ , boron carbide loading: 5-7 mg/cm<sup>2</sup>). (c) Corresponding *in situ* pressure analysis for cell depicted in (b).

Among other recently tested conducting ceramic electrode materials (FY 2016 Q3), boron carbide nanopowders (B<sub>4</sub>C) were shown to exert promising cycling behavior in the molten salt electrolyte (Figure 113b,c). In this quarter, e<sup>-</sup>/O<sub>2</sub> molar ratios was found to be 2.0 for both discharge and charge half-cycle, supporting reversible formation of Li<sub>2</sub>O<sub>2</sub> as the discharge product, with OER/ORR ratio of 0.85, consistent with solution-phase mechanism of Li<sub>2</sub>O<sub>2</sub> growth and/or side reaction with the carbide material to form lithium carbonate. SEM analysis of a discharged electrode showed micron-sized ORR product deposited onto glass fibers (separator material), leading to electrical disconnection and low CE ( $\approx 85\%$ ). XRD and XPS measurements are in progress to characterize B<sub>4</sub>C surface during cycling in a molten nitrate lithium/oxygen cell.

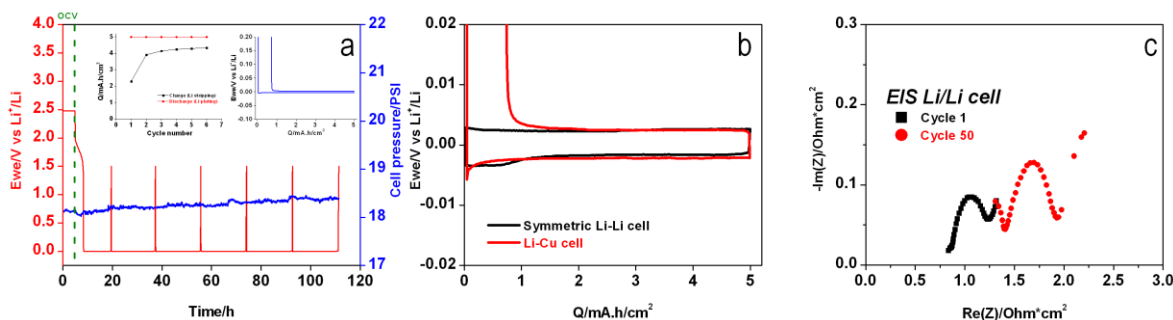


Figure 114. (a) Lithium plating/stripping onto Cu ( $\text{ALi}=\text{ACu}=0.502 \text{ cm}^2$ ) at  $j = 0.5 \text{ mA/cm}^2$ , at 150°C, under Ar, in LiNO<sub>3</sub>-KNO<sub>3</sub> melt (Inset: Q vs cycle number and lithium plating/stripping load curve). (b) Cycling curve comparison between Li-Li symmetric cell and Li-Cu cell employing LiNO<sub>3</sub>-KNO<sub>3</sub> melt, at 0.5 mA/cm<sup>2</sup>, at 150°C. (c) Electrochemical impedance spectroscopy data derived from cycled Li-Li symmetric cell (estimated electrolyte thickness: 0.5 mm,  $\text{ALi} = 0.502 \text{ cm}^2$ ).

Study of the Li-metal/molten-nitrate interface shows an increase in ASR with cycle number (both bulk and interfacial resistances), continuous increase in pressure (Figure 114a), consistent with SEI reaction:  $2\text{Li} + \text{NO}_3^- = \text{Li}_2\text{O} + \text{NO}_2^-$ , with nitrite anion being further reduced by lithium to yield nitric oxide and nitrogen (confirmed by MS), and low CE for lithium stripping/plating ( $\approx 87\%$ ). The addition of few wt% CsNO<sub>3</sub> into the melt to stabilize the lithium interface has shown promising results and is being explored, along with stable ceramic electrolytes to eliminate reaction between Li-metal anode and the molten nitrate electrolyte.

## Patents/Publications/Presentations

### Publication

- Burke, C. M., et al. “Implications of 4 e<sup>-</sup> Oxygen Reduction via Iodide Redox Mediation in Li-O<sub>2</sub> Batteries.” *ACS Energy Lett.* 1, no. 4 (2016): 747–756.

### Presentation

- 2016 PRIME / ECS, Honolulu (October 2016): “Cathode Design for High Energy Molten Salt Lithium-Oxygen Batteries”; D. Tozier (California Institute of Technology); V. Giordani, J. Uddin, and H. Tan (Liox); B. D. McCloskey (LBNL); J. R. Greer (California Institute of Technology); and G. V. Chase and D. Addison (Liox).

## Task 9.3 – Lithium–Air Batteries (Khalil Amine and Larry A. Curtiss, Argonne National Laboratory)

**Project Objective.** This project will develop new cathode materials and electrolytes for Li-air batteries for long cycle life, high capacity, and high efficiency. The goal is to obtain critical insight that will provide information on the charge and discharge processes in Li-air batteries to enable new advances to be made in their performance. This will be done using state-of-the-art characterization techniques combined with state-of-the-art computational methodologies to understand and design new materials and electrolytes for Li-air batteries.

**Project Impact.** The instability of current nonaqueous electrolytes and degradation of cathode materials limits the performance of Li-air batteries. The project impact will be to develop new electrolytes and cathode materials that are stable and can increase cycle life and improve efficiency of Li-air batteries.

**Approach.** The project is using a joint theoretical/experimental approach for design and discovery of new cathode and electrolyte materials that act synergistically to reduce charge overpotentials and increase cycle life. Synthesis methods, in combination with design principles developed from computations, are used to make new cathode architectures. Computational studies are used to help understand decomposition mechanisms of electrolytes and how to design electrolytes with improved stability. The new cathodes and electrolytes are tested in Li-O<sub>2</sub> cells. Characterization along with theory is used to understand the performance of the materials used in the cell and make improved materials.

**Out-Year Goals.** The out-year goals are to find catalysts that promote discharge product morphologies that reduce charge potentials and find electrolytes for long cycle life through testing and design.

**Collaborations.** This project engages in collaboration with Professor Kah Chun Lau (University of California – Norridge), Professor Amin Salehi (University of Illinois – Chicago), Professor Yang-Kook Sun (Hanyang University), Professor Yiyang Wu (Ohio State University), and Dr. Dengyun Zhai (China).

### Milestones

1. Investigation of new architectures for platinum catalysts using hollow nanocarbon cages. (Q1 – Complete)
2. Design and synthesis of new catalysts for cathode materials based on metal organic frameworks for low charge overpotentials. (Q2 – In progress)
3. Development of new characterization techniques for determination of the composition and conductivity of discharge products in Li-O<sub>2</sub> batteries. (Q3)
4. Investigation of uniformly synthesized metal clusters as catalysts and nucleation sites for controlling efficiency of Li-O<sub>2</sub> cells. (Q4)

## Progress Report

One of the formidable challenges facing aprotic Li-O<sub>2</sub> batteries is the high charge overpotential, which causes formation of by-products, loss in efficiency, and poor cycling performance. To solve this challenge, ultra-small Pt-coated HGN have been synthesized as cathodes for Li-O<sub>2</sub> batteries. The charge voltage plateau is 3.2 V at the current density of 100 mA/g and is even still below 3.5 V when the current density is increased to 500 mA/g. The unique HGN matrix can not only provide numerous nano-scale tri-phase regions as active sites for efficient oxygen reduction, but also offer a sufficient amount of meso-scale pores for rapid oxygen diffusion. Furthermore, with strong atomic-level oxygen absorption into its subsurface, ultra-small platinum particles can serve as the nucleation site for Li<sub>2</sub>O<sub>2</sub> growth. The Li<sub>2</sub>O<sub>2</sub> has a favorable morphology with small size and amorphous state, which can decompose more easily during recharge. Meanwhile, the conductive hollow graphene substrate can enhance the catalytic activity of noble metal platinum catalysts due to the graphene-metal interfacial interaction.

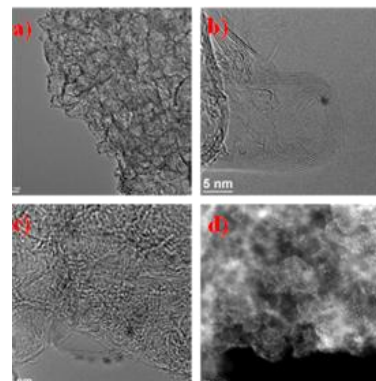


**Figure 115.** (a) Transmission electron microscopy (TEM) image of Platinum-hollow graphene nanocages (Pt-HGNs). (b, c) High-magnification TEM images of Pt-HGNs. (d) Dark-field scanning transmission electron microscopy (DF-STEM) image of Pt-HGNs.

The synthetic strategy for HGNs involves the combustion of metal manganese with dry ice to produce cubic nanoparticles of MgO covered by few graphite carbon layers. The HGNs are obtained by removing the cubic MgO from inside of the graphene with dilute hydrochloric acid. Finally, the platinum nanoparticles were homogeneously deposited on the surface of the HGNs by PVD. The porous hollow nanocage architecture of HGNs, and the homogeneity of platinum catalysts were confirmed with TEM at different magnifications shown in Figure 115. The electrochemical performances of pristine and Pt-HGNs as the cathodes in a Li-O<sub>2</sub> cell were investigated under capacity-controlled conditions to minimize side reactions. With a nano-Pt catalyst, the Pt-HGNs electrode exhibited a stable discharge curve at approximately 2.75 V. It also showed a charge voltage below 3.2 V closing with a value of 2.96 V after initial three cycles, and steadily remained below 3.5 V for at least 10 cycles (see Figure 116). Thus, with enhanced conductivity and unique porous structure, the Pt-HGNs exhibit a very low charge overpotential for a Li-O<sub>2</sub> battery using a platinum cathode catalyst.

Moreover, the poor rate performance of the typical aprotic Li-O<sub>2</sub> cell was found to be improved by using the Pt-HGNs cathode. The Pt-HGN cathode showed the discharge plateau staying above 2.6 V, and the charge mid-capacity potential below 3.5 V. The excellent electrochemical performance may be attributed to improved OER kinetics facilitating efficient decomposition of Li<sub>2</sub>O<sub>2</sub>.

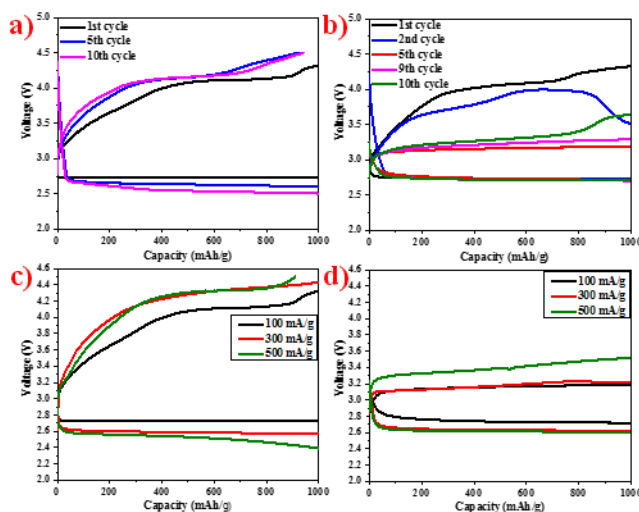


**Figure 116.** Galvanostatic discharge/charge profiles of Li-O<sub>2</sub> batteries with (a) hollow graphene nanocages (HGNs) and (b) Pt-HGNs as cathode catalysts at 100 mA/g in the voltage range of 2.2 – 4.5 V vs. Li+/Li with the fixed capacity of 1000 mAh/g. Discharge/charge profiles of Li-O<sub>2</sub> batteries with (c) Pristine HGNs and (d) Pt-HGNs cathode catalysts at different current densities.



## Patents/Publications/Presentations

### Publication

- He, M., and K. C. Lau, X. Ren, N. Xiao, W. D. McCulloch, L. A. Curtiss, and Y. Wu. “Concentrated Electrolyte for the Sodium–Oxygen Battery: Solvation Structure and Improved Cycle Life.” *Angewandte Chemie* 128, no. 49 (2016): 15536–15540.

## TASK 10 – SODIUM-ION BATTERIES

### Summary and Highlights

To meet the challenges of powering the PHEV, the next generation of rechargeable battery systems with higher energy and power density, lower cost, better safety characteristics, and longer calendar and cycle life (beyond Li-ion batteries, which represent today's state-of-the-art technology) must be developed. Recently, Na-ion battery systems have attracted increasing attention due to the more abundant and less expensive nature of the sodium resource. The issue is not insufficient lithium on a global scale, but what fraction can be used in an economically effective manner. Most untapped lithium reserves occur in remote or politically sensitive areas. Scale-up will require a long lead time, involve heavy capital investment in mining, and may require the extraction and processing of lower quality resources, which could drive extraction costs higher. Currently, high costs remain a critical barrier to the widespread scale-up of battery energy storage. Recent computational studies on voltage, stability, and diffusion barriers of Na-ion and Li-ion materials indicate that Na-ion systems can be competitive with Li-ion systems.

The primary barriers and limitations of current state-of-the-art of Na-ion systems are as follows:

- Building a sodium battery requires redesigning battery technology to accommodate the chemical reactivity and larger size of sodium ions.
- Lithium batteries pack more energy than sodium batteries per unit mass. Therefore, for sodium batteries to reach energy densities similar to lithium batteries, the positive electrodes in the sodium battery need to hold more ions.
- Since Na-ion batteries are an emerging technology, new materials to enable sodium electrochemistry and the discovery of new redox couples along with the diagnostic studies of these new materials and redox couples are quite important.
- In sodium electrochemical systems, the greatest technical hurdles to overcome are the lack of high-performance electrode and electrolyte materials that are easy to synthesize, safe, and non-toxic, with long calendar and cycling life and low cost.
- Furthermore, fundamental scientific questions need to be elucidated, including (1) the difference in transport and kinetic behaviors between sodium and lithium in analogous electrodes; (2) sodium insertion/extraction mechanism; (3) SEI layer on the electrodes from different electrolyte systems; and (4) charge transfer in the electrolyte–electrode interface and Na<sup>+</sup> ion transport through the SEI layer.

This task will use synchrotron-based *in situ* X-ray techniques and other diagnostic tools to evaluate new materials and redox couples, to explore fundamental understanding of the mechanisms governing the performance of these materials, and provide guidance for new material developments. This task will also be focused on developing advanced diagnostic characterization techniques to investigate these issues, providing solutions and guidance for the problems. The synchrotron based *in situ* X-ray techniques (XRD and hard and soft XAS) will be combined with other imaging and spectroscopic tools such as HRTEM, MS, and TXM.

## Task 10.1 – Exploratory Studies of Novel Sodium-Ion Battery Systems (Xiao-Qing Yang and Xiqian Yu, Brookhaven National Laboratory)

**Project Objective.** The primary objective is to develop new advanced *in situ* material characterization techniques and to apply these techniques to explore the potentials, challenges, and feasibility of new rechargeable battery systems beyond the Li-ion batteries, namely the Na-ion battery systems for PHEVs. To meet the challenges of powering the PHEV, new rechargeable battery systems with high energy and power density, low cost, good abuse tolerance, and long calendar and cycle life must be developed. This project will use synchrotron-based *in situ* X-ray diagnostic tools developed at BNL to evaluate the new materials and redox couples, exploring the fundamental understanding of the mechanisms governing the performance of these materials.

**Project Impact.** The VTO Multi-Year Program Plan describes the goals for battery: “Specifically, lower-cost, abuse-tolerant batteries with higher energy density, higher power, better low-temperature operation, and longer lifetimes are needed for the development of the next-generation of HEVs, PHEVs, and EVs.” If this project succeeds, the knowledge gained from diagnostic studies and collaborations with U.S. industries and international research institutions will help U.S. industries develop new materials and processes for a new generation of rechargeable battery systems beyond Li-ion batteries, such as Na-ion battery systems, in their efforts to reach these VTO goals.

**Approach.** This project will use synchrotron-based *in situ* X-ray diagnostic tools developed at BNL to evaluate the new materials and redox couples to enable a fundamental understanding of the mechanisms governing the performance of these materials and to provide guidance for new material and new technology development regarding Na-ion battery systems.

**Out-Year Goals.** The out-year goals are as follows: (1) Complete the synchrotron based *in situ* XRD and absorption studies of MXene type material  $V_2C$  as new cathode material for Na-ion batteries during charge-discharge cycling, and (2) complete the preliminary synchrotron based X-ray absorption studies of  $NaCuMnO_2$  as new cathode material for Na-ion batteries.

**Collaborations.** The BNL team has been working closely with top scientists on new material synthesis at ANL, LBNL, and PNNL, with U.S. industrial collaborators at GM and Johnson Controls, and with international collaborators.

### Milestones

1. Complete the *in situ* XRD studies of one type of MXene material  $V_2C$  as new anode material for Na-ion batteries during charge-discharge cycling. (December 2016 – Complete)
2. Complete *in situ* hard X-ray absorption studies at vanadium K-edge of one type of MXene material  $V_2C$  as new anode material for Na-ion batteries during charge-discharge cycling. (March 2017 – In progress)
3. Complete soft X-ray absorption studies at vanadium L-edge, carbon, and oxygen K-edge of one type of MXene material  $V_2C$  as new anode material for Na-ion batteries at different charge-discharge states. (June 2017 – In progress)
4. Complete the synchrotron based X-ray absorption at copper and manganese K-edge for a new  $NaCuMnO_2$  cathode material for Na-ion batteries during charge-discharge cycling. (September 2017 – In progress)

## Progress Report

The first milestone for FY 2017 has been completed. This quarter, BNL has focused on studies of a new cathode material for Na-ion batteries. A  $V_2C$  material, as a new member of the two-dimensional TM carbides, so-called MXenes, was synthesized in a way containing surface functional groups (denoted as  $V_2CT_x$ , where  $T_x$  are surface functional groups) and studied as anode materials for Na-ion batteries.  $V_2CT_x$  anode exhibits reversible charge storage with good cycling stability and high rate capability through electrochemical test. The charge storage mechanism of  $V_2CT_x$  material during  $Na^+$  intercalation/deintercalation and the redox reaction of vanadium were studied using a combination of synchrotron-based XRD and hard XANES. Figure 117a presents *ex situ* XRD patterns at the  $2\theta$  angle range corresponding the (002) reflection of  $V_2CT_x$  at several charge/discharge (that is, sodiation/desodiation) states during first cycle (the charge-discharge curve is also plotted on the right panel of Figure 117a). During the first sodiation process, the (002) diffraction peak in the XRD pattern moved from  $9.3^\circ$  to  $8.1^\circ$  from the OCV state to the 0.1 V state, corresponding an expansion of the interlayer distance from  $9.53 \text{ \AA}$  to  $10.93 \text{ \AA}$ . As illustrated in Figure 117b, beside the  $Na^+$  absorption at the surface of  $V_2CT_x$ , resulted in the capacitor-like capacity, additional energy storage also occurred through  $Na^+$  intercalation between layers of  $V_2CT_x$ . This behavior is similar to those of previous reports on  $Ti_2CT_x$  and  $V_2CT_x$  MXene materials. However, during subsequent desodiation (or deintercalation) process, the contraction of interlayer distance ( $\sim 1.03 \text{ \AA}$ ) is much smaller than the  $1.40 \text{ \AA}$  expansion during first sodiation.

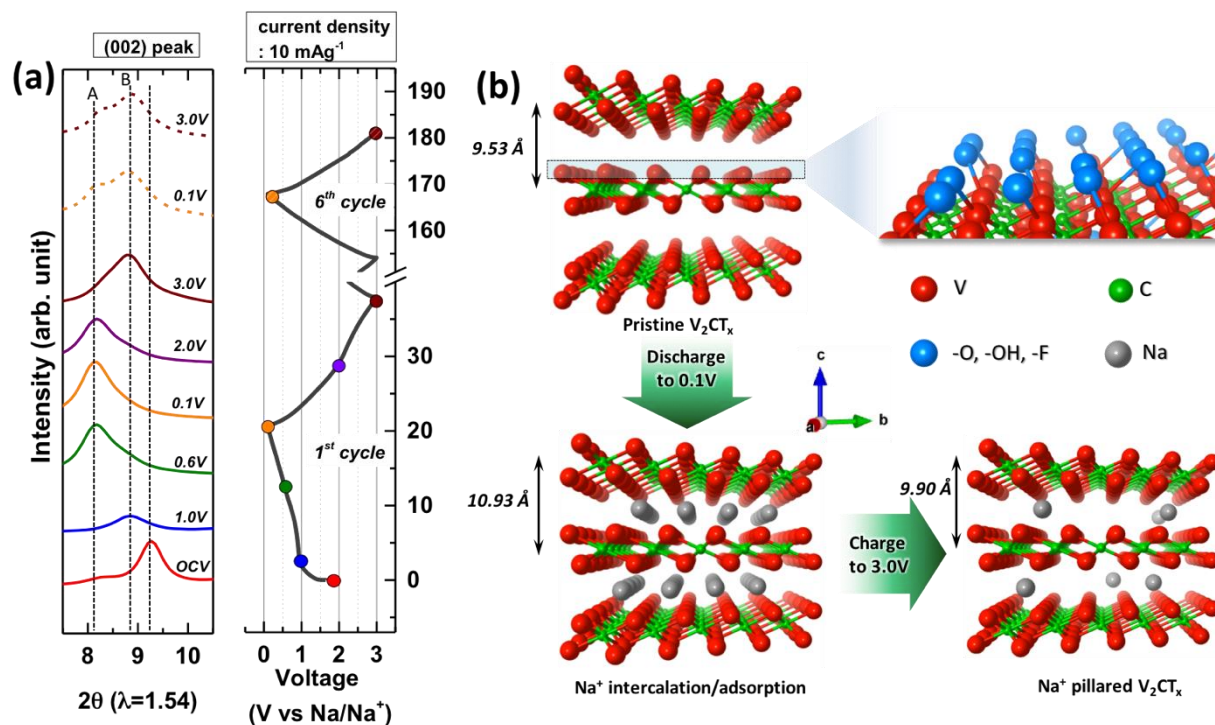


Figure 117. (a) *Ex situ* X-ray diffraction patterns (left) for  $V_2CT_x$  upon electrochemical sodiation/desodiation cycling (right). (b) Schematic illustration of the expansion/contraction behavior of  $V_2CT_x$  during sodiation/desodiation process: the interlayer distance of  $V_2CT_x$  is increased upon  $Na^+$  intercalation during sodiation process, then partially reduced upon  $Na^+$  deintercalation due to the trapped  $Na^+$  between  $V_2CT_x$  layers that behaves as a pillar during desodiation process.

## Patents/Publications/Presentations

### Publication

- Zhang, Zhizhen, and Qinghua Zhang, Jinan Shi, Yong S. Chu, Xiqian Yu, Kaiqi Xu, Mingyuan Ge, Hanfei Yan, Wenjun Li, Lin Gu\*, Yong-Sheng Hu\*, Hong Li, Xiao-Qing Yang, Liquan Chen, and Xuejie Huang. “A Self-Forming Composite Electrolyte for Solid-State Sodium Battery with Ultra-Long Cycle Life.” *Adv. Energy Mater.* (2016). doi: 10.1002/aenm.201601196.

### Presentation

- 11<sup>th</sup> International Forum on Li-ion Battery Technology & Industrial Development, Hefei, China, (October 23-24, 2016): “Using Synchrotron Based *In situ* X-ray Diffraction and Absorption and TXM Techniques to Study the New Electrode Materials for Next Generation of Batteries”; Yongning Zhou, Xiqian Yu, Enyuan Hu, Xiao-Qing Yang\*, Seong-Min Bak, Hung-sui Lee, Yijin Liu, Hong Li, Xuejie Huang, and Liquan Chen. Invited.